LINEAR AND MULTI-ARM FUNCTIONALIZABLE POLYMERIC CONSTRUCTS FOR TARGETED DRUG DELIVERY AND IMAGING APPLICATIONS

by

Özgül Gök

B.S., Chemistry, Boğaziçi University, 2007

M.S., Chemistry, Boğaziçi University, 2010

Submitted to the Institute for Graduate Studies in
Science and Engineering in partial fulfillment of
the requirements for the degree of
Doctor of Philosophy

Graduate Program in Chemistry

Boğaziçi University

LINEAR AND MULTI-ARM FUNCTIONALIZABLE POLYMERIC CONSTRUCTS FOR TARGETED DRUG DELIVERY AND IMAGING APPLICATIONS

APPROVED BY:

Assoc. Prof. Rana Sanyal (Thesis Supervisor)	……...
Assoc. Prof. Amitav Sanyal (Thesis Co-Advisor)	……
Assist. Prof. Necla Birgül İyison	……
Assoc. Prof. Seyda Bucak Malta	……
Prof. Selim Küsefoğlu	……
Prof. Mustafa Fethi Şahin	……

DATE OF APPROVAL: 23.09.2014

Dedicated to my beloved family

ACKNOWLEDGEMENTS

I would like to express my sincere gratitude to my thesis supervisors Assoc. Prof. Rana Sanyal and Assoc. Prof. Amitav Sanyal for their encouraging attitude and support through all the years I spent in their laboratory. Their valuable scientific guidance and helpful discussions regarding my thesis work directed me to think about chemistry in a more innovative way, to practice problems and develop concrete solutions. I really do appreciate their endless attention and encouragement. It was great pleasure for me to work with them.

I wish to express my thanks to Jean-François Lutz, Nathalie Baradel and Mirela Zamfir in Precision Macromolecular Chemistry Group at Institut Charles Sadron for their contributon, support and advice for the collaborrative work in 'sequence controlled polymers' project.

I also thank Assist. Prof. Necla Birgül İyison at Molecular Biology and Genetics Department, Boğaziçi University for kindly providing the healthy cell line.

I would like to extend my thanks to my committee Prof. Selim Küsefoğlu, Prof. Fethi Şahin, Assoc. Prof. Seyda Bucak Malta and Assist. Prof. Necla Birgül İyison for their careful and constructive review of the final manuscript.

I would like to express my gratitude to Burcu Sümer, Sadık Kağa, Aslı Erdoğ, Tuğçe Nihal Gevrek, Pelin Ertürk and Merve Karaçivi for their contribution to my research and their kind friendship.

I wish to thank to my present labmates Nergiz Cengiz, Özlem Kalaoğlu Altan, Duygu Aydın, Filiz Çalık, Janset Yener, Harun Utku Aksoy, Sesil Genç, Mehmet Arslan, Yavuz Öz, Yasemin Üzüm, Laura Chambre, Hazal İpek and Hasancan Helvacı for their enjoyable company and valuable friendship. They helped to enrich my experience by our chemistry debates, exchanges of knowledge and skills during my graduate program.

Also, I want to thank to my former labmates Melike Eceoğlu, Betül Bingöl, Nazlı Böke, Merve Coşar, İrem Kosif, Merve Köse, Sebla Onbulak, Ece Geçici, Oyuntuya Munkhbat,

Duygu Çıtak, Merve Türksoy, Tuğba Dışpınar, Sezin Yiğit, Gülen Yeşilbağ Tonga, Murat Tonga and Rabia Arslan for their kind friendship and support.

I would like to express my gratitude to Emine Dindar, Şule Erol Günay, Jesmi Çavuşoğlu, Sevgi Sarıgül, Çimen Özgüç, Zeynep Bilgici, Selda Erkoç and Melis Çağdaş for their friendship, support and encouragement throughout these years.

I am so much thankful to my beloved friend Tuğçe Nihal Gevrek for her endless friendship and support for years both in the laboratory and outside.

I would like to thank to all my other friends and all the members of the faculty in the Chemistry Department.

Finally, my deepest thanks go to my whole family for their great support, encouragement throughout my education life and for their endless love.

This research has been supported by The Scientific and Technological Research Council of Turkey (TÜBİTAK) (109T493) and by Ministry of Science, Industry and Technology of Turkey (00589.STZ). I want to thank to the graduate scholarship program by The Scientific and Technological Research Council of Turkey (TÜBİTAK) (2211-D) during my Phd program.

ABSTRACT

LINEAR AND MULTI-ARM FUNCTIONALIZABLE POLYMERIC CONSTRUCTS FOR TARGETED DRUG DELIVERY AND IMAGING APPLICATIONS

Multifunctional polymers with different architectures were designed as macromolecular carriers for drug delivery and imaging applications. To this end, linear and multiarm copolymers incorporated with reactive groups were synthesized. The first study outlines the design of a thiol-reactive water soluble maleimide-based copolymer that can be utilized for targeted delivery system. Water soluble thiol-reactive linear copolymers were conjugated with a thiol-containing hydrophobic fluorescent dye and a peptide based targeting group. *In vitro* studies over both cancerous and healthy cells demonstrated non-toxicity of the polymeric carrier and enhanced uptake for polymers containing the targeting group. The second project involves the synthesis of polymer-drug conjugates where a chemotherapy drug was attached to linear polymers. These were investigated for *in vitro* cytotoxicity and *in vivo* pharmacokinetic profiles to demonstrate benefits of drug conjugation to polymers. The third project involves development of polymers containing clusters of functional groups as side chains at precise location along the polymer backbone. Linear copolymers of styrene and maleimide containing polyester dendrons were synthesized via nitroxide-mediated radical polymerization. Successful incorporation of dendrons containing alkene units was undertaken and these were modified with thiol-containing molecules. Fourth part of thesis focuses on the design of orthogonally reactive multiarm star polymers as drug delivery vehicles. Polyester dendrons containing initiators were designed to obtain multiarm copolymers. Obtained copolymers contained thiol reactive maleimide group at the core and activated esters along the polymeric arms. These copolymers were efficiently conjugated with a hydrophobic fluorescent dye at the core and an anti-cancer drug gemcitabine along the side chains. *In vitro* studies over cancerous cells displayed the reduced toxicity of drug upon polymer conjugation. Final project outlines the design of multiarm water soluble polymers containing a pyridyl disulfide based reversible linker for conjugation of peptides and small molecules. In summary, various linear and multiarm functional polymers were designed for facile conjugation of drugs, imaging and targeting groups to fabricate ideal drug delivery systems.

ÖZET

HEDEFLENDİRİLMİŞ İLAÇ SALIMI VE GÖRÜNTÜLEME UYGULAMALARI İÇİN LİNEER VE ÇOK KOLLU FONKSİYONELLEŞTİRİLEBİLİR POLİMERİK YAPILAR

İlaç salımı ve görüntüleme uygulamaları için çok fonksiyonlu ve farklı yapılara sahip makromoleküller tasarlanmıştır. Reaktif gruplarla donatılmış lineer ve çok kollu kopolimerler sentezlenmiştir. İlk çalışma, hedeflendirilmiş ilaç salım sistemi olarak kullanılmak üzere suda çözünebilen ve tiyol gruplarına karşı oldukça reaktif olan maleimid bazlı kopolimerlerin tasarımını anlatmaktadır. Bu polimerler, tiyol grubu içeren hidrofobik boya ve peptit bazlı hedefleyici gruplarla konjuge edilmiştir. Hem kanserli hem de sağlıklı hücre hatlarında yapılan *in vitro* çalışmalar, bu polimerik yapıların toksik etki göstermediğini ve hedefleyici grupları barındıran polimerlerin hücre içine daha fazla girdiğini göstermiştir. İkinci proje, lineer polimerlere kemoterapi ilaçlarının bağlandığı polimer-ilaç konjugelerinin sentezlerini içermektedir. Elde edilen polimerlerin *in vitro* sitoksisite ve *in vivo* farmakokinetik profilleri araştırılmıştır. Üçüncü projede ise lineer polimerlerin yan dallarında belirli noktalarda toplu fonksiyonel grupların yerleştirilmesi tasarlanmıştır. Stiren monomer ve maleimid grubu içeren polyester dendronlardan, nitroksit-aracılı radikalik polimerizasyon yöntemi kullanılarak lineer polimerler sentezlenmiştir. Yüzeyinde alkin grubu bulunan dendronlar, serbest tiyol içeren moleküller kullanılarak fonksiyonelleştirilmiştir. Tezin dördüncü kısmı, ilaç salım sistemleri olarak kullanılmak üzere orthogonal reaktif grupları içeren çok kollu polimer sentezleri üzerine yoğunlaşmaktadır. Çok kollu polimer sentezi için, başlatıcılar içeren poliester dendronlar kullanılmıştır. Elde edilen kopolimerlerin çekirdeğinde tiyollere karşı reaktif olan maleimid grubu, yan dallarında ise aktifleştirilmiş ester grupları bulunmaktadır. Bu polimerler etkin bir şekilde hidrofobik florasan boyaya ve kemoterapi ilacına konjuge edilmiştir. *In vitro* sitotoksisite ve hücre alım deneyleri, ilacın polimere bağlandığında toksisitesinin düştüğünü göstermektedir. En son proje ise peptid ve küçük biyomoleküllerin pridil disülfit gibi tersinir bağlarla suda çözünebilen çok kollu polimerlere bağlanmasını kapsamaktadır. Özet olarak, ideal ilaç salım sistemleri oluşturmak için ilaç, hedefleyici ve görüntüleme ajanlarının konjuge edilebileceği çeşitli lineer ve çok kollu fonksiyonel polimerler sentezlenmiştir.

TABLE OF CONTENTS

ACKNOWLEDGEMENTS iv
ABSTRACT vi
ÖZET vii
LIST OF FIGURES xi
LIST OF TABLES xix
LIST OF ACRONYMS/ABBREVIATIONS xx
1. INTRODUCTION 1
1.1. Cancer and Chemotherapy 1
1.2. Polymer Therapeutics 3
1.2.1. EPR effect 8
1.2.2 . Active Targeting 11
1.2.3. Polymeric nanomedicines: from Clinical Trials to Market 12
1.3. Preparation of Reactive Polymeric Platforms 25
1.3.1. Polymerization Techniques 25
1.4. Polymeric Architectures for Delivery of Therapeutics 27
1.4.1. Dendrimers 28
1.4.2. Dendronized polymers 36
1.4.3 . Star Polymers 39
1.4.4. Post-Polymerization Modification Strategies for Efficient Bio-Functionalizations 42
2. RESEARCH OVERVIEW 52
3. WATER SOLUBLE THIOL REACTIVE POLYMERIC SUPPORTS AS PROMISING CANDIDATES FOR HUMAN THERAPEUTICS 53
3.1. Introduction 53
3.2. Experimental 56
3.2.1. Materials 56
3.2.2. Instrumentation 57
3.2.3. Copolymerization of Latent Reactive Monomer and PEGMEMA 58
3.2.4. Activation of Copolymers by retro-Diels/Alder Reaction 59
3.2.5. Conjugation of Polymers with Bodipy-SH via Thiol-ene Reaction 60
3.2.6. Conjugation of Polymers with cRGDfC via Thiol-ene Reaction 61

3.2.7. *In vitro* Experiments..……..……63
3.3. Results and Discussion.. 64
3.3.1. Synthesis of Polymers with Naked Maleimide Units..……64
3.3.2. Conjugation of Polymers with Bodipy-SH and cRGDfC..……..……67
3.3.3. *In vitro* Experiments..……..71
3.4. Conclusion.. 76
4. CHEMOTHERAPY DRUG CONJUGATED POLYMERIC SCAFFOLDS: SMART FORMULATIONS AS POLYMER THERAPEUTICS. 77
5. SEQUENCE-CONTROLLED POLYMERIZATION USING DENDRTITIC MACROMONOMERS: PRECISE CHAIN-POSITIONING OF BULKY FUNCTIONAL CLUSTERS.....81
5.1. Introduction.....81
5.2. Experimental..……..84
5.2.1. Materials..……84
5.2.2. Instrumentation..……..85
5.2.3. Synthesis of Dendron-Functionalized Maleimides.……86
5.2.4. General Procedure for the Direct NMP Copolymerization of Styrene with Macromonomers D1-D5..……88
5.2.5. General Procedure for the Time-Controlled Addition of Macromonomers D1-D5 During the NMP of Styrene..…….…….……..89
5.2.6. General Procedure for the Time-Controlled Addition of D6 in Styrene NMP……..……89
5.2.7. Procedure for the Thiol-ene Modification of the Copolymer P(S-*co*-D6) with Thio-glycerol.……..…… 90
5.3. Results and Discussion.. 90
5.3.1. Polyester Dendron Substituted-Maleimides (MIs) Syntheses.……...90
5.3.2. Local Incorporation of Dendron-Substituted MIs in Polystyrene Chains.….92
5.3.3. Thiol-ene Modification of the Copolymer P(S-*co*-D6) with Thio-glycerol...96
5.4. Conclusion. 99
6. ORTHOGONALLY REACTIVE MULTIARM POLYMER- DRUG CONJUGATES……...…….….101
6.1. Introduction.....101
6.2. Experimental.....106

6.2.1. Materials.……..…….……106
6.2.2. Instrumentation.……107
6.2.3. Synthesis of 2-arm Multiarm Star Copolymers via G1 Dendriti..…….……108
6.2.4. Synthesis of 4-arm Multiarm Star Copolymers via G2 Initiator..…….109
6.2.5. Synthesis of 8-arm Multiarm Star Copolymers via G3 Dendriti..…….112
6.2.6. Activation of Copolymer P6 by Retro-Diels/Alder Reaction (P11)..……114
6.2.7. Conjugation of Copolymer P11 with Bodipy-SH&Thiol-ene Reaction..…..114
6.2.8. Conjugation of Copolymers with Gemcitabine via Amidation Reaction..…114
6.2.9. *In vitro* Experiments..……116
6.3. Results and Discussion 116
6.3.1. Synthesis of Multiarm Star Copolymers with Naked Maleimide Units..…..117
6.3.2. Conjugation of Multiarm Copolymer with Bodipy-S..……..123
6.3.3. Conjugation of Multiarm Copolymer with Gemc&Amidation Reaction.…125
6.3.4. *In vitro* Experiments..……129
6.4. Conclusion. 133
7. BIODEGRADABLE MULTIARM POLYMERS FOR REVERSIBLE CONJUGATION: SYNTHESIS & FUNCTIONALIZATION 134
7.1. Introduction.....134
7.2. Experimental. 138
7.2.1. Materials..……..…138
7.2.2. Instrumentation.……139
7.2.3. Synthesis of G2PDS initiator (7).……139
7.2.4. Synthesis of 4-arm Multiarm Star Polymer via G2PDS Initiator (P1).……140
7.2.5. Reversible Conjugation of Multiarm Star Polymer with Glutathione and BodipyC10SH.……..…….. 141
7.3. Results and Discussion. 142
7.3.1. Synthesis of Multiarm Star Polymer with PDS..……..……142
7.3.2. Conjugation of Multiarm Star Copolymer with Glutathione&Bodipy..……148
7.4. Conclusion. 156
8. CONCLUSIONS. 157
9. APPENDIX A: SPECTROSCOPY DATA. 159
10. REFERENCES. 213

LIST OF FIGURES

Figure 1.1. Cell divisions of normal and cancerous cells 2
Figure 1.2. Drug level in the blood with a conventional dosing. 3
Figure 1.3. Design of a regular polymeric drug delivery system. 4
Figure 1.4. Examples of water soluble polymers. 6
Figure 1.5. Examples of (A) enzymatically cleavable and (B) pH sensitive linkers. 7
Figure 1.6. Drug level in the blood with a controlled delivery dosing. 7
Figure 1.7. A representation for EPR effect. 9
Figure 1.8. A representation for passige of (a) linear and (b) branched polymers from pores of kidney. 10
Figure 1.9. Blood pharmacokinetics of bow-tie polymers. 11
Figure 1.10. Interaction of folic acid with its receptor on the cell surface. 12
Figure 1.11. Schematic representation of polymer therapeutic families. 13
Figure 1.12. Structural details of therapeutic polypeptides. 14
Figure 1.13. A representation showing the micellization process of NK012. 16
Figure 1.14. Synthesis of HPMA based polymer - drug conjugate and its *in vitro* evaluation design. 18
Figure 1.15. Chemical structure of a part of the PGA conjugated paclitaxel, showing the tubulin binding site. 19
Figure 1.16. Representations of Doxorubicine conjugated PAMAM-PEG constructs via (a) linker and (b) linker. 20
Figure 1.17. Synthesis scheme for EZN-2208 conjugate. 21
Figure 1.18. Heterotelechelic polymer conjugation with biotin and BSA/glutathione. 24
Figure 1.19. Mechanism of Atom Transfer Radical Polymerization. 26
Figure 1.20. Mechanism of Nitroxide-Mediated Polymerization. 27
Figure 1.21. Classes of polymeric architectures. 28
Figure 1.22. Schematic representation showing subunits of dendrimers. 29
Figure 1.23. General structure of a dendron. 29
Figure 1.24. Synthesis of dendrimers via divergent and convergent method. 31
Figure 1.25. Types of block dendrimers. 31
Figure 1.26. Synthesis of first layer block dendrimer. 32
Figure 1.27. Synthesis of surface block polyester dendrimer. 33

Figure 1.28. Synthesis of the segment blocks dendrimer. 34
Figure 1.29. Schematic representation of monovalent and multivalent interactions. 35
Figure 1.30. Orthogonal functionalization of biodegradable polyester dendrons. 36
Figure 1.31. Three types of hybrids of PEG and [G-4] polyester dendrons obtained from PEGs with one, two, or four reactive ends. 38
Figure 1.32. Dendron–polymer block copolymers via Diels–Alder "click" reaction..... 39
Figure 1.33. Categories of star polymers. 40
Figure 1.34. Methods for the synthesis of multiarm star polymer: (a) 'arm-first' methodology; (b) 'core-first' methodology; (c) conjugation/coupling reactions. 41
Figure 1.35. General strategy for the synthesis of multiarm polymers containing reactive maleimide core. 42
Figure 1.36. General mechanism for DA and rDA reactions. 43
Figure 1.37. General mechanism for thiol-ene reaction. 44
Figure 1.38. A representation for 1,4-Michael addition reaction. 45
Figure 1.39. Possible 'Click' reactions of maleimide functionality. 45
Figure 1.40. Synthesis of maleimide based reactive copolymer..... 46
Figure 1.41. Sequential thiol addition via Michael and photo thiol-ene reactions. 47
Figure 1.42. General mechanism for thiol-exchange reactions. 47
Figure 1.43. A representation for PDS based thiol-exchange reactions. 48
Figure 1.44. Polymeric nanogel formation and BSA conjugation to its surface. 48
Figure 1.45. Orthogonal functionalization of copolymers with amine- and alkyne-containing molecules. 49
Figure 1.46. Dual functionalized polymeric micelles by click coupling chemistry. 50
Figure 1.47. Orthogonal and reversible functionalization or reactive copolymers..... 51
Figure 3.1. Synthetic approach towards maleimide with thiol reactive copolymers. 56
Figure 3.2. Synthesis of furan masked maleimide group containing copolymers. 65
Figure 3.3. Activation of maleimide groups of copolymers via retro Diels - Alder cycloreversion. 66
Figure 3.4. ^{1}H NMR spectra of P1 (a) and P3 (b) in $CDCl_3$. 67
Figure 3.5. Thiol-ene modification of copolymers with BodipyC10SH. 68
Figure 3.6. ^{1}H NMR spectra of P3 (a) and P5 (b) in $CDCl_3$. 69

Figure 3.7. Thiol-ene modification of BodipyC10SH conjugated copolymers with cRGDfC. 70
Figure 3.8. ^{1}H NMR spectra of P5 (a) in $CDCl_3$ and P6 (b) in $CDCl_3$, (c) in D_2O and (d) in DMSO. 71
Figure 3.9. Inhibition of MDA-MB-231 and MCF-10A cells proliferation by P1 (thiol reactive polymer), P5 (bodipy conjugated polymer) and P7 (both bodipy and cRGD conjugated polymer). Cell viability was determined by CCK-8 assay. Results were expressed as mean ± SD (n = 4). 72
Figure 3.10. Inhibition of MDA-MB-231 and MCF-10A cells proliferation by P2 (thiol reactive polymer), P6 (bodipy conjugated polymer) and P8 (both bodipy and cRGD conjugated polymer). Cell viability was determined by CCK-8 assay. Results were expressed as mean ± SD (n = 4). 73
Figure 3.11. Fluorescence images of MDA-MB-231 cells treated with Bodipy conjugated polymers. Cells were incubated at 37 ^{o}C for 24 h and nuclei were stained by DAPI just prior to imaging. (A) shows blue fluorescence of cell nuclei stained by DAPI, (B) shows green fluorescence of internalized Bodipy conjugated polymers, (C) shows the merged images. . 74
Figure 3.12. Fluorescence images of MCF-10A cells treated with Bodipy conjugated polymers. Cells were incubated at 37 ^{o}C for 24 h and nuclei were stained by DAPI just prior to imaging. (A) shows blue fluorescence of cell nuclei stained by DAPI, (B) shows green fluorescence of internalized Bodipy conjugated polymers, (C) shows the merged images. 75
Figure 4.1. Illustration of a typical polymeric construct for targeted drug delivery 78
Figure 4.2. Synthetic approach towards chemotherapy drug conjugated polymers via three different biodegradable linkers 80
Figure 5.1. Schematic representation showing subunits of dendrimers 82
Figure 5.2. Dendron containing macromolecular structures 82
Figure 5.3. Synthetic approach towards precise chain-positioning of bulky functional clusters 84
Figure 5.4. Synthesis of R-G1M-OH. 86
Figure 5.5. Synthesis of R-G2M-OH. 87
Figure 5.6. Synthesis of R-G2M-alkene. 88
Figure 5.7. Synthesized dendritic macromonomers (D1-6). 91

Figure 5.8. ^{1}H NMR (a) and ^{13}C NMR (b) spectra of R-G2M-alkene (D6). 92
Figure 5.9. Strategies studied for the local incorporation of dendron based macromonomers in polystyrene chains 93
Figure 5.10. (a) and (c) Semi-logarithmic plots of monomers conversion versus time for nitroxide-mediated copolymerization of styrene (Sty, 50 equiv.) (black squares) with D2 (R-G2M-X, 1 equiv.) (red dots) added at beginning or after 45 minutes of reaction. Experimental conditions: bulk, 120 °C, Sty/MI/BlocBuilder=50/1/1. (b) and (d) Size exclusion chromatograms of the isolated copolymers 95
Figure 5.11. ^{1}H NMR spectrum of a copolymer P(S-*co*-D2) recorded at RT in $CDCl_3$ 96
Figure 5.12. Semi-logarithmic plot of monomers conversion versus time for nitroxide-mediated copolymerization of styrene (Sty, 50 equiv.) (black squares) with D6 (R-G2M-alkene, 1 equiv.) (red dots) added after 55 minutes of reaction. Experimental conditions: bulk, 120 °C, Sty/MI/BlocBuilder=50/1/1. (b) Size exclusion chromatogram of the isolated copolymer. 97
Figure 5.13. Thiol-ene modification of the copolymer P(S-*co*-D6) with thio-glycerol. .. 98
Figure 5.14. ^{1}H NMR spectra of copolymers P(S-*co*-D6) (a) and P(S-*co*-D6') (b) recorded at RT in $CDCl_3$. 99
Figure 6.1. Synthesis route of multiarm polymers with reactive maleimide core. 103
Figure 6.2. Structures of Gemcitabine (a) and Deoxycytidine (b). 105
Figure 6.3. Illustration of an orthogonally reactive multiarm copolymer conjugated to both chemotherapy drugs and an imaging agent. 106
Figure 6.4. Synthesis of furan protected maleimide based initiators G1M-G3M. 118
Figure 6.5. Synthesis of multiarm copolymers with masked maleimide cores P4-7 using the second generation initiator G2M. 120
Figure 6.6. Activation of maleimide group of P6 via retro D/A reaction (P11). 122
Figure 6.7. ^{1}H NMR spectra of G2M-(DEGMEMA&NHSMA) copolymer P6 (a) and its retro product P11 (b) in $CDCl_3$. 123
Figure 6.8. Thiol - ene modification of multiarm star copolymer P11 with BodipyC10SH (P12). 124
Figure 6.9. ^{1}H NMR spectra of P11 (a) and P12 (b) in $CDCl_3$. 125

Figure 6.10. Conjugation of Gemcitabine to multiarm copolymer P6 via amidation reaction (P13). 126
Figure 6.11. ^{1}H NMR spectra of P6 (a) and P13 (b) in DMSO. 127
Figure 6.12. Conjugation of Gemcitabine to multiarm star copolymer P12 via amidation reaction (P14). 128
Figure 6.13. ^{1}H NMR spectra of P12 (a) and P14 (b) in DMSO. 129
Figure 6.14. Inhibition of MDA-MB-231 cells proliferation by Gemc itself and Gemcitabine conjugated copolymers P13 and P14, and their reactive precursors P6 and P11, respectively. Cell viability was determined by CCK-8 assay. Results were expressed as mean ± SD (n = 3). 130
Figure 6.15. Fluorescence images of MDA-MB-231 cells treated with Bodipy conjugated multiarm star polymers. Cells were incubated at 37 ^{o}C for 24 h and nuclei were stained by DAPI just prior to imaging. (A) shows blue fluorescence of cell nuclei stained by DAPI, (B) shows green fluorescence of internalized Bodipy conjugated polymers, (C) shows the merged images. 132
Figure 7.1. Illustration of a core reactive multiarm star polymer conjugated to an imaging agent and a tripeptide. 138
Figure 7.2. Synthesis of pyridyl disulfide based polyester dendrons G1-3. 143
Figure 7.3. Synthesis of pyridyl disulfide based initiator (7). 144
Figure 7.4. ^{1}H NMR (a) and ^{13}C NMR (b) spectra of pyridyl disulfide based initiator (7) in $CDCl_3$. 145
Figure 7.5. Synthesis of multiarm star polymer with pyridyl disulfide core P1 using the second generation initiator (7). 146
Figure 7.6. ^{1}H NMR spectrum of G2PDS-DEGMEMA polymer P1. 147
Figure 7.7. End group content determination for P1. 148
Figure 7.8. Conjugation of multiarm star polymer P1 with gluthatione via cleavable disulfide linkage (P2). 149
Figure 7.9. ^{1}H NMR spectra of P1 (a) in $CDCl_3$, P2 (b) in $CDCl_3$ and (c) in D_2O. 150
Figure 7.10. UV-Vis absorption spectra for glutathione with Pyridyl disulfide group containing 4-armed star polymer P1. 151
Figure 7.11. Conjugation of multiarm star polymer P1 with BodipyC10SH via cleavable disulfide linkage (P3). 152

Figure 7.12. ^{1}H NMR spectra of P1 (a) and P3 (b) in $CDCl_3$. 153
Figure 7.13. 5 % methanol containing aqueous solutions of free BodipyC10SH (a), polymer conjugated BodipyC10SH (b) and liberated BodipyC10SH from the polymer via DTT treatment (c). 154
Figure 7.14. UV-Vis absorption spectra for the time-dependent conjugation of BodipyC10SH to P1. 155
Figure 7.15. UV-Vis absorption spectra for time-dependent release of BodipyC10SH from P3 upon treatment with DTT. 156
Figure 3A.1. ^{1}H NMR spectrum of the copolymer P1 in $CDCl_3$ 160
Figure 3A.2. ^{1}H NMR spectrum of the copolymer P2 in $CDCl_3$ 161
Figure 3A.3. ^{1}H NMR spectrum of the copolymer P3 in $CDCl_3$ 162
Figure 3A.4. ^{1}H NMR spectrum of the copolymer P4 in $CDCl_3$ 163
Figure 3A.5. ^{1}H NMR spectrum of the copolymer P5 in $CDCl_3$ 164
Figure 3A.6. ^{1}H NMR spectrum of the copolymer P6 in $CDCl_3$ 165
Figure 3A.7. ^{1}H NMR spectrum of the copolymer P7 in $CDCl_3$ 166
Figure 3A.8. ^{1}H NMR spectrum of the copolymer P7 in D_2O 167
Figure 3A.9. ^{1}H NMR spectrum of the copolymer P7 in DMSO 168
Figure 3A.10. ^{1}H NMR spectrum of the copolymer P8 in $CDCl_3$ 169
Figure 3A.11. ^{1}H NMR spectrum of the copolymer P8 in D_2O 170
Figure 3A.12. ^{1}H NMR spectrum of the copolymer P8 in DMSO 171
Figure 3A.13. GPC traces of copolymers P1 and P2 in THF 172
Figure 5A.1. ^{1}H NMR (a) and ^{13}C NMR (b) spectra of R-G1M-OH (D4) 173
Figure 5A.2. FTIR spectrum of R-G1M-OH (D4) 174
Figure 5A.3. ^{1}H NMR (a) and ^{13}C NMR (b) spectra of R-G2M-OH (D5) 175
Figure 5A.4. FTIR spectrum of R-G2M-OH (D5) 176
Figure 5A.5. ^{1}H NMR (a) and ^{13}C NMR (b) spectra of R-G2M-alkene (D6) 177
Figure 5A.6. Maldi-TOF result of R-G2M-alkene (D6) 178
Figure 5A.7. (a) and (c) Semi-logarithmic plots of monomers conversion versus time for nitroxide-mediated copolymerization of styrene (Sty, 50 equiv.) (black squares) with D1 (R-G1M-X, 1 equiv.) (red dots) added at beginning or after 45 minutes of reaction. Experimental conditions: bulk, 120 °C, Sty/MI/BlocBuilder=50/1/1. (b) and (d) Size exclusion chromatograms of the isolated copolymers 179

Figure 5A.8. (a) and (c) Semi-logarithmic plots of monomers conversion versus time for nitroxide-mediated copolymerization of styrene (Sty, 50 equiv.) (black squares) with D2 (R-G2M-X, 1 equiv.) (red dots) added at beginning or after 45 minutes of reaction. Experimental conditions: bulk, 120 °C, Sty/MI/BlocBuilder=50/1/1. (b) and (d) Size exclusion chromatograms of the isolated copolymers 180

Figure 5A.9. (a) and (c) Semi-logarithmic plots of monomers conversion versus time for nitroxide-mediated copolymerization of styrene (Sty, 50 equiv.) (black squares) with D3 (R-G3M-X, 1 equiv.) (red dots) added at beginning or after 45 minutes of reaction. Experimental conditions: bulk, 120 °C, Sty/MI/BlocBuilder=50/1/1. (b) and (d) Size exclusion chromatograms of the isolated copolymers 181

Figure 5A.10. (a) and (c) Semi-logarithmic plots of monomers conversion versus time for nitroxide-mediated copolymerization of styrene (Sty, 50 equiv.) (black squares) with D4 (R-G1M-OH, 1 equiv.) (red dots) added at beginning or after 45 minutes of reaction. Experimental conditions: bulk, 120 °C, Sty/MI/BlocBuilder=50/1/1. (b) and (d) Size exclusion chromatograms of the isolated copolymers 182

Figure 5A.11. (a) and (c) Semi-logarithmic plots of monomers conversion versus time for nitroxide-mediated copolymerization of styrene (Sty, 50 equiv.) (black squares) with D5 (R-G2M-OH, 1 equiv.) (red dots) added at beginning or after 45 minutes of reaction. Experimental conditions: bulk, 120 °C, Sty/MI/BlocBuilder=50/1/1. (b) and (d) Size exclusion chromatograms of the isolated copolymer 183

Figure 5A.12. (a) Semi-logarithmic plot of monomers conversion versus time for nitroxide-mediated copolymerization of styrene (Sty, 50 equiv.) (black squares) with D6 (R-G2M-alkene, 1 equiv.) (red dots) added after 55 minutes of reaction. Experimental conditions: bulk, 120 °C, Sty/MI/BlocBuilder=50/1/1. (b) SEC of the isolated copolymer 184

Figure 5A.13. ^{1}H NMR spectra of copolymers P (S-*co*-D1) (a) and P (S-*co*-D4) (b) recorded at RT in $CDCl_3$ 185

Figure 5A.14. ^{1}H NMR spectra of copolymers P(S-*co*-D2) (a) and P(S-*co*-D5) (b) recorded at RT in $CDCl_3$ 186

Figure 5A.15. ^{1}H NMR spectra of copolymers P(S-*co*-D3) (a) and P(S-*co*-D6) (b) recorded at RT in $CDCl_3$ 187
Figure 5A.16. ^{1}H NMR spectrum of copolymer P(S-*co*-D6') recorded at RT in $CDCl_3$ 188
Figure 6A.1. ^{1}H NMR spectrum of G1M-(PMMA-*co*-NHSMA) (P1) in $CDCl_3$ 189
Figure 6A.2. ^{1}H NMR spectrum of G1M-(DEGMEMA-*co*-NHSMA) (P2) in $CDCl_3$. 190
Figure 6A.3. ^{1}H NMR spectrum of G1M-(PEGMEMA-*co*-NHSMA) (P3) in $CDCl_3$ .. 191
Figure 6A.4. ^{1}H NMR spectrum of G2M-(PMMA-*co*-NHSMA) (P4) in $CDCl_3$ 192
Figure 6A.5. ^{1}H NMR spectrum of G2M-(DEGMEMA-*co*-NHSMA) (P5) in $CDCl_3$. 193
Figure 6A.6. ^{1}H NMR spectrum of G2M-(DEGMEMA-*co*-NHSMA) (P6) in $CDCl_3$. 194
Figure 6A.7. ^{1}H NMR spectrum of G2M-(DEGMEMA-*co*-NHSMA) (P6) in DMSO 195
Figure 6A.8. ^{1}H NMR spectrum of G2M-(PEGMEMA-*co*-NHSMA) (P7) in $CDCl_3$ .. 196
Figure 6A.9. ^{1}H NMR spectrum of G3M-(PMMA-*co*-NHSMA) (P8) in $CDCl_3$ 197
Figure 6A.10. ^{1}H NMR spectrum of G3M-(DEGMEMA-*co*-NHSMA) (P9) in $CDCl_3$. 198
Figure 6A.11. ^{1}H NMR spectrum of G2M-(PEGMEMA-*co*-NHSMA) (P10) in $CDCl_3$ 199
Figure 6A.12. ^{1}H NMR spectrum of activated G2M-(DEGMEMA-*co*-NHSMA) (P11) in $CDCl_3$ 200
Figure 6A.13. ^{1}H NMR spectrum of Bodipy10CS-G2M-(DEGMEMA-*co*-NHSMA) (P12) in $CDCl_3$ 201
Figure 6A.14. ^{1}H NMR spectrum of Bodipy10CS-G2M-(DEGMEMA-*co*-NHSMA) (P12) in DMSO 202
Figure 6A.15. ^{1}H NMR spectrum of Gemc conjugated G2(DEGMEMA-*co*-NHSMA) (P13) in DMSO 203
Figure 6A.16. ^{1}H NMR spectrum of Bodipy10CSH and GEMC conjugated G2M-(DEGMEMA-*co*-NHSMA) (P14) in DMSO 204
Figure 6A.17. GPC traces of copolymers P1-10 in THF 205
Figure 7A.1. ^{1}H NMR spectrum of G2PDS initiator (7) in $CDCl_3$ 206
Figure 7A.2. ^{13}C NMR spectrum of G2PDS initiator (7) in $CDCl_3$ 207
Figure 7A.3. ^{1}H NMR spectrum of G2PDS-DEGMEMA (P1) in $CDCl_3$ 208
Figure 7A.4. ^{1}H NMR spectrum of Glutathione-G2-DEGMEMA (P2) in $CDCl_3$ 209
Figure 7A.5. ^{1}H NMR spectrum of Glutathione-G2-DEGMEMA (P2) in DMSO 210
Figure 7A.6. ^{1}H NMR spectrum of BodipyC10S-G2-DEGMEMA (P3) in $CDCl_3$ 211
Figure 7A.7. GPC trace of polymer P1 in THF 212

LIST OF TABLES

Table 3.1. Polymerization conditions and characterization details of P1-2. 65

Table 5.1. Kinetic data recorded for the nitroxide mediated copolymerization of styrene with dendron-functionalized *N*-substituted maleimides 94

Table 6.1. Polymerization conditions and characterization details of orthogonally reactive multiarm star copolymers 121

Table 6.2. The EC_{50} values for Gemcitabine, its conjugated copolymers P13/P14 and their reactive precursors P6/P12 against human breast cancer cell lines 131

LIST OF ACRONYMS/ABBREVIATIONS

J	Coupling constant
ν	Frequency
ALAL	Alanine-Leucine-Alanine-Leucine
ATCC	American Type Culture Collection
ATRP	Atom Transfer Radical Polymerization
BSA	Bovine Serum Albumine
CCK-8	Cell counting kit-8
$CDCl_3$	Deuterated Chloroform
CH_2Cl_2	Dichloromethane
cRGD	Cyclic Arginylglycylaspartic Acid
cRGDfC	Cyclic Arginine-Gylcine-Aspartic acid-Phenyl alanine-Cystine
D_2O	Deuterated Water
Da	Dalton
DA	Diels-Alder
DAPI	4',6-diamidino-2-phenylindole
DCC	*N*,*N'*-Dicyclohexylcarbodiimide
DEGMEMA	Di(ethylene glycol) monomethyl ether methacrylate
DLS	Dynamic light scattering
DMAP	4-Dimethylaminopyridine
DMSO	Dimethyl Sulfoxide
Dox	Doxorubicine
DTT	Dithiothreitol
EDCI	1-Ethyl-3-(3-dimethylaminopropyl) Carbodiimide
EPR	Enhanced Retention and Permeability
EtOAc	Ethyl Acetate
FDA	Food and Drug Administration
FT-IR	Fourier Transform Infrared
G	Generation
Gemc	Gemcitabine
GFLG	Glycine-Phenylalanine-Leucine-Glycine

GPC	Gel Permeation Chromotography
HPMA	Hydroxypropyl Methacrylate
Lys	Lysozyme
MALDI-TOF	Matrix-assisted laser desorption/ionization-Time of Flight
MeOH	Methanol
MHz	Mega Hertz
MMA	Methylmetacrylate
NHS	N-Hydroxy Succinimide
NMP	Nitroxide-Mediated Polymerization
NMR	Nuclear Magnetic Resonance
PAGE	Polyacrylamide gel electrophoresis
PAMAM	Poly(amidoamine)
PBS	Phosphate Buffer Saline
PEG	Poly(ethylene glycol)
PEGMEMA	Poly(ethylene glycol) monomethyl ether methacrylate
PDS	Pyridyl Disulfide
PGA	Poly(glycolic acid)
PMMA	Poly(methyl methacrylate)
PT	Polymer Therapeutics
R&D	Research&Development
RAFT	Reversible Addition-Fragmentation chain Transfer
RGD	Arginylglycylaspartic Acid
ROMP	Ring Opening Metathesis Polymerisation
ROP	Ring Opening Polymerisation
RT	Room Temperature
SD	Standard Deviation
SDS	Sodium dodecyl sulfate
SEC	Size-Exclusion Chromatography
TEA	Triethylamine
THF	Tetrahydrofuran
TLC	Thin Layer Chromatography
UV	Ultraviolet
Vis	Visible

1. INTRODUCTION

1.1. Cancer and Chemotherapy

Accounting for more than 8.2 million deaths in 2012, cancer figures among the leading causes of death worldwide. The world age-standardised (AS) states that there are almost 250 new cancer cases for every 100,000 men and 165 for every 100,000 women. Annual cancer cases was expected to rise from 14 million in 2012 to 22 within the next two decades, according to reports of WHO (World Health Organization) [1, 2].

Although the term ‘cancer’ represents a large group of diseases that affects any part of the body, especially lung, liver, stomach, colorectal and breast cancers cause the most cancer deaths each year. Abnormal cell growth in an unregulated manner is the result of deteriorations in apoptosis which is a mechanism to control cell death (Figure 1.1). Transformation of a normal cell into a cancerous one and generation of tumor tissue are mostly due to severe mutations caused by physical carcinogens like UV and ionizing radiations, chemical carcinogens like asbestos and arsenic, and biological carcinogens like viruses and bacterias. The majority of genes affected by the mentioned external changes are tumor supressor genes and oncogenes. The former ones are normal genes that slow down cell division, repair DNA mistakes, or tell cells when to die (a process known as apoptosis). When tumor suppressor genes don't work properly, cells can grow out of control, which can lead to cancer. On the other hand oncogenes are the mutated versions of proto-oncogenes which code for proteins that help to regulate cell growth and differentiation. Any distruption in the balance of those two gene types may affect the expression of proteins involved in cell proliferation and signal transduction. Proliferation of cancerous cells may go beyond their usual boundaries and invade nearby tissues, which brings the thread of spreading through the body by the limphatic system. This process is called as methastesis and it stands for the major cause of death from cancer [3].

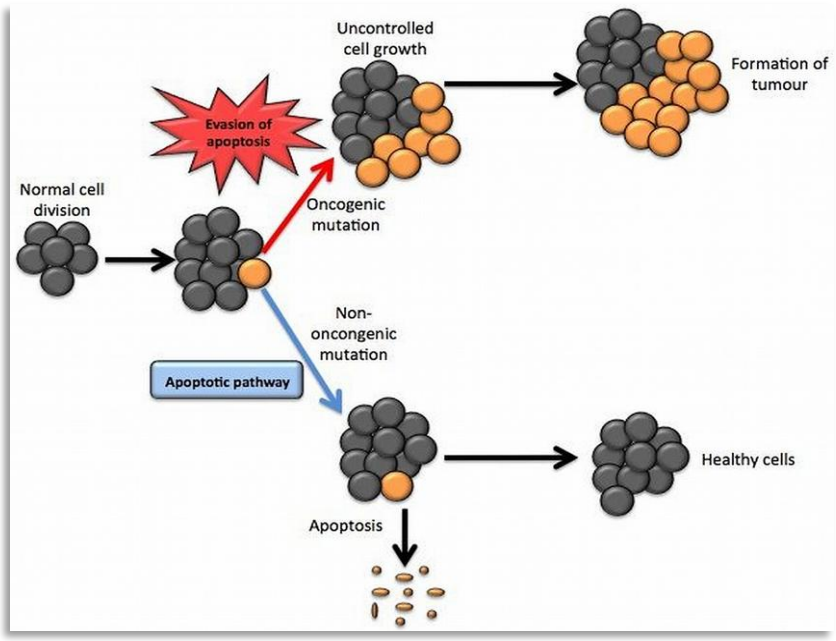

Figure 1. 1. Cell divisions of normal and cancerous cells [3].

Cancer mortality may be reduced if growing tumor tissue is detected early by either awareness of signal and symptoms or screening programs like mammography. For tumor tissues in advance stages and malignant ones, a selection of treatment methods have been developed to cure the cancer. Surgery, radiotherapy and chemotherapy are the major therapy strategies. Together with physiological support, the main aim of the mentioned therapies is to cure the disease and prolong patients' life, also to improve quality of life [4, 5].

Conventional chemotherapy methods require the use of agents like drugs and proteins that have therapeutic effect for the diseases. There is enormous endeavor in developments of newer and more potent chemotherapy agents with today's chemical and biological information accumulation and technological improvements. However most of chemotherapy drugs suffer from severe defects in treatment stages which limit their bioavailability and applicability. Rapid metabolism and clearance of low molecular weight drugs from kidney reduces the circulation time in the blood stream so frequent drug administration to the patient becomes inevitable to keep the blood concentration of drug above minimum effective level needed to obtain a benefit from the therapy [6, 7]. Since chemotherapy drugs are not directed to tumor tissues but programmed to kill all rapidly dividing cells, they are not selective and already damage fast-growing healthy cells like

hair follicles, white blood cells and sperms. Additionally if its concentration in the blood exceeds the maximum effective level, then the toxicity of drug molecules will rise dramatically due to increased penetration (Figure 1.2). That is why most of the time patients give a break to the therapy to allow enough time for the immune system to recover the white blood cell level. Also genomic instability of tumor cells leads to drug-resistant by decreasing activity of chemotherapy drugs. Along with poor water solubility and inability to access to site of infection, bioavailability of drugs decreases and applied therapy do not satisfy the desired curing protocol [8].

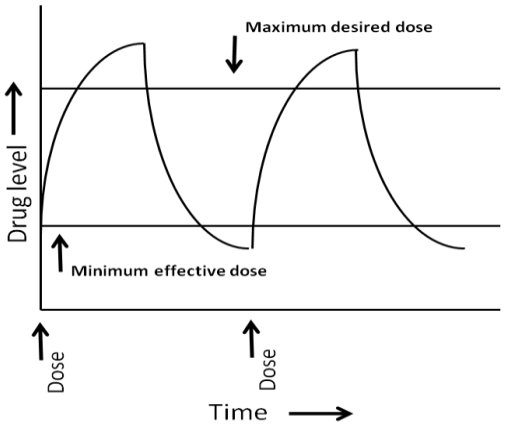

Figure 1. 2. Drug level in the blood with a conventional dosing.

1.2. Polymer Therapeutics

Drawbacks and limitations concerning the administration and efficacy of chemotherapy drugs have opened a new era to scientists to introduce drug carriers for their delivery to the desired pathology zone of the body safely. Designed drug delivery systems obey to the mechanism allowing the release of drug into the directed part of the body within appropriate time interval without losing the therapeutic effect. Polymers have involved into the drug delivery systems as carriers by firstly Ringsdorf in 1975 and become a biological rationale with the progress by Duncan and Kopecek in 1984. Polymers and associated nanomedicine technologies are termed as Polymer Therapeutics (PT) and these macromolecules conjugated to therapeutic agents (5-100 nm) have been evaluated as new

chemical entities with more complex architectures than conventional therapeutic drugs and proteins [9, 10].

Design of a regular polymer therapeutic system comprises of a biocompatible and preferably biodegradable polymeric support to which the bioactive compounds are conjugated either by biodegradable covalent linkers or by supramolecular interactions (Figure 1.3). Both natural and synthetic polymers can serve as suitable platforms for delivery of therapeutics. Increasing advances in organic chemistry enables the design and synthesis of polymer scaffolds with tunable physical properties and molecular weights [11]. Moreover installation of reactive groups to polymer chains with various architectures provides the attachment of solubilizing agents and targeting/imaging agents to improve the benefits of outcoming polymeric carriers [12].

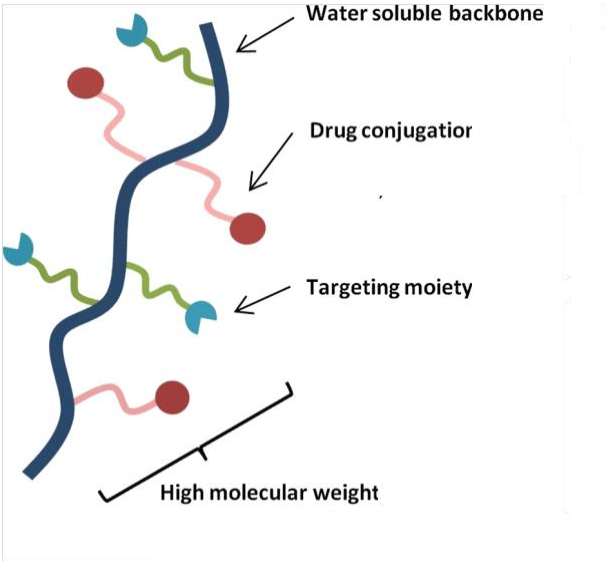

Figure 1. 3. Design of a regular polymeric drug delivery system [12].

Conjugation of therapeutics to water soluble polymers benefits from its hydrophilicity and high molecular weight as they contribute to (i) solubility of mostly hydrophobic drugs in aqueous media, (ii) increased half-life due to reduced renal clearance, (iii) protection against enzymatic degradation due to surrounding polymer chains, (iv) prevention of immunogenicity, (v) overpass drug resistance and (vi) passively tumor accumulation.

Water soluble polymers mostly utilized as carrier systems are poly(vinyl pyrrolidone) (PVP), poly(vinyl alcohol) (PVA), poly(maleic acid), Poly(ethylene glycol) (PEG), Poly(Hydroxypropyl methacrylate) (HPMA) and Poly(glycolic acid) (PGA). Their hydrophilic character increases the solubility of therapeutics in water, enhancing their bioavailabilities (Figure 1.4). HPMA based polymers are biocompatible and water soluble due to hydroxyl groups in the structure and being approved by FDA, its copolymers conjugated to several chemotherapy drugs have been clinically tested since 1984. It allows the copolymerization of various reactive group bearing monomers for post-polymerization functionalizations with drug molecules and there are a lot of examples of HPMA-drug conjugates in the literature as well as in clinical trails where drug molecule was incorporated into the polymer as a macromonomer [13].

Conjugation of proteins and drug molecules to poly(ethylene glycol) is referred as PEGylation and in recent years, this process has emerged as a widely utilized strategy to improve the stability and therapeutic activity of conjugated bioactive compounds. PEG is also water soluble and biocompatible, however its additional superior features like anti-biofouling, anti-immunogenicity and high flexibility contribute to its potential in bioconjugations. It reduces non-specific interactions with proteins and enzymes in the blood stream, leading to a protection towards immune system and enzymatic degradation. Surrounding of delivered therapeutics by PEG chains is like an umbrella effect that raises the stability while circulating in the blood. Especially for the protein conjugation, PEGylation is a very substantial strategy to increase the solubility and hydrodynamic volume in water, providing a reduced renal clearance rate and longer circulation time. There are several PEG-protein and PEG-drug conjugates in the market for the treatment of various cancers and other diseases [14].

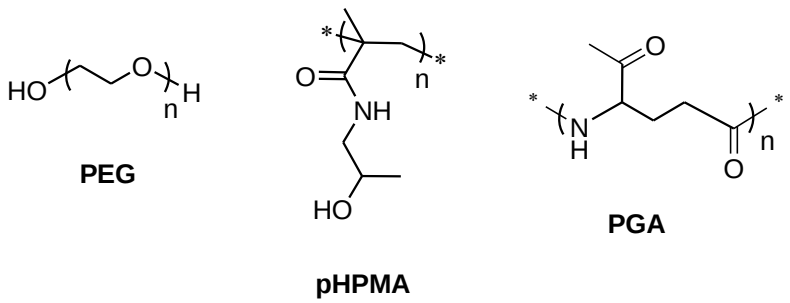

Figure 1. 4. Examples of water soluble polymers.

Advances in controlled polymerization techniques have enabled introduction of a wide spectrum of reactive groups into polymer structures to allow efficient functionalization with the bioactive molecule of interest. Multifunctional polymers serve as macromolecules with increased loading capacity for the conjugation of drugs which provides multivalent interactions of drugs. Upon delivery to tumor tissue, local concentration of drug molecules will be automatically raised, hence the therapeutic index [15].

What is attractive about polymer therapeutics is its ability to reduce toxicity of therapeutics to a remarkable extent since they are mostly inactive when bound to polymer scaffold and get released at the targeted site of the body. This issue is related to both nature of the linker and compactness of the macromolecular delivery system. Mostly utilized covalent linkers do not vary the function of the drug by chemical modification and sensitive towards the physiological changes in tumor tissue. Compared to healthy ones, tumor tissue has a lower pH around 5.5 due to increased amount of lactic acid generated as a result of glycolysis by rapidly proliferating cancerous cells. Moreover, increased transcription of lysozymes and matrix metalloproteases to create enough space in extracellular matrix of tumor tissue is a challenging target for the cleavage of linkers between drugs and polymer chains. Depending on the mentioned reasons, pH sensitive linkers like carboxyl, carbonate and carbamate esters, oximes and imines, and enzymatically cleavable small peptide sequences like GFLG and ALAL are very popular in design of drug delivery systems (Figure 1.5) [16].

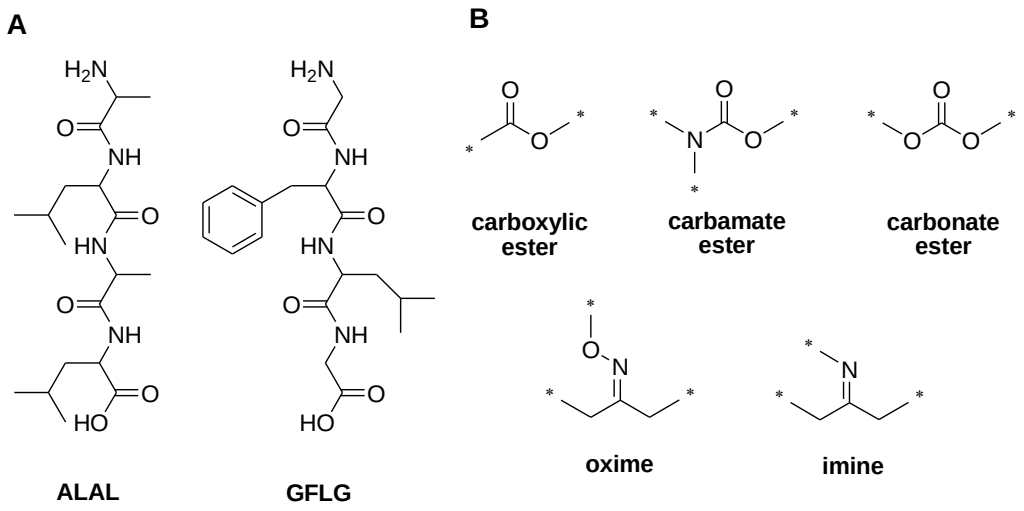

Figure 1. 5. Examples of (A) enzymatically cleavable and (B) pH sensitive linkers.

Due to steric hindrance of polymer chains, release profile of attached therapeutics at the site of infection will be at a constant predetermined rate that maintains the drug level in the therapeutic zone, which contributes to perhaps the major benefit of PT that is the controlled drug release (Figure 1.6). Drug concentration will be at enough level to efficiently continue to therapy but do not exceed the maximum level above which toxicity increases [8].

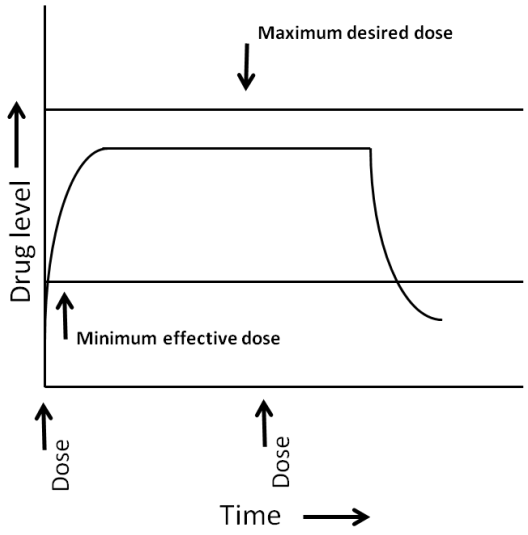

Figure 1. 6. Drug level in the blood with a controlled delivery dosing.

1.2.1. EPR effect

In the context of polymer therapeutics, conjugation of drugs and proteins to macromolecules enables their preferential accumulation in solid tumor by taking the advantage of differentiated morphology of tumor tissue. This phenomenon is called as "Enhanced Retention and Permeability" (EPR) effect (Figure 1.7) [17]. In 1986, Maeda and coworkers were investigated the biodistribution of a polymer-protein conjugate synthesized by styrene maleic anhydride (SMA) and neocarzinostatin (NCS) with a molecular weight of 16000 g mol^{-1}. They found out that concentration of conjugate in tumor tissue is more than 2500 times bigger compared to that in blood so they concluded that the observed accumulation is due to leaky structure of tumor tissue, and named this passive targeting as EPR effect [18].

It is well known that tumor tissue has a micro vascular hyper permeability with extensive angiogenesis and high vascular density together with lack of lymphatic drainage. The reason of this defective structure is the rapid vascularization to provide oxygen and nutrients to fast growing cancer cells. So while circulating in the blood stream, macromolecular drug delivery systems can be easily uptaken by the permeable tumor tissue and accumulate at a specific place. Due to regular and well packed organization of healthy cells, it is difficult for polymer-drug conjugates to snakes into and affect normal tissues adversely [19].

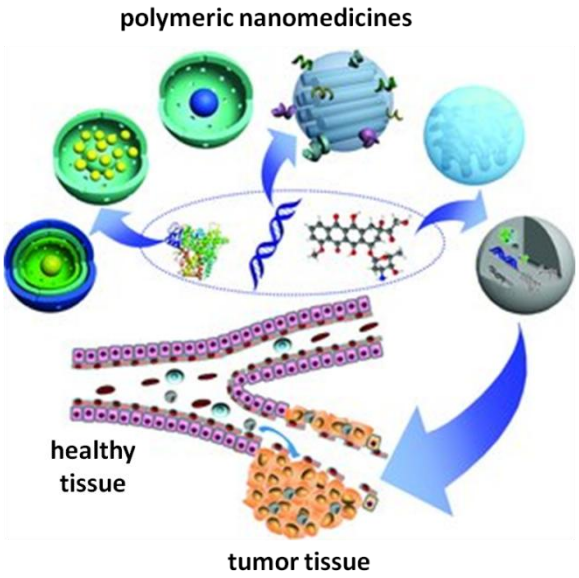

Figure 1. 7. A representation for EPR effect [19].

Accumulation process driven by EPR effect provides an increased local drug concentration at tumor tissue. Since the drug is expected to be inactive when bound to polymeric scaffold and intended to release after arrival to the desired place, systemic toxicity of drug is decreased and its pharmacokinetic efficacy is improved in parallel.

1.2.1.1. Effect of Polymer Architecture on Pharmacokinetics. Design of polymer architectures serving as carriers in drug delivery systems has a crucial effect on the accumulation of polymer-therapeutic agent in the tumor tissue. Effective polymeric drug delivery is a balance between the elimination of the conjugate from the pores of kidney (renal filtration) and their uptake from the blood vascular system into the disrupted tumor tissue (extravasation). Since the diameter of openings within cancerous cells is much greater than the pores of blood vessel structure, differences in molecular weights and hydrodynamic volumes of polymer-drug conjugates does not have a severe effect on extravasation. However, branching degree, flexibility and molecular conformation of polymer-drug conjugates have a direct impact on the rate of renal clearance (Figure 1.8). Compared to linear elongated polymer chains, more branched and compact ones of same molecular weights have less flexibility during the glomerular elimination from kidneys and

as a result they circulate in the blood stream for longer period of time. In this prolonged time interval, polymer-drug conjugates with branched architectures have more chance to accumulate in the tumor tissue [20].

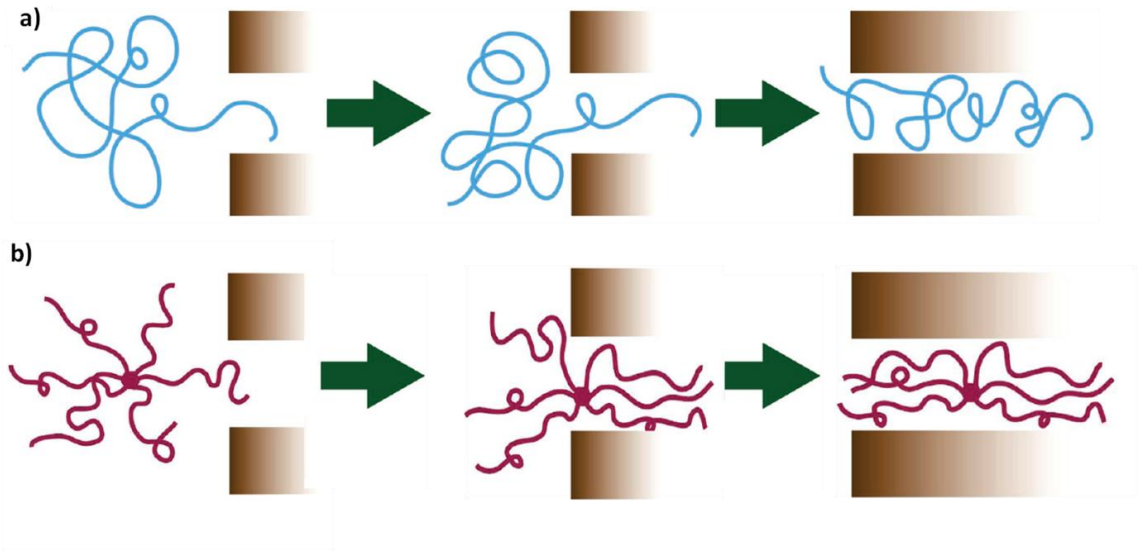

Figure 1. 8. A representation for passige of (a) linear and (b) branched polymers from pores of kidney [20].

Gillies and Fre´chet introduced a new architecture of branched polymers, called as "bow-tie" polymers, by combining polyester dendrimers with linear PEG chains in 2004 and 2005. Surface groups of first to third generation dendrimers were decorated with PEG polymers to generate 2, 4 and 8 armed multiarm polymers. Within the conjugates of almost same molecular weights, rigid and spherical ones were displayed decreased renal clearance and prolonged circulation time. Pharmocokinetic data clearly demonstrates that [G-3] polymer with 8 polymeric arms of 5K each circulate more in the blood and excrete at a lower rate compared to [G-2] polymer with 4 polymeric arms of 10K. Whereas [G-1] polymer with 2 polymeric arms of 20K each was observed to eliminate from the kidney rapidly within 48h. This study also indicated that as the number of polymeric arms increases in the dendron-polymer conjugate, it took more time to excrete from the kidney, which clearly points out the effect of polymer architecture on renal filtration (Figure 1.9) [21-23].

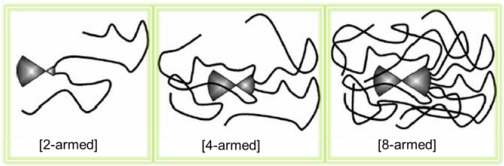

Polymer	MW	t ½
[G1]-10K	22kDa	8
[G1]-20K	44kDa	1.4
[G2]-5K	23kDa	11
[G2]-10K	43kDa	26
[G2]-20K	87kDa	25
[G3]-5K	45kDa	31
[G3]-10K	85kDa	40
[G3]20K	160kDa	50

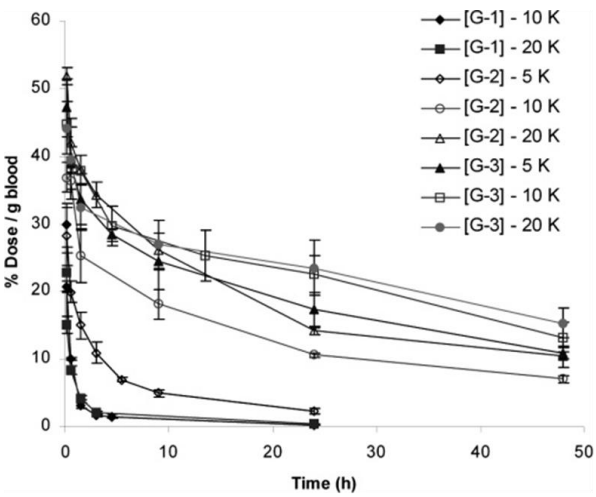

Figure 1. 9. Blood pharmacokinetics of bow-tie polymers [21].

1.2.2. Active Targeting

Delivery of therapeutics to the tumor tissue can also be achieved with the help of a targeting moiety that has higher affinity to specific molecules needed for carcinogenesis and tumor growth. Overexpression of certain receptors for enhanced uptake of nutrients in tumor tissue may lead to design of ligand type molecules which enhances the uptake of the whole drug delivery system by strong interaction of the targeted receptors [24]. As an example, sugar and vitamins are among the most needed metabolites for cancerous cells and they tend to uptake the systems bearing these molecules. For the receptor mediated targeting, folic acid is a very commonly examined natural ligand that is utilized for its specific binding ability to folate receptor with increased number in surface of cancerous cells. Likewise, a tripeptide RGD (Arg-Gly-Asp) sequence selectively goes and binds to α_v-β_3 integrin receptors, found abundantly in tumor tissue. Recent studies suggested new conformations of RGD containing peptides that function as targeting groups. Cyclized and even doubly cyclised RGD sequences bind to α_v-β_3 integrin receptors at least 40-fold more avidly. There are numerous studies in the literature that benefits from these strong and selective binding feature to target the designed drug carrying polymeric systems [25, 26].

Multifunctional polymer based carriers enable the conjugation several different agents to facilitate the delivery of therapeutics better and to improve their effectiveness. Multiple targeting groups attached to one polymer scaffold raise the binding efficiency remarkably due to increased local concentration and high entropic gain.

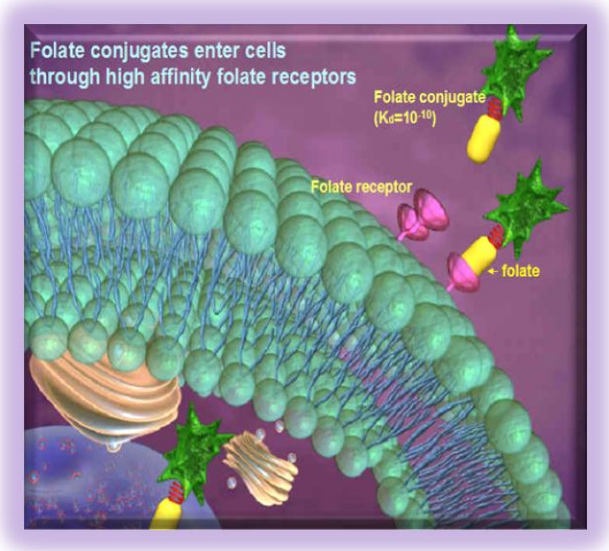

Figure 1. 10. Interaction of folic acid with its receptor on the cell surface [25].

1.2.3. Polymeric Nanomedicines: from Clinical Trials to Market

Design of innovative polymeric architectures and their smart decorations with unique reactive groups allow scientists to develop more comprehended and beneficial polymer-based pharmaceuticals. Conjugation of therapeutic drugs, proteins and DNA fragments to polymeric platforms improves their stability and efficacy. Polymeric delivery vehicles are ranges from polymer-drug and polymer-protein conjugates to polyplexes and micellar macromolecules [27]. Moreover special polymers themselves may display therapeutic activity. In laboratory scale, immense work has being afforded to design and synthesize various polymeric architectures conjugated to therapeutics that display severe side effects. Luckily, some of them are in clinical trials and most potent ones have switched to the market. Polymeric delivery systems providing slow and controlled release are of great interest as promising therapy strategies for several diseases [28].

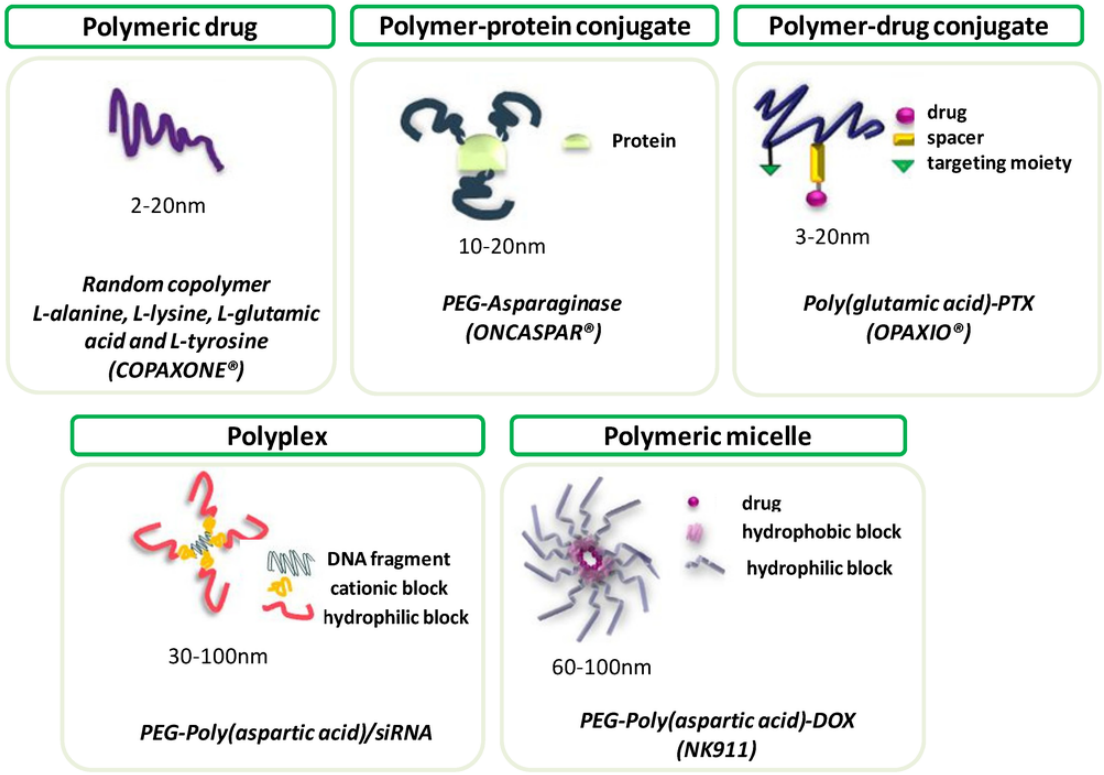

Figure 1. 11. Schematic representation of polymer therapeutic families [28].

1.2.3.1. Polymeric drugs. Polypeptides have been evaluated as promising candidates for drug delivery applications where they directly demostrate therapeutic activity for certain diseases. Their special structural characteristics contribute to special interactions with different biomolecules. Polypeptides refer to linear chains of amino acids or they may be composed by two or more aminoacids to form hybrid block copolymers. Functional groups in their structure with the capibility of forming strong hydrogen bonding enables site-specific interactions to either enhance ot inhibit the function of the target [29, 30]. Moreover, their degradation via hydrolysis yields non-toxic metabolites that can be removed or metabolized inside the body safely. Copolymers of poly(glutamic acid), poly(L-lysine) and poly(aspartate) are the most widely investigated polypeptides that can either act as polymeric drugs or serve as scaffolds for imaging agents and gene delivery [31]. Copaxone is a polymeric drug in the market by Teva and composed of alanin, glutamic acid, tyrosine and lysine aminoacds. It is currently used for the treatment of multiple sclerosis. Another example to polypeptides with therapeutic activity is a lysine

based dendrimer, namely Vivagel (Figure 1.12). Clinica trails are stil going on for this dendrimer in Phase II and III. Also they have special applicatons as non-immunogenic materials in implant coatings [32, 33].

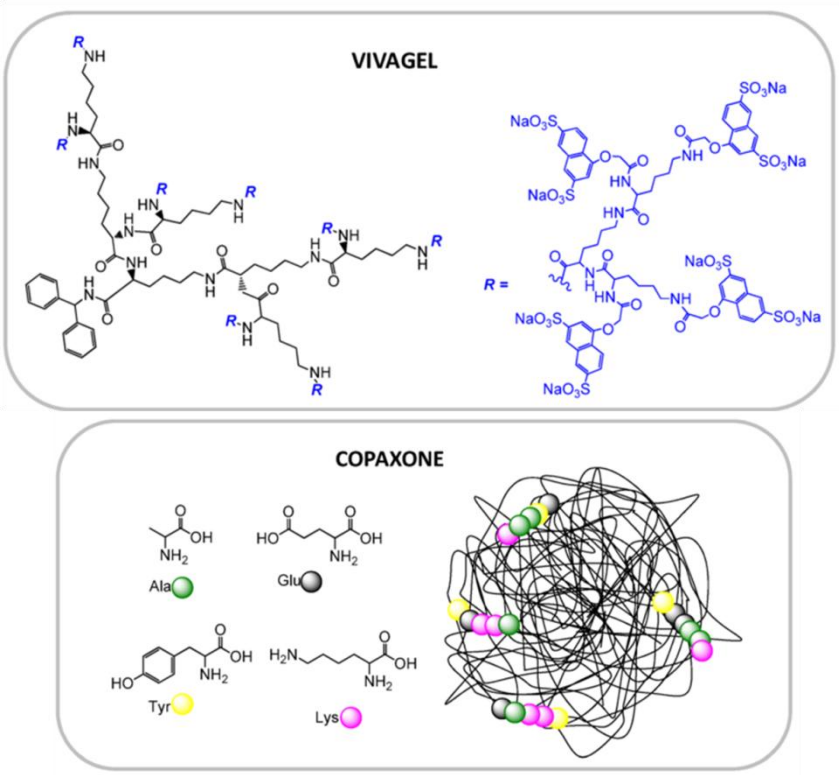

Figure 1. 12. Structural details of therapeutic polypeptides [32-33].

1.2.3.2. Polyplexes. Polyplexes are the complex architectures of polymers with gene fragments. Polymers utilized display inherent ionic character which enables the electrostatic interaction with charged biological compounds. Mostly polypeptides bearing positively charged aminoacids are preferred for the delivery of negatively charged DNA and siRNA. In the literature, a spectrum of charged polymeric scaffolds have been revealed to exhibit efficient complexation in the form of clusters, micelles and nanoparticles [34]. Poly (L-lysine) based copolymers and dendrimers have evaluated as promising candidates for the delivery of negatively charged gene fragments to serve as non-viral vectors [35, 36].

1.2.3.3. Polymeric micelle. Polymeric micelles are the self-assembled architectures of amphiphilic polymers in aqueous solutions and utilized to deliver hydrophobic drug molecules at physiological conditions. They are composed of two main parts: hydrophilic shell and hydrophobic core. Synthetic arrangements over these compartments have provided tunable physical properties depending on the choice of polymer on the surface together with enhanced drug loading capacity for the inner core part via introducing reactive groups for effiecient covalent conjugation. As compact macromolecules, polymeric micelles within size range of 10 – 200 nm have shown to accumulate in tumor tissue based on EPR effect. Their clearance from the body is achieved by the disruption of their supramolecular chemistry by time and biodegradability of polymer chains, if any [37, 38].

Kataoka and his group have mainly focused on the synthesis of polymeric micelles since 1990s and they have demonstrated their potential both for chemotherapy drug and genetic material delvery. Recently they published two studies in one of which they outline a strategy to design drug conjugated polymeric micelle out of poly(ethylene glycol)-poly(glutamic acid) (PEG-co-PGlu) copolymers and oxaliplatin as drug molecule was complexed with the carboxylate groups at the core. By releasing 30% of the loaded drug, these constructs are now in Phase I clinical trials [39]. The other study is about the delivery of siRNA by polyion complex micelles stabilized by cholesterol. PEG-PLL based cationic polymers were complexed with negatively charged siRNA fragments and the delivery was enhanced with the introduction of a targeting group, cRGD. It was reported that systemically administered micelles showed significant gene silencing activity in tumor [40].

Micellar structures that have switched to preclinical and clinical strudies in Japan are mostly the copolymers of PEG and polypeptides. A remarkable example would be an amphiphilic block copolymer, PEG–PGlu(SN-38), clinically tested in phase II. Sn-38 is an analog of campthotesin that targets DNA Topoisomerize II (Figure 1.13). It was incorporated into the structure by condensation reaction to the side chains of PGlu and then

micellization process took place. Obtained as a freeze-dried formulation, NK012 has being administered to the patients with colorectal cancer [41].

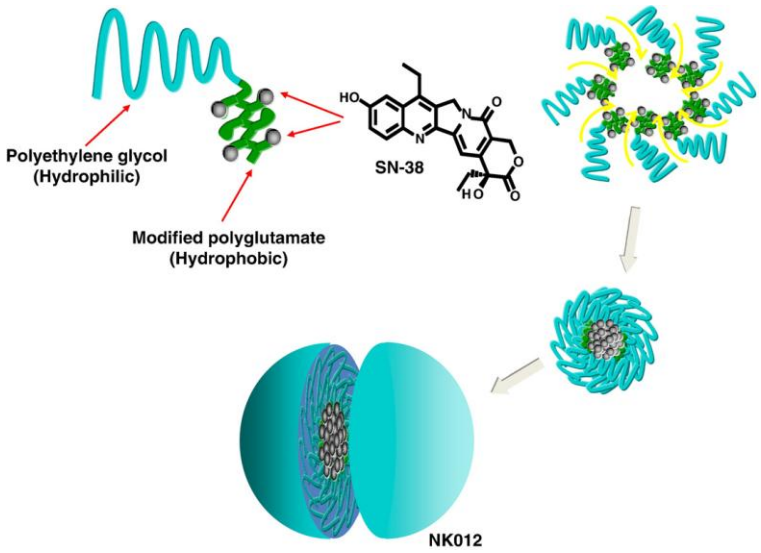

Figure 1. 13. A representation showing the micellization process of NK012 [41].

1.2.3.4. Polymer-drug conjugate. Today's nanomedicine understanding strongly supports the significance of polymer therapeutics since benefits of polymer conjugation for therapeutic acitivities of chemotherapeutic drugs have remarkably observed. A number of research groups along with several industrial companies have started to work on designing different and advantageous polymer architectures and attach chemotherapy agents currently in the market. Instead of modeling and synthesizing new active chemicals and test them for their effectiveness in both *in vitro* and *in vivo* studies, most of the scientists conjugate them to polymeric scaffolds to improve the pharmacokinetic efficacy of the existing ones that passed through all clinical studies. Based on EPR effect, drug conjugated polymeric macromolecules can be easily directed to cancerous cells by passive targeting that originates from the leaky morphology of tumor tissue. To enhance the targeting ability of the designed system, several targeting groups can be covalently introduced to the drug delivery system. There are more than fifteen constructs as polymer-drug conjugates in the clinical phases and some of them is in the market already for the treatment of various cancer types and other diseases [42].

Most widely used water soluble polymers are PEG, pHPMA and PLA, first two of which has approved by FDA. There are a lot of literature examples about their conjugation to chemotherapy agents. Copolymers of HPMA were firstly introduced as water soluble and biocompatible polymeric scaffolds by Kopecek and coworkers in the mid 1970s. First clinically tried HPMA based copolymer, called as PK1, was Doxorubicine conjugated HPMA polymer in 1998, where drug molecules were covalenly attached to polymer backbone via a tetrapeptide linker, GFLG. This construct was developed by attaching galactosamine as a targeting ligand for hepatocyte asialoglycoprotein receptor in the liver (PK2). This lysosomally cleavable linker has been utilized as a mean for drug attachment to polymer backbone in several literature studies, some of which has passed to clinics. HPMA based polymers were conjugated to severalcheotherapy drugs to improve their effectiveness such as gemcitabine, campthotesin, taxanes and geldanamycine. As an example, DACH platinium and carboplatinate analogues conjugated HPMA polymers with around 25K g/mol molecular weight are now in Phase II clinical trials [43-45].

Ghandehari and coworkers have also immensely working on HPMA based polymer-drug conjugates and one of their recent studies is about the conjugation of aminohexylgeldanamycin (AH-GDM) to side chains of HPMA copolymer via above-mentioned GFLG linker. AH-GDM is an anti-angiogenic drug which functions by interruptimg the new vessel formation (Figure 1.14). Due to EPR effect, drug molecules were passively directed to tumor tissue and compared to equimolar doses of drug, polymer conjugated ones demonstrated higher antitumor activity in nude mice bearing DU-145 human prostate cancer xenografts [46].

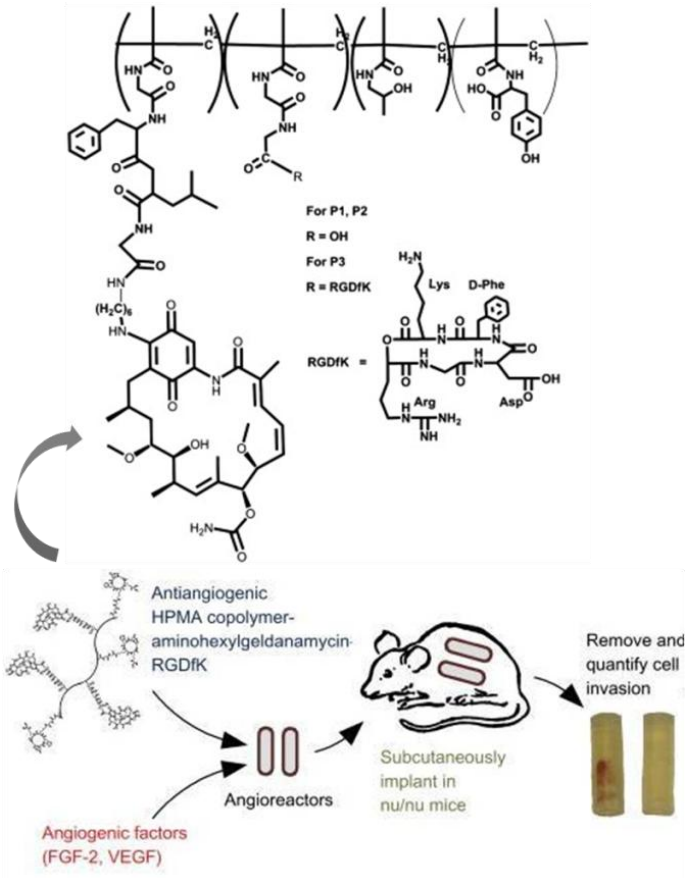

Figure 1. 14. Synthesis of HPMA based polymer-drug conjugate and its in vitro evaluation design [46].

Known with the name ‘Opaxio’ (or previously Xyotax), paclitaxel poliglumex (PPX) is a polymer-drug conjugate where paclitaxel is linked to poly-L-glutamic acid of 40K g/mol with the aim of benefiting from EPR effect (Figure 1.15). Release of drug molecules from the polymer scaffold depends on the lysosomal degradation by cathepsin B. The conjugate has now being tested in Phas III clinical trials over advanced lung cancer and ovarian cancer. For the former case, it was detected that conjugate activity may be modulated by estrogens, mostly efficient in womens. Fot the other cancer type, the results were pointed out 98% response when used in combination with carboplatin [47, 48].

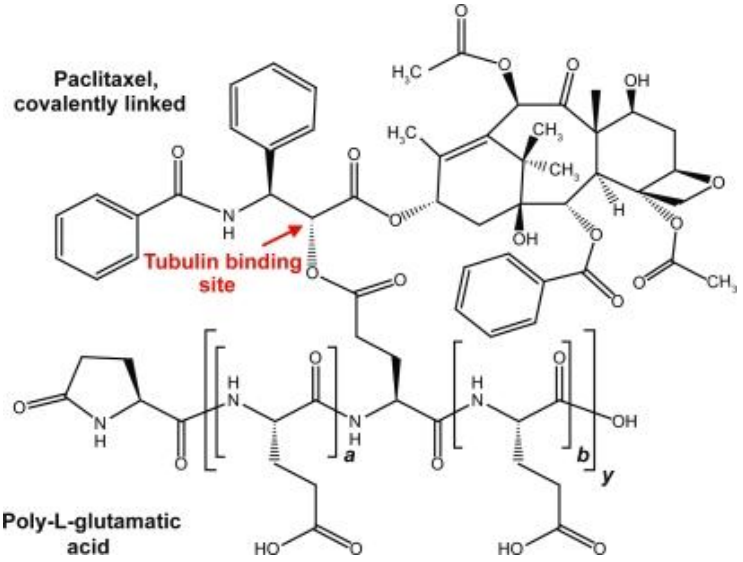

Figure 1. 15. Chemical structure of a part of the PGA conjugated paclitaxel, showing the tubulin binding site [48].

Concerning the ethylene glycol based polymers; PEGylation is now an attractive option for drug conjugation studies as well as protein therapies. Due to its superior features like water solubility, anti-biofouling and anti-immunogenicity, there is an increasing trend in the field of polymer therapeutics to inset PEG chains into the system and improve the stability of the delivered agent in physiological conditions. As in the case of other polymeric constructs, it provides passive targeting by EPR effect and also PEG methacrylate based polymers have developed as both biodegradable and biocompatible scaffolds. In the case of linear chains, mostly NHS activated end groups were utilized for bioconjugation, however the mentioned PEG methacrylate monomer allows the incorporation of several different reactive groups during the copolymerization process, like maleimide, azide, alkene, alkyne, amine groups [49].

Jiang and coworkers from China described the synthesis of efficient carriers for selective targeting of anti-cancer drug, Doxorubicin in 2010. 4th generation PAMAM dendrimer surface was partly functionalized by linear NHS-PEG chains of around 5000 g/mol via amidation reaction (Figure 1.16). Drug molecule was inserted to the system either via acid sensitive cis-aconityl linkage or acid sensitive succinic linkage and obtained drug conjugates are named as PCD or PPSD, respectively. It was observed that drug

release is triggered in acidic environment and increased as PEGylation degree increases. PPCD conjugates were demonstrated increased drug release upon entering the lysozyme and nuclei, however PPSD conjugates showed negligible drug release at any tested pH condition and were less cytotoxic. PEGylated at the same degree, PPSD conjugates accumulated more in tumor tissue compared to PPCD, however the latter one displayed more tumor activity due to higher concentration of the released drug. Together with the fact that PEGylation degree has a positive effect on antitumor activity for PPCD, this conjugate was evaluated as a promising candidate for solid tumor therapy [50].

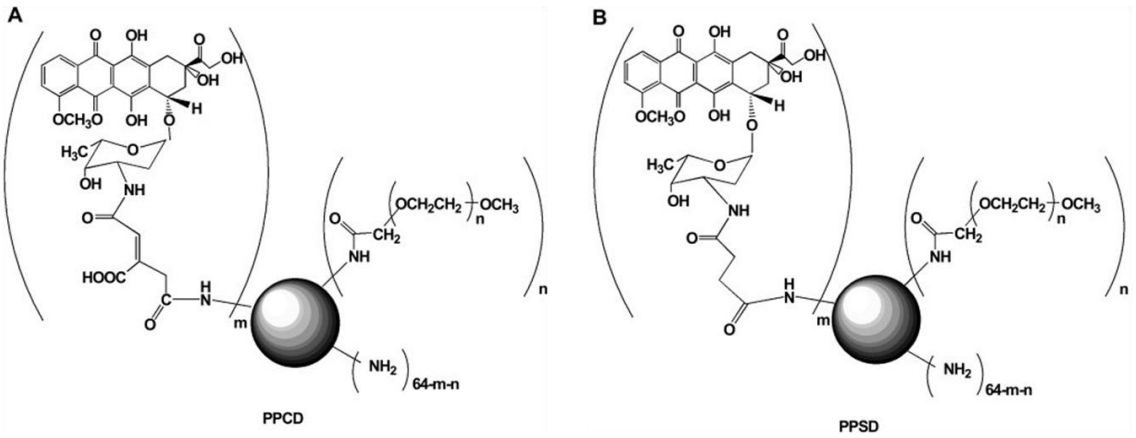

Figure 1. 16. Representations of Doxorubicine conjugated PAMAM-PEG constructs via (a) linker and (b) linker [50].

As an example to the PEGylated drugs in clinics is EZN-2208, that is composed by a 4 armed multiarm PEG polymer conjugated to SN38 which is an active metabolite of camptothecin-11 with poor water solubility (Figure 1.17). This drug was conjugated to the PEG polymer via a glycine linker. In vitro studies demonstrated that the conjugate was 10- to 245-fold more potent than CPT-11 in a panel of human tumor cell lines. Likewise, EZN-2208 administered to xenograft models of MX-1 breast, MiaPaCa-2 pancreatic, or HT-29 colon carcinoma was determined to be more efficacious compared to drug itself. EZN-2208 had prolonged circulation in the blood compared with CPT-11, resulting in high tumor exposure. Currently investigated in Phase II clinical trials, EZN-2208 is among the promising candidates for the treatment of metastatic breast cancer [51]. Preclinical data

suggest that EZN-2208 may be a promising anticancer agent in a wide variety of clinical settings, including tumors refractory to CPT-11 treatment.

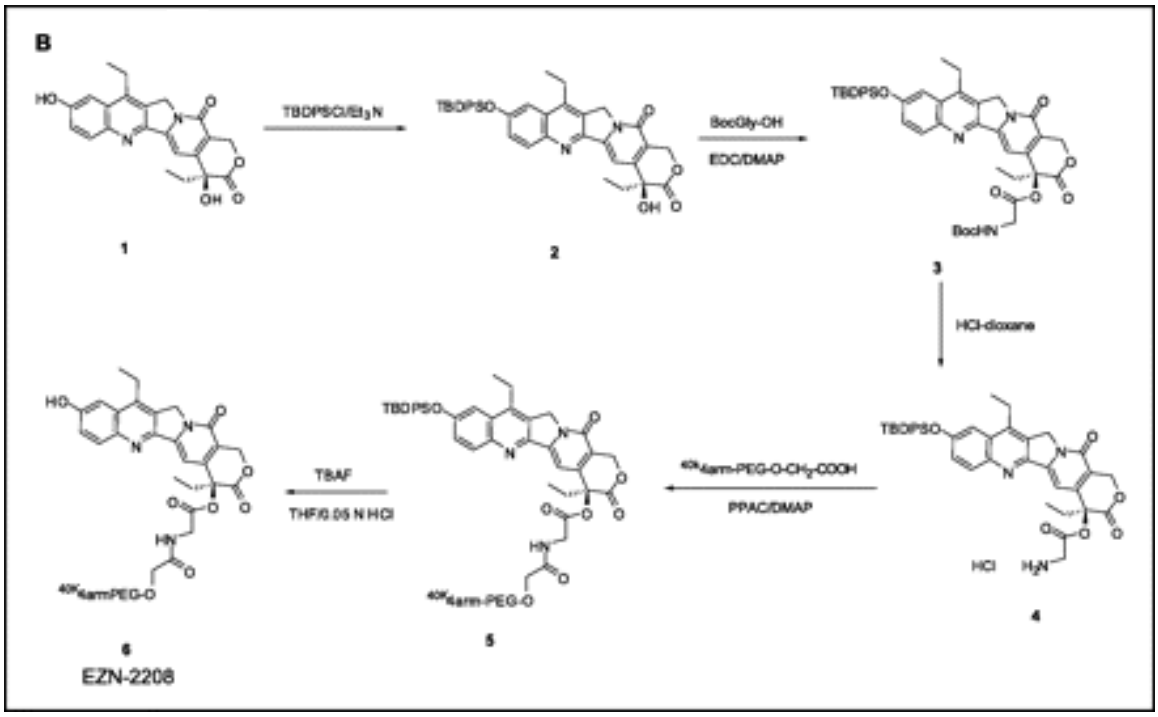

Figure 1. 17. Synthesis scheme for EZN-2208 conjugate [51].

In order to obtain more efficient and sustained therapy for the treatments of complex and advanced diseases, polymer based combinatorial chemistry may be a wise solution which involves the administration of polymer-drug conjugate together with a free drug or more than one drug either conjugated to same polymeric construct or as two separate polymer-drug conjugates. The main aim here is to benefit from the therapeutic effects of both drugs but they should display synergistic interactions with each other, not antagonistic. Design of these polymeric constructs nessesitates the overview of same fundamental issues such as selection of drugs, their optimum payload, best drug ratio and the linkers binding drug molecules to the system, enabling desired rate of release for each.

For example, a combination of PGA-paclitaxel and carboplatin has been investigated for the ovarian cancer therapy and initial results showed a positive response in 80 out of 82 patients. This interesting study was the sequential administration of polymer-drug and polymer-protein conjugates where firstly HPMA copolymer-Gly-Phe-Leu-Gly-doxorubicin

was injected to the body and after its accumulation in tumor site by the EPR effect, HPMA copolymer-chatepsin B was administered to stimulate the release of conjugated drug [52]. In 2009, Ulbrich and coworkers designed a multi-drug targeting polymeric scaffold that beared two chemotherapy drugs together. Copolymerization of HPMA, MA-GFLG-gemcitabine, MA-GFLG-doxorubicin and MA-Tyr-NH_2 monomers yielded a multiple drug carrying conjugate with a radiolabelling agent (6.4 wt% of gemcitabine, 5.7 wt% of doxorubicin and 1.0 mol% of tyrosinamide). Termed as P-Gem-Dox, this conjugate was evaluated *in vitro* to effectively kill cancer cells and *in vivo* studies indicated that this conjugate could circulate in the blood stream for longer period of time, accumulate in the tumor selectively and inhibit tumor growth more than both drugs when administered alone [53].

1.2.3.5. Polymer-protein conjugates. Conjugation of peptide, protein and antibody based drugs to polymeric scaffolds provides a remarkable increase in their therapeutic effect. Recent year have witnessed great interest over the attachment of water soluble polymer to mentioned polypeptide drugs that suffer from short plasma half-life, poor solubility and immunogenicity [54]. Surrounded by polymer chains, proteins are protected against proteolysis that is degradation process by enzymes in the blood stream. Since proteins bound to hydrophilic polymers possess larger hydrodynamic volume, their renal clearance will slow down and they selectively accumulate in the tumor tissue due to EPR effect. Mostly HPMA and PEG based polymers are preferred for the design of polymer-protein conjugates. In 2009, Davis and his coworkers demonstrated the synthesis of HPMA based polymers with reactive groups to modify protein and enzyme surfaces. In one of them they activated the end of HPMA chain with thiazolidine 2-thione to facilitate the attachment to BSA surface, where as in the other study they utilized pyridyl disulfide group inserted HPMA polymer to conjugate to lysozyme and control its stability [55, 56]. However especially clinical studies support the benefit of PEGylation due to anti-biofouling and anti-immunogenicity properties. Surrounded by PEG polymer, mostly transgenic and synthetically obtained therapeutic proteins are not affected by non-specific protein interactions and do not cause immunogenic response [57].

Traditional method for the synthesis of polymer-protein conjugates is to attach the polymer chains from their activated end groups. PEG chains are generally conjugated to proteins via reactive end groups. In 2004, Maynard published a study where PEG methacrylate based linear polymers functionalized with pyridyl disulfide units were conjugated to BSA via disulfide exchange reactions[58]. Likewise in 2006, Filpula and coworkers demonstrated efficient conjugation of NHS terminated linear or branched PEG chains to protein human interferon beta-1b (IFN-â-1b) that increased the half-life from hours to days compared to native protein [59]. This coupling is strongly affected by the polymer chain length due to steric hindrance problems, which lead to development of a new strategy depending on the polymerization from the surface of proteins [60]. Here, a small initiator molecule that has also the ability to interact with the proteins is synthesized and conjugated to the protein, and then polymerization takes place. There are numerous literature examples outlining interesting strategies that optimize the polymerization conditions so that protein conformation, hence its activity will not be affected extensively. ATRP and click chemistries have been mostly employed as the polymerization methods to obtain controlled molecular weights and low polydispersity index values [61]. However residual Cu catalyst may cause toxicity, if left any. So the trend switched to the copper free polymerization techniques like RAFT polymerization which takes place at mild conditions and in a more controlled way. A remarkable study was performed by Davis and coworkers in 2008 that they synthesized series of N-isopropyl acrylamide (NIPAAM) and poly(ethylene oxide)-acrylate (PEG-A) bearing pyridy disulfide unit in both water and acetonitrile and proved the intactness of this reactive group during the polymerization [62, 63].

Conjugation of either the polymer chain or the initiator for polymerization was achieved through with amine or thiol moieties in the protein structure. Due to large abundance of amine residues, conjugation mediated by aminolysis may not be site-specific. However thiol groups that do not participate into the disulfide bond formation can be utilized for the conjugation of proteins with maleimide, bisulfone and pyridyl disulfide functionalities and known positions of cystein amino acids contribute to site-specific conjugation [64, 65]. Among the linkages between polymer part and proteins, pyridyl

disulfide bond is a very attractive one since its reversible nature and ability to undergo disulfide exchange reaction in the presence of other thiol containing molecules allow controlled release of the protein.

In 2008, Stenzel and coworkers illustrated an example study for the polymer-protein conjugation concept. They employed for the synthesis of well-defined heterotelechelic polymers of PEG, PS or poly(NIPAAm) that were designed to possess an azide group on one end and a bioreactive group, pyridyl disulfide, on the other end. R-azide, *ω*-dithiopyridine polymers were successfully obtained in one step via the reversible addition-fragmentation chain transfer (RAFT) polymerization. Azide functionality was utilized for the conjugation of alkyne modified biotin via click chemistry to benefit from its strong binding capability to avidin protein. On the other hand, thiol reactive end of this conjugate was attached to BSA that has one available thiol unit with known position. This disulfide exchange reaction resulted in site-specific conjugation of polymer chains over BSA protein [66, 67].

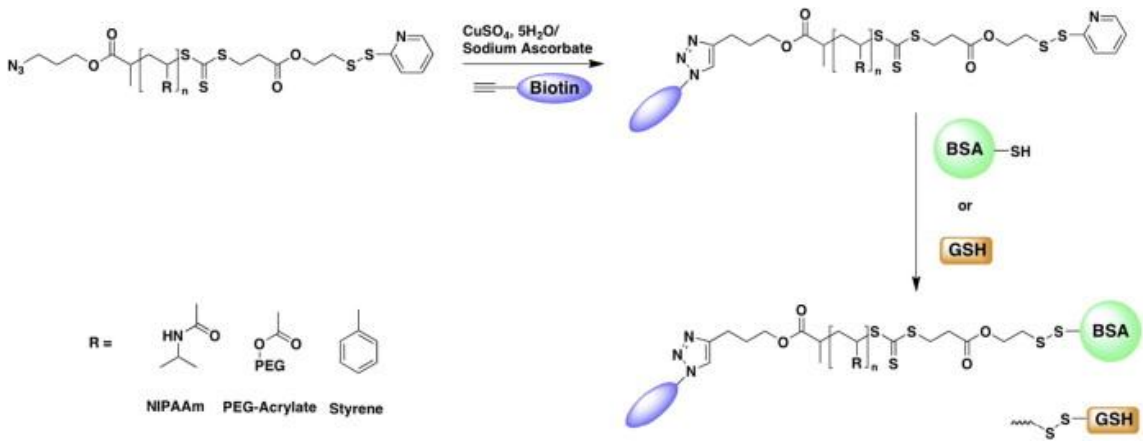

Figure 1. 18. Heterotelechelic polymer conjugation with biotin and BSA/glutathione [66].

Protein PEGylation has improved the therapeutic activity of several proteins used as drugs for certain diseases and some of them passed the clinical studies successfully and now in the market. The first conjugate that entered to the market was PEG-adenosine deaminase in 1990. Some of the following polymer-protein conjugates are Pegasys (PEG-

interferon α-2a), PEG-Intron (PEG-interferon α-2b), Neulasta (PEG-granulocyte colony-stimulating factor), Oncaspar (PEG-asparaginase) and Mircera (PEG-EPO (polyethylene glycol-epoetin beta). For example, Pegasys and PEG-Intron are conjugates of PEG polymers with proteins of cytokine family and these conjugates are used for the treatment of Hepatitis C. Moreover, Oncaspar is used as a treatment for acute lymphoblastic leukaemia, with the advantage of reduced hypersensitivity reactions and Neulasta is the PEGylated G-CFS which is a recombinant methionyl human granulocyte colony-stimulating factor and it is used to prevent chemnotherapy induced neutropaenia [68-70].

1.3. Preparation of Reactive Polymeric Platforms

1.3.1. Polymerization Techniques

Today, scientists have many opportunities to design macromolecules with highly uniform and specific characteristics via several different polymerization techniques that enable the synthesis of well-defined architectures with controlled molecular weights together with insertion of reactive groups of interests along the polymer chains. Out of this wide range of strategies, controlled chain growth depended polymerization techniques like ATRP, RAFT, NMP, ROMP and ROP outstand as useful handles to arrange the desired molecular weights with low polydispersity values. The polymerization techniques used in this thesis are briefly mentioned below.

1.3.1.1. Atom transfer radical polymerization (ATRP). ATRP is among the most widely used methods of controlled radical polymerization (CRP). Discovered by by Mitsuo Sawamoto and Krzysztof Matyjaszewski in 1995, this technique enables high degree of control over the architecture and molecular weight of the resultant polymer chains to yield a wide range of linear and branched polymers with highly specific, tailored functionalities to be used in many applications from coatings and adhesives to environmental, biotechnological and medical areas [71-73].

The components of ATRP are the monomer, initiator with a transferable halogen atom, and a catalyst which is composed of a transition metal species and ligand. Mechanism of ATRP is based on the halogen atom transfer between radical polymer and metal ion, contributing to the controlled chain growth. Polymerization reaction is initiated by halide unit of initiator and the catalyst provides an equilibrium between the active (propagating) and inactive (dormant) form of the polymer. This equilibrium mechanism reduces the concentration of propagating polymer chains and therefore minimizes termination steps (Figure 1.19) [74].

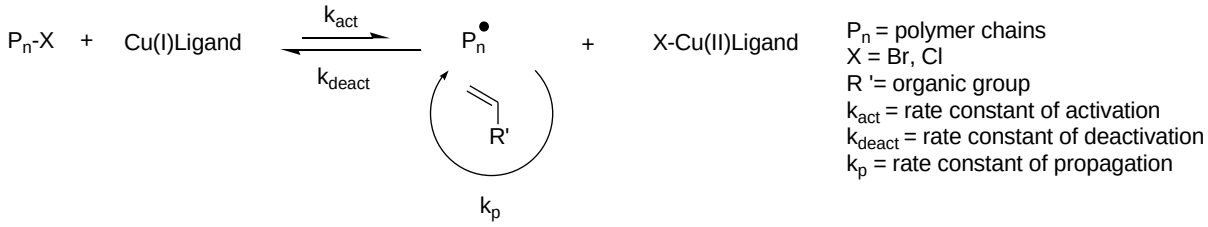

Figure 1. 19. Mechanism of Atom Transfer Radical Polymerization.

1.3.1.2. Nitroxide-Mediated Polymerization. NMP is a method of controlled radical polymerization which uses an alkoxyamine initiator for the generation of polymers with well-defined stereochemistry and low polydispersity index values. It is mostly applied for the polymerization of styrenes and its derivatives, acrylates, acrylamides, acrylontrile (and dienes) with tailored functionalities to serve as platforms in nanotechnology [75, 76].

Nitroxide radicals obtained at high temperatures via homolytic bond cleavage play the role of stable free radicals as reversible terminating agents to polymerize the growing number of monomers in a controlled manner. Control in NMP is achieved with dynamic equilibration between dormant alkoxyamines and actively propagating radicals. Due to reversible capping and de-capping of the growing polymer chains, it is assumed that at any given time, almost all chains are capped by a mediating nitroxide and grow at similar rates, which provide a precise control over both molecular weight and architecture of the resultant polymer (Figure 1.20) [77, 78].

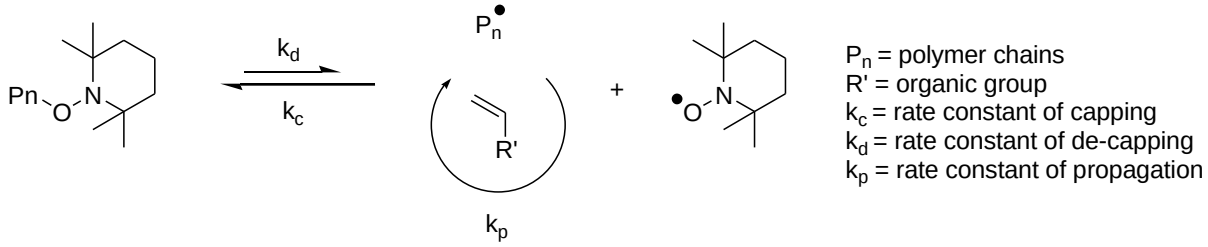

Figure 1. 20. Mechanism of Nitroxide-Mediated Polymerization.

An interesting class of polymers prepared by NMP obeys to sequence controlled polymerization where mostly styrene and its derivatives copolymerize with active maleimide group bearing reactive monomers in an alternative fashion. Initiated by a commonly used initiator TEMPO, this polymerization process results in synthetic sequence-regulated architectures with successful insertion of functional groups with almost known positions along the backbone. So obtained polymeric platforms are of high interest due to their similarity to natural sequence defined biopolymers like DNA and proteins [79–81].

1.4. Polymeric Architectures for Delivery of Therapeutics

Studies about the design of polymeric materials have been fueled by the established impact of polymer therapeutics in biomedical fields. Innovative architectures with tailored functionalities have been synthesized to be utilized as carrier systems for therapeutics like drugs and peptides. A variety of polymerization techniques allows scientists to obtained polymeric materials with appropriate molecular weights, flexibility and physical properties. Commonly used polymeric architectures consist of linear polymers, graft and star polymers, dendrimers and dendronized polymers (Figure 1.21) [27].

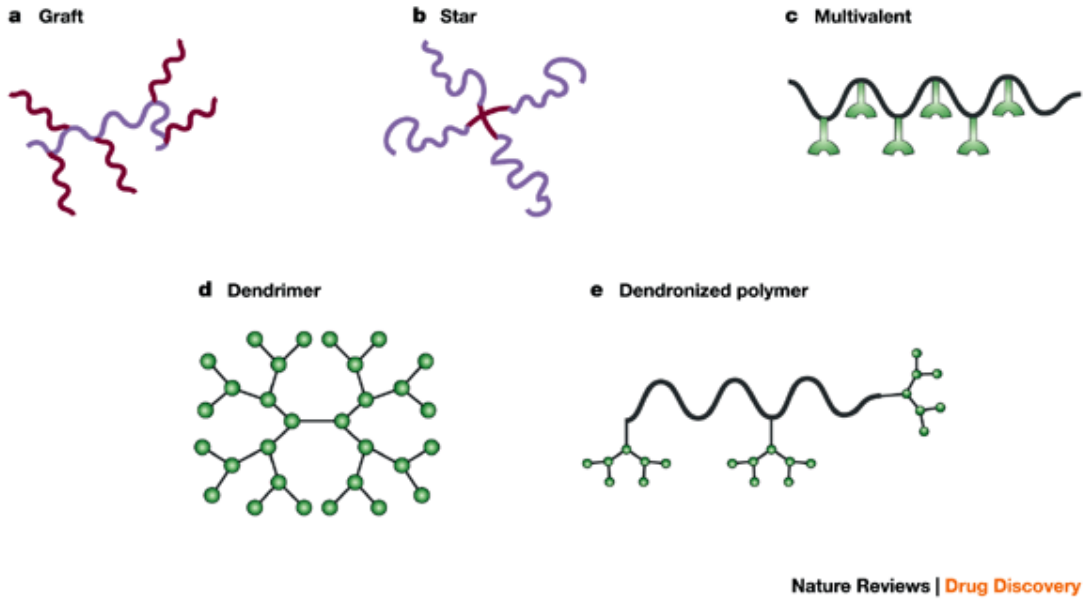

Figure 1. 21. Classes of polymeric architectures [27].

1.4.1. Dendrimers

Dendrimers, meaning treelike in Greek due to graphical representation of the dendrimer structure resembles the branches of a tree, are highly ordered, regularly branched globular macromolecules with well-defined monodisperse architectures synthesized by stepwise organic reactions [82]. Their structure involves three main architectural regions: a core, synthesized with stepwise organic reactions resulting in the structure mainly composed of three different units: a core, layers of branched repeat units emanating from the core and surface groups located at the periphery. Symmetrically placed branching units around the core contribute to its uniform 3-D structure. Degree of branching at the core determines the multiplicity of dendrimers. The number of branching units from the core to the periphery refers to the generation of the dendrimers (Figure 1.22) [83].

Each component of a dendrimer can be utilized as a powerful tool to attain molecules into dendrimer structure. While the core can be evaluated as a linker, branching units may contribute to hydrophilicity/hydrophobicity of the system to carry the appropriate drug or

other agents via non-covalent interactions. Internal cavities between the branching units also play significant role in the encapsulation of agents to be delivered for specific purposes. Last but not least, functional groups located at the periphery of dendrimers enables covalent attachment of (bio) molecule of interest in an organized manner providing better conjugation stability [84, 85].

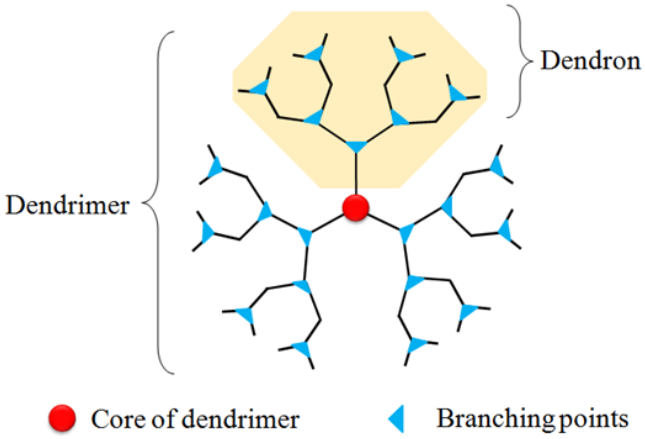

Figure 1. 22. Schematic representation showing subunits of dendrimers.

Dendron refers to a part of the dendrimer, and it starts from the core and ends at the periphery. A dendron does not possess a core but instead contains a focal point which may also have chemically reactive groups. The focal point is the fragment from which repeating units that built the dendron originates (Figure 1.23).

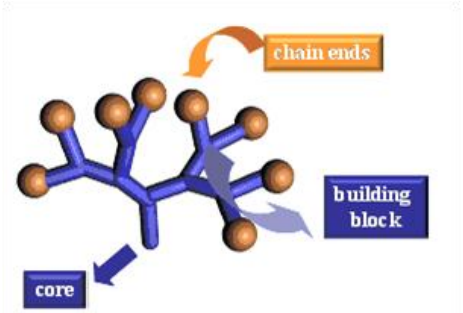

Figure 1. 23. General structure of a dendron.

Dendrimers with their monodisperse character present extremely attractive physical and chemical properties for covalent conjugation and supramolecular assemblies of diverse molecules such as drugs, imaging and targeting groups, peptides and proteins, etc. for

applications such as targeted drug delivery [86], formation of enzyme mimicking cavities [87], synthesis of multiarm star polymers [88], light harvesting systems [89], bio-molecular immobilization [90] and hydrogels [91].

1.4.1.1. Synthesis Methods. Dendrimer synthesis can be achieved by two different methodologies: convergent or divergent.

In the ‘convergent’ method, the synthesis starts with the branching units, in other words from the periphery to the core. Surface groups are attached onto the branching units and further coupling of these small dendrons to the multivalent core molecule results in formation of the desired dendrimer [92]. Due to steric hindrance, dendrimers with higher generations may contain defects while combining the building blocks towards the core, so the purification process becomes harder. Due to increased molecular weight and branching degree of the dendrimer after growing each generation, divergent synthesis is a desirable method for large scale dendrimer synthesis. However excess amount of building blocks should be used each time to obtain higher generations of dendrimers to make sure that all surface groups are reacted with no defects on the surface. Unreacted monomers can be removed by conventional separation techniques such as distillation, chromatography, crystallization etc.

Whereas in the other method, synthesis of the dendrimers starts from the core by attachment of branching units and finally installation of the surface groups at the periphery takes place [93]. Growth of dendrimer continues with the addition of building blocks to the periphery via surface groups which gets activated just before the building block addition to increase the generation number one more.

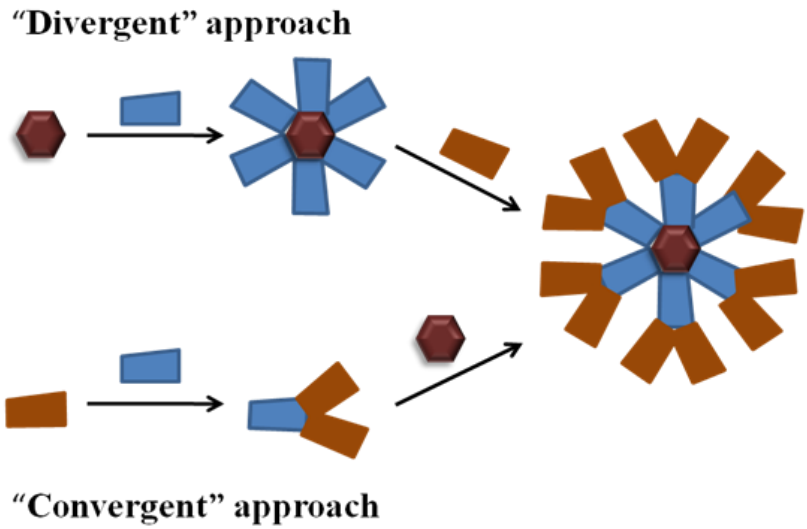

Figure 1. 24. Synthesis of dendrimers via divergent and convergent method [92-93].

1.4.1.2. Block Dendrimers. Different arrangements of clusters of building blocks of dendrimers facilitate their classification as three major subgroups: layer block, segment block and surface block (Figure 1.25). Along with the functional groups at the peripheries, building block nature of dendrons can be varied to possess different properties. Combination of these different blocks via a multifunctional core unit enables the introduction of novel dendrimers with enhanced architectures [94].

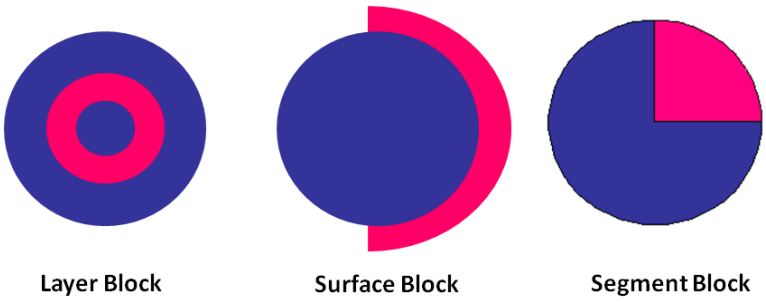

Figure 1. 25. Types of block dendrimers.

Layer block dendrimers are formed by attaching more than one type of repeating units to the core molecule in a layered way. The first example of a layer block dendrimer was demostrated by Hawker and Fréchet in 1992 where they have used convergent approach to attach poly (benzyl ether) dendrons to a triphenolic core resulting in formation of the layered dendrimers (Figure 1.26) [95].

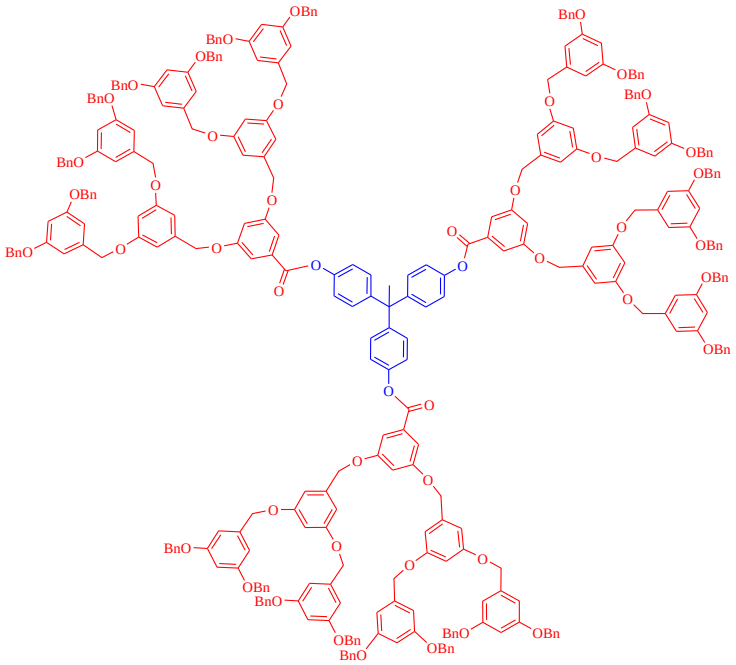

Figure 1. 26. Synthesis of first layer block dendrimer [95].

Another class of dendrimers is surface block dendrimers which consists of two or more different types of peripheral groups on the dendrimer surface. Dendrons built by same repeating units but bears different peripheral functionalities may be combined to each other from their focal points or around a multifunctional core to end up with surface block dendrimers. Hawker *et al.* have synthesized orthogonally functionalizable surface block polyester dendrimer by using click reaction to combine two polyester dendrons (Figure 1.27) [96].

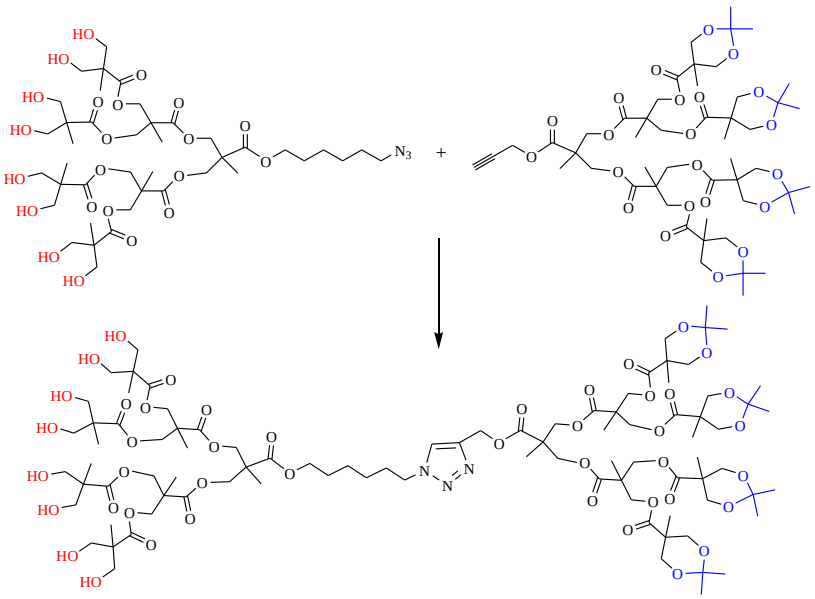

Figure 1. 27. Synthesis of surface block polyester dendrimer [96].

First example of this kind of structures was given by Hawker and Fréchet where they synthesized poly (benzyl ether) and poly (benzyl ester) dendrons and then via DDC mediated esterification these dendron parts were combined to each other [97]. Another outstanding study was published by Sanyal group in 2008, where they revealed the synthesis of polyarylether and polyester dendrons with furan and naked maleimide group at their focal points, respectively [98]. Three generations of dendrons were undergone Diels/Alder cycloaddition reaction to yield segment block dendrimers in high yields (Figure 1.28).

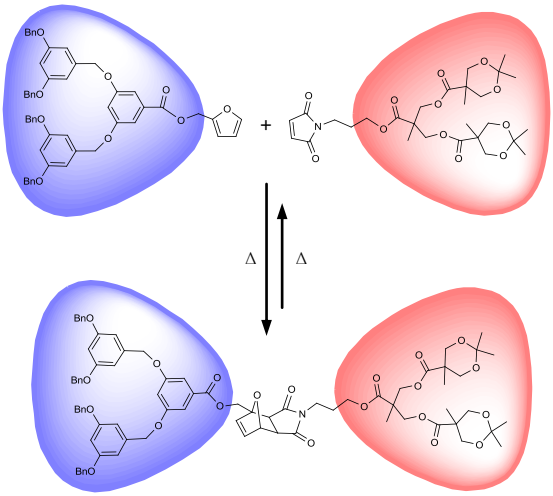

Figure 1. 28. Synthesis of the segment blocks dendrimer [98].

1.4.1.3. Enhanced multivalency by dendrimers. What is remarkable about the structure of dendrimers is the multivalency they provide due to surface groups that can be decorated with desired functionalities and internal cavity nature. As the generation number increases, more drugs, targeting groups and biomolecules can be covalently conjugated to the periphery or physically trapped to the internal cavities of dendrimers which increases their loading capacity. So, local concentration of the conjugated or complexed molecule dramatically rises in the form of clusters since they are kept in one delivery system. That is, multifunctionality of the dendrimer structure contributes to multivalency of the biomolecules of interest to improve their effectiveness [99].

It is well known that most of the biological interactions utilize interaction of multivalent ligands with receptors found on the cell surfaces. This behavior is significantly important in ligand mediated interactions of enzymes and proteins. Connecting to each other via “on-off” process, ligand-receptor interactions become stronger with increased number of ligand molecules around the receptor (Figure 1.29). Compared to monovalent interactions where binding of one ligand does not affect the interaction of the other ligand, each interaction is independent from each other and rates of processes are same. However, as the concentration of ligands increases around the receptor via a multifunctional ligand carrier system, binding of one ligand to receptor facilitates the binding of the other one, resulting in more and effective binding process [100].

At this point, dendrimers with increased number of reactive groups at the surface can bind to and interior cavities can accommodate more than one targeting group, imaging agent or drug molecules to improve their local concentration and effectiveness. As a result, one can obtain better and faster binding ability of targeting groups, enhanced intensity for the imaging agents and improved efficacy for drug molecules with decreased cytotoxicity [101].

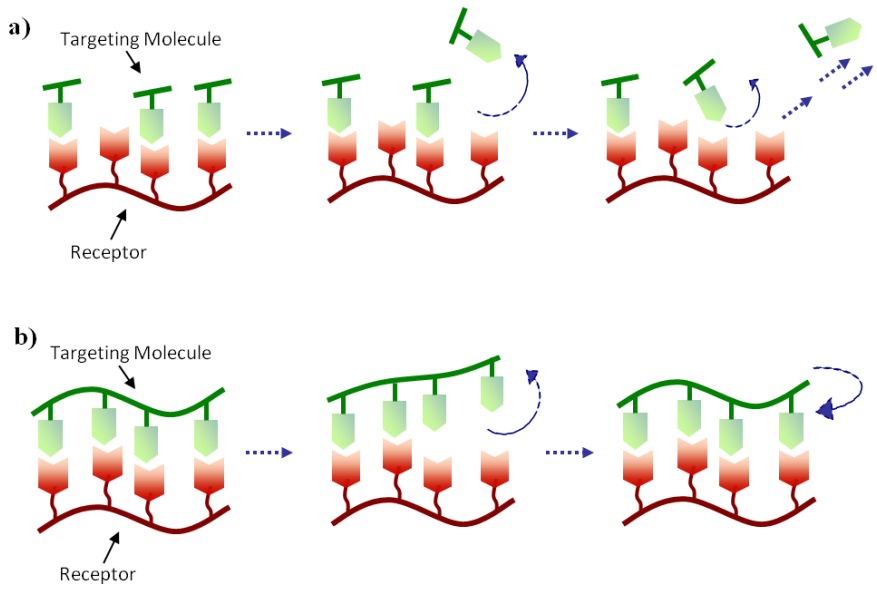

Figure 1. 29. Schematic representation of monovalent (a) and multivalent (b) interactions.

1.4.1.4. Orthogonally Functionalizable Dendrons. As alluded above, surface groups of dendrimers serves as potential conjugation sites for various (bio)molecules. However the nature of reactive groups can be tuned according to the synthesis methodologies of dendrimers and different types of functional groups such as hydroxyls, amines, thiols, carboxylic acids, and others, can be installed on the periphery of dendrimers. Dendrons possessing different reactive groups which do not interfere with each other during conjugation processes are called as 'orhogonally reactive dendrons' and combination of these dendrons via several different synthesis strategies yield dendrimers with orthogonal reactivities [102, 103].

Literature reveals several dendrimers and dendrimer inserted macromolecules with orthogonal reactive groups. An example regarding the dendrons functionalized with

different reactive units at both focal and peripheral regions were described by Sanyal and coworkers in 2011. They synthesized orthogonal dendritic scaffolds via novel biodegradable polyester dendrons and then demonstrated their multifunctionality. Dendron surface was appended with alkyne moeities which undergo lately Huisgen type ‘click’ cycloaddition reaction with PEG azide. At the same time, maleimide bearing core of dendron was functionalized with a thiol containing dye and orthogonal multifunctionality of these kind of systems has been successfully proved (Figure 1.30) [104].

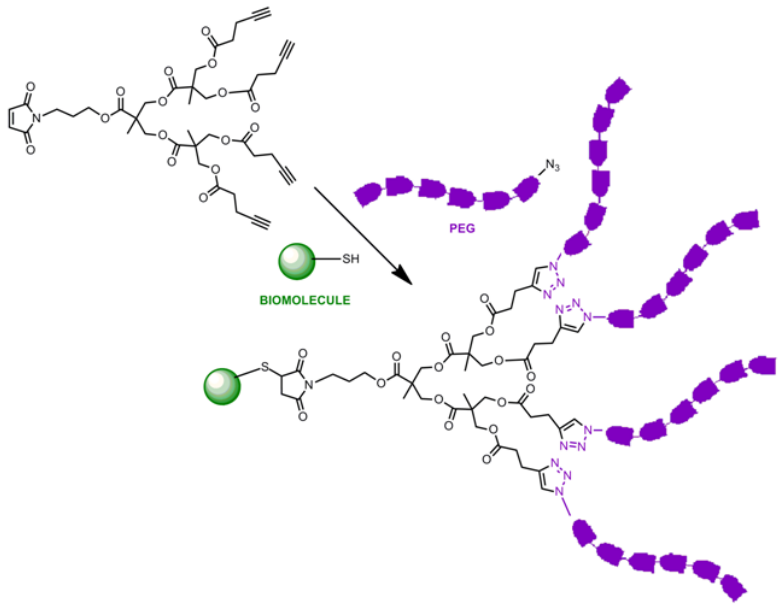

Figure 1. 30. Orthogonal functionalization of biodegradable polyester dendrons [104].

1.4.2. Dendronized polymers

Dendronized polymers are attractive subdivisions of comb polymers decorated with dendritic units. In recent years, substantial amount of effort is directed toward developing novel design of dendron-polymer conjugates enhancing their loading capacity. Incorparation of the dendrimers provides the polymers with special properties depending on the type and generation of dendron, attachment density along the backbone, functional groups at its periphery and degree of polymerization [105]. Molecular architecture of dendronized polymers can be controlled with high precision in terms of size, stiffness and surface decoration. Appended large dendrons to the backbone transform random coil conformation of backbone to extended conformation [106].

Linear polymers mostly form random-coil structures in solution, but upon attachment of several generations of dendrons either to side chains or to the ends of polymers, the backbone of the obtained macromolecule becomes more extended due to steric hindrance and the overall conformation switches to cylindrical, rodlike structures. With enhanced physical properties and gained multifunctionality, dendron conjugated polymers have being utilized widely in drug delivery and pharmaceutical applications together with material sciences like catalysis, electronic and photonic applications [107, 108]. Dendron-polymer conjugates can be obtained in an efficient and preferably in a modular manner by following three main routes; namely ‘graft from’ method, ‘macromonomer method’ and ‘graft-to’ method.

As an alternative approach for synthesis of dendron-polymer conjugates, block copolymer design have witnessed great attention. It includes the combination of focal points of dendrons with end groups of polymer chains by ‘graft-to’ method. Reactive end groups of polymers are attached to dendrons with appropriate functional units at their focal points. So di and triblock copolymer synthesis can be achieved with high efficiency. The principle advantage of these types of block constructs is due to insertion of more functional groups to the ends of polymers and improved loading capacity which provides multivalency for especially drug conjugations. Figure 1.31 represents one, two and four G4 polyester dendrons bearing PEG polymers synthesized by Frechet and coworkers in 2001. This report is accepted one of the leading examples in dendron-polymer conjugation [109].

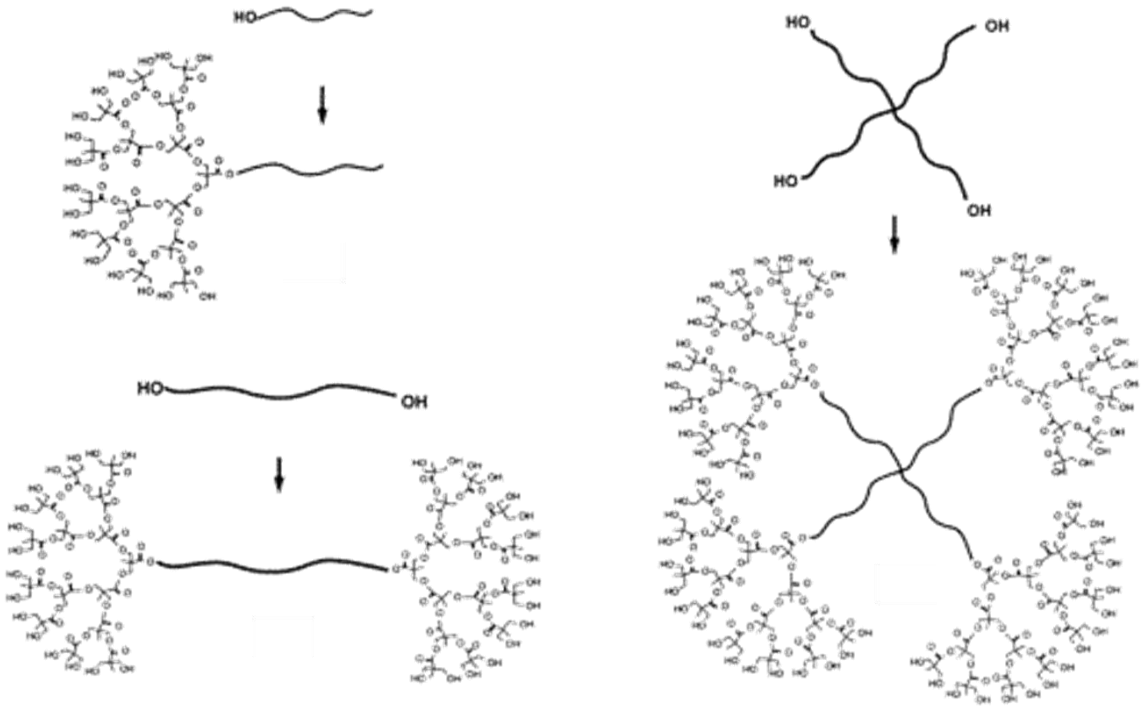

Figure 1. 31. Three types of hybrids of PEG and [G-4] polyester dendrons obtained from PEGs with one, two, or four reactive ends [109].

For bioconjugation and drug delivery applications, water soluble and biocompatible polymeric scaffolds are preferred. In recent years, a wide range of constructs were designed using PEG as the major component due to its improved contribution to hydrophilicity and immunogenicity of the system. Moreover, its anti-biofouling property reduces the non-specific interactions remarkably. However loading capacity of linear PEG chains should be improved to get better impact on especially pharmacokinetic profiles of conjugated biomolecules [49]. This can be achieved by introducing dendrons furnished with several functional groups. Hence the resultant macromolecule can be conjugated to more than one or two molecule of interest. In recent years, click reaction were readily utilized for the efficient coupling of dendrons to linear PEG chains. Sanyal and coworkers reported two attractive studies one of which consists of attachment of azide functionalized dendrons to alkyne terminated PEG chains. The obtained conjugates were further functionalized with alkyne groups and utilized for the synthesis of hydrogels with gelation efficiencies greater than 80 % [110]. Another study exploring Diels-Alder reaction for the synthesis of di and triblock dendron-polymer conjugates. Here, multivalent PEG polymers

were accessed by reaction of anthracene group at the focal points of three generations of biodegradable polyester dendrons with Furan masked maleimide ended linear PEG chains (Figure 1.32). Resultant conjugates were decorated with aklene units to demostrate efficient and multivalent attachment of a free thiol containing molecule [110].

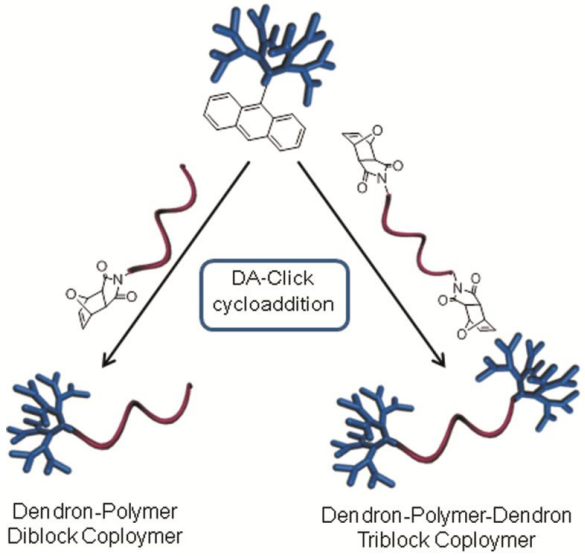

Figure 1. 32. Dendron–polymer block copolymers via the Diels–Alder "click" reaction [110].

1.4.3. Star Polymers

Star polymers have emerged as three-dimensional globular macromolecules that are composed of many linear arms extending from a core (Figure 1.33) [111]. What differentiate them from regular hyper branched polymers are their compact architectures with linear polymeric arms of almost same molecular weight and narrower polydispersity index values. That is why star polymers have witnessed great attraction as multi-armed polymeric platforms with interesting bulk and solution properties. Especially in biotechnology and material sciences, multiarm star polymers have found a wide range of applications. According to polymerization methodology employed to form these discrete architectures, reactive groups of interest can be inserted to final multiarm star polymers and any biomolecules or agent with suitable functional group can be conjugated with high efficiency via additional modifications or cross-linking [112, 113].

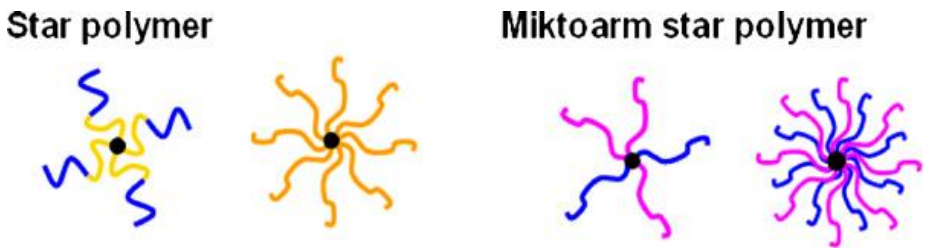

Figure 1. 33. Categories of star polymers [112].

Mostly controlled addition polymerization techniques have being applied for the sysnthesis of several monomers to yield well-defined multiarm star polymers with desired functionalities. Among living anionic and cationic polymerizations, nitroxide mediated polymerizations (NMP) and atom transfer radical polymerizations (ATRP) methods are the outstanding ones applied to obtain multiarm star polymers due to their improved control over molecular weight, functional group tolerance and less-stringent experimental conditions [114, 115].

1.4.3.1. Preparation of multiarm star polymers. Approaches to synthesize multiarm star polymers can be catogerized into three parts, namely “arm-first”, “core-first” and “couling-onto” methods. In the first method, pre-synthesized terminally reactive living polymer chains are cross-linked from their reactive ends with the help of difunctional vinyl compounds. If the mentioned polymer chains with suitable functional groups for the coupling reaction are combined to each other by a multifunctional core, then it is called as “couling-onto” method. Both methods suffer from low reaction efficiency due to steric hinderance around the core. The other is the *‘core first’* approach which involves the polymerization of monomers of interest initiated by a multifunctional core. Here, the resultant star polymer has arms with the same number of initiators in the structure of the core, which leads to more organized arms around the core [116].

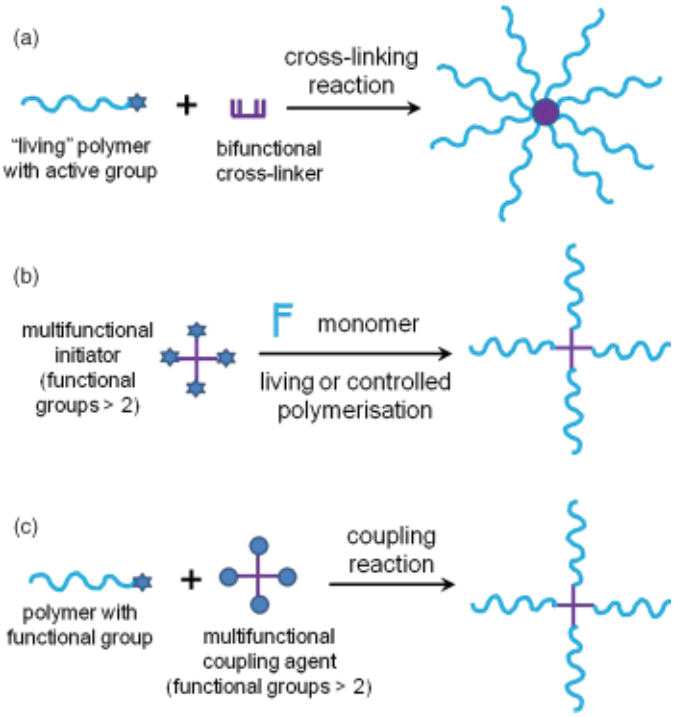

Figure 1. 34. Methods for the synthesis of multiarm star polymer: (a) 'arm-first' methodology; (b) 'core-first' methodology; (c) conjugation/coupling reactions [116].

Multiarm star polymers with well-defined shapes and attractive physical properties have potential for bio-conjugation studies. According to nature of polymer chains, biomolecules or agents can be physically doped into the compact structure or they can be conjugated to the system via reactive groups on star polymers, if any.

Water soluble polymeric constructs both as dendritic structures and as linear scaffolds are known to extensively increase bioavailability of drug molecules. In this regard, Sanyal and coworkers presented the synthesis of functional multiarm star polymers in 2010 [117]. They synthesized thiol reactive dendron based multi initiator to polymerize several monomers via ATRP. Furan masked maleimide group located at the core of multiarm star polymers obtained by "core-first" method was then activated via retro Diels/Alder cycloreversion strategy to yield naked maleimide functionality for further conjugation of a tripeptide via Michael addition reaction (Figure 1.35).

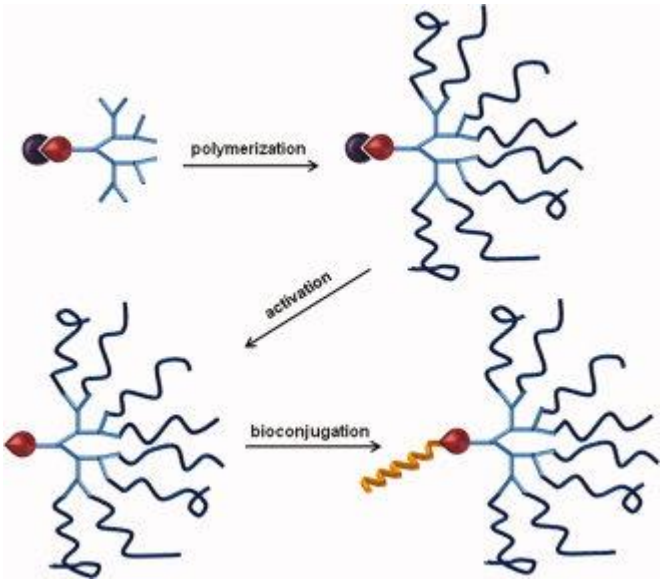

Figure 1. 35. General strategy for the synthesis of multiarm polymers containing reactive maleimide core [117].

1.4.4. Post-Polymerization Modification Strategies for Efficient Bio-Functionalizations

Covalent attachment of polymeric architectures to several drugs, targeting and imaging agents, proteins and peptides requires the reactive groups in their structure through which the conjugation occurs. To date, organic chemistry offers a wide range of efficient modification strategies to synthesize functionalizable polymeric constructs for the conjugation and immobilization of bio-molecules of interest. More readily used coupling strategies are click reactions involving [3+2] Huisgen cycloaddition, [4+2] Diels-Alder cycloaddition, thiol-ene and thiol-yne reactions together with a popular disulfide exchange reaction. A number of drug and protein delivery systems benefits from the versatility, robustness and efficiency of these mentioned strategies depending on the reactive groups on the conjugated bio-molecules. Some of the utilized click reactions that are utilized in this thesis are briefly described below.

1.4.4.1. Diels-Alder cycloaddition reaction. Diels-Alder reaction is a type of click reactions which describes a [4+2] cycloaddition reaction taking place between an electron rich diene group and an electron poor dienophile (Figure 1.36). This electrocyclic reaction involves

the generation of new σ-bonds that are energetically more stable than π-bonds and results in a six membered ring formation, referred to as an adduct. Due to high yields and mild reaction conditions without any need for additional reagents, it is widely utilized in organic chemistry and conjugation studies [118].

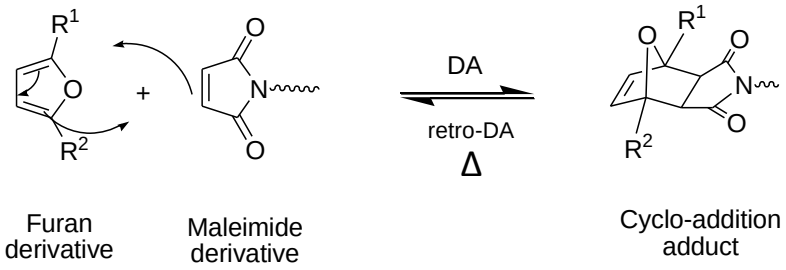

Figure 1. 36. General mechanism for DA and rDA reactions.

Diels-Alder reaction ends up with two stereoisomers named as the *endo* and *exo* products. The *exo* product is the thermodynamically controlled product formed by a more stable conformation with less steric hindrance and it is favored at high temperatures. Whereas, the *endo* product is the kinetically controlled one due to lower activation energy concerning the orbital overlap in the transition state.

As the diene component, mostly furan and anthracene groups have being used in macromolecular construction. One of the popular dienophiles preffered due to its high reactivity and structural variability is the maleimide moiety. For furan-malemide cycloadduct, it is possible to shift the reaction towards the reactants by only heating to elevated temperatures. The reverse reaction is named as retro Diels-Alder reaction (rDA). The uniqueness of mentioned reversibility phenomenon appears as a versatile strategy for the synthesis of theroreversible polymeric systems including dendrimers, linear and cross-linked polymers, multiarm star block copolymers and conjugation of bio-molecules like antibodies [119-123].

Use of DA reaction in polymer chemistry dates back to 1932 that Alder and coworkers explored the formation of oligomers of cyclopentadiene by this strategy. Then,

DA chemistry between cyclopentadiene based dimers and bis maleimides was used as a handle to synthesize high molecular weight polymers by Stille and his team in 1961. By time, the advantages of DA chemistry have been evaluated to obtain linear polymers as well as thermally responsive polymeric platforms. Gandini and coworkers illustrated several examples of linear and branched polymers using furan-maleimide cycloadduct based DA strategy [124, 125].

1.4.4.2. Thiol-ene chemistry. Thiol-ene chemistry is a special type of click reactions mostly utilized for the construction of thioethers. Taking place between a free thiol group and an aklene moiety, thiol-ene reaction end up with the formation of carbon-sulfur bond which is synthetically important due to resemblence of the system to sulfur-containing natural products. Driven by UV light or heat, the mechanism depends on the radical formation which provides external control over the reaction rate [126].

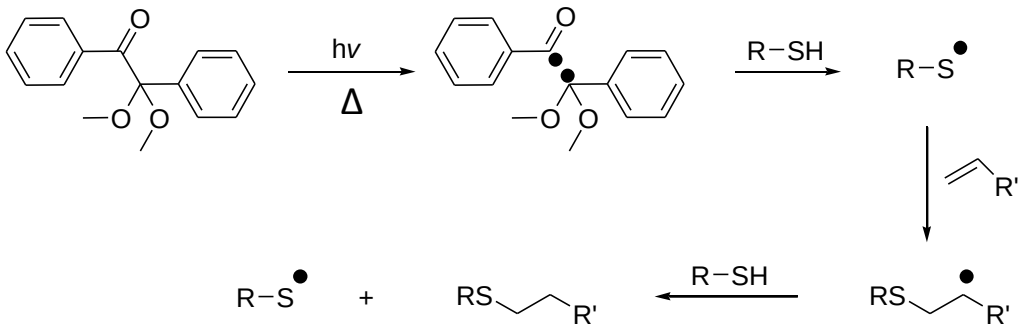

Figure 1. 37. General mechanism for thiol-ene reaction.

Combining the classical advantages of click reactions with the benefits of photo/heat-initiated processes, thiol-ene chemistry has seen as an efficient methodology to modify surface and polymers for bio-conjugation and bio-immobilization of several biologically active molecules. Its robust and efficient attribute together with high yields and tolerance to a number of functional groups clearly account for its applicability to linear and cross-linked materials synthesis, protein modifications and surface immobilizations [127-128]. There are seveal literature examples employing thiol-ene chemistry to functionalize linear polymers like poly(oxazolines) and poly(butadiene) with an array of thiols to build glycodendrons. Likewise, polymers with any type of ene functionality can be conjugated to

proteins via free thiols in their conformations. Uniform network and lowered shrinkage gathered by the step-growth mechanism of thiol-ene chemistry allow the scientists modify the surfaces by photolithography and microdevice techniques [129].

1.4.4.3. 1,4-Michael addition reaction. A special type of thiol-ene reaction is the 1,4-Michael addition reaction which depends on the nucleophilic attack of an electron rich thiol to an electron deficient N-substituted maleimides with two electron withdrawing groups. Reagent free conditions of this reaction and elimination of side reactions makes this reaction extremely attractive especially for the modification of proteins and peptides. Steric hindrance or solubility problems may require the use of mild bases to initiate the reaction, such as triethylamine. Due to absence of any metal or catalyst, this addition technique is very suitable in biomedical applications [130, 131].

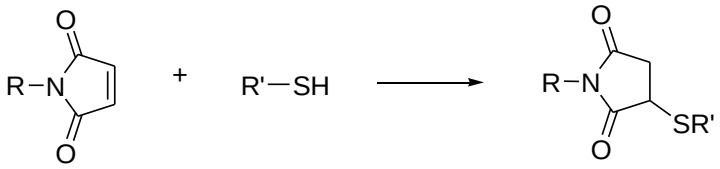

Figure 1. 38. A representation for 1,4-Michael addition reaction.

As an outstanding functionality, maleimide group has a significant role in bioconjugation experiments that requires efficient and reagent free conditions. It can undergo both DA cycloaddition reaction and Michael addition reaction, most commonly with furan and thiol reactive groups, respectively. Highlighted by many literature reports, maleimide group is very valuable placed in the toolbox of functional groups organic chemistry offers. Maleimide based materials have found application areas in synthesis and functionalization of polymers and proteins as well as modification of nanoparticle and planar surfaces [132-134].

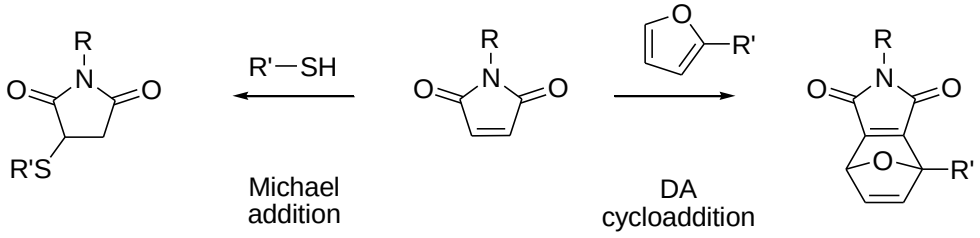

Figure 1. 39. Possible ‘Click’ reactions of maleimide functionality.

Combination of both modification strategies in the cross-line of chemistry and biology by maleimide group contributes to the design of novel polymeric scaffolds in biotechnology. However, presence of a double bond prone to rapid polymerization necessitates a protection step. Sanyal and Dove used a protection/deprotection strategy to synthesize thiol reactive biodegradable polymers (Figure 1.40). Furan-masked maleimide-containing diol was copolymerized with dl-lactide by ring opening polymerization via organobase catalyst, followed by retro Diels/Alder reaction to remove furan groups and generate naked maleimide functionalities appended to polymer backbone. The efficiency of post-polymerization modification was demostrated by Michael type thiol-ene chemistry with a thiol containing small molecule [135].

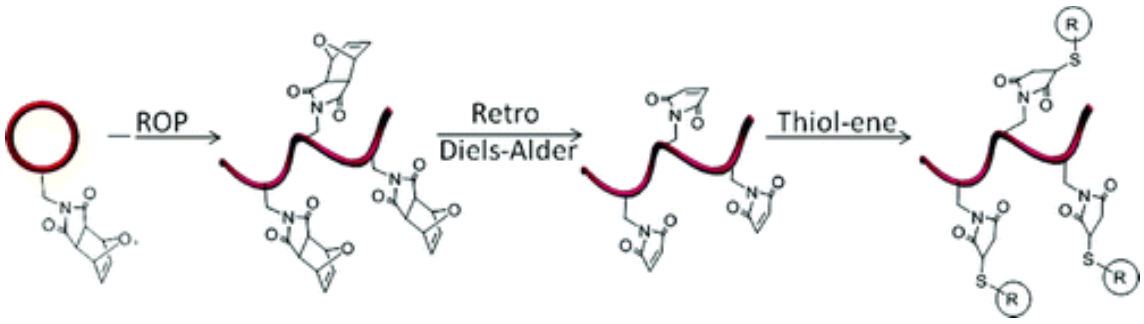

Figure 1. 40. Synthesis of maleimide based reactive copolymer [135].

In recent years, metal free thiol-ene click reactions have attracted great attention so that their advantages have been combined to synthesize polymeric scaffolds that can be functionalized by both strategies [136]. Sanyal and coworkers designed both amine and thiol reactive polymers as well as polymers that can be functionalized by two different thiol group containing molecules via the nucleophilic thiol-ene and the free-radical thiol-ene “click” reactions (Figure 1.41). Sequential conjugation of maleimides by hexane-thiol via Michael type click reaction was followed by radicalic thiol-ene reaction of thioglycerol to alkene units at side chains of polymers [137].

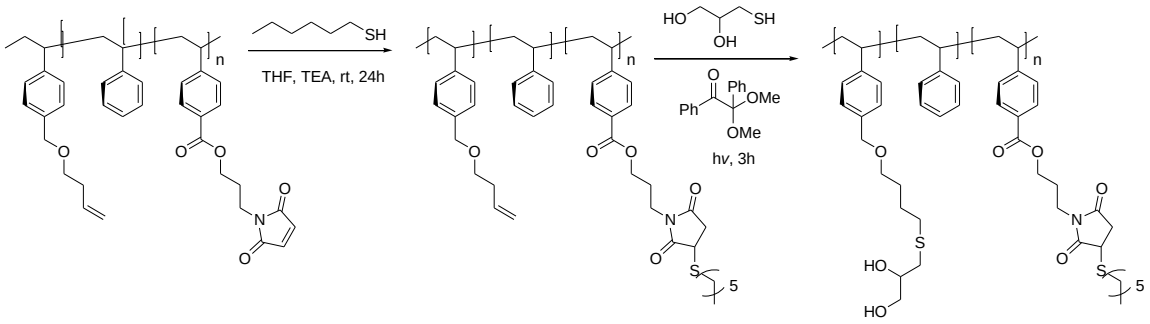

Figure 1. 41. Sequential thiol addition via Michael and photo thiol-ene reactions [137].

1.4.4.4. Disulfide exchange reaction. Thiol-disulfide interchange reaction is based on the reaction of a thiol molecule (RSH) with a disulfide containing one (R'SSR') to form a new disulfide bond (RSSR') in between and replace the thiol (R'SH) in the original disulfide (Figure 1.42). This reaction is unique in organic chemistry due to its ability to its capability to break and reform a disulfide bond that is covalent, strong and directional at room temperature. This rapid reversibility property can be controlled by adjusting the pH of the environment [138, 139].

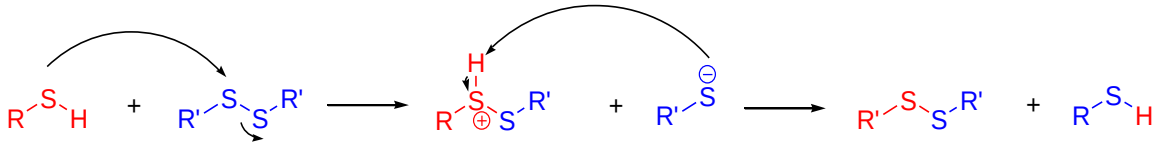

Figure 1. 42. General mechanism for thiol-exchange reactions.

Being one of the special reactions utilized in molecular biology due to disulfide groups located in protein conformations and cystein moieties in their sequences, disulfide exchange reaction has being immensely examined for the modification of proteins and enzymes by mostly attaching thiol containing polymers and dendrimers. Nature demonstrates that thiol groups on polymers are not tend to interfere with other functional groups on protein and nucleic acid structures which enables the usage of disulfide exchange reactions in orthogonal functionalization strategies [140].

As an attractive chemical handle, pyridyl disulfide (PDS) group provides a modular approach for the conjugation of polymers and molecules of interest to biological

compounds. Its fast exchange ability with free thiol groups enables the efficient disulfide exchange reaction. This group leaves the system as pyridine-2-thione and due to its absorption feature, it becomes possible to monitor the release rate of this byproduct and hence the rate of disulfide exchange reaction (Figure 1.43). So any polymer or bio-molecule attached to proteins via disulfide bond can be cleaved due to either reductive cellular environment or increased transcription of free thiol containing molecules like glutathione in case of tumor tissues and the conjugated protein can be easily liberated [142, 143].



Figure 1. 43. A representation for PDS based thiol-exchange reactions.

An elegant utilization of PDS group for bioconjugation was reported by the collaboration of Maynard and Thayumanavan. Poly(ethylene glycol) methylether methacrylate and pyridyl disulfide methacrylate were copolmerized by RAFT to yield PDS groups at the side chains of the polymers, some of which then reduced by DTT to obtain cross-linked nanogels (Figure 1.44). PDSMA serves as both a crosslinking agent and a reactive handle for the surface modification of the nanogels. Remaining PDS groups were conjugated to free thiol containing dye molecule and thiol-modified BSA protein that was proven by several analysis methods like SDS-PAGE and DLS [144].

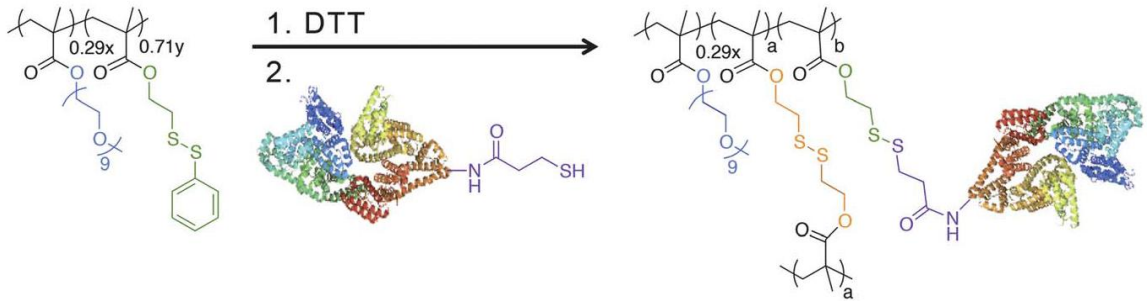

Figure 1. 44. Polymeric nanogel formation and BSA conjugation to its surface [144].

1.4.4.5. Orthogonally Functionalizable Polymers. Oftentimes combination of efficient post-polymerization functionalization strategies have been applied in to generate functional materials. Reactive groups that do not interfere with each other during conjugation reactions are installed in the same macromolecular construct and modified sequentially or one-pot conjugation with molecules with different functionalities [145-148].

As a recent example, reactive polymers allowing both amidation and Huisgen type click reactions were reported by Sanyal and coworkers in 2010. They synthesized two different orthogonally functionalizible polymeric constructs, in one of which a novel N-hydroxysuccinimide carbonate containing methacrylate monomer and azide functionalized monomer were copolymerized with PEG methacrylates to obtain both amine and alkyne reactive polymers (Figure 1.45). This carbonate monomer was also copolymerized with NHS methacrylate and PEG methacrylate monomers to yield second orthogonally reactive polymer which was shown to be functionalized with two different amine containing molecules without interfering with each other [149].

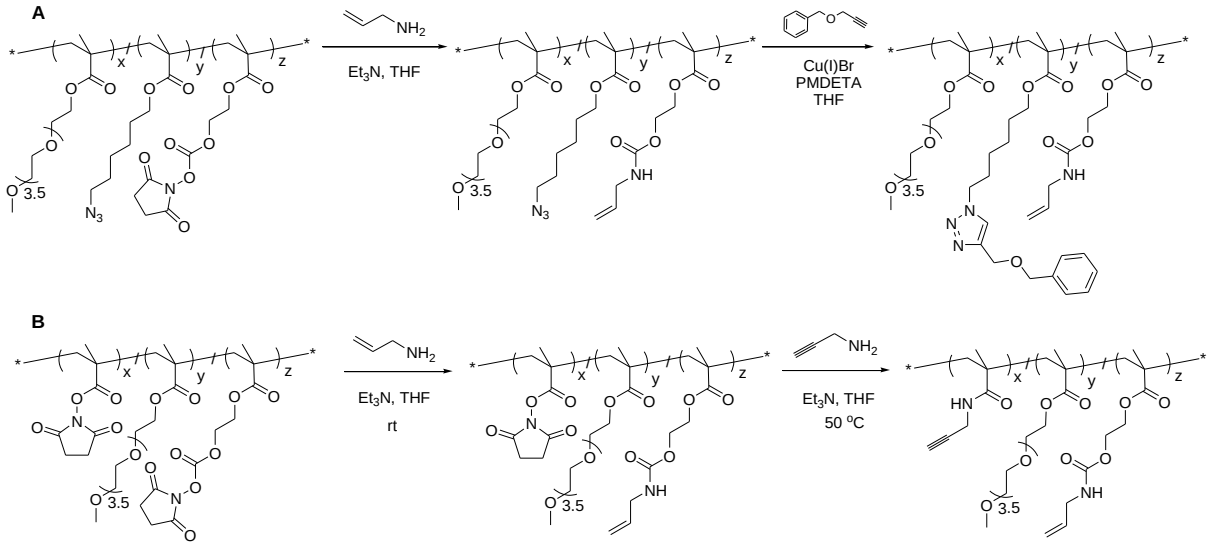

Figure 1. 45. Orthogonal functionalization of copolymers with amine- and alkyne-containing molecules [149].

In another example, Shoichet and his team published a study about design of micellar platforms for theranostic delivery in 2013. Dual functional micelles were gathered by self-

assembly of amphiphilic copolymers, poly(dl-lactide- co-2-methyl-2-carboxytrimethylene carbonate)-graft poly(ethylene glycol)-X (P(LA-co-TMCC)-g-PEG-X) with X representing either azide or furan groups (Figure 1.46). Diels-Alder reaction was carried out to conjugate trastuzumab-maleimide antibodies to furan ended polymers and on the other side FLAG-dibenzylcyclooctyne peptides were attached to azide ended polymers via Huisgen type click reaction. Obtained micelles were investigated for their ability to localize in SKOV-3luc cells [150].

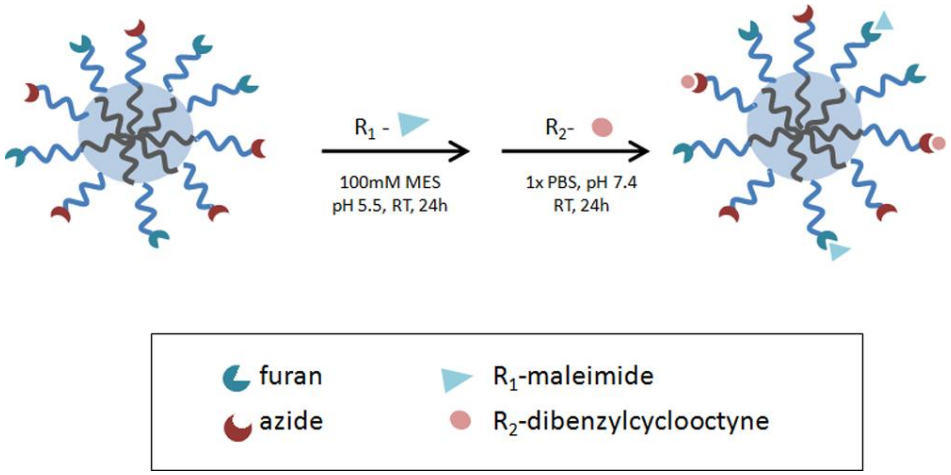

Figure 1. 46. Dual functionalized polymeric micelles facilitated by click coupling chemistry [150].

As mentioned above, bioconjugation of proteins and peptides have been driven by the utility of pyridyl disulfide (PDS) moiety that results in disulfide bond reversible in physiological conditions. Thayumanavan and coworkers synthesized both amine and thiol reactive polymers by copolymerization of NHS and PDS containing methacrylates via ATRP (Figure 1.47). Sequential functionalization of NHS group by propylamine and followed by PDS group modification by thiol modified anthracene molecule was undertaken. As an extention, reversibility of disulfide bond appended to polymer chain was demonstrated by a reducing agent, DTT and removal of anthrace unit was monitored by UV-Vis spectra [151].

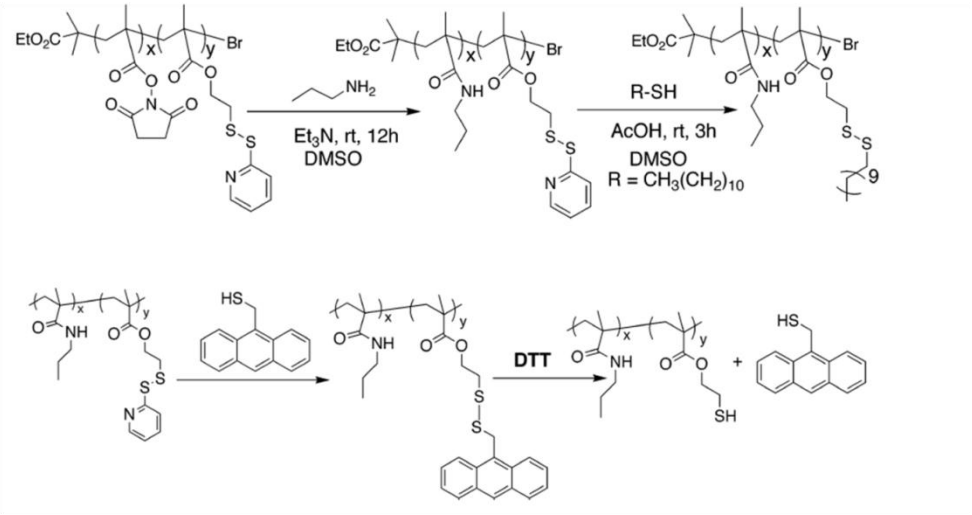

Figure 1. 47. Orthogonal and reversible functionalization or reactive copolymers [151].

2. RESEARCH OVERVIEW

The main objective of this thesis is to design, synthesize and evaluate functional polymeric platforms for therapeutic and diagnostic purposes. Based on polymer therapeutics, novel reactive macromolecular constructs that could be incorporated with drug, imaging and targeting groups were synthesized and evaluated as promising candidates to improve uptake in cancer cells, reduce the overall toxicity of chemotherapy drugs that already in the market and are used for treatments of various cancer types.

To achieve this goal, various linear and multiarm polymers decorated with reactive units were obtained by employing controlled radical polymerization techniques. It is well known that upon conjugation to high molecular weight polymers, drug molecules preferentially accumulate in tumour tissue due to its leaky structure. With this notion, reactive groups in polymers were utilized for the attachment of targeting groups to enhance the selectivity. Also, some copolymers were designed in a manner to enable orthogonally functionalization so that different molecules of interest can be attached utilizing chemistries that do not interfere with each other. For example, orthogonal reactivity was utilized for conjugation of both chemotherapy and imaging agents on the same construct. Another attractive application of multiarm copolymers is their utilization as a protective sheath for therapeutic agents in the harsh biological milieu of the body. Various peptide based drugs are often conjugated with polymers to protect them from proteolytic degradation. So, multiarm polymers were designed for reversible conjugation of therapeutics. Constructs allowing facile conjugation of peptides but also allow deconjugation under thiol-rich environment was obtained.

In short, combining advancements in synthetic organic and polymer chemistry with newly developed technologies in drug delivery, novel polymeric scaffolds were synthesized. Conjugation of drugs, targeting and imaging agents to both linear and multiarm polymers was undertaken to fabricate various drug delivery systems, some of which were evaluated for their both *in vitro* and *in vivo* activities to demonstrate their viable candidacy as drug carriers.

3. WATER SOLUBLE THIOL REACTIVE POLYMERIC SUPPORTS AS PROMISING CANDIDATES FOR HUMAN THERAPEUTICS

3.1. Introduction

The driving force for development of novel polymeric materials is their ever-increasing applications to areas such as tissue engineering, gene therapy, drug delivery and biosensors [42], [152, 153]. Synthetic polymers incorporating various functional groups are of high interest to serve as solid or soluble supports for conjugation and/or bioimmobilization of chemotherapy agents, biomolecules, peptides, and imaging agents [154-157].

In this regard, synthesis of well defined biocompatible and preferably biodegradable polymeric scaffolds have attracted great attention especially in the human therapeutics where proteins and peptides are also utilized as therapy agents along with regularly used chemotherapy drugs [158]. Recently, polymer-peptide and polymer-protein assemblies have witnessed an increasing interest due to improved stability and pharmacological properties of peptides and proteins upon conjugation to polymers. Although many of the pharmaceuticals based on peptide structures suffer from short circulating half-life due to rapid kidney clearance, immunogenicity, proteolytic degradation and low solubility, attachment of these proteins and peptides to polymers may lead to improved physical properties and pharmacological behavior such as longer half-life, reduced proteolytic degradation, slower clearance rate and diminished immunogenicity [159, 160].The increasing demand of such polymers in biomedical fields necessitates expanding the toolbox of reactive water soluble polymers that can be easily decorated with (bio)molecules of interest for particular applications [161].

Being one of the most investigated polymers, poly(ethylene glycol) (PEG) provides a number of advantages to improve the properties of conjugated peptides and proteins [162, 163]. This modification strategy opens up interesting avenues in the context of addressing

the activity and stability of the peptides and proteins. PEG improves the biocompatibility and hydrophilicity, and offers increased circulation time of the resultant conjugate in the body [14]. Due to its anti-biofouling property, proteins conjugated to PEG are less subjected to non-specific protein-protein interactions, so immunogenic response of the body towards the protein/peptide acting as therapy agent decreases to a serious extend. Regarding the conjugation process, the coupling reaction between PEG and biomolecules requires mild, preferable reagent free chemical conditions. So far, the literature reveals several methods for the attachment of PEG chains to proteins. The most common reactive groups in polypeptides are nucleophiles such as thiol, alpha amino group, carboxylic acid and hydroxyl group. The carboxylic groups cannot be easily activated without having reaction with the protein amino groups, which results in intra or inter molecular cross-linking. Designing of PEG mostly with N-succinimidyl ester and α-aldehyde-functional poly(methoxy PEG methacrylate) groups results in efficient reaction of polymer chains with amine functionalities present at the surface of proteins [54], [164].

Keeping in mind that proteins have a lot of amine groups randomly distributed in their structure, conjugation via amine-based coupling reactions do not bring out structurally well-defined macromolecules. However, utilization of thiol groups derived from cystein amino acids of proteins with precise locations comes up with the desired specificity for the polymer location around the protein of interest [165]. Although thiol reactive polymers with terminal maleimide, vinyl sulfone and activated disulfides have been synthesized to achieve conjugation to proteins, there are very few of polymers with thiol reactive groups on the side chain. These are interesting platforms for conjugation of a number of small active peptides. Among these available thiol reactive functional groups, maleimide group seems to be an attractive candidate since it is very stable and reactive under appropriate conditions [166, 167]. However, it is difficult to design polymeric materials containg a reactive maleimide group that is available for post-polymerization modification because the maleimide group is itselp prone to participate in polymerization to to the presence of an activated unsaturation. Recently, remarkable advances have been made in this area by utilization of protected maleimide based initiators to obtain polymers with maleimide as their end groups. Haddleton et al. has disclosed an approach to obtain

maleimide end functionalized macromolecules to target cysteine residues on the proteins [168]. They introduced the maleimide moiety into the polymers by utilizing a "protected" maleimide initiator for the polymerization step followed by deprotection to give the active maleimide terminated polymers.

In the light of many such endeavors, it may be beneficial to extend this display of a single conjugation site to multivalent. Thus, the limited loading capacity can be increased by the incorporation of reactive group containing thiol-reactive maleimide monomers into the system [134, 135], [169]. Sanyal and coworkers have demonstrated that by using the protection/deprotection strategy of maleimide functional group by Diels-Alder/retro Diels-Alder (DA/rDA) cycloaddition reactions, maleimide functionalities can be incorporated as side chains of polymers [170-172].

The first chapter of this dissertation involves the design of a route to synthesize and characterize a family of well-defined poly(ethylene glycol) based water-soluble thiol reactive copolymers using ATRP and demonstrate their potential to create a targeted drug delivery platform via post-polymerization modifications (Figure 3.1). To obtain such copolymers, a furan-masked maleimide monomer is copolymerized with water soluble PEG-methacrylate monomer using ATRP in a methanol-water solvent system. ATRP is a controlled living radical polymerization that leads a great control over the molecular weight distribution and the architecture of polymers. Activation of maleimide groups was achieved quantitatively by heating at elevated temperatures. The copolymers are characterized for their purity and maleimide content via ^{1}HNMR spectroscopy. Due to their biocompatibility and anti-biofouling properties, naked maleimide groups located at the side chains of these polymers were evaluated for the conjugation of a free thiol group containing a model hydrophobic drug/imaging agent, a hydrophobic dye, namely, Bodipy-SH, and a peptide as a well-established targeting group, cRGDfC. To prove the potent of these biodegradable reactive copolymers as delivery platforms for drugs and biomolecules, *in vitro* cytotoxicity experiments and cell internalization studies were performed on both cancerous and healthy breast cell lines.

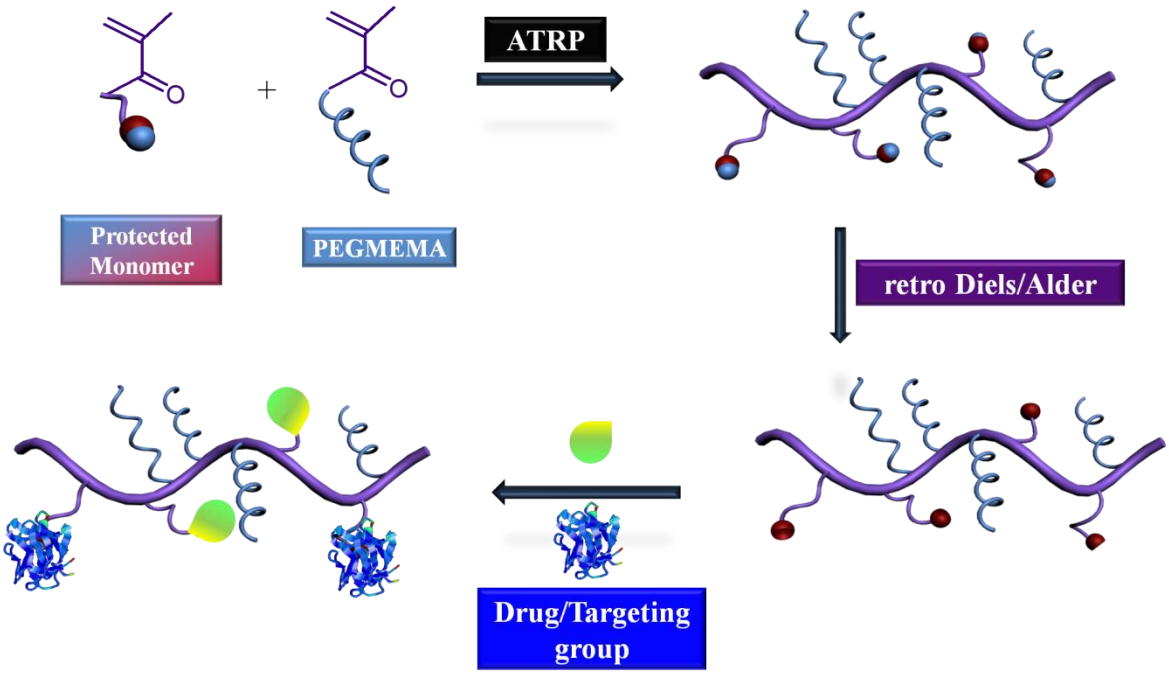

Figure 3. 1. Synthetic approach towards maleimide containing thiol reactive copolymers.

3.2. Experimental

3.2.1. Materials

3.2.1.1. Chemicals. All reagents were obtained from commercial sources and were used as received unless other-wise stated. Poly(ethylene glycol) methylether methacrylate (M_n = 300) (PEGMEMA, 99%, Aldrich) was passed through basic alumina column to remove inhibitor prior to use *N, N, N', N'', N''*-pentamethyldiethylenetriamine (PMDETA, 99%, Aldrich). Methacryloylchloride and 2-bromo-2-methyl propionyl bromide were obtained from Alfa Aesar and used as received. Triethylene glycol monometyl ether (TEGME, 99%, Aldrich), Copper(I)Bromide (CuBr, 99.9%, Aldrich) and 2-(pyridin-2-yl)pyridine (2,2'bipyridine, 99%, Aldrich) were used as received. 2-methoxyethyl 2-bromo-2-methylpropanoate (**3**), BodipyC10SH were prepared according to literature procedures [170] [173] [174]. Alcohol exo-3a,4,7,7a-tetrahydro-2- (3-hydroxypropyl)-4,7-epoxy-1H-isoindole-1,3(2H)- dione (**1**) and derived monomer (**2**) were synthesized by following literature [134]. cRGD was synthesized by Dr. Rana Sanyal using standard solid phase

synthesis. Anhydrous solvents (CH_2Cl_2, THF, toluene) was obtained from ScimatCo Purification System, other solvents were dried over molecular sieves. The dialysis bags (Spectra/Por® Biotech Regenerated Cellulose Dialysis Membranes, MWCO 1000 Da) were purchased from Spectrum Labs. All other chemicals were used as received from manufacturer (Merck, Aldrich, Alfa Aesar. Column chromatography was performed using silicagel–60 (43–60 nm). Thin layer chromatography was performed using silica gel plates (Kiesel gel 60 F254, 0.2mm, Merck).

3.2.1.2. Cells. Human breast adenocarcinoma MDA-MB-231 and healthy MCF-10A cell lines were obtained from ATCC (Wessel, Germany). Cells were kept in the logarithmic phase of cell growth for the duration of experiments. MDA-MB-231 cells were maintained in RPMI-1640 culture medium (Roswell Park Memorial Institute) [Gibco, Invitrogen] supplemented with 10% fetal bovine serum [FBS] [Lonza], 100 U/mL penicillin, 100 g/mL streptomycin, and 0.25 g/mL amphotericin B at 37 °C, 5% CO_2, and 95% relative humidity. MCF-10A cells were maintained in Endothelial Cell Growth Medium-2 (EMB-2) [Lonza, Invitrogen] supplemented with EGM™-2 Bulletkit™ containing hEGF, hydrocortisone, GA-1000 (Gentamicin, Amphotericin-B), FBS (Fetal Bovine Serum) 10 ml, VEGF, hFGF-B, R3-IGF-1, Ascorbic Acid, Heparin and 0.01 % insulin [Lonza], at 37 °C, 5% CO_2, and 95% relative humidity. Cell counting kit-8 (CCK-8) and DAPI was obtained from Sigma Aldrich.

3.2.2. Instrumentation

3.2.2.1. Nuclear Magnetic Resonance Spectroscopy (NMR). The NMR spectra were recorded using a 400 MHz Varian spectrometer at 25 °C. ^1H NMR measurements were made at frequency of 400 MHz, and calibrated with respect to the solvent signal. The measurements were performed in deuterated chloroform ($CDCl_3$), water (D_2O) and dimethyl sulfoxide (DMSO).

3.2.2.2. Size Exclusion Chromatography (SEC). The molecular weights of the copolymers were estimated by GPC analysis using a Shimadzu PSS-SDV (length/ID 8 × 300 mm, 10 mm particle size) mixed-C column calibrated with polystyrene standards (1–400 kDa) using a refractive-index detector. Tetrahydrofuran (THF) was used as eluent at a flow rate of 1 mL/min at 30 °C.

3.2.2.3. MultiscanTM FC Microplate Photometer. Cell viability values for the cytotoxicity experiments were determined by measuring the absorbance of 96-well plates in use at 450 nm by Multiscan^{TM} FC Microplate Photometer from Thermo Scientific^{TM} equipped with a quartz halogen light source of a precision CV≤0.2% (0.3-3 Abs). It has an excitation wavelength range 340 to 850 nm with excitation filters are installed at 405, 450 and 620 nm.

3.2.2.4. Fluorescent Microscopy. Cell internalization studies were performed with Zeiss Observer Z1 fluorescence microscope connected to Axiocam MRc5 using a Zeiss Filter set 38 (Excitation BP 470/40, Emission BP 525/50) for imaging the functionalized polymers and a Zeiss Filter set 49 (Excitation G365, Emission BP 445/50) was used for imaging DAPI stained nuclei. Images were merged to visualize cell nuclei and morphology using Zeiss AxioVision software.

3.2.3. Copolymerization of Latent Reactive Monomer and PEGMEMA

3.2.3.1. Synthesis of Copolymer **P1**. Furan protected maleimide monomer (**2**) (0.64 g, 0.22 mmol) dissolved in minimum amount of degassed MeOH was introduced into a flask containing 2,2'bipyridine (6.15 mg, 0.040 mmol), CuBr (2.8 mg, 0.020 mmol) and PEGMEMA (0.50 mL, 1.75 mmol) dissolved in degassed MeOH (1.65 mL) and H_2O (1.65 mL) under stirring. To the stirring mixture was added TEGME-Br initiator (**3**) (6.16 mg, 0.020 mmol) and stirred at room temperature for 10 minutes At the end of the reaction, MeOH was evaporated under vacuum and water was removed with the help of lyophilizer. The polymer was dissolved in minimum amount of dichloromethane and precipitated in cold diethyl ether and the passed through aluminum oxide to remove cupper catalyst. **P1** was obtained as a viscous solid. ($[M]_0/[I]_0$= 100, [**2**]:[PEGMEMA]= 1:8.3, $[I]_0$:[CuBr]:[PMDETA]=1:2:4, conversion = 61 %, $M_{n,theo}$ = 18430, $M_{n,NMR}$ = 8387, $M_{n,GPC}$ = 30260, M_w/M_n= 1.52, relative to PS).

For polymer **P1**: ^{1}H NMR ($CDCl_3$, δ, ppm) 6.52 (s, 2H, CH=CH), 5.23 (s, 2H, CH bridgehead protons), 4.06 (s, 2H, OCH_2 ester protons of PEGMEMA), 3.89 (br s, 2H, OCH_2), 3.63-3.52 (m, 4H, OCH_2 of PEGMEMA and NCH_2), 3.45 (br s, 3H, OCH_3), 3.35

(s, 3H, OCH_3 of PEGMEMA), 2.86 (s, 2H, CH-CH, bridge protons), 1.92–0.85 (m, 7H, $NCH_2CH_2CH_2O$, CH_2 and CH_3 along polymer backbone).

3.2.3.2. Synthesis of Copolymer **P2.** Furan protected maleimide monomer (**2**) (0.32 g, 0.11 mmol) dissolved in minimum amount of degassed MeOH was introduced into a flask containing 2,2'bipyridine (5.80 mg, 0.037 mmol), CuBr (2.7 mg, 0.019 mmol) and PEGMEMA (0.50 mL, 1.75 mmol) dissolved in degassed MeOH (1.65 mL) and H_2O (1.65 mL) under stirring. To the stirring mixture was added TEGME-Br initiator (**3**) (5.8 mg, 0.019 mmol) and stirred at room temperature for 10 minutes. At the end of the reaction, MeOH was evaporated under vacuo and water was removed with the help of lyophilizer. The polymer was dissolved in minimum amount of dichloromethane and precipitated in cold diethyl ether and the passed through aliminium oxide to remove cupper catalyst. **P2** was obtained as a viscous solid. ($[M]_0/[I]_0$= 100, [**2**]:[PEGMEMA]= 1:15.8, $[I]_0$:[CuBr]:[PMDETA]=1:2:4, conversion = 73 %, $M_{n,theo}$ = 22090, $M_{n,NMR}$ = 7950, $M_{n,GPC}$ = 35330, M_w/M_n= 1.51, relative to PS).

For polymer **P2**: ^{1}H NMR ($CDCl_3$, δ, ppm) 6.53 (s, 2H, CH=CH), 5.24 (s, 2H, CH bridgehead protons), 4.06 (s, 2H, OCH_2 ester protons of PEGMEMA), 3.89 (br s, 2H, OCH_2), 3.64-3.52 (m, 4H, OCH_2 of PEGMEMA and NCH_2), 3.46 (br s, 3H, OCH_3), 3.36 (s, 3H, OCH_3 of PEGMEMA), 2.87 (s, 2H, CH-CH, bridge protons), 1.87–0.85 (m, 7H, $NCH_2CH_2CH_2O$, CH_2 and CH_3 along polymer backbone).

3.2.4. Activation of Copolymers by retro-Diels/Alder Reaction

3.2.4.1. Activation of Copolymer P1 (**P3**). Polymer **P1** (40.0 mg, 4.77 μmol) was dissolved in anhydrous toluene and heated at 110 °C for 24 hours. ^{1}H NMR analysis indicated a quantitative conversion of the oxabicyclic moiety to the maleimide functional group (36.0 mg, 93 % yield).

For polymer **P3**: ^{1}H NMR ($CDCl_3$, δ, ppm) 6.76 (s, 2H, CH=CH), 4.06 (s, 2H, OCH_2 ester protons of PEGMEMA), 3.92 (br s, 2H, OCH_2), 3.64-3.52 (m, 5H, OCH_2 of PEGMEMA and NCH_2), 3.46 (br s, 3H, OCH_3), 3.35 (s, 3H, OCH_3 of PEGMEMA), 1.92–0.83 (m, 7H, $NCH_2CH_2CH_2O$, CH_2 and CH_3 along polymer backbone).

3.2.4.2. Activation of Copolymer P2 (**P4**). Polymer **P2** (50.0 mg, 6.3 μmol) was dissolved in anhydrous toluene and heated at 110 °C for 24 hours. ^{1}H NMR analysis indicated a quantitative conversion of the oxabicyclic moiety to the maleimide functional group (48.0 mg, 97 % yield).

For polymer **P4**: ^{1}H NMR ($CDCl_3$, δ, ppm) 6.64 (s, 2H, CH=CH), 4.06 (s, 2H, OCH_2 ester protons of PEGMEMA), 3.93 (br s, 2H, OCH_2), 3.64-3.52 (m, 5H, OCH_2 of PEGMEMA and NCH_2), 3.46 (br s, 3H, OCH_3), 3.36 (s, 3H, OCH_3 of PEGMEMA), 1.86–0.85 (m, 7H, $NCH_2CH_2CH_2O$, CH_2 and CH_3 along polymer backbone).

3.2.5. Conjugation of Polymers with Bodipy-SH via Thiol-ene Reaction

3.2.5.1. Conjugation of Copolymer P3 with Bodipy-SH (**P5**). Polymer **P3** (15.0 mg, 1.85 μmol) and BodipyC10SH (1.60 mg, 3.70 μmol) were dissolved in THF (0.15 mL) and triethylamine (0.07 μL, 0.46 μmol) was added into the reaction mixture. The reaction was allowed to proceed at room temperature for 24 h. Unreacted dye was removed by washing the conjugate with cold diethyl ether several times. ^{1}H NMR analysis revealed that 80% of maleimides appended to the polymer chains were attached to BodipyC10SH. Dye conjugated polymer was obtained as a fluorescent viscous solid **P5** (12 mg, 72 % yield).

For polymer **P5**: ^{1}H NMR ($CDCl_3$, δ, ppm) 6.76 (s, 2H, C*H*=C*H*), 6.03 (s, 2H, *H*C=CCH_3 of Bodipy), 4.06 (s, 2H, OCH_2 ester protons of PEGMEMA), 3.92 (br s, 2*H*, OCH_2), 3.64-3.53 (m, 5H, OCH_2 of PEGMEMA and NCH_2), 3.46 (br s, 3H, OCH_3), 3.36 (s, 3H, OCH_3 of PEGMEMA), 3.20-3.12 (m, 1H, C*H*SCH2), 2.93-2.83 (m, 3H, CH_2S of Bodipy and CH_2CHS), 2.76-2.69 (m, 1H, CH_2CHS), 2.49 (s, 6H, NCCH_3 of Bodipy), 2.40 (s, 6H, CH_3C=C of Bodipy), 2.33 (t, 2H, *J* = 7.6 Hz, CCH_2 of Bodipy), 1.88–0.84 (m, 23H, $NCH_2CH_2CH_2O$, CH_2 and CH_3 of Bodipy, CH_2 and CH_3 along polymer backbone).

3.2.5.2. Conjugation of Copolymer P4 with Bodipy-SH (**P6**). Polymer **P4** (15.0 mg, 1.19 μmol) and BodipyC10SH (0.83 mg, 1.19 μmol) were dissolved in THF (0.15 mL) and triethylamine (0.07 μL, 0.48 μmol) was added into the reaction mixture. The reaction was allowed to proceed at room temperature for 24 h. Unreacted dye was removed by washing

the conjugate with cold diethyl ether several times. ^{1}H NMR analysis revealed that 52% of maleimides appended to the polymer chains were attached to BodipyC10SH. Dye conjugated polymer was obtained as a fluorescent viscous solid **P6** (13 mg, 83 % yield).

For polymer **P6**: ^{1}H NMR ($CDCl_3$, δ, ppm) 6.76 (s, 2H, C*H*=C*H*), 6.03 (s, 2H, *H*C=CCH_3 of Bodipy), 4.06 (s, 2H, OCH_2 ester protons of PEGMEMA), 3.92 (br s, 2*H*, OCH_2), 3.63-3.51 (m, 5H, OCH_2 of PEGMEMA and NCH_2), 3.45 (br s, 3H, OCH_3), 3.35 (s, 3H, OCH_3 of PEGMEMA), 3.19-3.11 (m, 1H, C*H*SCH_2), 2.93-2.82 (m, 3H, CH_2S of Bodipy and CH_2CHS), 2.75-2.69 (m, 1H, CH_2CHS), 2.48 (s, 6H, NCCH_3 of Bodipy), 2.39-2.32 (m, 8H, CH_3C=C and CCH_2 of Bodipy), 1.86–0.85 (m, 23H, $NCH_2CH_2CH_2O$, CH_2 and CH_3 of Bodipy, CH_2 and CH_3 along polymer backbone).

3.2.6. Conjugation of Polymers with cRGDfC via Thiol-ene Reaction

3.2.6.1. Conjugation of Copolymer P5 with cRGDfC (**P7**). Fluorescent dye conjugated polymer **P5** (5.0 mg, 0.57 μmol) and cRGDfC (0.49 mg, 0.86 μmol) were dissolved in distilled H_2O (0.10 μL) and the mixture was degassed for 3 minutes. Then, triethylamine (0.02 μL, 0.14 μmol) was added into the reaction mixture. The reaction was allowed to proceed at room temperature for 24 h. Unreacted peptide was removed by dialysis over distilled water using 1000 Da cut-off cellulose generated membrane. ^{1}H NMR analysis revealed that rest of maleimide groups appended to the polymer chains were conjugated to cRGDfC. Both dye and peptide conjugated polymer was obtained as a fluorescent viscous solid **P7** (4.3 mg, 81 % yield). ([BodipyC10SH]:[cRGDfC]= 4:1)

For polymer **P7**: ^{1}H NMR ($CDCl_3$, δ, ppm) 6.03 (s, 2H, *H*C=CCH_3 of Bodipy), 4.07 (s, 4H, OCH_2 ester protons of PEGMEMA and OCH_2), 3.64-3.53 (m, 5H, OCH_2 of PEGMEMA and NCH_2), 3.48-3.44 (m, 3H, OCH_3), 3.36 (s, 3H, OCH_3 of PEGMEMA), 3.23-3.17 (m, 1H, C*H*SCH_2), 2.93-2.83 (m, 2H, CH_2S of Bodipy), 2.49 (s, 6H, NCCH_3 of Bodipy), 2.40 (s, 6H, CH_3C=C of Bodipy), 2.33 (t, 2H, *J*= 7.7 Hz, CCH_2 of Bodipy), 1.66–0.84 (m, 25H, $NCH_2CH_2CH_2O$, CH_2 of Bodipy, CH_2 of cRGDfC, CH_2 and CH_3 along polymer backbone). ^{1}H NMR (D_2O, δ, ppm) 7.46-7.27 (m, 1H, N*H* of cRGDfC), 4.21 (br s, 4H, OCH_2 ester protons of PEGMEMA and OCH_2), 3.81-3.66 (m, 5H, OCH_2 of

PEGMEMA and NCH_2), 3.42 (br s, 3H, OCH_3 of PEGMEMA and OCH_3), 2.06–0.63 (m, 25H, NCH$_2$CH_2CH$_2$O, CH_2 of Bodipy, CH_2 of cRGDfC, CH_2 and CH_3 along polymer backbone). ^{1}H NMR (DMSO, δ, ppm) 8.00-7.93 (m, 2H, Ar-*H* of cRGDfC), 7.56-7.36 (m, 3H , Ar-*H* of cRGDfC), 7.34-7.14 (m, 1H, N*H* of cRGDfC), 6.22 (s, 2H, *H*C=CCH$_3$ of Bodipy), 4.02 (br s, 4H, OCH_2 ester protons of PEGMEMA and OCH_2), 3.60-3.43 (m, 5H, OCH_2 of PEGMEMA and NCH_2), 3.25 (br s, 3H, OCH_3 of PEGMEMA and OCH_3), 3.12 (br s, 1H, C*H*SCH2), 2.98-2.75 (m, 4H, CH_2S of Bodipy and CH_2CHS), 2.67 (br s, 2H, CH_2S of cRGDfC), 2.54 (s, 6H, NCCH_3 of Bodipy), 2.39 (br s, 2H, CH_2 of cRGDfC), 2.33 (br s, 3H, N*H* and NH_2 of cRGDfC), 1.73–0.79 (m, 25H, NCH$_2$CH_2CH$_2$O, CH_2 of Bodipy, CH_2 of cRGDfC, CH_2 and CH_3 along polymer backbone).

3.2.6.2. Conjugation of Copolymer P6 with cRGDfC (**P8**). Fluorescent dye conjugated polymer **P6** (5.0 mg, 0.61 μmol) and cRGDfC (0.35 mg, 0.61 μmol) were dissolved in distilled H_2O (0.10 μL) and the mixture was degassed for 3 minutes. Then, triethylamine (0.02 μL, 0.15 μmol) was added into the reaction mixture. The reaction was allowed to proceed at room temperature for 24 h. Unreacted peptide was removed by dialysis over distilled water using 1000 Da cut-off cellulose generated membrane. ^{1}H NMR analysis revealed that rest of maleimide groups appended to the polymer chains were conjugated to cRGDfC. Both dye and peptide conjugated polymer was obtained as a fluorescent viscous solid **P8** (3.8 mg, 72 % yield). ([BodipyC10SH]:[cRGDfC]= 2:1)

For polymer **P8**: ^{1}H NMR ($CDCl_3$, δ, ppm) 6.03 (s, 2H, *H*C=CCH$_3$ of Bodipy), 4.06 (s, 4H, OCH_2 ester protons of PEGMEMA and OCH_2), 3.64-3.54 (m, 7H, OCH_2 of PEGMEMA, NCH_2 and OCH_3), 3.36 (br s, 8H, OCH_3 of PEGMEMA, CH_2S of Bodipy, CH_2CHS and C*H*SCH$_2$), 2.49 (s, 6H, NCCH_3 of Bodipy), 2.40 (s, 6H, CH_3C=C of Bodipy), 1.87–0.83 (m, 25H, NCH$_2$CH_2CH$_2$O, CH_2 of Bodipy, CH_2 of cRGDfC, CH_2 and CH_3 along polymer backbone). ^{1}H NMR (D_2O, δ, ppm) 8.43 (s, 1H, COO*H* of cRGDfC), 7.44-7.22 (m, 1H, N*H* of cRGDfC), 4.17 (br s, 4H, OCH_2 ester protons of PEGMEMA and OCH_2), 3.77-3.62 (m, 5H, OCH_2 of PEGMEMA and NCH_2), 3.38 (br s, 3H, OCH_3 of PEGMEMA and OCH_3), 1.96–0.89 (m, 25H, NCH$_2$CH_2CH$_2$O, CH_2 of Bodipy, CH_2 of cRGDfC, CH_2 and CH_3 along polymer backbone). ^{1}H NMR (DMSO, δ, ppm) 8.50 (br s,

2H, Ar-*H* of cRGDfC), 7.98-7.85 (m, 3H , Ar-*H* of cRGDfC), 7.32-7.22 (m, 1H, N*H* of cRGDfC), 6.22 (s, 2H, *H*C=CCH$_3$ of Bodipy), 5.32 (br s, 1H, HNC*H* of cRGDfC), 5.00 (br s, 1H, HNC*H* of cRGDfC), 4.66-4.46 (m, 3H, HNC*H* of cRGDfC), 4.02 (br s, 2H, OCH_2 ester protons of PEGMEMA), 3.92-3.82 (m, 2H, OCH_2), 3.60-3.44 (m, 5H, OCH_2 of PEGMEMA and NCH_2), 3.25 (br s, 3H, OCH_3 of PEGMEMA and OCH_3), 2.89 (m, 2H, CH_2S of Bodipy), 2.73 (s, 6H, NCCH_3 of Bodipy), 2.67 (br s, 8H, CH_3C=C of Bodipy and CH_2S of cRGDfC), 2.47-2.40 (m, 2H, CH_2 of cRGDfC), 2.33 (br s, 3H, N*H* and NH_2 of cRGDfC), 2.15 (t, 2H, *J*= 7.6 Hz, CCH_2 of Bodipy), 1.66–0.79 (m, 25H, NCH$_2$CH_2CH$_2$O, CH_2 of Bodipy, CH_2 of cRGDfC, CH_2 and CH_3 along polymer backbone).

3.2.7. *In vitro* Experiments

3.2.7.1. Cytotoxicity Experiments. Cytotoxicity of thiol reactive copolymers and its imaging agent and targeting group conjugated versions were assessed by CCK-8 viability assay against adenocarcinoma MDA-MB-231 and healthy MCF-10A human breast cell lines. Cells (5000 cells/well) were seeded in a 96-well plate as quadruplet in 100 μL appropriate culture medium and incubated at 37 ^{o}C for 24 h for cells to adhere completely. Naked and functionalized polymers were dissolved in DMSO at 10^{-2} M stock concentration and seven different concentrations (0.1 nM to 0.1 mM) of samples were prepared via serial dilutions. Cells were treated with these samples and incubated at 37 C for 72 h. After removal of sample solutions, wells were washed with 100 μL PBS twice. The amount of viable cells was determined by CCK-8 cell viability assay by adding 10 μL CCK-8 reagent in 100 μL fresh medium onto wells and at the end of 1 h incubation absorbance values at 450 nm were measured via a microplate reader. EC50 values were calculated by GraphPad prism software using non-linear regression mode.

3.2.7.2. Internalization Experiments. Adenocarcinoma MDA-MB-231 and healthy MCF-10A human breast cells (10000 cells/well) were seeded in a 24-well plate as quadruplet in 500 μL appropriate culture medium and incubated at 37 ^{o}C for 24 h for cells to adhere completely. Then the culture medium was aspirated and replaced with fresh medium containing imaging agent functionalized copolymers at a concentration of 10^{-5} M. The experiments were completed in triplicate. After incubation at 37 ^{o}C for 12 h, sample solutions were removed. Wells were washed with 500 μL PBS twice and cells were

mounted with PBS containing DAPI (5 mg/mL) at 37 ^{o}C for 30 min. Then washed with PBS three times, cells were fixed with 4% formaline solution at 37 ^{o}C for 5 min. Images were collected by Zeiss Observer Z1 fluorescence microscope at room temperature.

3.3. Results and Discussion

As potential scaffolds for therapeutic agents, water soluble biocompatible and biodegradable polymers were designed and synthesized to bear furan-masked maleimide functionalities at their side chains. After the removal of furan molecules at high temperatures, obtained thiol reactive groups appended to polymer chains were furnished with a hydrophobic dye, Bodipy-SH, and a targeting peptide, cRGDfC using nucleophilic thiol-ene chemistry. Results of cytotoxicity experiments verify their strong potential in bio-applications.

3.3.1. Synthesis of Polymers with Naked Maleimide Units

Reactive polymeric scaffolds discussed in this study were attained by the copolymerization reaction of a PEG based methacrylate monomer and a furan masked maleimide containing monomer. Design of the project was based on the presence of furan masked maleimide units located at the side chains of the main polymer. To achieve this architecture, a methacrylate monomer possessing furan protected maleimide group was synthesized according to the literature [134]. Next, this reactive group containing monomer was copolymerized with a commercially available poly(ethylene glycol) monomethyl ether methacrylate (PEGMEMA, *Mn*= 300) monomer under mild conditions (Figure 3.3).

Regarding their utilization in various bioapplications, monomers constituting the polymeric scaffold play a very crucial role. Herein, PEGMEMA monomer increases degree of hydrophilicity and provides better water solubility to the system involved in. ATRP was chosen as a method of polymerization since it proceeds at low temperatures, that is important to keep the maleimide group in its masked form. Also the method enables

good control over molecular weight distribution with narrow polydisperties. In particular, a triethylene glycol based water soluble initiator was used as the alkyl halide initiator and polymerization was initiated by a complex of an alkyl halide (Cu(I)Br) and a transition metal complex (2,2'-bipyridine). Reaction time and solvent ratio were investigated for obtaining polymers with narrow polydispersities.

Table 3. 1. Polymerization conditions and characterization details of copolymers P1 and P2

No	Polymer	Dilution a) Solvent:M_{total} (w/v) b) MeOH:H_2O (v/v)	Feed Ratio [M1]:[M2][a]	Obtained Ratio [M1]:[M2][a,b]	GPC[c]		*M*n, theo (g/mol)	*M*n, NMR[b] (g/mol)	Conv. (%)
					M_n (g/mol)	M_w/M_n			
1	P1	a)6:1 b)1:1	8:1	8.3:1	30260	1.52	18430	8387	61
2	P2	a)6:1 b)1:1	16:1	16.2:1	35330	1.51	22090	7950	73

[a]M1:PEGMEMA, M2: latent reactive monomer (2), $[I]_0:[M_{total}]_0:[CuBr]:[Bipy]=1:100:1:2$, [b]calculated by integration values in ^{1}H NMR spectra, [c]estimated by SEC eluted with THF, relative to linear PS standards.

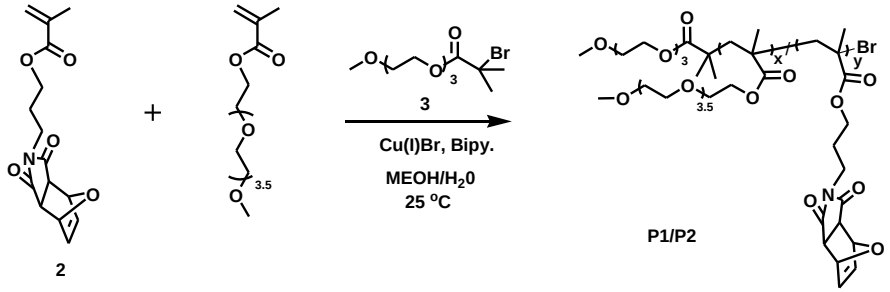

Figure 3. 2. Synthesis of furan masked maleimide group containing copolymers.

Based on same architecture, two copolymers were synthesized, namely **P1** and **P2**, differing from each other in terms of maleimide group content. By adjusting the feed ratio of latent reactive monomer with constant amount of PEGMEMA, P1 was synthesized to bear two times more maleimide groups at its side chain compared to P2. All conditions for the copolymerization reaction and characterization details of synthesized copolymers were reported in Table 3.1.

Utilization of the latent reactive monomer containing furan-maleimide cycloadduct unit relies on protection/deprotection strategy of maleimide group which is thermoreversible, since the Diels-Alder reaction (DA) between furan and maleimide units occurs at 80 ^{o}C and retro Diels-Alder reactionoccurs at 110 ^{o}C. So upon furan protection, polymerizable double bond of maleimide group can not participate into the copolymerization at ambient temperature which prevents cross-linking of monomers within each other.

After the polymerization, copolymers in hand were heated in toluene at 110 ^{o}C until all furan groups were removed from the polymer via the retro Diels-Alder reaction to reveal the maleimide units in active form (Figure 3.4). Complete cycloreversion of the furan-maleimide cycloadducts was verified by ^{1}H NMR spectroscopy.

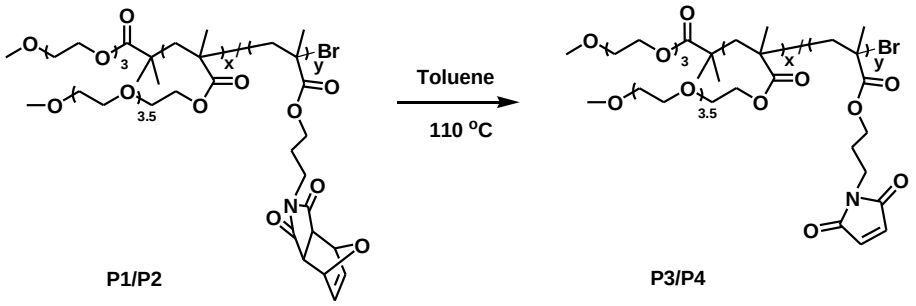

Figure 3. 3. Activation of maleimide groups of copolymers via retro Diels-Alder cycloreversion.

Synthesized reactive copolymers were analyzed by ^{1}H NMR spectroscopy to determine the degree of incorporation of maleimide monomer into the system and ratio of monomers after the polymerization. For example, characteristic peaks of furan-maleimide cycloadduct for P1 copolymer are easily seen at 6.52, 5.23 and 2.86 ppm (peaks a, b and c respectively, Figure 3.5a). Ratio of integration values for these peaks with that of a singlet belonging to methoxy group of PEGMEMA monomer at 3.35 ppm (peak d, Figure 3.5a) reveals the monomer ratios incorporated into the polymer structure. For both polymers, obtained monomer ratio is found to be almost same with the feed ratio of them.

Comparing ^{1}H NMR spectrum of P1 with that of its retro product P3, it can be clearly seen that disappearance of proton resonances belonging to furan group at 6.52 and 5.23 ppm, and shift of the peak representing maleimide group bridgehead protons from 2.86 ppm (peak c, Figure 3.5a) to 6.76 ppm (peak c, Figure 3.5b) indicates complete cycloreversion reaction and activation of all maleimide groups appended to polymer chain.

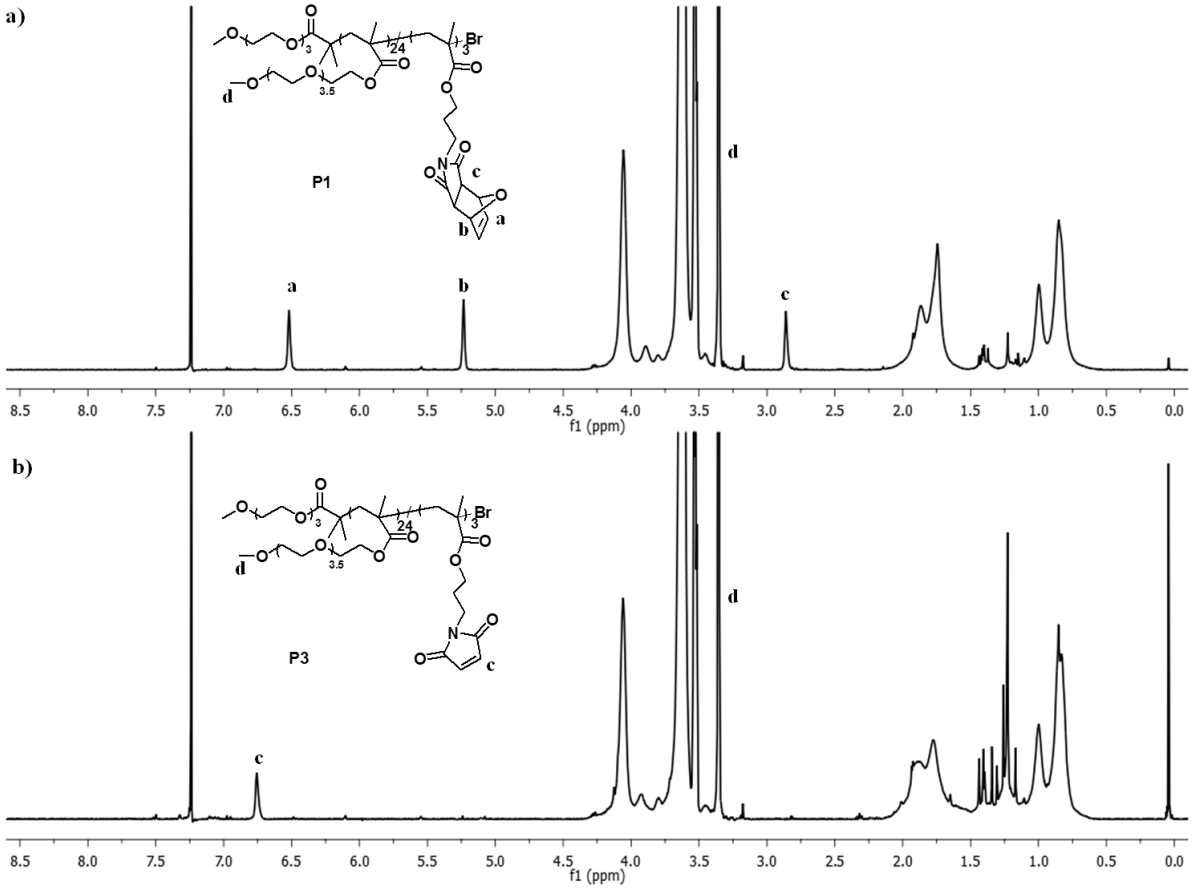

Figure 3. 4. ^{1}H NMR spectra of P1 (a) and P3 (b) in $CDCl_3$.

3.3.2. Conjugation of Polymers with Bodipy-SH and cRGDfC

Following activation of all maleimide units at side chains of copolymers, post-polymerization functionalization were exploited by two different compounds in a step-wise manner. Free thiol groups of these compounds enable their conjugation to copolymers via Michael type thiol-ene chemistry. Preferably, one of these free thiol bearing molecules is a hydrophobic dye, Bodipy C10SH. It has derivatized from a core bodipy structure which

consist of dipyrromethene complexed with a disubstituted boron atom. The fluorescent property originating from this structure allows them to serve as imaging agents upon attachment to scaffolds used for chemotherapy drug or protein delivery. BODIPY derivates are also known for their photodynamic properties and hence their chice also represents a model drug conjugation. Thiol-modified Bodipy molecule was synthesized according to literature procedures and purified by column chromatography [170].

Conjugation of the mentioned dye to copolymers was carried out in basic media. After generating a strong nucleophile of thiol with the help of triethylamine, some portions of maleimide groups appended to copolymer chains were attached to bodipy dye (Figure 3.6).

Amount of dye per polymer chain can be adjusted by playing with the stoichiometric ratios of BodipyC10SH and maleimide units of copolymers. This reaction was carried out in THF due to the hydrophobic nature of the dye, however its conjugation to PEG based copolymers solubilized it in water, thus demonstrating advantage of the designed copolymer to improve drug solubility.

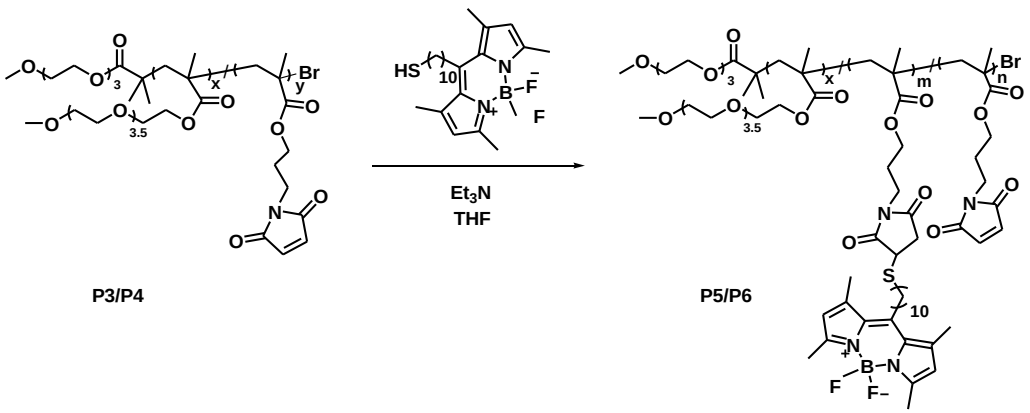

Figure 3. 5. Thiol-ene modification of copolymers with BodipyC10SH.

Efficiency of conjugation can be evaluated by comparing the integration values of characteristic peaks of both dye molecule and copolymer itself. ^{1}H NMR spectroscopy results clearly demonstrate proton resonances of polymer, dye and residual maleimide groups. In case of P1, for example, appearance of new peaks at 6.03, 2.49 and 2.40 ppm

(peaks e, f and g respectively, Figure 3.7b) distinctly indicates the conjugation of dye where the first mentioned peak coming from the pyrrole part of bodipy and the latter two peaks belong to methyl groups. Moreover, integration value of newly emerged bodipy peak at 6.03 ppm and decrease in integration value of proton resonance of maleimide unit at 6.76 ppm (peak c, Figure 3.7) correlate with each other, which suggests 80% conjugation.

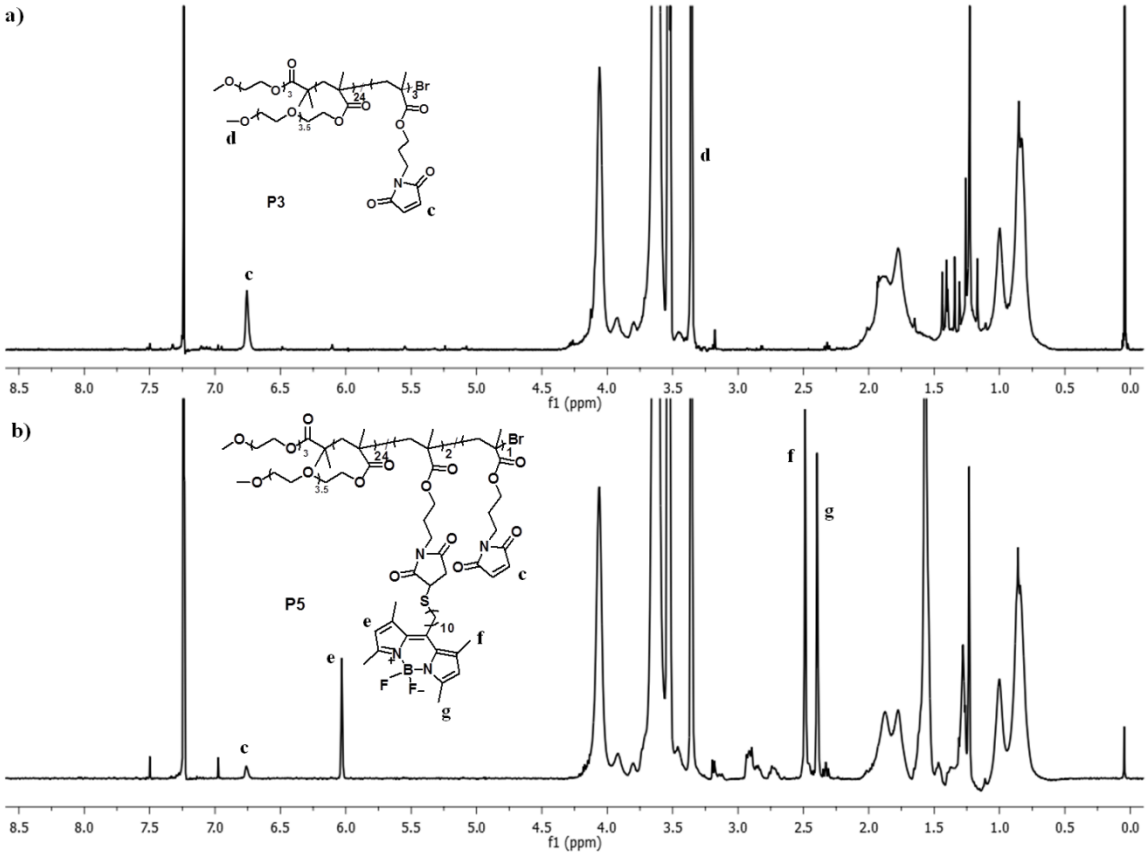

Figure 3. 6. ^{1}H NMR spectra of P3 (a) and P5 (b) in $CDCl_3$.

Remaining maleimide functionalities of copolymers were utilized for the attachment of a second thiol group containing compound, cRGDfC. This peptide composed of five amino acids is a commonly ligand used for the targeting integrin receptors located on the outer surface of cell membrane. Its cyclic structure makes the binding stronger and thiol functionality is gained by cystein residue.

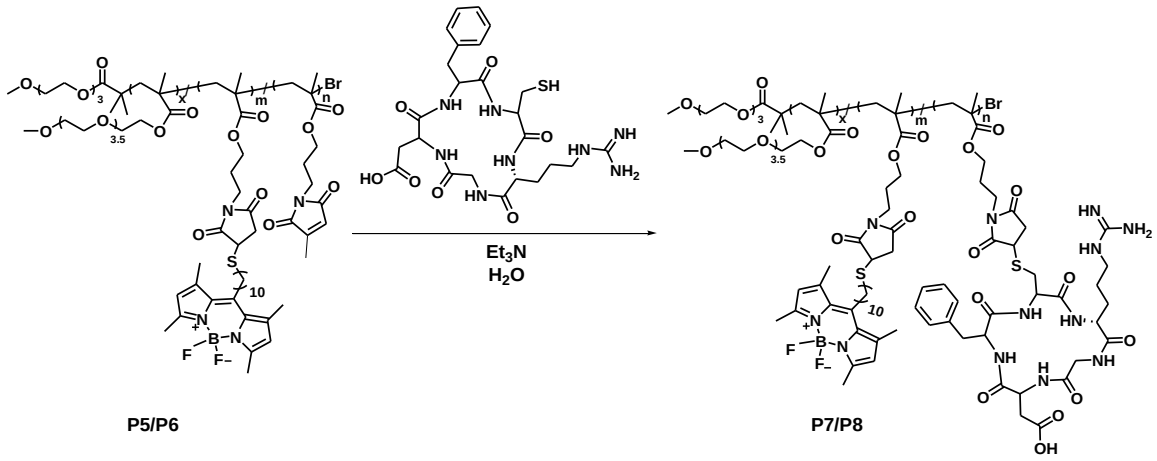

Figure 3. 7. Thiol-ene modification of BodipyC10SH conjugated copolymers with cRGDfC.

Due to hydrophilic nature of cRGDfC, conjugation reaction was performed in water medium in the presence of a base, triethylamine (Figure 3.8). After removal of excess peptide from the system by dialysis in distilled water, the resultant copolymers were characterized by ^{1}H NMR spectroscopy. For P1, high efficiency can be easily apprehended from the complete disappearance of proton resonance of maleimide group and emergence of new peaks of peptide in down field region between 7-8 ppm. At the same time proton resonances of bodipy dye seen at 6.03, 2.49 and 2.40 ppm (Figure 3.9b). Conjugation of peptide to polymer backbone was confirmed by NMR analysis performed in D_2O and DMSO. In Figure 3.9c, proton resonances coming from labile hydroxyl and amine hydrogens points to the presence of peptide cRGDfC. Considering the hydrophobic nature of bodipy dye, it was not surprising to see the absence of any characteristic peaks belonging to dye in this spectrum. However, all proton resonances specifying the presence of dye, peptide and polymer itself could be detected by performing ^{1}H NMR analysis in DMSO. Presence of resonances at 6.22 ppm originating from the proton on the pyrrole ring of bodipy dye, and labile hydrogens and aromatic protons of phenylalanine unit of peptide around 7-8 ppm prove successful conjugation to copolymer (Figure 3.9d).

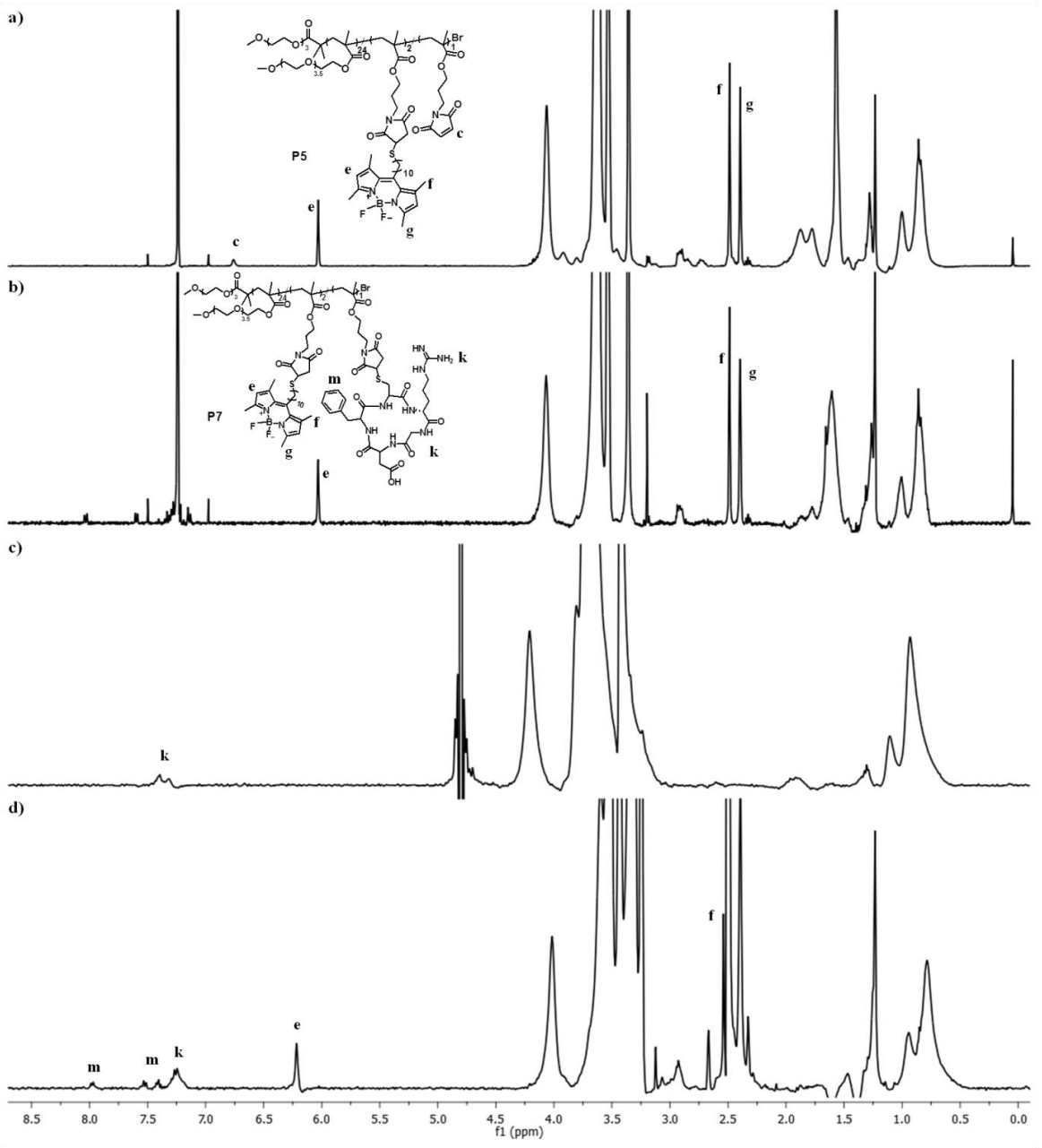

Figure 3. 8. ^{1}H NMR spectra of P5 (a) in $CDCl_3$ and P6 (b) in $CDCl_3$, (c) in D_2O and (d) in DMSO.

3.3.3. *In vitro* Experiments

3.3.3.1. *In vitro* cytotoxicity assay. Cytotoxic activities of thiol reactive polymers and their conjugates with imaging agent, BodipyC10SH and targeting group, cRGD were investigated over MDA-MB-231 and MCF-10A human breast adenocarcinoma and healthy

cell lines, respectively and compared with each other. Cells adhered to 96-well plates were treated with drug and polymer-drug samples at 37 ^{o}C for 72h. Cell viability was evaluated by a colorimetric assay, CCK-8 and obtained absorbance values at 450 nm were processed by GraphPad prism software using non-linear regression curve with a sigmodial dose response equation. By this way, EC_{50} values, concentration at which the molecule displaces half of its toxic activity over cells, for all polymers were calculated from the cytoxicity graphs. Results demosnstrated the EC_{50} values for all polymers examined as more than 100 μM which reveal almost no toxicity for all of them. In each case, cell viability did not decrease remarkably even at high concentrations of polymers (Figure 3.10&3.11). P1 and P2 are the polymers decorated with furan masked maleimide groups where the ratio of PEGMEMA to maleimide containing monomer is 8:1 for P1 and 16:1 for P2. Their imaging agent conjugated forms are P5 and P6, respectively. Ratio of imaging agent and targeting group for P7 and P8 are 4:1 and 2:1 respectively.

Growth inhibition results showed that all conjugates P5-8 are almost not toxic to both cancerous and healthy breast cells, which supports their potential as delivery vehicles for several therapeutic agents with free thiol groups.

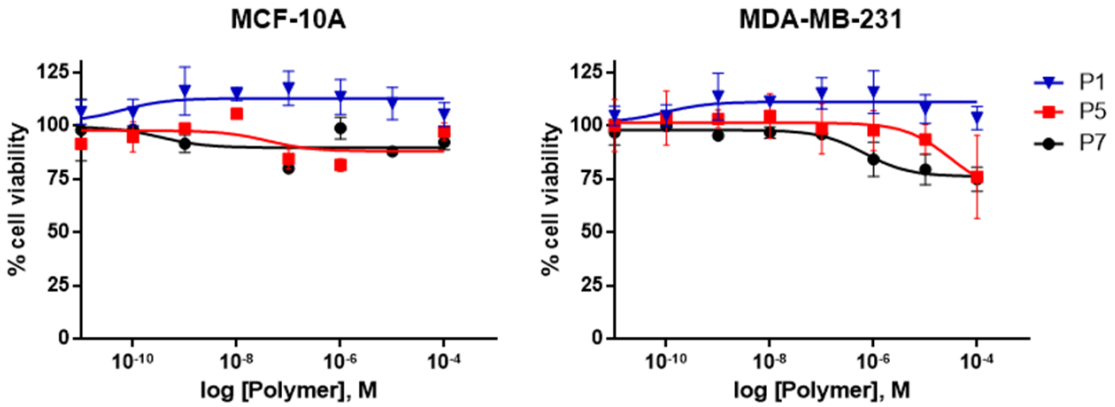

Figure 3. 9. Inhibition of MDA-MB-231 and MCF-10A cells proliferation by P1 (thiol reactive polymer), P5 (bodipy conjugated polymer) and P7 (both bodipy and cRGD conjugated polymer). Cell viability was determined by CCK-8 assay. Results were expressed as mean ± SD (n = 4).

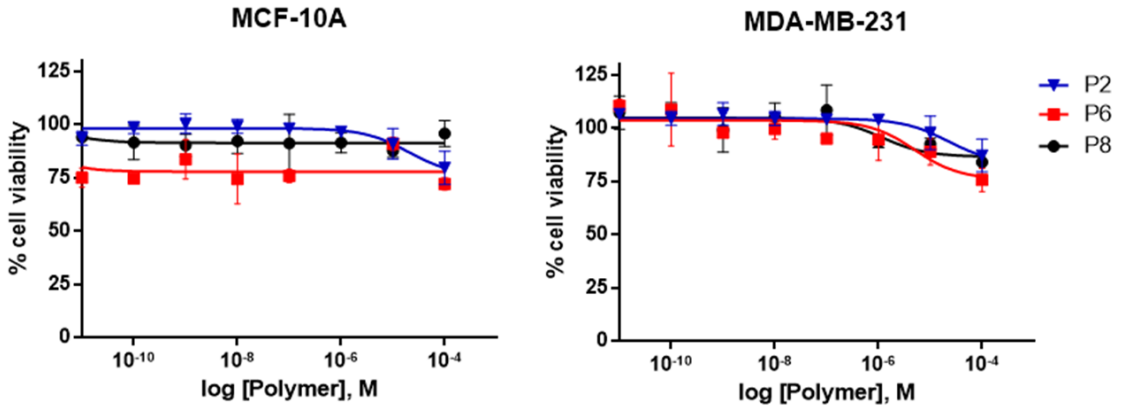

Figure 3. 10. Inhibition of MDA-MB-231 and MCF-10A cells proliferation by P2 (thiol reactive polymer), P6 (bodipy conjugated polymer) and P8 (both bodipy and cRGD conjugated polymer). Cell viability was determined by CCK-8 assay. Results were expressed as mean ± SD (n = 4).

3.3.3.2. *In vitro* internalization assay. Uptake of bodipy conjugated polymers was examined over adenocarcinoma MDA-MB-231 and healthy MCF-10A human breast cell lines. Bodipy molecule is already fluorescent and can be visualized by green fluorescence filter. However cell nuclei were detected by staining with DAPI, which can be visualized by a blue fluorescence filter. Cultured cells with a density of 10000 cells per well were treated with polymer samples of 10^{-5} M and incubated at 37 ^{o}C for 24 h for efficient internalization. After removal of sample solutions, wells were washed with PBS and DAPI staining was examined. Following the fixation process by formalin, cells were visualized by appropriate fluorescence filters at room temperature. Figure 3.12 displays the fluorescence patterning of internalized polymers from which P5 and P6 bears just bodipy, and P7 and P8 consist of both bodipy and cRGD over both cancerous and healthy cells. Results clearly indicates that cell internalization were observed for all polymers over almost same cell density, however green fluorescence intensity is remarkably higher for both P7 and P8 due to presence of the targeting group, cRGD which binds to integrin receptors located on the outer surface of cells with strong affinity.

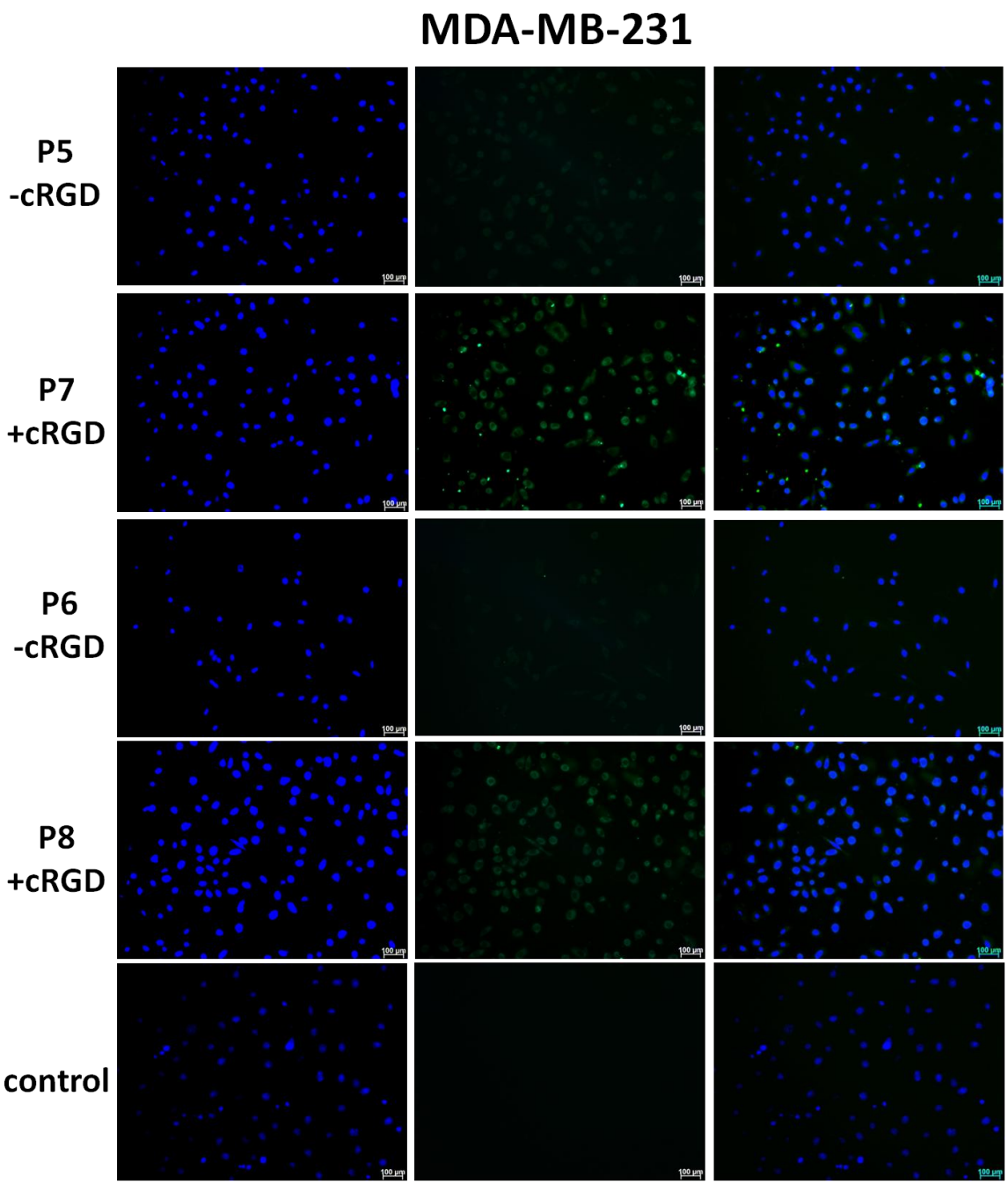

Figure 3. 11. Fluorescence images of MDA-MB-231 cells treated with Bodipy conjugated polymers. Cells were incubated at 37 ^{o}C for 24 h and nuclei were stained by DAPI just prior to imaging. (A) shows blue fluorescence of cell nuclei stained by DAPI, (B) shows green fluorescence of internalized Bodipy conjugated polymers, (C) shows the merged images.

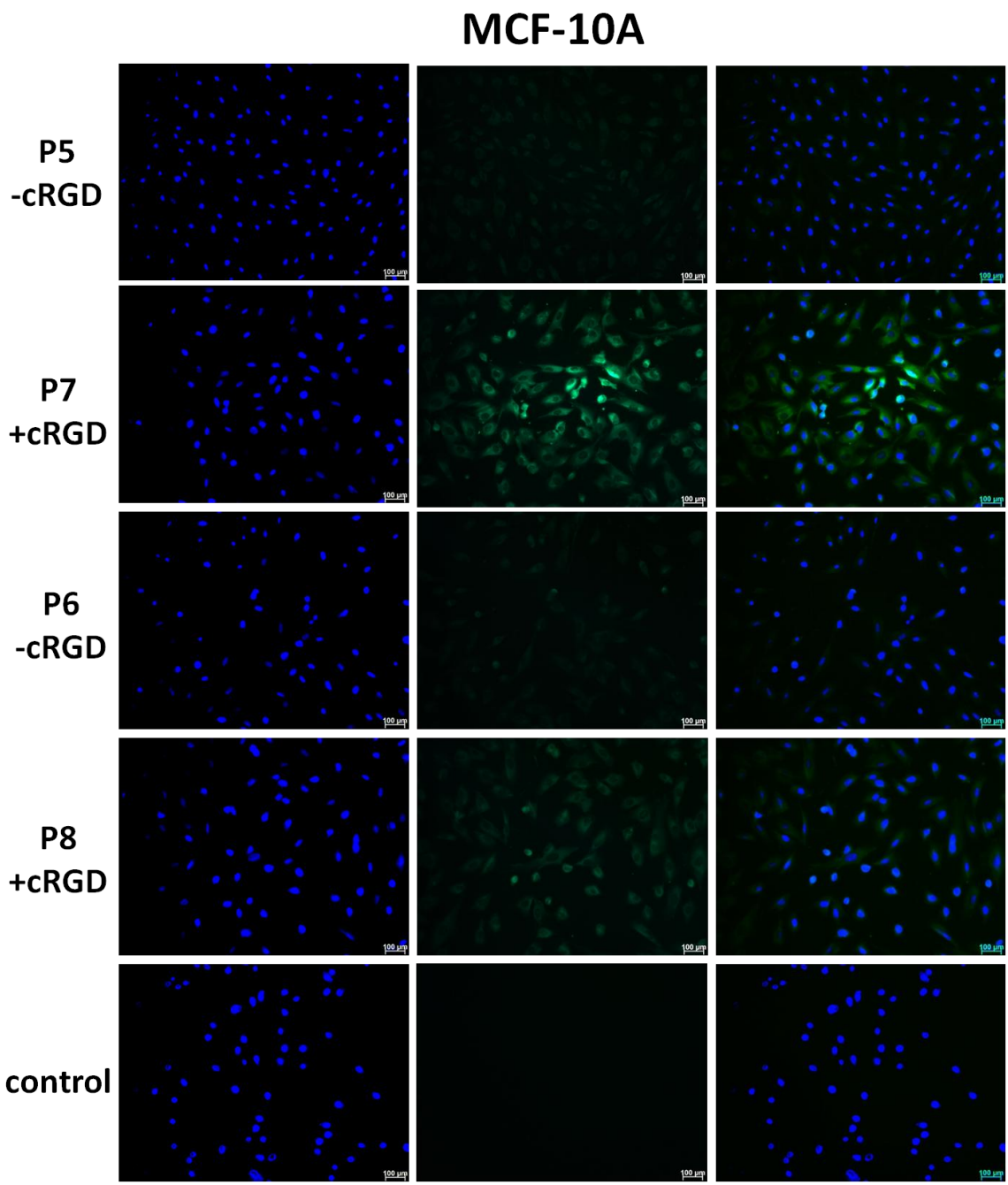

Figure 3. 12. Fluorescence images of MCF-10A cells treated with Bodipy conjugated polymers. Cells were incubated at 37 ^{o}C for 24 h and nuclei were stained by DAPI just prior to imaging. (A) shows blue fluorescence of cell nuclei stained by DAPI, (B) shows green fluorescence of internalized Bodipy conjugated polymers, (C) shows the merged images.

3.3. Conclusion

In summary, a novel class of functional thiol reactive polymers was developed as drug delivery and targeted imaging platforms. Maleimide groups were incorporated into the copolymer using a furan-protected methacrylate based monomer and incorporated as side chains of PEG methacrylate based polymers to enable the attachment of thiol group containing dyes(imaging agents) and peptides (targeting groups). These water soluble PEG-based copolymers were designed to increase the surface hydrophilicity of the carrier and decrease the non-specific interactions with biomolecules. Copolymerization was carried out by utilization of ATRP since this method provides polymers with good control over molecular weight and narrow polydispersity value. Importantly, the polymerization can be conducted at ambient temperatures to avoid any unmasking of the reactive maleimide group. Maleimide groups in the copolymers were obtained quantitatively in their native form by heating the polymer after polymerization. Efficiency of post-polymerization functionalization was evaluated by conjugation of a hydrophobic dye, Bodipy-SH, and a targeting peptide, cRGDfC from their available thiol groups via Michael type nucleophilic thiol-ene reaction. These conjugates were subjected to *in vitro* experiments over both cancerous (MDA-MB-231) and healthy (MCF-10A) breast cell lines. Obtained results show that these conjugates can be uptaken by both cell types and are non-toxic to cancer and healthy cells, which raises their potential to be used as platforms in bioapplications. The presence of the peptide based targeting group had a clear effect in increasing the uptake of the dye-conjugated polymer into cells when compared to the construct devoid of the peptide.

4. CHEMOTHERAPY DRUG CONJUGATED POLYMERIC SCAFFOLDS: SMART FORMULATIONS AS POLYMER THERAPEUTICS

The materials in this chapter have been adapted with modifications from the following project: “Drug Delivery Systems for Chemotherapy” No: 00589.STZ. This project was based on university-industry collaboration for innovation and R&D between 2010 and 2014 in the field of cancer therapies and supported by Ministry of Science, Industry and Technology of Turkey. Due to confidential issues, industrial company and the chemotherapy drug investigated in this project could not be revealed in this dissertation.

Recent advances in designing versatile synthetic macromolecular structures provide new-era investigators with attractive drug delivery systems where it becomes possible to combine cooperative contributions of scientific fields like organic chemistry, molecular biology, medicine, pharmacology, biomedical engineering, etc [175, 176]. Interesting architectures of polymeric materials that can be engineered to behave like natural ones open the door to promising approaches and formulations to introduce and device new drug carriers for treatment of several different diseases [177-180].

Current technologies modifying drug molecules and developing new delivery systems were evaluated with considerable attention in cancer therapy [181]. Immense work has being endeavored for cancer patients to prolong life time or reduce symptoms by removing the tumor tissue. Conventional cancer therapies including surgery, chemotherapy and radiotherapy play a limited but significant role in the overall treatment of most solid tumors. However, therapeutic activity of most anticancer drugs in clinics or market is not sufficient due to limited accessibility of drugs to the tumor tissue, their intolerable toxicity, development of multi-drug resistance and dynamic heterogeneous biology of the growing tumors.

It is well-known that tumor tissue is generated by abnormally growing mutated cancerous cells and has the potential to invade nearby tissues and spread throughout the

body by the lymphatic system. That is why most of the chemotherapy agents utilized for the treatments of cancer are programmed to prevent the proliferation of rapidly growing cells through various mechanisms to inhibit cell division process [182-184]. Unfortunately they are not targeted to the cell or tissue type and this non-specificity makes it inevitable for other healthy rapidly dividing cells in the body to be damaged including bone marrow, hair follicles, lining of the digestive tract, etc. Shortly, resultant toxicity may cause side effects that can vary from person to person and limit the drug administration dose to the patient which prolongs the therapy period. Moreover, that chemotherapy drugs are low molecular weight compounds accounts for their reduced circulation time in blood stream and low degree of bioavailability due to rapid clearance through the kidneys once they are administered to the patient [185, 186].

At this crutial point, better understanding of tumor tissue structure and defects of chemotherapy agents allow the scientists to develop new drug delivery approaches suggesting successful drug carriers for cancer therapy. Out of these innovative platforms, polymer therapeutics concept has been distinguished as a promising strategy to overcome the toxicity and bioavailability problems of chemotherapy drugs [11], [181], [187]. Recent years have witnessed great attention towards synthesizing novel polymeric materials with superior physical properties and versatile chemical functionalities for conjugating drugs, targeting and imaging agents for addressing the tumor tissue [12], [188-190].

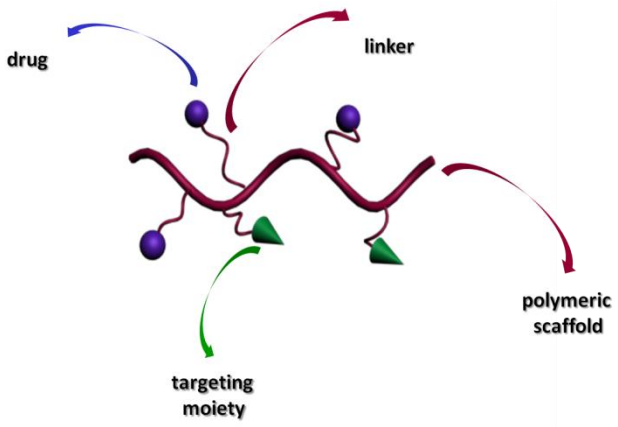

Figure 4. 1. Illustration of a typical polymeric construct for targeted drug delivery.

Undoubtedly, high molecular weight polymers conjugated to drug molecules enable their passive targeting to tumor tissue by a phenomenon called “enhanced permeability and retention effect” (EPR effect) explained more in Chapter 1. Through the leaky structure of unorganized cancerous cells, mentioned conjugate can pass easily and accumulate in tumor tissue to a great extent whereas this possibility is almost not valid for well-packed healthy tissue. Furthermore, compared to small drug molecules, these high molecular weight and compact polymeric materials are excreted from the kidney at a slower rate enabling the latter to circulate in the blood stream for a longer time which is needed for its accumulation in the tumor. So conjugating chemotherapy drugs to polymers localizes them at one place decreasing toxicity and side effects to healthy tissues. It is evident from this elucidation that desired efficacy within a longer half-life period is directly related to an increase in bioavailability of chemotherapy drugs in tumor tissue upon conjugation to polymeric scaffolds. Along with the contribution of higher loading capacity of polymer chains due to multivalency of reactive groups per chain, polymer therapeutics provides less frequent dose application and decreased administration rate which is a serious issue for the patient convenience and compliance [17-19], [191, 192].

Following the challenging breakthroughs of polymer therapeutics, in this part of thesis work, a chemotherapy drug was conjugated to high molecular weight HPMA polymers with unique formulations in its structure to form its reactive monomers. Instead of post-polymerization modification methods where drug molecules are attached to side chains of polymer after polymerization step, in this study drug molecule was introduced to the system in the polymerization process which eliminates the solubility problems of chemotherapy drugs and low degree of conjugation due to steric hindrance of polymer chains.

As its name implies, the content of this chapter is related to design and synthesis of polymer-drug conjugates with novel formulations of an anti-metabolite chemotherapy drug that was introduced with polymerizable methacrylate functionality with the help of three different naturally degradable linking options. Specifically acid labile and enzymatically cleavable linkers were utilized in drug containing monomer synthesis and as a next step,

copolymerization with HPMA monomer over free radical polymerization yielded water soluble and biocompatible drug conjugated high molecular weight copolymers (Figure 4.3). Drug molecule was modified through necessary reagents to form its monomer versions. In the first case, it was conjugated to copolymer via ortho-ester, an acid labile group and it was expected to hydrolize in more acidic environment of tumor tissue due to increased level of glycolysis there [193]. Switching to other monomer was realized by conjugating drug to a tetrapeptide Gly-Phe-Leu-Gly (GFLG) degraded by thiol-dependant proteases, particularly cathepsin B [194]. In the structure of last monomer, drug molecule was conjugated to copolymer backbone via an amide group where drug was envisioned to release from the system depending on enzymatic hydrolysis of glutamic acid peptides [195]. As a result of many efforts to synthesize and purify these drug conjugated monomers and polymers together with their characterization studies, first two constructs mentioned above were evaluated for their *in vitro* activity on two different breast cancer cell lines and *in vivo* behavior to support their potent as tumor seeking polymeric prodrugs utilizing EPR-effect.

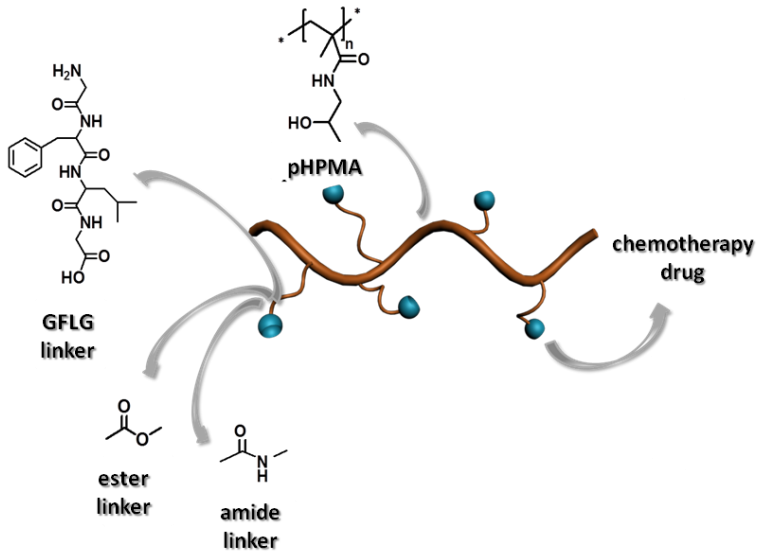

Figure 4. 2. Synthetic approach towards chemotherapy drug conjugated polymers via three different biodegradable linkers.

5. SEQUENCE-CONTROLLED POLYMERIZATION USING DENDRITIC MACROMONOMERS: PRECISE CHAIN-POSITIONING OF BULKY FUNCTIONAL CLUSTERS

The materials in this chapter have been adapted with modifications from the following article: Baradel, N., O. Gok, M. Zamfir, A. Sanyal and J.-F. Lutz, *Chem. Commun.*, Vol. 49, pp. 7280-7282, 2013.

5.1. Introduction

Especially in the last decades, the design and synthesis of macromolecular structures with high degree of structural and functional control have been widely investigated [196]. Despite the diversity of living polymerization methods, control over the molecular weight, size and topology of macromolecules needs to be improved to structurally resemble and therewith act as those found in nature [197].

An important breakthrough in the field was the discovery of dendrimers, which are highly ordered, spherical and monodisperse macromolecules which can be synthesized by stepwise organic reactions [198]. A dendron is a part of the dendrimer that starts from a single, chemically addressable focal point and ends at the periphery (Figure 5.1). Large number of functional groups enables multivalency to the dendritic construct [199]. Dense functional clusters are present in many biological systems and play a pivotal role in multivalent biological recognition processes [117]. Due to the multivalency displayed by dendritic structures, they have been incorporated into polymeric materials to promote interactions with biomolecules [200].

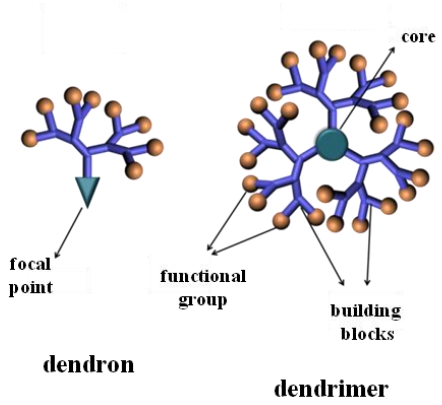

Figure 5. 1. Schematic representation showing subunits of dendrimers [3].

Although functional polymeric materials provide scaffolds with a wide range of improved properties, positioning of reactive groups along the polymer backbone is a crutial issue for the generation of clusters of functional groups [201]. Shortly after, dendrimers have been utilized to introduce reactive groups to the polymer structure [202], [110]. This interesting class of macromolecules combines some features of dendrimers and linear polymers [203]. For instance, such polymers often exhibit a high persistence length and a high density of functional groups. Molecular architecture of dendronized polymers can be controlled with high precision in terms of size, stiffness and surface decoration. Using modern polymerization strategies, various types of dendronized architectures have been reported in recent literature (Figure 5.2) [204- 206].

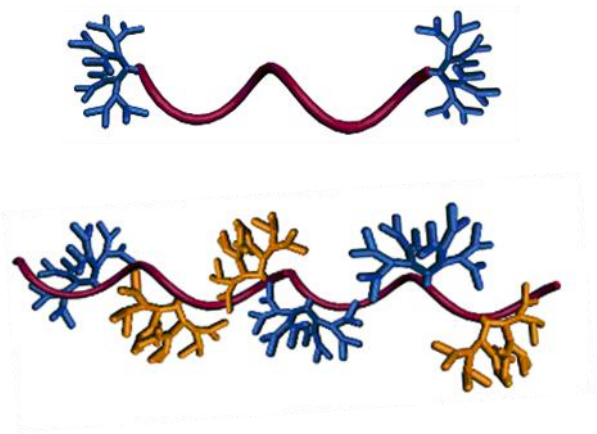

Figure 5. 2. Dendron containing macromolecular structures.

Needless to say, in order to design and create functional macromolecular constructs like the ones in nature, monomer sequence control at the primary level will play a pivotal role [207]. In this light, the design of sequence-controlled polymers is becoming an active area of research [208]. Some years ago, Lutz and coworkers proposed a strategy to obtain polymers with precise positioning of monomers at desired locations along the polymer backbone. The strategy relies on the kinetically favored cross-propagation of two comonomers in the polymerization feed. In particular, the poor tendency of an *N*-substituted maleimide (MI) to homopolymerize but efficiently copolymerize with a styrenic monomer can be utilized to obtain polymers with high degree of positional control [209]. Introduction of an amount of MI comparable to the amount of the initiator, into the feed of an ongoing polymerization results in rapid incorporation of the MI into the growing chain. Moreover, the methodology allows the introduction of a variety of different functional groups along a single polymer chain sequentially [210]. All these features open up interesting avenues for the design of complex functional macromolecular structures [211-212].

The present study demonstrates that this methodology can be extended to install a bulky functional dendron at a precise location in a polymer chain (Figure 5.3). This new strategy provides a modular approach towards the synthesis of polymers bearing clusters of functional groups.

To achieve the disposition of clusters of functional groups at precise locations along the polymer backbone, dendrons bearing a maleimide unit at their focal points were utilized as monomers (Figure 5.3). Nitroxide-mediated polymerization (NMP) using a commercially available alkoxyamine initiator, BlocBuilder MA®, was used to synthesize these copolymers. In this study, various generations of dendrons containing either acetal or hydroxyl groups at their periphery were synthesize. The pendant hydroxyl group containing dendron can be utilized as a handle for facile post-polymerization modification to install well-positioned clusters of desired functionality along the polymeric backbone. We also investigated the direct installation of a dendron containing several alkene units at the periphery along with the required maleimide group at the focal point. While the

electron-deficient maleimide group participates in the polymerization reaction, the alkene moiety should be an inert functional group. More importantly, the insertion of alkene groups yields a polymer that can be appended with desired molecules using a thiol-ene click reaction [137], [213].

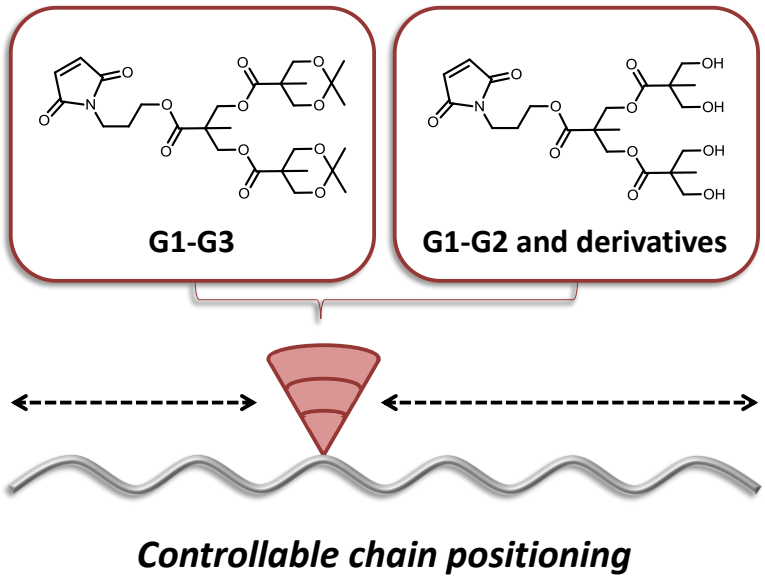

Figure 5. 3. Synthetic approach towards precise chain-positioning of bulky functional clusters.

5.2. Experimental

5.2.1. Materials

The maleimide-containing dendrons 3-(2,5-dioxo-2,5-dihydro-1H-pyrrol-1-yl)propyl 2,2,5-trimethyl-1,3-dioxane-5-carboxylate (**D1** R-G1M-X), 2-((3-(2,5-dioxo-2,5-dihydro-1H-pyrrol-1-yl)propoxy)carbonyl)-2-methylpropane-1,3-diyl bis(2,2,5-trimethyl-1,3-dioxane-5-carboxylate) (**D2** R-G2M-X), (((2-((3-(2,5-dioxo-2,5-dihydro-1H-pyrrol-1-yl)propoxy)carbonyl)-2-methylpropane-1,3-diyl)bis(oxy))bis(carbonyl))bis(2-methylpropane-3,2,1-triyl)tetrakis(2,2,5-trimethyl-1,3-dioxane-5-carboxylate) (**D3** R-G3M-X) were synthesized according to literature procedures [98], [104]. 3-(2,5-dioxo-2,5-dihydro-1H-pyrrol-1-yl)propyl 3-hydroxy-2-(hydroxymethyl)-2-methylpropanoate (**D4** R-

G1M-OH), 2-((3-(2,5-dioxo-2,5-dihydro-1H-pyrrol-1-yl)propoxy)carbonyl)-2-methylpropane-1,3-diyl bis(3-hydroxy-2-(hydroxymethyl)-2-methylpropanoate) (**D5** R-G2M-OH), and 2-((3-(2,5-dioxo-2,5-dihydro-1H-pyrrol-1-yl)propoxy)carbonyl)-2-methylpropane-1,3-diyl bis(2-methyl-3-(pent-4-enoyloxy)-2-((pent-4-enoyloxy)methyl)propanonate) (**D6** R-G2M-alkene) were synthesized as explained below. The *N*-(2-methylpropyl)-*N*-(1-diethylphosphono-2,2-dimethylpropyl)-*O*-(2-carboxylprop-2-yl)-hydroxylamine initiator (BlocBuilder®, Arkema, 99 %), 4-dimethylaminopyridine (DMAP, 99%, Sigma Aldrich), 4-pentenoic anhydride (98%, Sigma Aldrich) and pyridine (99%, Merck) were used as received without further purification. Styrene (Sigma Aldrich, 99%) was distilled over CaH_2 and stored under argon atmosphere at low temperature prior to use. Column chromatography was performed using silicagel–60 (43–60 nm). Thin layer chromatography was performed using silica gel plates (Kiesel gel 60 F254, 0.2mm, Merck).

5.2.2. Instrumentation

5.2.2.1. Nuclear Magnetic Resonance Spectroscopy (NMR). The NMR spectra were recorded using a 400 MHz Bruker Avance or a 400 MHz Varian spectrometer at 25 °C. ^{1}H NMR measurements were made at frequency of 400.13 MHz, and calibrated with respect to the solvent signal. The measurements were performed in deuterated chloroform ($CDCl_3$).

5.2.2.2. Size Exclusion Chromatography (SEC). Characterizations of copolymers were performed at 30 °C in THF at a flow rate of 1 mL/min. The number-average molar mass (M_n) and the polydispersity index (M_w/M_n=PDI) were estimated using a calibration based on linear polystyrene standards (PSS, Germany). The SEC set-up was equipped with four 5 µ-SDV columns (PLgel mixed C, one guard column and three columns of 4.10^3, 3.10^5, 2.10^6 Å). The detection was performed with a refractometer (DN-1000, WGE Dr. Bures) and a UV/Vis detector (UV 2000, 260 nm).

5.2.2.3. MALDI-TOF Mass Spectroscopy (MS). The MALDI-TOF MS spectrum acquisition for R-G2M-alkene was obtained on a Shimadzu Biotech Axima Performance System using 2,5-dihydroxybenzoic acid as a matrix.

5.2.2.4. Fourier Transform Infrared Spectroscopy (FT-IR). Functional group analysis was performed for R-G1M-OH and R-G2M-OH by Fourier transform infrared (ATR-FT-IR) spectroscopy as Thermo Fisher Scientific Inc. Nicolet 380 with 7800 – 350 cm^{-1} using proprietary KBr beamsplitter.

5.2.3. Synthesis of Dendron-Functionalized Maleimides

5.2.3.1. Synthesis of R-G1M-OH. Furan protected maleimide containing first generation polyester dendron with acetal units at the periphery (G1M-X) was synthesized according to the literature. This compound (1.00 g, 2.64 mmol) was dissolved in THF (10 mL) and to this solution 1M HCl solution (10 mL) was added. The resulting mixture was stirred at 25 ^{o}C until the consumption of G1M-X was observed via thin layer chromatography. Then, THF was evaporated and the resulting aqueous solution was extracted with CH_2Cl_2, and the organic layer was dried over anhydrous Na_2SO_4. The residue was concentrated *in vacuo*. The crude product was purified by column chromatograpy to give G1M-OH (0.78 g, 89 %). The obtained product (0.30 g, 0.88 mmol) was then dissolved in toluene (100 mL) and heated up to 100 ^{o}C. After the reaction mixture was stirred for 24 hours, toluene was evaporated and the crude product was purified by column chromatograpy to give R-G1M-OH as a white solid (0.21 g, 88 %).^{1}H NMR ($CDCl_3$, δ, ppm) 6.69 (s, 2H, CH=CH), 4.11 (t, 2H, *J* = 6.0 Hz, OCH_2), 3.88 (d, 2H, *J* = 11.2 Hz, $HOCH_2$), 3.74 (d, 2H, *J* = 11.2 Hz, $HOCH_2$ protons), 3.64 (t, 2H, *J*= 6.8 Hz, NCH_2), 2.91 (br s, 2H, OH), 2.02-1.94 (m, 2H, $NCH_2CH_2CH_2O$), 1.09 (s, 3H, $C(CH_3)$). ^{13}C NMR ($CDCl_3$, δ, ppm) 175.7, 170.8, 134.2, 68.1, 61.3, 49.5, 34.3, 27.5, 17.2. Anal. calcd. for R-G1-OH [$C_{12}H_{17}NO_6$]: C, 53.13; H, 6.32; N, 5.16. Found: C, 53.17; H, 6.42; N, 5.32.

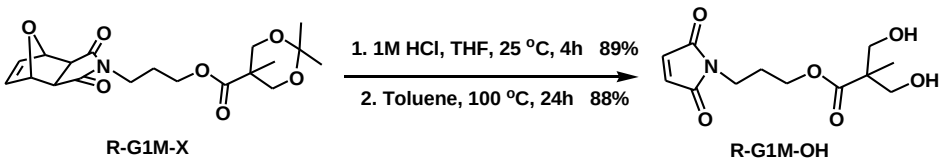

Figure 5. 4. Synthesis of R-G1M-OH.

5.2.3.2. Synthesis of R-G2M-OH. Furan protected maleimide containing second generation polyester dendron with acetal units at the periphery (G2M-X) was synthesized according to the literature. This compound (3.70 g, 5.68 mmol) was dissolved in THF (30 mL) and to this solution 1M HCl solution (30 mL) was added. The resulting mixture was stirred at 25 ^{o}C until the consumption of G2M-X was observed via TLC. Then, THF was evaporated and the resulting aqueous solution was extracted with CH_2Cl_2, and the organic layer was dried over anhydrous Na_2SO_4. The residue was concentrated in *vacuo*. The crude product was purified by column chromatograpy to give G2M-OH (2.70 g, 84 %). The obtained product (0.60 g, 1.05 mmol) was then dissolved in toluene (200 mL) and heated up to 100 ^{o}C. After the reaction mixture was stirred for 24 hours, toluene was evaporated and the crude product was purified by column chromatograpy to give R-G2M-OH as a white solid (0.39 g, 74 %). ^{1}H NMR ($CDCl_3$, δ, ppm) 6.70 (s, 2H, CH=CH), 4.43 (d, 2H, *J* = 11.2 Hz, CH_2 ester protons), 4.28 (d, 2H, *J* = 11.2 Hz, CH_2 ester protons), 4.10 (t, 2H, *J* = 5.8 Hz, OCH_2), 3.81 (dd, 4H, *J* = 11.4, 2.4 Hz, $HOCH_2$ protons), 3.69 (dd, 4H, *J* = 11.4, 2.4 Hz, $HOCH_2$ protons), 3.61 (t, 2H, *J*= 6.4 Hz, NCH_2), 2.50 (br s, 4H, OH protons), 1.98-1.92 (m, 2H, $NCH_2CH_2CH_2O$), 1.31 (s, 3H, $C(CH_3)$), 1.04 (s, 6H, $C(CH_3)_2$). ^{13}C NMR ($CDCl_3$, δ, ppm) 175.1, 172.8, 170.7, 134.2, 60.8, 64.9, 62.4, 49.8, 46.5, 34.5, 27.6, 18.0, 17.1. Anal. calcd. for R-G2-OH [$C_{22}H_{33}NO_{12}$]: C, 50.91; H, 6.74; N, 2.70. Found: C, 50.74; H, 6.68; N, 2.69.

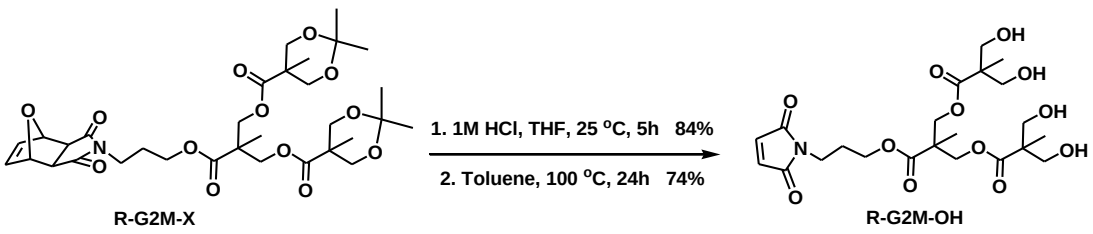

Figure 5. 5. Synthesis of R-G2M-OH.

5.2.3.3. Synthesis of R-G2M-alkene. Furan protected maleimide containing second generation polyester dendron with hydroxyl units at the periphery (G2M-OH) was synthesized as described before. To a solution of G2M-OH (0.40 g, 0.61 mmol) in CH_2Cl_2 (25 mL), 4-pentenoic anhydride (1.02 g, 5.60 mmol), DMAP (0.14 g, 1.15 mmol) and pyridine (0.51 mL) were added. The mixture was stirred at 25 ^{o}C for 24 hours followed by

quenching of excess anhydride with (1:1 v/v) mixture of pyridine and water (1.00 mL) for 2 h. Then, the reaction mixture was extracted with 1 M $NaHSO_4$ (3 x 20 mL), 10 % Na_2CO_3 (3 x 20 mL) and then with brine (1 x 20 mL), and combined organic layers were dried over anhydrous Na_2SO_4. The residue was concentrated *in vacuo*. The product (G2M-alkene) was obtained as a light yellow solid (0.45 g, 71 %). The obtained product (0.20 g, 0.22 mmol) was then dissolved in toluene (200 mL) and heated up to 100 ^oC. After the reaction mixture was stirred for 10 hours, toluene was evaporated and the crude product was purified by column chromatography to give R-G2M-alkene as a light yellow solid (0.14 g, 77 %). ^1H NMR ($CDCl_3$, δ, ppm) 6.69 (s, 2H, C*H*=C*H*), 5.82-5.72 (m, 4H, C*H*=CH_2), 5.05-4.96 (m, 8H, CH=C*H*$_2$), 4.26 (s, 4H, CH_2 ester protons), 4.28 (dd, 8H, *J* = 11.2, 2.4 Hz, CH_2 ester protons), 4.07 (t, 2H, *J* = 6.2 Hz, OCH_2), 3.60 (t, 2H, *J*= 6.6 Hz, NCH_2), 2.41-2.30 (m, 16H, $OCCH_2CH_2$ protons), 1.98-1.92 (m, 2H, $NCH_2CH_2CH_2O$), 1.26 (s, 3H, $C(CH_3)$), 1.21 (s, 6H, $C(CH_3)_2$). ^{13}C NMR ($CDCl_3$, δ, ppm) 172.4, 172.0, 171.9, 170.6, 136.4, 134.2, 115.6, 65.7, 65.1, 62.2, 46.6, 46.4, 34.4, 33.2, 28.7, 27.5, 17.8, 17.5. Calculated: $[M]^+$ m/z = 831.9. Found: MALDI-TOF MS: $[M]^+$ m/z = 833.5, $[M+Na]^+$ m/z = 854.8.

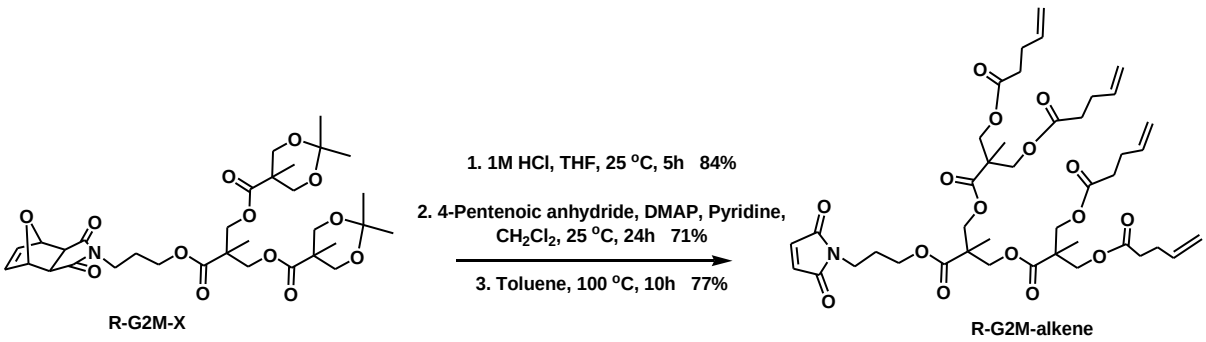

Figure 5. 6. Synthesis of R-G2M-alkene.

5.2.4. General Procedure for the Direct NMP Copolymerization of Styrene with Macromonomers D1-D5

BlocBuilder MA® (1 equiv.) and a dendron-functionalized maleimide (1 equiv.) were added into a flask, sealed with a septum and purged with dry argon for 30 minutes. Then degassed styrene (50 equiv.) was added with a degassed syringe. The mixture was

immersed in a preheated oil bath at 120 °C. During the polymerization, aliquots were taken from the reaction mixture with a degassed syringe in order to monitor the incorporation of maleimide in the growing copolymer chains by ^{1}H NMR spectroscopy. After approximately 240 minutes of polymerization, the reaction mixture was cooled down to RT, diluted in a small amount of THF and poured in a large amount of cold methanol. The precipitated copolymer was filtered and dried *in vacuo* at RT.

5.2.5. General Procedure for the Time-Controlled Addition of Macromonomers D1-D5 During the NMP of Styrene

BlocBuilder MA® (1 equiv.) was added into a flask, sealed with a septum and purged with dry argon for 30 minutes. Then degassed styrene (50 equiv.) was added with a degassed syringe. The mixture was then immersed in a preheated oil bath at 120 °C. After 45 minutes of polymerization, a degassed solution of dendron-functionalized maleimide (1 equiv.) in degassed anisole was added with a degassed syringe. During the copolymerization, aliquots were taken from the mixture with a degassed syringe in order to monitor the incorporation of maleimide in the growing copolymer chains. After 240 minutes of polymerization, the reaction mixture was cooled down to RT, diluted in a small amount of THF and poured in a large amount of cold methanol. The precipitated copolymer was filtered and dried *in vacuo* at RT.

5.2.6. General Procedure for the Time-Controlled Addition of D6 in Styrene NMP

BlocBuilder MA® (1 equiv.) was added into a flask, sealed with a septum and purged with dry argon for 30 minutes. Then degassed styrene (50 equiv.) was added with a degassed syringe. The mixture was immersed in a preheated oil bath at 120 °C. After 55 minutes of polymerization, a degassed solution of **D6** (1 equiv.) in degassed anisole was added with a degassed syringe. During the polymerization, aliquots were taken from the mixture with a degassed syringe in order to monitor the incorporation of maleimide in the growing copolymer chains by ^{1}H NMR spectroscopy. After 240 minutes of polymerization, the reaction mixture was cooled down to RT, diluted in a small amount of

THF and poured in a large amount of cold methanol. The precipitate copolymer was filtered and dried *in vacuo* at RT.

5.2.7. Procedure for the Thiol-ene Modification of the Copolymer P(S-*co*-D6) with Thio-glycerol

Alkene functionalized copolymer P(S-*co*-D6) (20.0 mg, $3x10^{-3}$ mmol) and 2,2'-dimethoxy-2-phenylacetophonone (DMPA) were added into a vial, sealed with a teflon cap and purged with nitrogen for 10 minutes. Then they were dissolved in degassed DMF (0.1 mL) and finally thio-glycerol (2.08 μL, $24x10^{-3}$ mmol) was added into the vial. Then, the vial content was purged with nitrogen for an additional 10 min and irradiated for 3 hours with 365 nm light at room temperature. Subsequently, the crude mixture was precipitated in cold methanol. The precipitated copolymer was filtered and dried *in vacuo* to give thio-glycerol conjugated copolymer (18.2 mg, 78 % yield). $M_{n,theo}$= 7515, $M_{n,SEC}$= 7440, M_w/M_n= 1.21.

5.3. Results and Discussion

Sequence controlled copolymerization methodology was applied to insert functional dendrons at precise positions along a linear polymer backbone. Styrene and polyester dendrons containing maleimide unit at their focal point were copolymerized to yield polymers bearing clusters of functional groups. These functional groups placed at the side chain of the polymer can be utilized for further conjugation approaches. Herein, use of dendrons furnished with alkene units allows the conjugation of thio-glycerol to the side chain of the resultant polymer via thiol-ene chemistry.

5.3.1. Polyester Dendron Substituted-Maleimides (MIs) Syntheses

Planned to be used as macromonomers, various polyester based dendrons differing from each other with respect to their generations and surface groups were synthesized (Figure 5.7). Thanks to naked maleimide moieties at their focal points, they can

incorporate into nitroxide-mediated copolymerization. Dendrons containing acetal groups at the periphery (**D1-D3**) were prepared using a previously established protocol that uses the divergent synthesis of polyester dendrons using an acetonide-protected bis(hydroxy)propionic acid building block [214], [215]. Briefly, a furan-protected maleimide containing alcohol was treated with acetonide-protected bis(hydroxy)propionic anhydride to obtain an acetal protected dendron. Retro Diels-Alder reaction by refluxing in toluene releases the furan moiety to yield the first generation dendron **D1** containing a reactive maleimide unit at the focal point. The removal of acetal groups under acidic conditions prior to the retro Diels-Alder reaction furnishes the corresponding alcohol containing dendron **D4**. Higher generations of the dendrons were obtained by iterative deprotection of acetal units followed by reaction with acetal-containing anhydride. The alkene appended dendron **D6** was synthesized by reaction of the hydroxyl groups at the periphery of a second generation dendron with pentenoic anhydride.

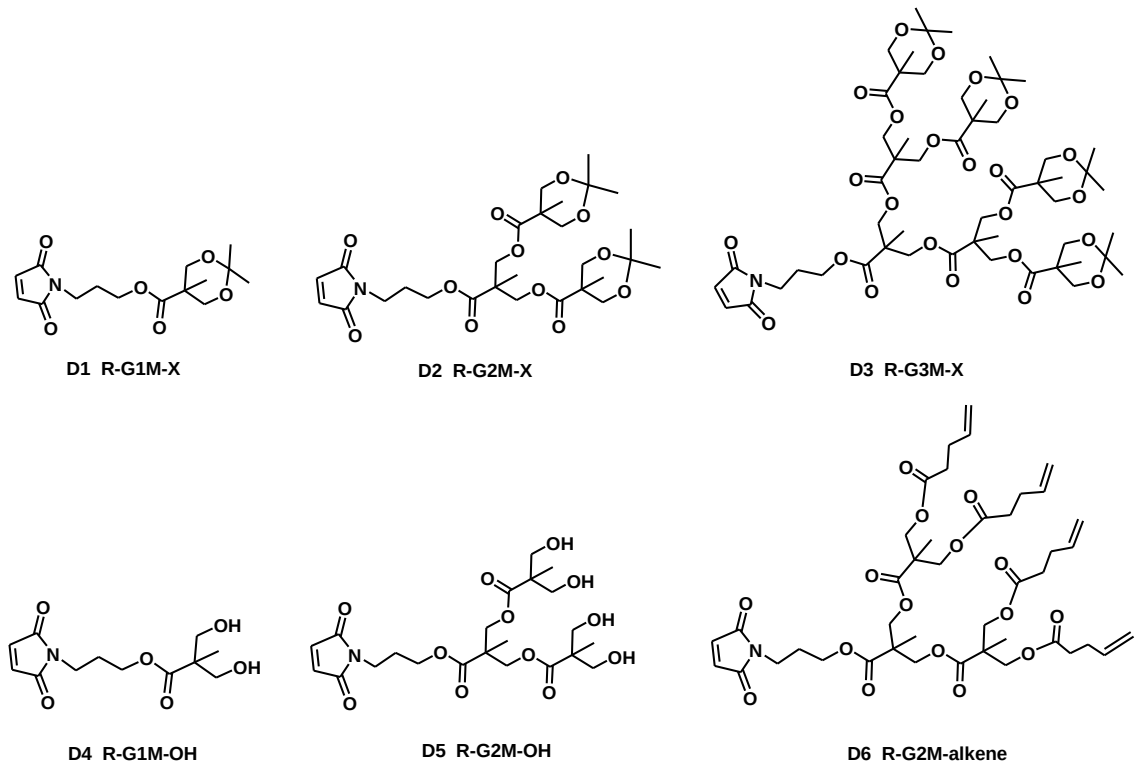

Figure 5. 7. Synthesized dendritic macromonomers (D1-6).

All dendritic macromolecules were obtained in pure form after column chromatography, and they were characterized with ^{1}H NMR and ^{13}C NMR for their structural assignments and purity. For example, presence of alkene units in structure of **D6** was evident from the proton resonances around 5.8 and 5.0 ppm. Also the peak at 6.69 ppm belonging to maleimide double bond confirms the polymerizibility of this macromonomer (Figure 5.8). ^{13}C NMR provides further support of the structure due to the presence of four different carbonyl peaks and two ethylene carbons as expected.

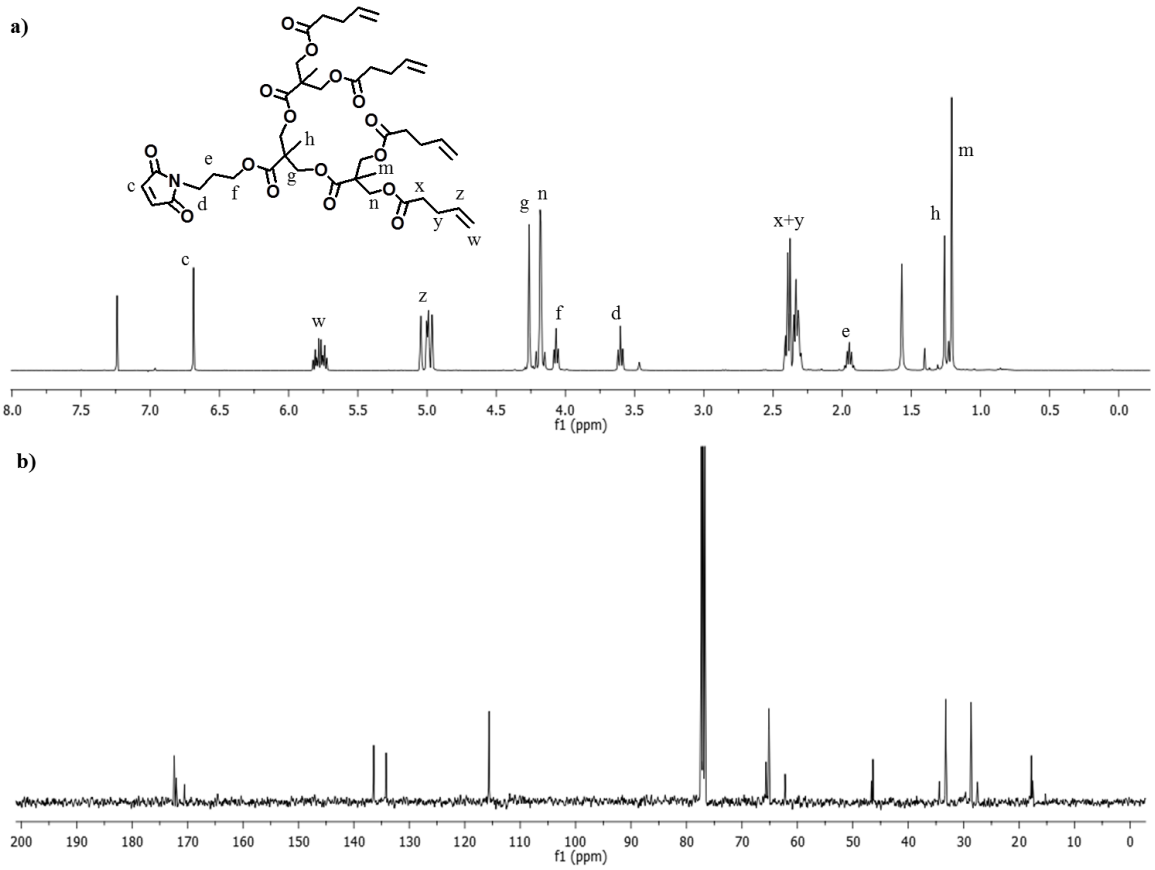

Figure 5. 8. ^{1}H NMR (a) and ^{13}C NMR (b) spectra of R-G2M-alkene (D6).

5.3.2. Local Incorporation of Dendron-Substituted MIs in Polystyrene Chains

Synthesized dendritic macromonomers were introduced into sequence controlled polymerization with styrene in collaboration with Nathalie Baradel from Prof. Dr. Jean-François Lutz's group at Charles Sadron Institute in Strasbourg, France. Control over the

position of dendrons along the growing polymer chain was derived from the higher tendency of maleimide groups to copolymerize with styrene instead of homopolymerize with each other. Local incorporation of dendritic macromonomers into polystyrene chains was achieved by arranging the time of addition of these dendrons into the polymerization. In order to install the dendron close to the chain end, polymerizations were carried out with the dendron-substituted MIs in the initial feed (Figure 5.9a). For introducing the dendrons in the middle of the polymer chains, the MIs were introduced after a certain period of time in styrene homopolymerizations (Figure 5.9b).

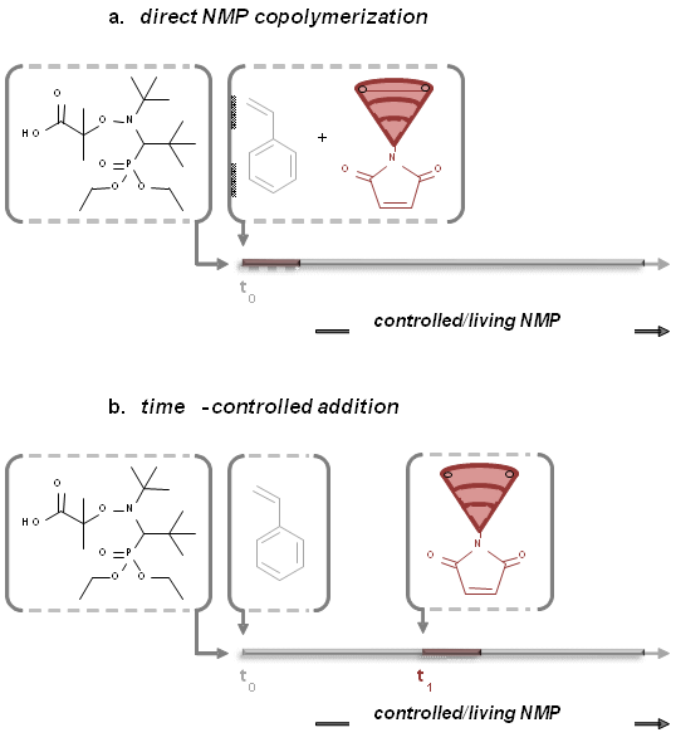

Figure 5. 9. Strategies studied for the local incorporation of dendron based macromonomers in polystyrene chains.

Nitroxide-mediated polymerization (NMP) using a commercially available alkoxyamine initiator, BlocBuilder MA®, was used to synthesize these copolymers. Following the approaches mentioned above, two different model microstructures were synthesized. In both of them, consumption of dendron-substituted maleimides was monitored by ^{1}H NMR spectroscopy by taking aliquots from the reaction mixture during

the polymerization. Monomer conversions calculated by integration values of proton resonances belonging to both monomers indicate the consumption of dendritic macromonomers within a short time after its introduction in the reaction medium (Table 5.1).

Table 5. 1. Kinetic data recorded for the nitroxide mediated copolymerization of styrene with dendron-functionalized *N*-substituted maleimides[a]

Entry	MI	t_{add} [min][b]	conv.$_S$ at t_{add} [c]	t_{MI} [min][d]	conv.$_S$ at t_{MI} [c]	t_{end} [min][e]	conv.$_S$ at t_{end} [c]	M_n [f]	$M_{n\ theo}$ [g]	M_w/M_n [f]
1	**D1**	0	0	20	0.17	240	0.94	4030	5583	1.14
2	**D1**	45	0.26	65	0.38	260	0.87	4235	5218	1.13
3	**D2**	0	0	20	0.13	240	0.96	4550	5959	1.15
4	**D2**	45	0.42	65	0.49	260	0.97	4400	6011	1.14
5	**D3**	0	0	20	0.17	220	0.95	5230	6451	1.13
6	**D3**	45	0.31	65	0.41	240	0.72	5340	5255	1.17
7	**D4**	0	0	20	0.13	240	0.84	4370	5022	1.15
8	**D4**	45	0.26	65	0.39	260	0.82	4870	4918	1.12
9	**D5**	0	0	20	0.11	240	0.84	4330	5254	1.12
10	**D5**	45	0.25	65	0.33	260	0.86	4945	5358	1.13
11	**D6**	55	0.29	75	0.40	240	0.77	6650	5271	1.15

[a] Experimental conditions: bulk, 120 °C, [S]/[MI]/[BlocBuilder] = 50:1:1. [b] t_{add} denotes the time at which the MI was added to the polymerization mixture. [c] Styrene conversion calculated from ^{1}H NMR spectra. [d] t_{MI} denotes the time at which nearly-quantitative MI conversion was observed. [e] t_{end} denotes the final polymerization time. [f] Measured by SEC in THF. [g] $M_{n\ theo} = M_{BlocBuilder} + M_{S.} \cdot conv._S \cdot [S]/[BlocBuilder] + M_{MI.} \cdot conv._{MI} \cdot [MI]/[BlocBuilder]$.

Moreover, the controlled/'living' nature of the NMP was preserved after dendron incorporation. In Figure 5.10, it was clearly seen from the semi-logarithmic plots of monomers conversion that after consumption of dendritic macromonomer **D2**, styrene homopolymerization continued and the resultant dendron-modified polystyrene was obtained with controlled molecular weight and narrow molecular weight distributions.

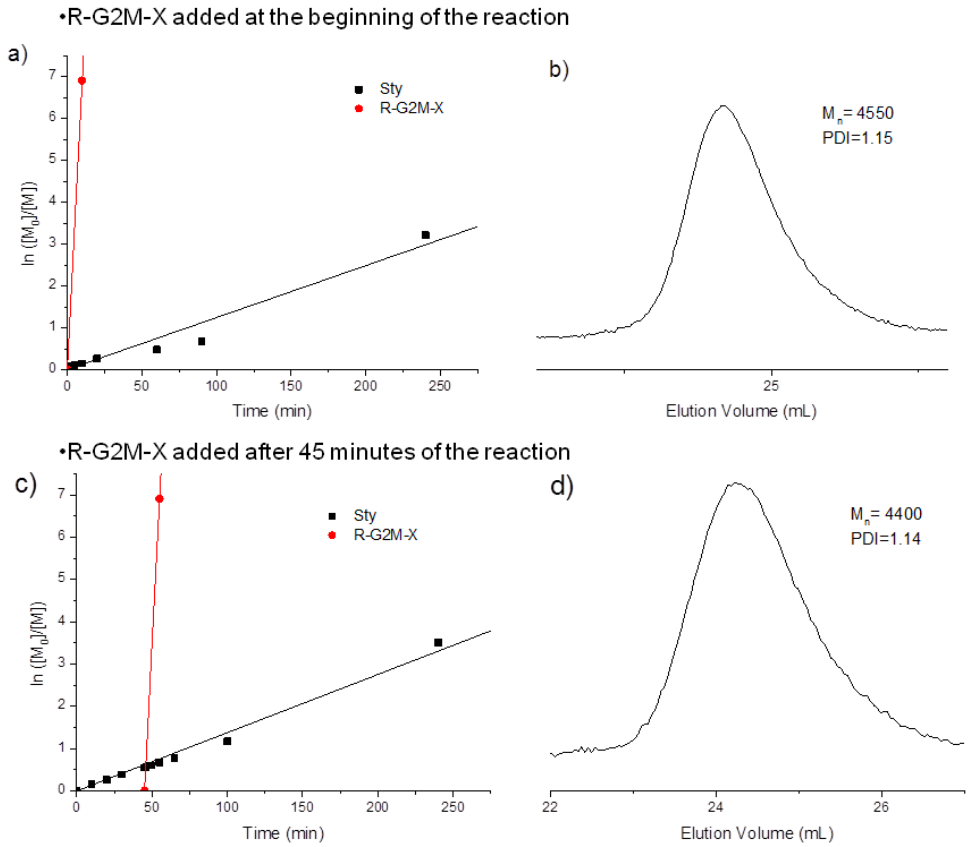

Figure 5. 10. (a) and (c) Semi-logarithmic plots of monomers conversion versus time for nitroxide-mediated copolymerization of styrene (Sty, 50 equiv.) (black squares) with D2 (R-G2M-X, 1 equiv.) (red dots) added at beginning or after 45 minutes of reaction. Experimental conditions: bulk, 120 °C, Sty/MI/BlocBuilder=50/1/1. (b) and (d) Size exclusion chromatograms of the isolated copolymers.

Chemical composition of all dendron-inserted polymers was analyzed by ^{1}H NMR spectroscopy. All the polymer samples isolated from the reactions preserved all the signature peaks of the dendrons, along with the expected proton resonances from the polystyrene polymer chain. For example, for the polymers obtained using the second

generation maleimide dendron **D2**, the resonances from the protons adjacent to the ester functional groups can be seen around 4.3 ppm, while the peaks from the diastereotopic methylene protons on the acetal units can be seen around 4.1 and 3.6 ppm (Figure 5.11). Altogether, NMR and size exclusion chromatography (SEC) results indicate that all generations of maleimide containing dendrons performed well in sequence-controlled copolymerizations with styrene. Facile reaction with a G3-dendron containing the maleimide group at the focal point highlights that the reactive nature of the maleimide functional group enables effective incorporation into the polymer backbone in spite of the steric bulk of the dendron.

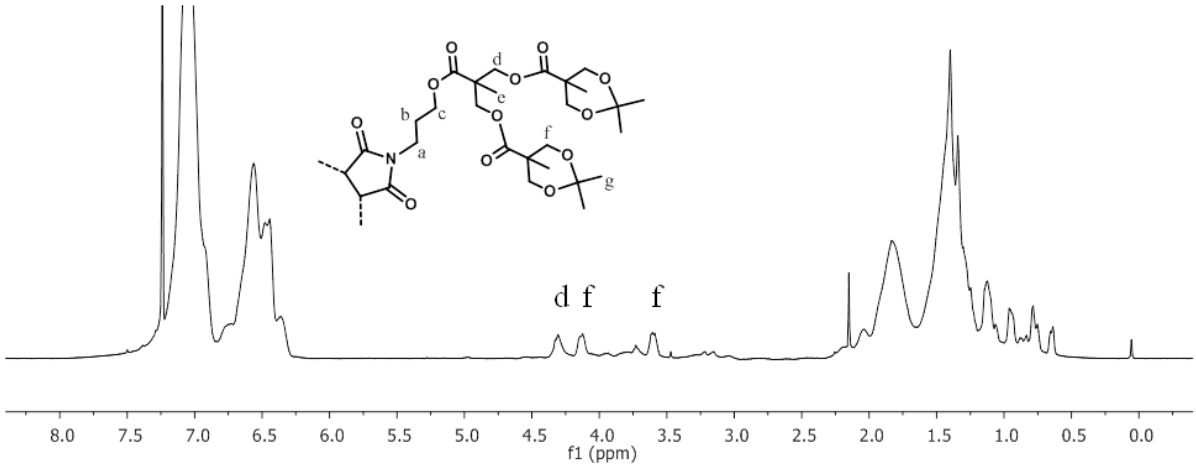

Figure 5. 11. ^{1}H NMR spectrum of a copolymer P(S-*co*-D2) recorded at RT in $CDCl_3$.

5.3.3. Thiol-ene Modification of the Copolymer P(S-*co*-D6) with Thio-glycerol

As an alternative, alkene units were appended to the side chains of polystyrenes by the incorporation of dendritic macromonomers with alkene functionalities at the periphery. After 55 minutes, the second generation dendron **D6** containing four alkene groups at the periphery and a reactive maleimide unit at the focal point was introduced into the polymerization reaction and from the monomer conversion plots, it is obvious that alkene functionalized dendron was consumed within a very short time so that the local insertion of dendron was achieved successfully (Figure 5.12). The kinetic analysis of the polymerization suggests that the presence of multiple alkene functional groups at the periphery of the dendrons did not interfere significantly with the polymerization reaction.

A slight high molecular weight shoulder was detectable in the SEC chromatogram of the corresponding polymer, while all other polymers obtained with dendrons **D1**-**D5** were monomodal. Importantly, the ^{1}H NMR spectrum of the **D6**-containing polymer exhibited all the expected characteristic peaks from the polymeric backbone and the appended dendron (Figure 5.14). The integration of the different signals suggested that about 85% of the alkene functions were preserved after copolymerization.

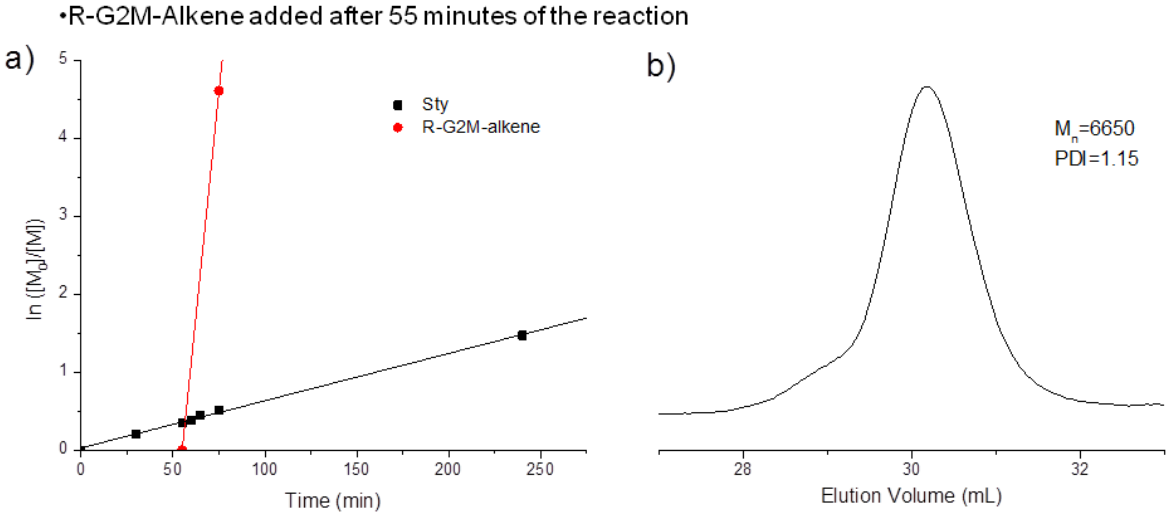

Figure 5. 12. Semi-logarithmic plot of monomers conversion versus time for nitroxide-mediated copolymerization of styrene (Sty, 50 equiv.) (black squares) with D6 (R-G2M-alkene, 1 equiv.) (red dots) added after 55 minutes of reaction. Experimental conditions: bulk, 120 °C, Sty/MI/BlocBuilder=50/1/1. (b) Size exclusion chromatogram of the isolated copolymer.

Utilization of orthogonally reactive dendron based building block **D6** yielded polymers enabling post-functionalization modifications. Functionalization of the double bonds was demonstrated by using a free-thiol group containing molecule, thio-glycerol using thiol-ene chemistry.

Alkene groups at the side chains of copolymer P(S-*co*-D6) was treated with thio-glycerol in the presence of 2,2-dimethoxy-2-phenylacetophenone as the photoinitiator (Figure 5.13). After irradiation for 3 hours with 365 nm light at room temperature, the modified polymer was purified by precipitation in cold methanol.

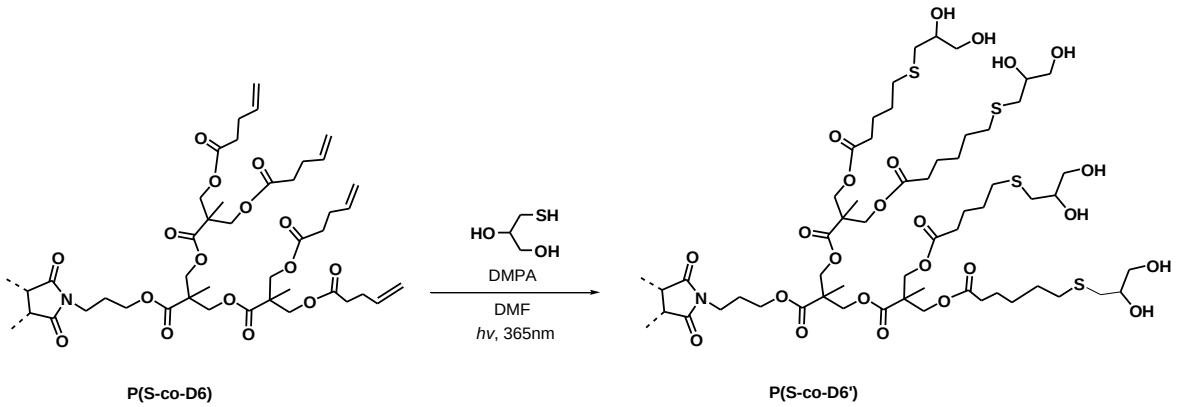

Figure 5. 13. Thiol-ene modification of the copolymer P(S-*co*-D6) with thio-glycerol.

Thio-glycerol conjugated copolymer was then analyzed by ^{1}H NMR spectroscopy to determine the efficiency of the thiol-ene modification. Complete disappearance of proton resonances from the alkene units at 5.0 and 5.8 ppm, and the appearance of new proton resonances between 3.4-3.8 ppm belonging to the thioglycerol unit, demonstrated highly efficient post-polymerization modification (Figure 5.14).

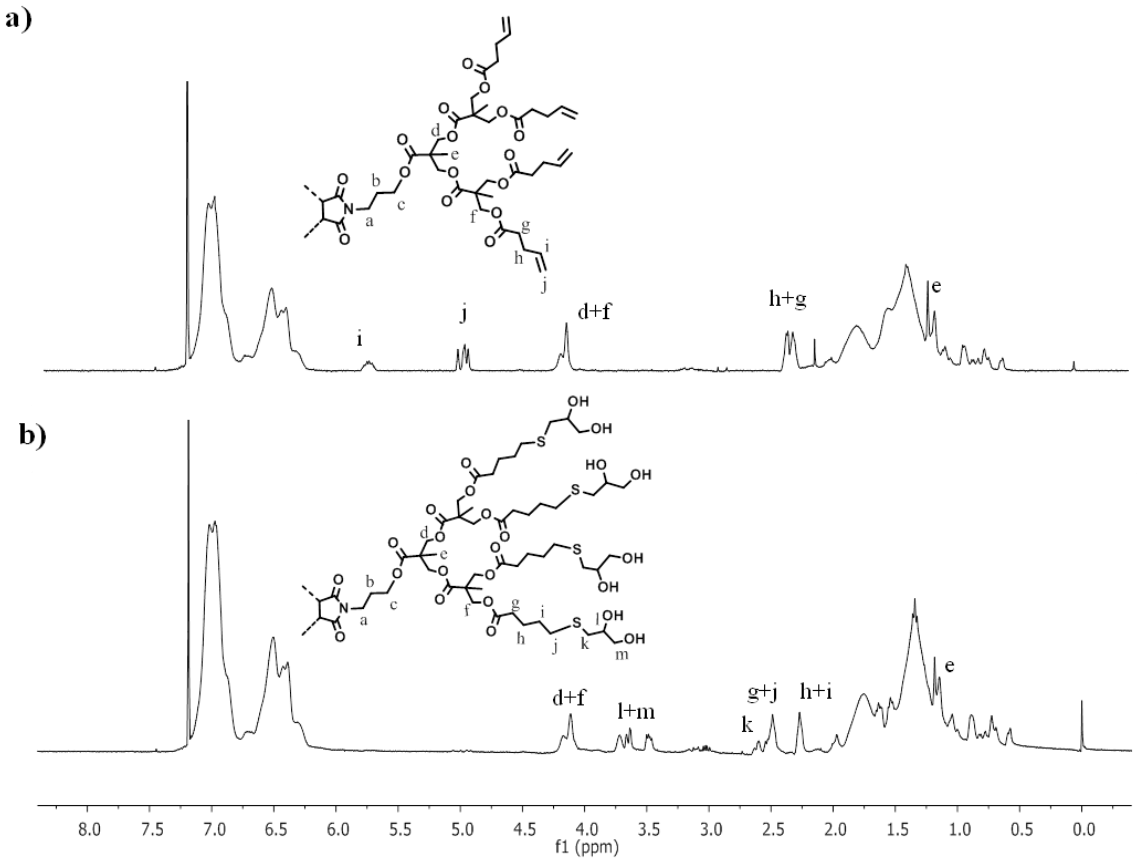

Figure 5. 14. ^{1}H NMR spectra of copolymers P(S-*co*-D6) (a) and P(S-*co*-D6') (b) recorded at RT in $CDCl_3$.

5.4. Conclusion

In this study, a new strategy towards precise chain positioning of macromolecules along polymer chains was presented. Various dendron-substituted maleimides with different generations were synthesized and act as macromonomers during the copolymerization with styrene via sequence-controlled copolymerization. Two routes were followed during Nitroxide-mediated polymerization (NMP) to arrange the position of the dendrons along the growing polymer chain. Dendritic macromolecules were either added to the polymerization mixture at the beginning of the reaction or they were introduced after a certain period of time. In both cases, monomer conversions and molecular weights of the polymers were traced with ^{1}H NMR spectroscopy and it was seen that the resultant polymers have proton resonances coming from both dendrons and styrene. Thus, polymers

bearing dendrons with acetal, hydroxyl or alkene groups as pendant groups were obtained. Furthermore, functional groups placed at the periphery of dendrons allow post-polymerization modifications. As an example, a polymer containing a cluster of alkene functional units was efficiently modified by thiol-ene chemistry. Alkene units were reacted with a free-thiol group containing molecule, thio-glycerol, via thiol-ene reaction and successful conjugation was proved by ^{1}H NMR spectroscopy. The methodology can be extended to sequentially insert two or more different dendrons along the polymer backbone at desired locations to access multi-functional dendronized polymers.

6. ORTHOGONALLY REACTIVE MULTIARM POLYMER-DRUG CONJUGATES

6.1. Introduction

Synthetic biomaterials are finding increasing applications in various areas of biomedical sciences including approaches to address potential limitations in chemotherapy [42], [216]. To date, various polymeric nanomedicines including polymer-drug and polymer-protein conjugates, polymeric micelles and polyplexes have been employed to improve the therapeutic effect of chemotherapy agents in eradicating solid tumors [11, 12], [175], [217]. Polymer-drug conjugates account for slower renal clearance rate of the drug, thus allowing more circulation time in the blood stream and consequent decrease in toxicity by passive targeting of chemotherapy drugs to leaky tumor tissue [17]. In general, hydrophilic polymers are utilized to increase the water solubility of many of the hydrophobic anti-cancer agents via conjugation using biodegradable linkers responsive towards biological composition or pH of the tumor tissue. It is well established that polymeric carriers selectively accumulated in tumor tissue tend to enhance *in vivo* efficacy of therapeutic drugs by increasing their bioavailability in fast growing tumor [158], [187].

Recent investigations related to the penetration of polymer-drug conjugates acting as prodrugs into tumor tissue have pointed out the diversity in the molecular architecture [20]. A bioconjugate carrier delivering the drug payload effectively should be considered for its molecular weight and hydrodynamic volume as well as the molecular conformation and flexibility. Abovementioned parameters have direct impact on their excretion rate from the pores of kidney where slower clearance ends up with an increase in the circulation time of the drug conjugate in the blood stream that enhances accumulation in tumor tissue. Since the size of the pores generated in leaky tumor vasculature is larger than the hydrodynamic volumes of utilized polymeric drug carriers, mechanism of extravasation through the blood vessels seems to have little impact on their accumulation [218, 219].

In this regard, tuning of polymer architecture can be employed to regulate the elimination process through the pores of kidney. Several findings report thatpolymeric constructs that have higher molecular weight and more branched structures with less flexibility inhibit renal filtration. Compared to linear elongated versions of same molecular weight, polymers with high branching degree and increased arms, exclusively star polymers and dendrimers, provide longer blood circulation half-life due to restricted flexibility in glomerular filtration process. In 2004 and 2005, Gillies and Fre´chet introduced a new polymeric architecture by using dendrimer based building blocks to design bow-tie polymers as drug carriers. They utilized first, second and third generations polyester dendrons and attached them to PEG chains. Rigid and spherical Dendron-conjugated polymers had decreased renal filtration and longer blood circulation time, whereas flexible and elongated linear polymers were filtered rapidly. Furthermore, increasing the number of polymer arms seemed to prolong the blood circulation time due to decreased pore penetration during renal filtration. According to the pharmacokinetic data [G-3] polymers with almost same molecular weights circulated longer in the blood and excreted slower than [G-2] polymers, and [G-1] polymers similar to their linear counterparts were rapidly cleared through urine and feces [21-23].

The clear trend of branching degree observed for the above-mentioned multiarm polymers pioneers the combinations of dendrimers with multifarious polymers to stimulate the accumulation of chemotherapy agents in the pathology zone [110], [206], [220, 221]. This motivation leads to emanate the concept to new developments for drug carriers. As an alternative, polymer chains may be combined to each other with the help of peripheral groups of dendrimers to figure out attractive dendritic macromolecules as well-defined and uniform nanostructures. Most of the published dendritic multiarm star polymers rely on the ‘arm-first’ methodology where pre-synthesized polymeric arms are attached to the dendrons via functional groups located at the periphery [222-224]. However as the generation of the dendron increases, not all surface groups may be conjugated to polymer chains due to the steric hindrence generated by already bounded ones. This deterioration can be overcome by ‘core-first’ methodology enabling the use of dendritic initiators for the polymerization of several different monomers with desired functionalities. Monodisperse

architecture of these dendritic initiators provides the fabrication of well-defined compact multiarm star polymers with known number of arms determined by the number of initiators installed by the dendritic initiator [225-229]. In recent years, we reported the synthesis of bis-MPA based biodegradable first through third generation dendritic initiators with furan protected maleimide functionality at the focal points for the preparation of 2, 4 and 8 arm star polymers via ATRP [117]. After unmasking the maleimide group at the core via the retro Diels-Alder reaction a 4-armed water soluble star polymer was obtained. Facile conjugation was demonstrated using a thiol containing tripeptide, glutathione, via the Michael type nucleophilic thiol-ene addition reaction (Figure 6.1).

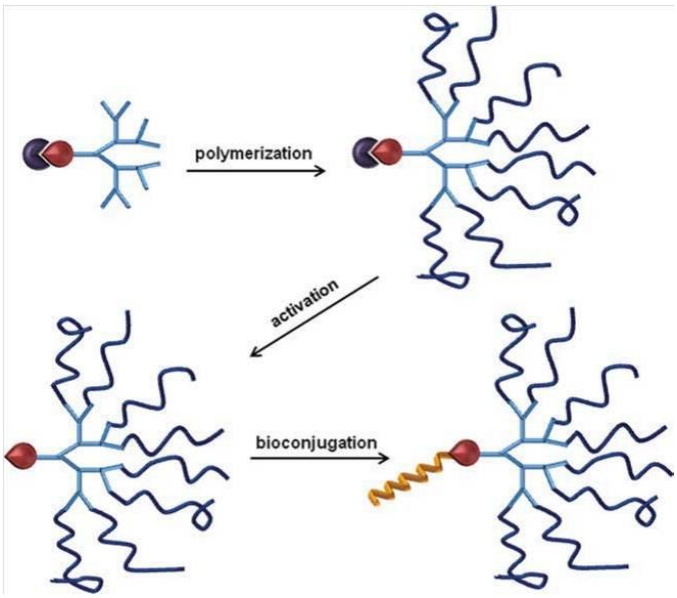

Figure 6. 1. Synthesis route of multiarm polymers containing reactive maleimide core [159].

An extension to the approach disclosed in above study is inevitably the incorporation of reactive group along the polymeric arms. With a furan protected maleimide at the core, these dendritic initiators allow the installation of different functional groups appended to polymeric arms growing from the periphery. Monomers with reactive group of interest introduced into the polymer architecture subsequently contribute to its multifunctionality

increases the drug loading capacity of the resultant macromolecule to get maximum therapeutic effect.

Multifunctionality of the designed multiarm star polymers may be enhanced by the insertion of orthogonally reactive groups enabling the conjugation of several biomolecules, drugs or peptides with various functionalities [96], [136], [149], [230, 231]. The methodology described here involves the synthesis of orthogonally reactive linear and multiarm star polymers as viable platforms for drug delivery. Along with a thiol reactive maleimide group provided by the initiator itself, polymeric arms were introduced with amine reactive N-hydroxy succinimide (NHS) groups so the conjugation reactions to these separate moieties can be performed without interfering with each other.

In this approach the number of polymeric arms relies on the number of initiation sites located at the dendron surface. Polymerization of an organosoluble and water soluble methacrylate monomers from multifunctional initiators yielded corresponding multiarm star polymers with protected maleimide units at the core. Mediated with a metal complex, ATRP method results in well-defined polymeric scaffolds with improved polydispersity index values. Due to mild reaction conditions and its applicability to methacrylate and acrylate compounds, this polymerization technique has been extensively used to obtain multi-arm polymers [232, 233]. NHS functionality was introduced into the polymer chains since activated esters are known to react readily with free amine groups upon aminolysis which is a very facile coupling reaction for the conjugation of peptides [144], [234, 235]. These orthogonally reactive polymeric carriers were utilized to achieve the simultaneous conjugation of a chemotherapy agent, gemcitabine and an imaging agent, BodipyC10SH.

With the brand name Gemzar and marketed by Eli Lilly and Company, gemcitabine is a chemotherapy drug currently used in the treatment of various carcinomas like non-small cell lung cancer, pancreatic cancer, bladder cancer and breast cancer (Figure 6.2). It is a nucleoside analog in which the hydrogen atoms on the 2' carbon of deoxycytidine are replaced by fluorine atoms [236]. Mechanism of action depends on the inhibition of DNA replication by replacing cytidine, one of the building blocks of DNA, resulting in

apoptosis. While it emerged as an antiviral drug during the early 1980s, in vitro studies showed that it also killed the leukemia cells. Afterevaluation as an anticancer agent, in 2006 it received FDA approval in the treatment of advanced ovarian cancer for use with carboplatin and then combinations with cisplatin and paclitaxel were clinically investigated for several cancer types. [237-240]. However it displays severe side effects like neutropenia due to its toxicity to healthy tissues and low bioavailability originating from its metabolism by the plasmatic enzyme cytidine-deaminase, yielding its inactive uracil derivative 2′,2′-difluorodeoxyuridine (dFdU) [241]. Most prodrugs prepared for gemcitabine revealed in the literature are based on the design of linear architectures with a kidney excretion that is not long enough to yield maximum therapeutic effect of administred drug [242-244].

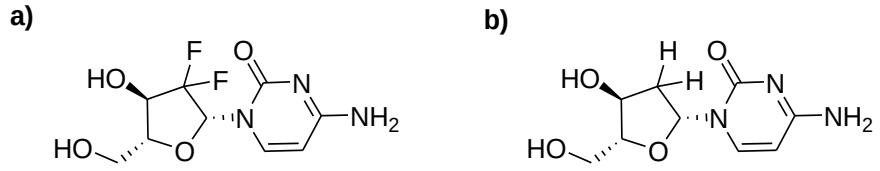

Figure 6. 2. Structures of Gemcitabine (a) and Deoxycytidine (b).

The focus of this study is to utilize the orthogonally functionalized copolymers as macromolecular carriers for the chemotherapy drug, gemcitabine. NHS groups were replaced by the free amine containing drug molecules to form polymer-drug conjugates with multiarm architectures. Out of the broad library of copolymers, DEGMEMA based polymers were preferred due to the biodegradable and water soluble character provided by small ethylene glycol chains attached to the backbone via acid labile ester linkage. The single maleimide group in polymeric scaffolds was evaluated as a tool for the incorporation of an imaging agent, BodipyC10SH, to these drug delivery systems, which facilitates the monitoring of their pathway in the body (Figure 6.3). As stated previously, ultimate goal of synthesizing polymeric platforms of multiarm architectures was to investigate their impact on renal clearance rates which reversely related to the drug efficacy. So far, preliminary tests were undertaken to evaluate *in vitro* viability and uptake in cancerous breast cell line (MDA-MB-231).

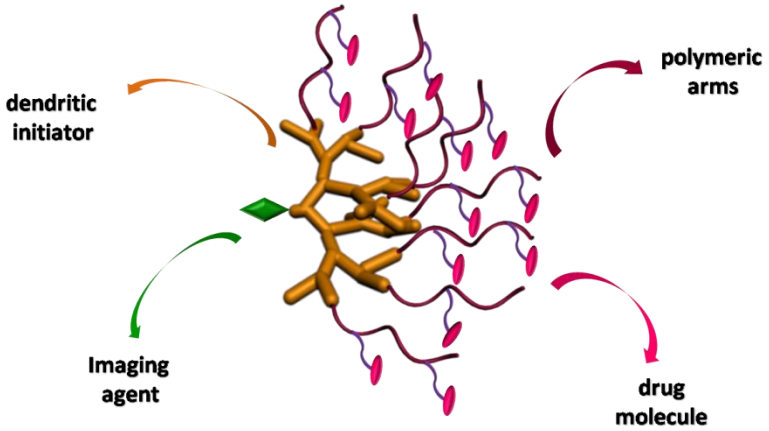

Figure 6. 3. Illustration of an orthogonally reactive multiarm star copolymer conjugated to both chemotherapy drugs and an imaging agent.

6.2. Experimental

6.2.1. Materials

6.2.1.1. Chemicals. All reagents were obtained from commercial sources and were used as received unless other-wise stated. N-hydroxysuccinimidyl methacrylamide monomer (NHSMA), dendritic initiators and BodipyC10SH were synthesized according to literature procedures [170], [245]. Methyl methacrylate (M_n = 100.12 g/mol) (MMA, 99%, Aldrich), Di(ethylene glycol) methylether methacrylate (M_n = 188 g/mol) (DEGMEMA, 99%, Aldrich), Poly(ethylene glycol) methylether methacrylate (M_n = 300 g/mol) (PEGMEMA, 99%, Aldrich) were passed through basic alumina column to remove inhibitor prior to use *N, N, N', N'', N''*-pentamethyldiethylenetriamine (PMDETA, 99%, Aldrich). Methacryloylchloride, DMAP and EtN_3 were obtained from Alfa Aesar and used as received. Ethylene glycol (99%, Aldrich), 2-bromo-2-methyl propionyl bromide (99.9%, Aldrich), DCC (99.9%, Aldrich), Copper(I)Bromide (Cu(I)Br, 99.9%, Aldrich) and EDCI (99.9%, Aldrich) were used as received. Chemotherapy drug Gemcitabine was purchased from IS Chemical Technology. Anhydrous solvents (CH_2Cl_2, THF, toluene) was obtained from ScimatCo Purification System, other solvents were dried over molecular sieves. The centrifugal filtration tubes (Spectra/Por® Amicon Ultra-4 Regenerated Cellulose Membranes MWCO 3000 Da) were purchased from Spectrum Labs. All other chemicals

were used as received from manufacturer (Merck, Aldrich and Alfa Aesar). Column chromatography was performed using silicagel–60 (43–60 nm). Thin layer chromatography was performed using silica gel plates (Kiesel gel 60 F254, 0.2mm, Merck).

6.2.1.2. Cells. Human breast adenocarcinoma MDA-MB-231 cell lines were obtained from ATCC (Wessel, Germany). Cells were kept in the logarithmic phase of cell growth for the duration of experiments. Cells were maintained in RPMI-1640 culture medium (Roswell Park Memorial Institute) [Gibco, Invitrogen] supplemented with 10% fetal bovine serum [FBS] [Lonza], 100 U/mL penicillin, 100 g/mL streptomycin, and 0.25 g/mL amphotericin B at 37 °C, 5% CO_2, and 95% relative humidity. Cell counting kit-8 (CCK-8) and DAPI was obtained from Sigma Aldrich.

6.2.2. Instrumentation

6.2.2.1. Nuclear Magnetic Resonance Spectroscopy (NMR). The NMR spectra were recorded using a 400 MHz Varian spectrometer at 25 °C. ^{1}H NMR measurements were made at frequency of 400 MHz, and calibrated with respect to the solvent signal. The measurements were performed in deuterated chloroform ($CDCl_3$) and dimethyl sulfoxide (DMSO).

6.2.2.2. Size Exclusion Chromatography (SEC). The molecular weights of the copolymers were estimated by GPC analysis using a Shimadzu PSS-SDV (length/ID 8 × 300 mm, 10 mm particle size) mixed-C column calibrated with polystyrene standards (1–400 kDa) using a refractive-index detector. Tetrahydrofuran (THF) was used as eluent at a flow rate of 1 mL/min at 30 °C.

6.2.2.3. MultiscanTM FC Microplate Photometer. Cell viability values for the cytotoxicity experiments were determined by measuring the absorbance of 96-well plates in use at 450 nm by Multiscan^{TM} FC Microplate Photometer from Thermo Scientific^{TM} equipped with a quartz halogen light source of a precision CV≤0.2% (0.3-3 Abs) at 405nm. It has an excitation wavelength range 340 to 850 nm with excitation filters are installed at 405, 450 and 620 nm.

6.2.2.4. Fluorescent Microscopy. Cell internalization studies were performed with Zeiss Observer Z1 fluorescence microscope connected to Axiocam MRc5 using a Zeiss Filter set

38 (Excitation BP 470/40, Emission BP 525/50) for imaging the functionalized polymers and a Zeiss Filter set 49 (Excitation G365, Emission BP 445/50) was used for imaging DAPI stained nuclei. Images were merged to visualize cell nuclei and morphology using Zeiss AxioVision software.

6.2.3. Synthesis of 2-arm Multiarm Star Copolymers via G1 Dendritic Initiator

6.2.3.1. Synthesis of G1M-(PMMA-*co*-NHSMA) (**P1**). G1M-(PMMA-*co*-NHSMA) was prepared by ATRP of MMA and NHSMA. Furan protected maleimide containing G1-initiator (**4)** (20.0 mg, 0.031 mmol) dissolved in minimum amount of degassed anisole was introduced into a flask containing Cu(I)Br (9.0 mg, 0.063 mmol), degassed PMDETA (26.0 µL, 0.125 mmol), degassed MMA (0.63 mL, 5.88 mmol) and NHSMA (72.0 mg, 0.39 mmol) dissolved in degassed anisole (6.30 mL) under stirring. The flask was then placed in a thermostated oil bath at 40 °C for 180 min. After polymerization, the reaction mixture was cooled down to room temperature, passed through a neutral alumina column to remove the catalyst and precipitated in methanol twice. **P1** was filtered and obtained as a white solid (0.23 g). ($[I]_0$:$[M]_0$:[CuBr]:[PMDETA]=1:200:2:4, [MMA]:[NHSMA] = 15:1, conversion = 34 %, $M_{n,theo}$ = 7380, $M_{n,NMR}$ = 17850, $M_{n,GPC}$ = 11920, M_w/M_n= 1.25, relative to PS).

For Polymer **P1**: ^{1}H NMR ($CDCl_3$, δ, ppm) 6.51 (s, 2H, C*H*=C*H*), 5.24 (s, 2H, C*H* bridgehead protons), 4.26-4.01 (m , 6H, CH_2 ester protons), 3.75-3.39 (m , 5H, CH_3 ester protons and NCH_2), 2.80 (br s, 6H, C*H*-C*H* bridge protons and NCCH_2), 2.15-0.82 (m, 22H, $NCH_2CH_2CH_2O$, C(CH_3), CBr(CH_3) , CH_2 and CH_3 along polymer backbone).

6.2.3.2. Synthesis of G1M-(DEGMEMA-*co*-NHSMA) (**P2**). G1M-(DEGMEMA-*co*-NHSMA) was prepared by ATRP of DEGMEMA and NHSMA. Furan protected maleimide containing G1-initiator (**4)** (20.0 mg, 0.031 mmol) dissolved in minimum amount of degassed anisole was introduced into a flask containing Cu(I)Br (9.0 mg, 0.063 mmol), degassed PMDETA (26.0 µL, 0.125 mmol), degassed DEGMEMA (1.08 mL, 5.88 mmol) and NHSMA (72.0 mg, 0.39 mmol) dissolved in degassed anisole (10.8 mL) under stirring. The flask was then placed in a thermostated oil bath at 40 °C for 180 min. After polymerization, the reaction mixture was cooled down to room temperature, passed

through a neutral alumina column to remove the catalyst and precipitated in diethyl ether twice. **P2** was filtered and obtained as a viscous solid (0.32 g). ($[I]_0$:$[M]_0$:[CuBr]:[PMDETA]=1:200:2:4, [DEGMEMA]:[NHSMA] = 15:1, conversion = 28 %, $M_{n,theo}$ = 10690, $M_{n,NMR}$ = 24650, $M_{n,GPC}$ = 16180, M_w/M_n= 1.17, relative to PS).

For Polymer **P2**: ^{1}H NMR ($CDCl_3$, δ, ppm) 6.48 (s, 2H, C*H*=C*H*), 5.20 (s, 2H, C*H* bridgehead protons), 4.06 (br s , 8H, CH_2 ester protons), 3.75-3.51 (br s, 6H, OCH_2 of DEGMEMA), 3.35 (br s, 5H, OCH_3 of DEGMEMA and NCH_2), 2.75 (s, 6H, C*H*-C*H* bridge protons and NCCH_2), 2.00-0.84 (m, 22H, $NCH_2CH_2CH_2O$, C(CH_3), CBr(CH_3), CH_2 and CH_3 along polymer backbone).

6.2.3.3. Synthesis of G1M-(PEGMEMA-*co*-NHSMA) (**P3**). G1M-(PEGMEMA-*co*-NHSMA) was prepared by ATRP of PEGMEMA and NHSMA. Furan protected maleimide containing G1-initiator (**4)** (20.0 mg, 0.031 mmol) dissolved in minimum amount of degassed anisole was introduced into a flask containing Cu(I)Br (9.0 mg, 0.063 mmol), degassed PMDETA (26.0 μL, 0.125 mmol), degassed PEGMEMA (1.42 mL, 4.96 mmol) and NHSMA (0.23 g, 1.24 mmol) dissolved in degassed anisole (14.2 mL) under stirring. The flask was then placed in a thermostated oil bath at 40 °C for 120 min. After polymerization, the reaction mixture was cooled down to room temperature, passed through a neutral alumina column to remove the catalyst and precipitated in diethyl ether twice. **P3** was filtered and obtained as a viscous solid (0.31 g). ($[I]_0$:$[M]_0$:[CuBr]:[PMDETA]=1:200:2:4, [PEGMEMA]:[NHSMA] = 4:1, conversion = 18 %, $M_{n,theo}$ = 10070, $M_{n,NMR}$ = 10240, $M_{n,GPC}$ = 7900, M_w/M_n= 1.21, relative to PS).

For Polymer **P3**: ^{1}H NMR ($CDCl_3$, δ, ppm) 6.48 (s, 2H, C*H*=C*H*), 5.21 (s, 2H, C*H* bridgehead protons), 4.07 (br s , 8H, CH_2 ester protons), 3.62-3.51 (br s, 14H, OCH_2 of PEGMEMA), 3.34 (br s, 5H, OCH_3 of PEGMEMA and NCH_2), 2.77 (s, 6H, C*H*-C*H* bridge protons and NCCH_2), 2.02-0.85 (m, 22H, $NCH_2CH_2CH_2O$, C(CH_3), CBr(CH_3), CH_2 and CH_3 along polymer backbone).

6.2.4. Synthesis of 4-arm Multiarm Star Copolymers via G2 Dendritic Initiator

6.2.4.1. Synthesis of G2M-(PMMA-*co*-NHSMA) (**P4**). G2M-(PMMA-*co*-NHSMA) was prepared by ATRP of MMA and NHSMA. Furan protected maleimide containing G2-

initiator (**5)** (20.0 mg, 0.017 mmol) dissolved in minimum amount of degassed anisole was introduced into a flask containing Cu(I)Br (9.8 mg, 0.068 mmol), degassed PMDETA (28.4 µL, 0.136 mmol), degassed MMA (0.68 mL, 6.38 mmol) and NHSMA (77.8 mg, 0.42 mmol) dissolved in degassed anisole (6.80 mL) under stirring. The flask was then placed in a thermostated oil bath at 40 °C for 180 min. After polymerization, the reaction mixture was cooled down to room temperature, passed through a neutral alumina column to remove the catalyst and precipitated in methanol twice. **P4** was filtered and obtained as a white solid (0.25 g). ($[I]_0$:$[M]_0$:[CuBr]:[PMDETA]=1:400:4:8, [MMA]:[NHSMA] = 15:1, conversion = 34 %, $M_{n,theo}$ = 14720, $M_{n,NMR}$ = 21280, $M_{n,GPC}$ = 14270, M_w/M_n= 1.20, relative to PS).

For Polymer **P4**: ^{1}H NMR ($CDCl_3$, δ, ppm) 6.50 (s, 2H, C*H*=C*H*), 5.21 (s, 2H, C*H* bridgehead protons), 4.21-4.03 (m , 14H, CH_2 ester protons), 3.73-3.38 (m , 5H, CH_3 ester protons and NCH_2), 2.79 (br s, 6H, C*H*-C*H* bridge protons and NCCH_2), 2.15-0.80 (m, 40H, $NCH_2CH_2CH_2O$, C(CH_3), CBr(CH_3) , CH_2 and CH_3 along polymer backbone).

6.2.4.2. Synthesis of G2M-(DEGMEMA-*co*-NHSMA) (**P5**). G2M-(DEGMEMA-*co*-NHSMA) was prepared by ATRP of DEGMEMA and NHSMA. Furan protected maleimide containing G2-initiator (**5)** (20.0 mg, 0.017 mmol) dissolved in minimum amount of degassed anisole was introduced into a flask containing Cu(I)Br (9.8 mg, 0.068 mmol), degassed PMDETA (28.4 µL, 0.136 mmol), degassed DEGMEMA (1.18 mL, 6.38 mmol) and NHSMA (77.8 mg, 0.42 mmol) dissolved in degassed anisole (11.8 mL) under stirring. The flask was then placed in a thermostated oil bath at 40 °C for 180 min. After polymerization, the reaction mixture was cooled down to room temperature, passed through a neutral alumina column to remove the catalyst and precipitated in diethyl ether twice. **P5** was filtered and obtained as a viscous solid (0.20 g). ($[I]_0$:$[M]_0$:[CuBr]:[PMDETA]=1:400:4:8, [DEGMEMA]:[NHSMA] = 15:1, conversion = 16 %, $M_{n,theo}$ = 12200, $M_{n,NMR}$ = 57450, $M_{n,GPC}$ = 21030, M_w/M_n= 1.20, relative to PS).

For Polymer **P5**: ^{1}H NMR ($CDCl_3$, δ, ppm) 6.51 (s, 2H, C*H*=C*H*), 5.21 (s, 2H, C*H* bridgehead protons), 4.09 (br s , 16H, CH_2 ester protons), 3.66-3.31 (br s, 6H, OCH_2 of DEGMEMA), 3.35 (br s, 5H, OCH_3 of DEGMEMA and NCH_2), 2.75 (s, 6H, C*H*-C*H*

bridge protons and NCCH_2), 2.00-0.84 (m, 40H, NCH$_2$CH_2CH$_2$O, C(CH_3), CBr(CH_3), CH_2 and CH_3 along polymer backbone).

6.2.4.3. Synthesis of G2M-(DEGMEMA-*co*-NHSMA) (**P6**). G2M-(DEGMEMA-*co*-NHSMA) was prepared by ATRP of DEGMEMA and NHSMA. Furan protected maleimide containing G2-initiator (**5)** (50.0 mg, 0.043 mmol) dissolved in minimum amount of degassed anisole was introduced into a flask containing Cu(I)Br (24.6 mg, 0.171 mmol), degassed PMDETA (71.5 µL, 0.343 mmol), degassed DEGMEMA (2.96 mL, 16.06 mmol) and NHSMA (196.2 mg, 1.07 mmol) dissolved in degassed anisole (29.6 mL) under stirring. The flask was then placed in a thermostated oil bath at 40 °C for 180 min. After polymerization, the reaction mixture was cooled down to room temperature, passed through a neutral alumina column to remove the catalyst and precipitated in diethyl ether twice. **P6** was filtered and obtained as a viscous solid (0.98 g). ($[I]_0$:$[M]_0$:[CuBr]:[PMDETA]=1:400:4:8, [DEGMEMA]:[NHSMA] = 15:1, conversion = 30 %, $M_{n,theo}$ = 22870, $M_{n,NMR}$ = 55590, $M_{n,GPC}$ = 24100, M_w/M_n= 1.21, relative to PS).

For Polymer **P6**: ^{1}H NMR ($CDCl_3$, δ, ppm) 6.51 (s, 2H, C*H*=C*H*), 5.21 (s, 2H, C*H* bridgehead protons), 4.09 (br s , 16H, CH_2 ester protons), 3.66-3.54 (br s, 6H, OCH_2 of DEGMEMA), 3.37 (br s, 5H, OCH_3 of DEGMEMA and NCH_2), 2.78 (s, 6H, C*H*-C*H* bridge protons and NCCH_2), 2.03-0.87 (m, 40H, NCH$_2$CH_2CH$_2$O, C(CH_3), CBr(CH_3), CH_2 and CH_3 along polymer backbone).

6.2.4.4. Synthesis of G2M-(PEGMEMA-*co*-NHSMA) (**P7**). G2M-(PEGMEMA-*co*-NHSMA) was prepared by ATRP of PEGMEMA and NHSMA. Furan protected maleimide containing G2-initiator (**5)** (20.0 mg, 0.017 mmol) dissolved in minimum amount of degassed anisole was introduced into a flask containing Cu(I)Br (9.8 mg, 0.068 mmol), degassed PMDETA (28.4 µL, 0.136 mmol), degassed PEGMEMA (1.79 mL, 6.26 mmol) and NHSMA (95.8 mg, 0.52 mmol) dissolved in degassed anisole (17.9 mL) under stirring. The flask was then placed in a thermostated oil bath at 40 °C for 180 min. After polymerization, the reaction mixture was cooled down to room temperature, passed through a neutral alumina column to remove the catalyst and precipitated in diethyl ether twice. **P7** was filtered and obtained as a viscous solid (0.41 g).

($[I]_0$:$[M]_0$:[CuBr]:[PMDETA]=1:400:4:8, [PEGMEMA]:[NHSMA] = 12:1, conversion = 19 %, $M_{n,theo}$ = 22340, $M_{n,NMR}$ = 62560, $M_{n,GPC}$ = 15020, M_w/M_n= 1.17, relative to PS).

For Polymer **P7**: ^{1}H NMR ($CDCl_3$, δ, ppm) 6.51 (s, 2H, C*H*=C*H*), 5.22 (s, 2H, C*H* bridgehead protons), 4.07 (br s , 16H, CH_2 ester protons), 3.64-3.53 (br s, 14H, OCH_2 of PEGMEMA), 3.36 (br s, 5H, OCH_3 of PEGMEMA and NCH_2), 2.80 (s, 6H, C*H*-C*H* bridge protons and NCCH_2), 1.93-0.86 (m, 40H, $NCH_2CH_2CH_2O$, C(CH_3), CBr(CH_3), CH_2 and CH_3 along polymer backbone).

6.2.5. Synthesis of 8-arm Multiarm Star Copolymers via G3 Dendritic Initiator

6.2.5.1. Synthesis of G3M-(PMMA-*co*-NHSMA) (**P8**). G3M-(PMMA-*co*-NHSMA) was prepared by ATRP of MMA and NHSMA. Furan protected maleimide containing G3-initiator (**6)** (20.0 mg, 8.97 μmol) dissolved in minimum amount of degassed anisole was introduced into a flask containing Cu(I)Br (10.32 mg, 0.072 mmol), degassed PMDETA (30.0 μL, 0.144 mmol), degassed MMA (0.72 mL, 6.73 mmol) and NHSMA (82.2 mg, 0.45 mmol) dissolved in degassed anisole (7.2 mL) under stirring. The flask was then placed in a thermostated oil bath at 40 °C for 180 min. After polymerization, the reaction mixture was cooled down to room temperature, passed through a neutral alumina column to remove the catalyst and precipitated in methanol twice. **P8** was filtered and obtained as a white solid (0.31 g). ($[I]_0$:$[M]_0$:[CuBr]:[PMDETA]=1:800:8:16, [MMA]:[NHSMA] = 15:1, conversion = 41 %, $M_{n,theo}$ = 36730, $M_{n,NMR}$ = 50470, $M_{n,GPC}$ = 22660, M_w/M_n= 1.19, relative to PS).

For Polymer **P8**: ^{1}H NMR ($CDCl_3$, δ, ppm) 6.51 (s, 2H, C*H*=C*H*), 5.21 (s, 2H, C*H* bridgehead protons), 4.32-4.97 (m , 30H, CH_2 ester protons), 3.75-3.38 (m , 5H, CH_3 ester protons and NCH_2), 2.80 (br s, 6H, C*H*-C*H* bridge protons and NCCH_2), 2.26-0.81 (m, 76H, $NCH_2CH_2CH_2O$, C(CH_3), CBr(CH_3) , CH_2 and CH_3 along polymer backbone).

6.2.5.2. Synthesis of G3M-(DEGMEMA-*co*-NHSMA) (**P9**). G3M-(DEGMEMA-*co*-NHSMA) was prepared by ATRP of DEGMEMA and NHSMA. Furan protected maleimide containing G3-initiator (**6)** (20.0 mg, 8.97 μmol) dissolved in minimum amount of degassed anisole was introduced into a flask containing Cu(I)Br (10.32 mg, 0.072 mmol), degassed PMDETA (30.0 μL, 0.144 mmol), degassed DEGMEMA (1.24 mL, 6.73

mmol) and NHSMA (82.2 mg, 0.45 mmol) dissolved in degassed anisole (12.4 mL) under stirring. The flask was then placed in a thermostated oil bath at 40 °C for 180 min. After polymerization, the reaction mixture was cooled down to room temperature, passed through a neutral alumina column to remove the catalyst and precipitated in diethyl ether twice. **P9** was filtered and obtained as a viscous solid (0.19 g). ($[I]_0$:$[M]_0$:[CuBr]:[PMDETA]=1:800:8:16, [DEGMEMA]:[NHSMA] = 15:1, conversion = 14 %, $M_{n,theo}$ = 23250, $M_{n,NMR}$ = 34440, $M_{n,GPC}$ = 20230, M_w/M_n= 1.08, relative to PS).

For Polymer **P9**: ^{1}H NMR ($CDCl_3$, δ, ppm) 6.50 (s, 2H, C*H*=C*H*), 5.20 (s, 2H, C*H* bridgehead protons), 4.08 (br s , 30H, CH_2 ester protons), 3.66-3.53 (br s, 6H, OCH_2 of DEGMEMA), 3.37 (br s, 5H, OCH_3 of DEGMEMA and NCH_2), 2.77 (s, 6H, C*H*-C*H* bridge protons and NCCH_2), 2.03-0.86 (m, 76H, $NCH_2CH_2CH_2O$, C(CH_3), CBr(CH_3), CH_2 and CH_3 along polymer backbone).

6.2.5.3. Synthesis of G3M-(PEGMEMA-*co*-NHSMA) (**P10**). G3M-(PEGMEMA-*co*-NHSMA) was prepared by ATRP of PEGMEMA and NHSMA. Furan protected maleimide containing G3-initiator (**6)** (20.0 mg, 8.97 μmol) dissolved in minimum amount of degassed anisole was introduced into a flask containing Cu(I)Br (10.32 mg, 0.072 mmol), degassed PMDETA (30.0 μL, 0.144 mmol), degassed PEGMEMA (1.92 mL, 6.73 mmol) and NHSMA (82.2 mg, 0.45 mmol) dissolved in degassed anisole (19.2 mL) under stirring. The flask was then placed in a thermostated oil bath at 40 °C for 180 min. After polymerization, the reaction mixture was cooled down to room temperature, passed through a neutral alumina column to remove the catalyst and precipitated in diethyl ether twice. **P10** was filtered and obtained as a viscous solid (0.41 g). ($[I]_0$:$[M]_0$:[CuBr]:[PMDETA]=1:800:8:16, [PEGMEMA]:[NHSMA] = 15:1, conversion = 20 %, $M_{n,theo}$ = 49060, $M_{n,NMR}$ = 133250, $M_{n,GPC}$ = 33910, M_w/M_n= 1.09, relative to PS).

For Polymer P10: ^{1}H NMR ($CDCl_3$, δ, ppm) 6.50 (s, 2H, C*H*=C*H*), 5.17 (s, 2H, C*H* bridgehead protons), 4.06 (br s , 30H, CH_2 ester protons), 3.63-3.53 (br s, 14H, OCH_2 of PEGMEMA), 3.35 (br s, 5H, OCH_3 of PEGMEMA and NCH_2), 2.79 (s, 6H, C*H*-C*H* bridge protons and NCCH_2), 1.92-0.84 (m, 76H, $NCH_2CH_2CH_2O$, C(CH_3), CBr(CH_3), CH_2 and CH_3 along polymer backbone).

6.2.6. Activation of Copolymer P6 by Retro-Diels/Alder Reaction (P11)

Polymer **P6** (300.0 mg, 5.4 μmol) was transferred into a flask. Then it was connected to a vacuum line and heated at 100 °C for 5 hours. ^{1}H NMR analysis indicated a quantitative conversion of the oxabicyclic moiety to the maleimide functional group (293.0 mg, 98 % yield).

For Polymer **P11**: ^{1}H NMR ($CDCl_3$, δ, ppm) 6.74 (s, 2H, C*H*=C*H*), 4.10 (br s , 16H, CH_2 ester protons), 3.68-3.55 (br s, 6H, OCH_2 of DEGMEMA), 3.39 (br s, 5H, OCH_3 of DEGMEMA and NCH_2), 2.79 (s, 4H, NCCH_2), 1.90-0.88 (m, 40H, $NCH_2CH_2CH_2O$, C(CH_3), CBr(CH_3), CH_2 and CH_3 along polymer backbone).

6.2.7. Conjugation of Copolymer P11 with Bodipy-SH via Thiol-ene Reaction (P12)

Polymer **P11** (250.0 mg, 4.5 μmol) and BodipyC10SH (2.35 mg, 5.4 μmol) were dissolved in THF (1.0 mL) and triethylamine (0.16 μL, 1.12 μmol) was added into the reaction mixture. The reaction was allowed to proceed at room temperature (25 ^{o}C) for 24 hours. Unreacted dye was removed by washing the conjugate with cold diethyl ether several times. Dye conjugated multiarm star copolymer **P12** was obtained as a fluorescent viscous solid (240.0 mg, 95 % yield).

For Polymer **P12**: ^{1}H NMR ($CDCl_3$, δ, ppm) 6.11 (s, 2H, *H*C=CCH_3 of Bodipy), 4.08 (br s , 16H, CH_2 ester protons), 3.66-3.53 (br s, 6H, OCH_2 of DEGMEMA), 3.37 (br s, 5H, OCH_3 of DEGMEMA and NCH_2), 2.77 (s, 8H, NCCH_2, C*H*SCH2 and CH_2S of Bodipy), 2.52 (br s, 1H, CH_2CHS), 2.48 (s, 6H, NCCH_3 of Bodipy), 2.39 (s, 6H, CH_3C=C of Bodipy), 1.92-0.87 (m, 56H, $NCH_2CH_2CH_2O$, C(CH_3), CBr(CH_3), CH_2 of Bodipy, CH_2 and CH_3 along polymer backbone).

6.2.8. Conjugation of Copolymers with Gemcitabine via Amidation Reaction

6.2.8.1. Conjugation of Copolymer P6 with Gemcitabine (**P13**). Multiarm star copolymer **P6** (10.0 mg, 0.18 μmol) and Gemcitabine (4.6 mg, 17.8 μmol) were dissolved in anhydrous pyridine (0.10 mL) and the reaction was allowed to proceed at 40 ^{o}C for 48 hours. After reaction mixture was cooled down to room temperature, unreacted

Gemcitabine was removed by centrifugal filtration (MWCO: 3000 Da, 5 times, 7000 rpm, 10 min per time) over MeOH:H_2O (1:1) mixture, and the concentrated solution was lypholized to give the resultant drug conjugated multiarm star copolymer as viscous solid **P13** (7.5 mg). ([P25]:[Gemcitabine]= 1:7, Drug content by weight = 3.25 %, Conjugation efficiency = (7/20)*100 = 35 %).

For Polymer **P13**: ^{1}H NMR (DMSO, δ, ppm) 7.95 (d, 1H, NC*H*, *J* = 8.0), 6.10 (t, 1H, NC*H*O, *J* = 8.0), 6.01 (d, 1H, C=C*H*, *J* = 8.0), 6.55 (s, 2H, C*H*=C*H*), 5.10 (s, 2H, C*H* bridgehead protons), 4.02 (br s , 16H, CH_2 ester protons), 3.60-3.46 (br s, 6H, OCH_2 of DEGMEMA), 3.36 (br s, 5H, OCH_3 of DEGMEMA and NCH_2), 2.80 (s, 6H, C*H*-C*H* bridge protons and NCCH_2), 1.83-0.80 (m, 40H, NCH$_2$CH_2CH$_2$O, C(CH_3), CBr(CH_3), CH_2 and CH_3 along polymer backbone).

6.2.8.2. Conjugation of Copolymer P12 with Gemcitabine (**P14**). Dye conjugated multiarm star copolymer **P12** (10.0 mg, 0.18 μmol) and Gemcitabine (4.7 mg, 17.9 μmol) were dissolved in anhydrous pyridine (0.10 mL) and the reaction was allowed to proceed at 40 ^{o}C for 48 hours. After reaction mixture was cooled down to room temperature, unreacted Gemcitabine was removed by centrifugal filtration (MWCO: 3000 Da, 5 times, 7000 rpm, 10 min per time) over MeOH:H_2O (1:1) mixture, and the concentrated solution was lypholized to give the resultant fluorescent dye and drug conjugated multiarm star copolymer as a fluorescent viscous solid **P14** (8.2 mg). ([P26]:[BodipyC10SH]:[Gemcitabine]= 1:1:6, Drug content by weight = 2.78 %, Conjugation efficiency = (6/20)*100 = 30 %).

For Polymer **P14**: ^{1}H NMR (DMSO, δ, ppm) 7.89 (d, 1H, NC*H*, *J* = 8.0), 6.11 (t, 1H, NC*H*O, *J* = 8.0), 6.03 (s, 2H, *H*C=CCH$_3$ of Bodipy), 5.96 (d, 1H, C=C*H*, *J* = 8.0), 4.02 (br s , 16H, CH_2 ester protons), 3.60-3.46 (br s, 6H, OCH_2 of DEGMEMA), 3.36 (br s, 5H, OCH_3 of DEGMEMA and NCH_2), 2.79 (s, 8H, NCCH_2, C*H*SCH2 and CH_2S of Bodipy), 2.40 (s, 6H, NCCH_3 of Bodipy), 2.33 (s, 6H, CH_3C=C of Bodipy), 1.88-0.80 (m, 56H, NCH$_2$CH_2CH$_2$O, C(CH_3), CBr(CH_3), CH_2 of Bodipy, CH_2 and CH_3 along polymer backbone).

6.2.9. *In vitro* Experiments

6.2.9.1. Cytotoxicity Experiments. Cytotoxicity of orthogonally reactive copolymers and its imaging agent and drug conjugated versions were assessed by CCK-8 viability assay against MDA-MB-231 human adenocarcinoma breast cell lines. Cells (5000 cells/well) were seeded in a 96-well plate as quadruplet in 100 μL appropriate culture medium and incubated at 37 ^{o}C for 24 h for cells to adhere completely. Polymers were dissolved in DMSO at 10^{-2} M stock concentration and seven different concentrations (0.1 nM to 0.1 mM) of samples were prepared via serial dilutions. Cells were treated with these samples and incubated at 37 C for 72 h. After removal of sample solutions, wells were washed with 100 μL PBS twice. The amount of viable cells was determined by CCK-8 cell viability assay by adding 10 μL CCK-8 reagent in 100 μL fresh medium onto wells and at the end of 1 h incubation absorbance values at 450 nm were measured via a microplate reader. EC50 values were calculated by GraphPad prism software using non-linear regression mode.

6.2.9.2. Internalization Experiments. MDA-MB-231 human adenocarcinoma breast cells (10000 cells/well) were seeded in a 24-well plate as quadruplet in 500 μL of RPMI-1640 medium and incubated at 37 ^{o}C for 24 h for cells to adhere completely. Then the culture medium was aspirated and replaced with fresh medium containing imaging agent functionalized copolymers at a concentration of 10^{-5} M. The experiments were completed in triplicate. After incubation at 37 ^{o}C for 12 h, sample solutions were removed. Wells were washed with 500 μL PBS twice and cells were mounted with PBS containing DAPI (5 mg/mL) at 37 ^{o}C for 30 min. Then washed with PBS three times, cells were fixed with 4% formaline solution at 37 ^{o}C for 5 min. Images were collected by Zeiss Observer Z1 fluorescence microscope at room temperature.

6.3. Results and Discussion

Several unique polymeric constructs with different architectures were successfully synthesized and decorated with orthogonal functional groups for convenient conjugation of drug molecules and an imaging agent. Depending on the generation of dendritic initiators utilized for the copolymerization of three different monomers (MMA, DEGMEMA and

PEGMEMA) with an amine reactive monomer (NHSMA), resultant star copolymers possessed 2, 4 and 8 polymeric arms A 4-armed water soluble multiarm scaffold was evaluated for its conjugation efficiency through post-polymerization modification with a thiol-containing hydrophobic dye, BodipyC10SH through attachment to the maleimide unit and a chemotherapy drug, gemcitabine, via appending to the side chains of polymeric arms by replacing the NHS groups. The ultimate goal of this project is to investigate the effect of this architecture in *in vivo* studies. To date, this polymeric platform was evaluated for its *in vitro* cytotoxicity and internalization studies over breast cancer cell line.

6.3.1. Synthesis of Multiarm Star Copolymers with Naked Maleimide Units

Multiarm star polymers explored in this project were synthesized starting with first through third generation dendritic initiators that were obtained according to the literature procedures [117]. Reactivity of maleimide unit during the polymerization reactions necessitates its protection/deprotection by furan group based on the sequential Diels-Alder/retro Diels-Alder strategy. Polyester dendrons furnished with acetal groups at the periphery (**3-5**) were prepared using a previously established protocol that utilizes the divergent synthesis of dendrons using an acetonide-protected bis(hydroxy)propionic acid building block [98]. In short, a furan protected N-hydroxy propyl maleimide was reacted with acetonide-protected bis(hydroxy)propionic anhydride to obtain a first generation dendron decorated with acetal groups, which then converted into polyols by an acidic resin DOWEX 50W-X2. Reserving the core with the furan protected maleimide moiety, higher generations of polyester dendrons were obtained by iterative reaction of hydroxyl units at the periphery with acetal-containing anhydride and subsequent removal of the acetal groups. Consequently, the hydroxyl groups at the periphery of several generations of dendrons were esterified by 2-bromoisobutyryl bromide in the presence of triethylamine and DMAP to efford multiarm initiators with tailored initiator density at the periphery in sufficient yields and they are named with their generation numbers with “M” standing for the maleimide unit at their core (Figure 6.4).

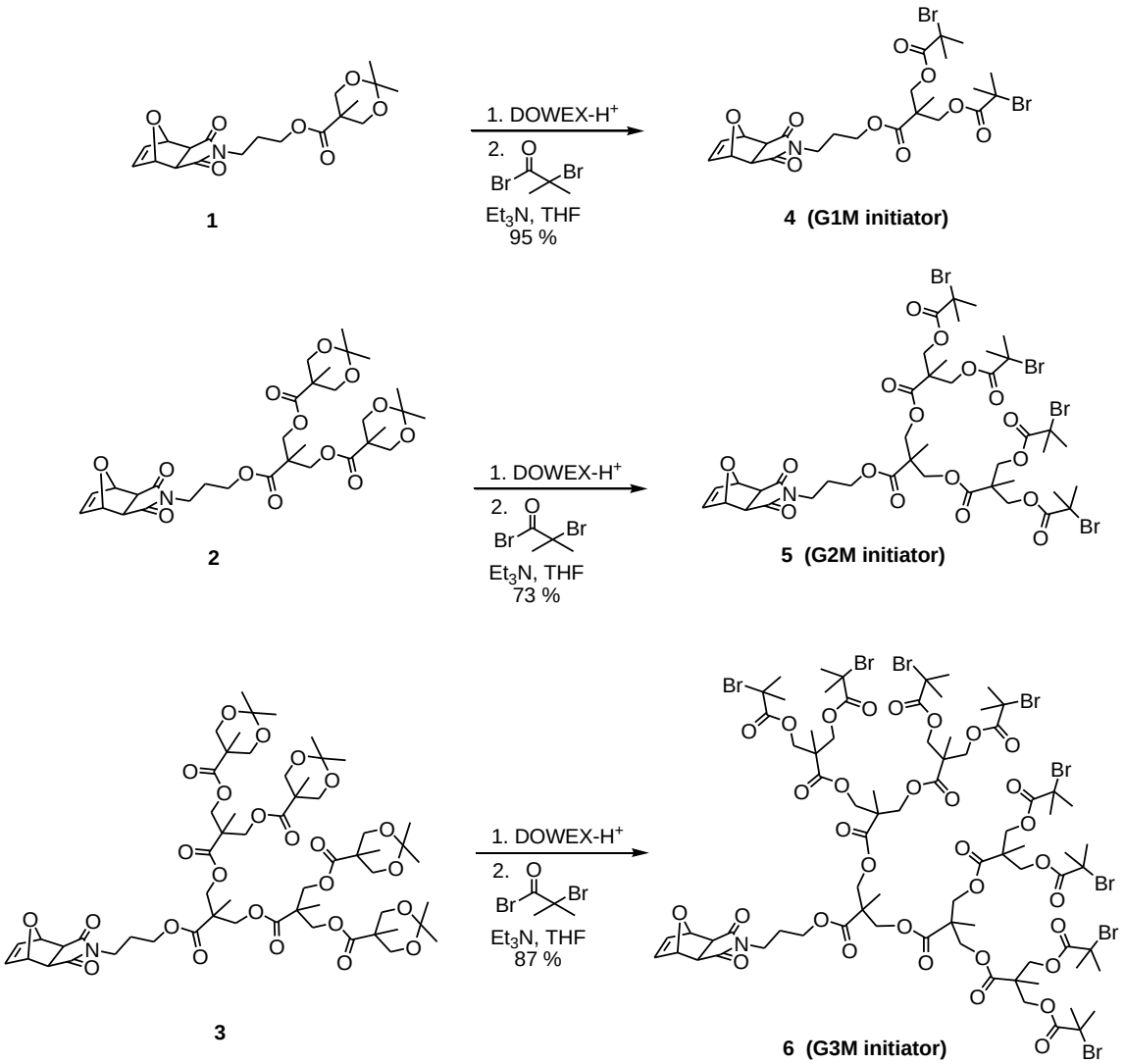

Figure 6. 4. Synthesis of furan protected maleimide based dendritic initiators G1M-G3M.

Dendritic initiators, obtained in pure form and well-characterized by NMR spectroscopy were evaluated for the polymerization of various monomers by ATRP method. Polymerizations initiated by the radical of tertiary halogens at the periphery enable the incorporation of several reactive groups to side chains of polymeric arms. Herein, N-hydroxysuccinimide functionality was preferred to be introduced into polymeric scaffolds due to orthogonality of this amine reactive group with respect to thiol reactive maleimide unit at the core. All dendritic initiators were utilized for the copolymerization of an organosoluble and water soluble monomers with NHS containing methacrylate monomer. Synthesis of the NHSMA monomer was achieved by treatment of N-hydroxy succinimide with methacryloyl chloride [245].

Depending on the generation number, dendritic initiators were utilized for the synthesis of 2, 4 and 8 arm copolymers. A series of multiarm star copolymers were prepared with the copolymerization of organosoluble monomer MMA and water soluble monomers PEGMEMA and DEGMEMA with a NHS-containing methacrylate monomer. The numerous amine-reactive NHS groups appended along the polymeric arms provide multifunctionality to the construct. Thiol reactive maleimide group at the core does not interfere with the NHS functionalities at the side chains of polymeric arms, hence the resultant constructs are orthogonally reactive towards thiol and amine containing molecules

Copolymers were obtained using ATRP in the presense of a Cu(I)Br salt and a PMDETA ligand in anisole as a solvent. Polymerization temperatures were kept at 40 ^{o}C to prevent any removal of the furan masking group from the core of the initiators (Figure 6.5). ^{1}H NMR spectra of all copolymers ensure the intactness of furan-maleimide cycloadduct during the polymerization processes. Reactions were terminated at low conversions in order to obtain copolymers with well-defined arms and low polydispersity values (Table 6.1).

Synthesized copolymers were characterized by GPC and ^{1}H NMR analysis for their structural assignments and purity for further modification and conjugation steps. Table 6.1 demonstrates polymerization conditions for three combinations of monomers associated with all dendritic initiators. Monomer compositions of obtained copolymers were calculated from the integration values of characteristic peaks of monomers, namely peak d (OCH_3 of DEGMEMA) at 3.37 ppm and peak e (CH_2 of NHSMA) at 2.78 ppm, and number of monomers incorporated into polymerization was determined by comparing them with the proton resonances of furan-maleimide cycloadduct (peaks a, b and c at 6.51, 5.21 and 3.19 ppm, respectively in Figure 6.7a) at the core of the initiators handled. It is evident from the data collected that the ratio of NHS units inserted into the structure of copolymers was close to its feed ratio Difference between molecular weights calculated according to integration values in ^{1}H NMR spectra and measured by SEC was expected due to changes

in hydrodynamic volumes of star polymers when compared to to the employed linear calibration standards.

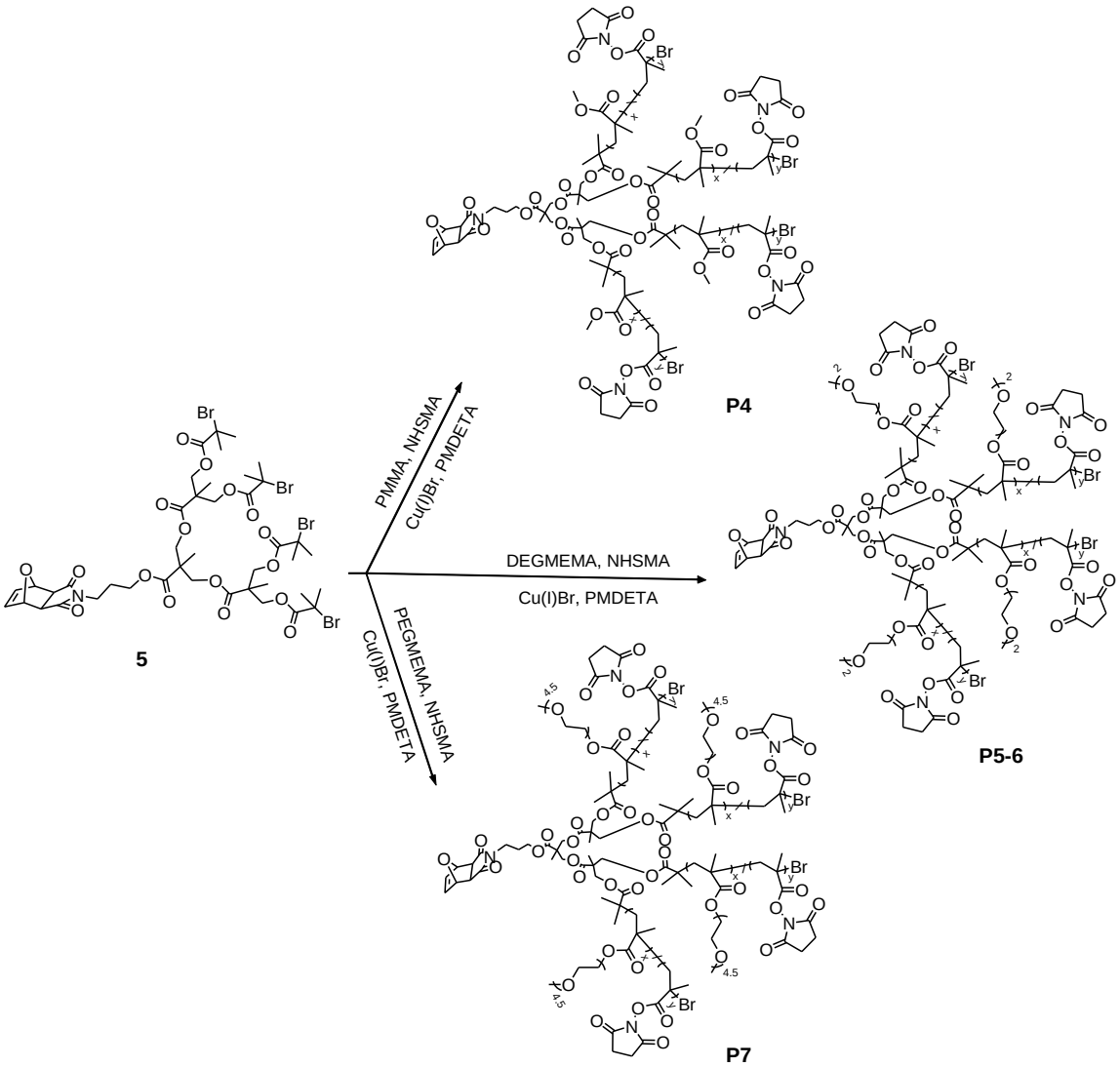

Figure 6. 5. Synthesis of multiarm star copolymers with masked maleimide cores P4-7 using the second generation initiator G2M.

Table 6. 1. Polymerization conditions and characterization details of orthogonally reactive multiarm star copolymers

Entry	Polymer No	Polymer[a]	Time (min)	Feed Ratio (% mol) $[M_1]_0/[M_2]_0$[b]	Obtained Ratio (% mol) $[M_1]_0/[M_2]_0$[b,c]	GPC[d]		$M_{n,NMR}$	Mn_{Theo} (g/mol)	Conv. (%)
						M_n (g/mol)	M_w/M_n			
1	P1	G1M-(PMMA&NHSMA)	180	15	12	11920	1.25	17850	7380	34
2	P2	G1M-(DEGMEMA&NHSMA)	180	15	12	16180	1.17	24650	10690	28
3	P3	G1M-(PEGMEMA&NHSMA)	120	4	2	7900	1.21	10240	10070	18
4	P4	G2M-(PMMA&NHSMA)	180	15	8	14270	1.20	21280	14720	34
5	P5	G2M-(DEGMEMA&NHSMA)	180	15	11	21030	1.20	57448	12200	16
6	P6	G2M-(DEGMEMA&NHSMA)	180	15	13.5	24100	1.21	55590	22870	30
7	P7	G2M-(PEGMEMA&NHSMA)	120	12	7	15020	1.17	62560	22340	19
8	P8	G3M-(PMMA&NHSMA)	180	15	12	22660	1.19	50470	36730	41
9	P9	G3M-(DEGMEMA&NHSMA)	180	15	10	20230	1.08	34440	23250	14
10	P10	G3M-(PEGMEMA&NHSMA)	180	15	12	33910	1.09	133250	49060	20

[a] $[I]_0:[M_{total}]_0:[CuBr]:[PMDETA]$ = 1:200:2:4 (entries 1-3), 1:400:4.8 (entries 4-7), 1:800:8:16 (entries 7-10), M_1:Anisole (v/v): 1:10 and Temperature = 40 ^oC (entries 1-10), [b]M_1: MMA, DEGMEMA, PEGMEMA. M_2: NHSMA, [c]calculated by integration values in ^1H NMR spectra, [d]estimated by SEC eluted with THF, relative to linear PS standards.

After establishment of copolymerization protocols, the second generation initiator based DEGMEMA-*co*-NHSMA copolymer was synthesized on a large scale for bioconjugation studies. P6 copolymer was found to bear 13.5% (mol%) NHS functionality that corresponds to to about 20 NHS groups distributed on 4 polymeric arms randomly. Its high molecular weight ($M_{n\ NMR}$: 55590 g/mol) together with hydrophilic and biodegradable nature underlines its potential as a scaffold for drug delivery and bioconjugation.

The maleimide group at the core of P6 (G2M-(DEGMEMA-co-NHSMA)) was activated by the removal of furan molecule via retro-Diels/Alder reaction at elevated temperature for 5 hours. The maleimide group at the core of this four-armed star copolymer becomes available for conjugation of free thiol containing compounds (Figure 6.6). The quantitative nature of the cycloreversion of the furan-maleimide cycloadduct at the core was established by ^{1}H NMR spectroscopy.

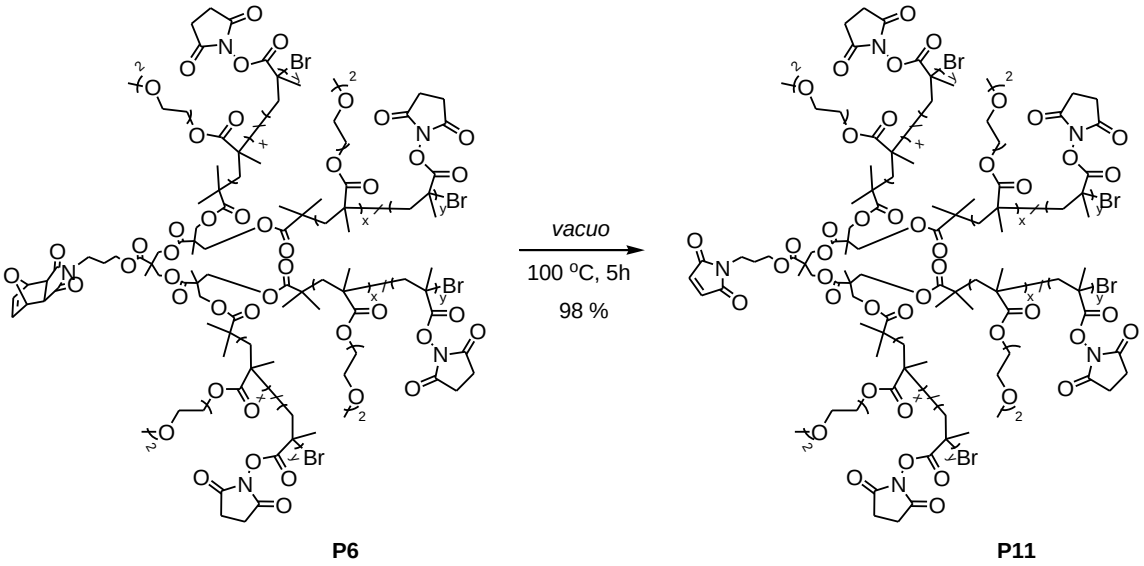

Figure 6. 6. Activation of maleimide group of P6 via retro Diels-Alder reaction (P11).

^{1}HNMR spectrum of P6 clearly demonstrates the characteristic peaks of furan-maleimide cycloadduct a, b and c at 6.51, 5.21 and 2.85 ppm, respectively along with peak d belonging to methoxy group of DEGMEMA monomer at 3.37 ppm and CH_2 protons of NHS groups at 2.78 ppm (Figure 6.7a). Upon retro-Diels/Alder reaction, disappearance of b and c peaks representing protons of furan molecules and shift of bridgehead protons

belonging to maleimide moiety from 2.85 ppm to 6.71 ppm clearly indicate the quantitative unmasking of maleimide group at the core of 4-arm multiarm star copolymer (peak c in Figure 6.7b). Almost same integration values of methoxy protons of DEGMEMA and CH_2 protons of NHS group for P6 and its retro form P11 confirms that NHS functionality is not affected by the polymerization conditions and high temperature of retro-Diels/Alder reaction.

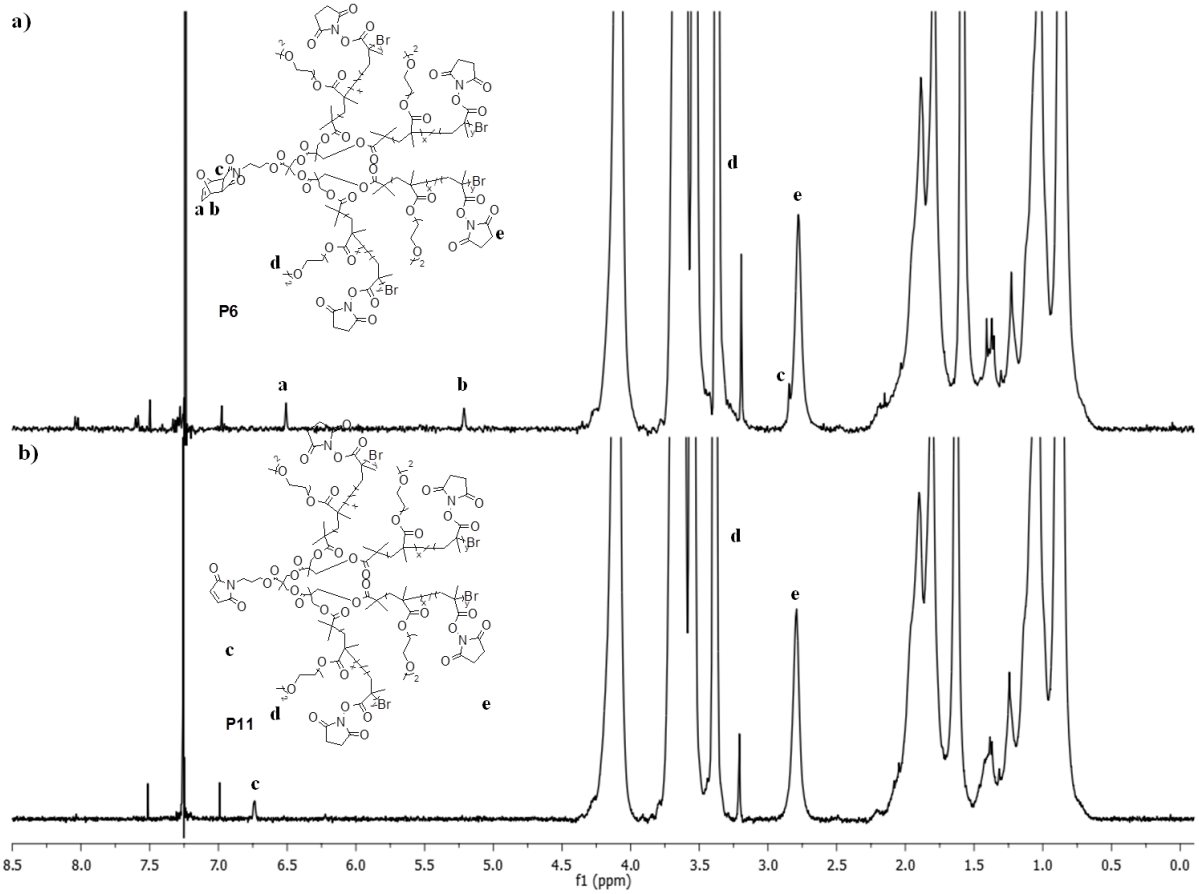

Figure 6. 7. ^{1}H NMR spectra of G2M-(DEGMEMA&NHSMA) copolymer P6 (a) and its retro product P11 (b) in $CDCl_3$.

6.3.2. Conjugation of Multiarm Copolymer with Bodipy-SH via Thiol-ene Reaction

Post-polymerization functionalization of orthogonally reactive multiarm star copolymer was explored by first attaching a thiol containing hydrophobic dye molecule,

namely Bodipy C10SH to the maleimide unit via Michael type thiol-ene chemistry. Due to the dipyrromethene complexed with a disubstituted boron atom in its structure, it imparts a fluorescence behavior at a specific wavelength, hence it is capable of functioning as an imaging agent in drug delivery applications. Especially for the multiarm star copolymers, location of the activated maleimide unit at the core enables an exclusive position for placing the imaging agent, providing the opportunity of its protectionby the surrounding polymeric arms. Furthermore, single maleimide unit in the scaffold is suitable for imaging agent attachment since a single dye molecule is enough to get the necessary signal for the determination of location of the polymeric system in the cells or the body for *in vitro* and *in vivo* studies, respectively.

The dye molecule was conjugated to copolymer P6 in the presence of an organobase, triethylamine. For the nucleophilic addition reaction represented in Figure 6.8, BodipyC10SH was efficiently attached to the polymer architecture. Although the mentioned reaction was performed in THF due to the hydrophobicity of the dye, its conjugation to high molecular weight copolymer improved its solubility in water, transferring its fluorescence property to this polymeric system.

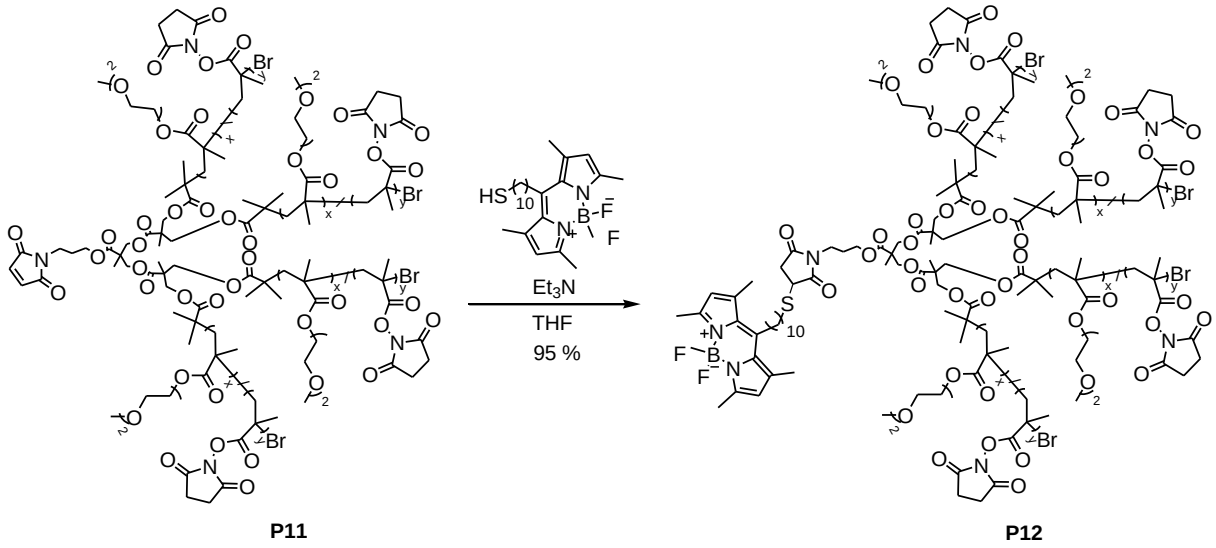

Figure 6. 8. Thiol-ene modification of multiarm star copolymer P11 with BodipyC10SH (P12).

Complete conjugation of all maleimide units with the hydrophobic dye was confirmed by ^{1}H NMR spectroscopy after removal of excess dye washing with diethyl ether (Figure 6.9). Near-quantitative attachment of bodipy dye to maleimide units was evident from disappearance of proton resonance c at 6.71 ppm representing double bond of maleimide. The newly emerged proton resonances f at 6.06 ppm belonging to pyrrole ring and resonances g and k at 2.52 and 2.41 ppm belonging to the methyl groups on this ring confirms conjugation of the dye (Figure 6.9).

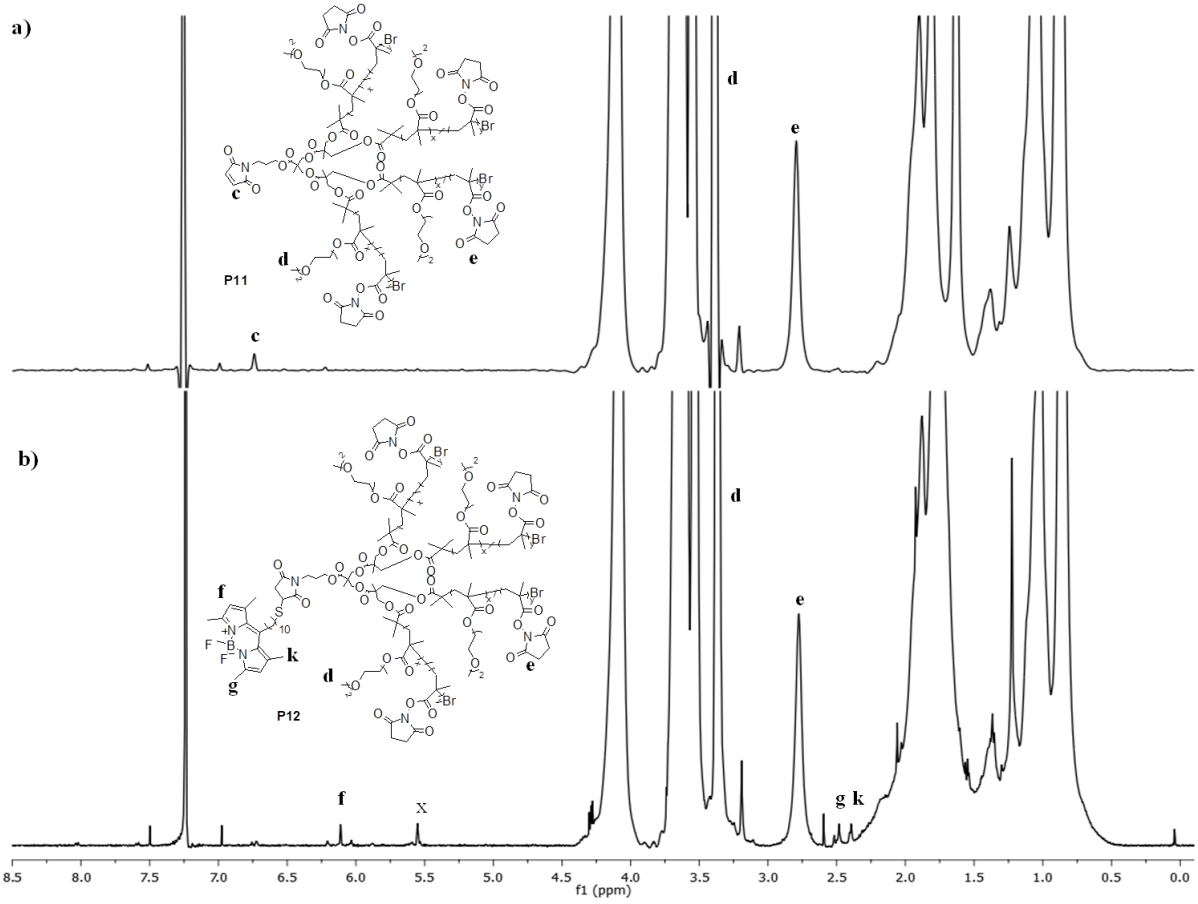

Figure 6. 9. ^{1}H NMR spectra of P11 (a) and P12 (b) in $CDCl_3$.

6.3.3. Conjugation of Multiarm Copolymer with Gemcitabine via Amidation Reaction

Synthesized multifunctional polymeric scaffold was evaluated as drug delivery systems in order to improve the efficacy of chemotherapy agent ‘gemcitabine’. Although it

is one of the frontline drugs in the market for the treatment of several solid tumors like ovarian, breast, pancreatic etc., gemcitabine still has severe side effects to the patients during the chemotherapy process due to its toxicity to healthy tissues and fast renal clearance from the kidneys.

Purified and well-characterized copolymer P6 was conjugated to gemcitabine via aminolysis reaction between the amine group of drug molecule and NHS activated ester appended to polymer chains. Gemcitabine was neutralized with an organobase prydine that was also served as the solvent of this reaction. Conditions for drug conjugation reaction were optimized by trials over 4-armed star copolymer with a protected maleimide group at the core. Incubation of excess drug molecules with the activated ester groups at the polymer chains at 40 ^{o}C for 2 days resulted in gemcitabine attached star copolymer P13 (Figure 6.10).

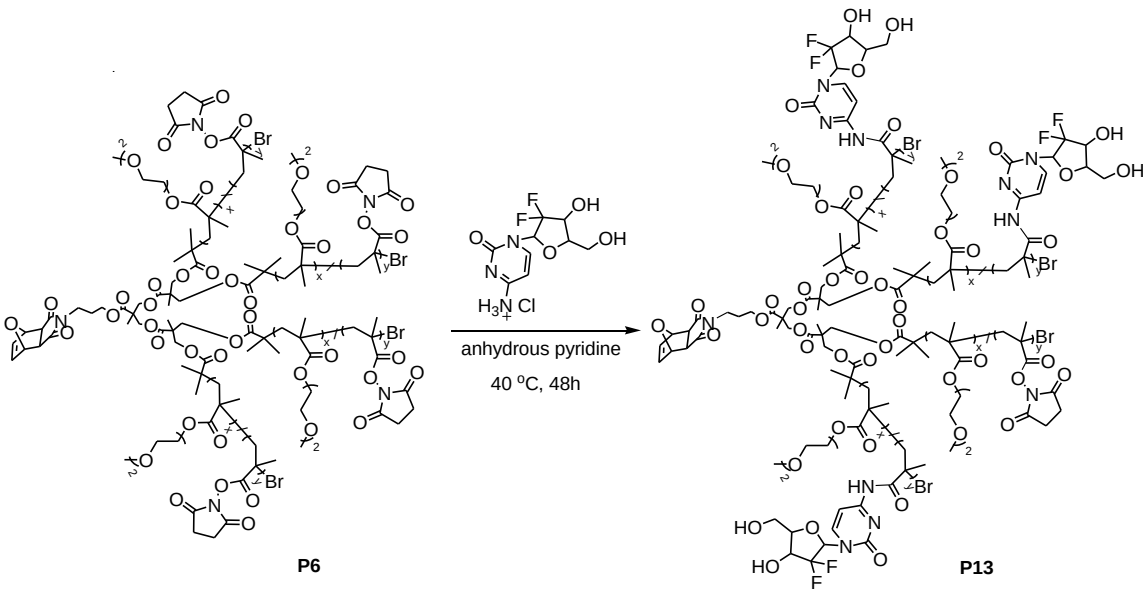

Figure 6. 10. Conjugation of Gemcitabine to multiarm star copolymer P6 via amidation reaction (P13).

Structural assignments and purity of the synthesized conjugate was verified by ^{1}H NMR spectroscopy. A quick glance to the spectrum of the conjugate clearly reveals the characteristic peaks of drug molecule together expected peaks of copolymer. Two doublets observed at 7.95 and 6.00 ppm and the triplet at 6.10 ppm is the proton resonances

originated from the drug structure (peaks n, m and r, respectively Figure 6.11). Presence of singlets at 6.55 and 5.10 ppm proves the conserved structure of furan-maleimide cycloadduct at the core. Decreased integration of the peak at 2.80 ppm for CH_2 of NHS groups (peak e), together with the methoxy protons appeared at 3.27 ppm (peak d) confirms the attachment of drug molecules to side chains of polymeric arms. Calculations from integration values of proton resonances belonging to both drug molecule and furan masked maleimide cycloadduct at the core, it is determined that 7 drug molecules were conjugated to this carrier, corresponding to 3.25 % drug content by weight.

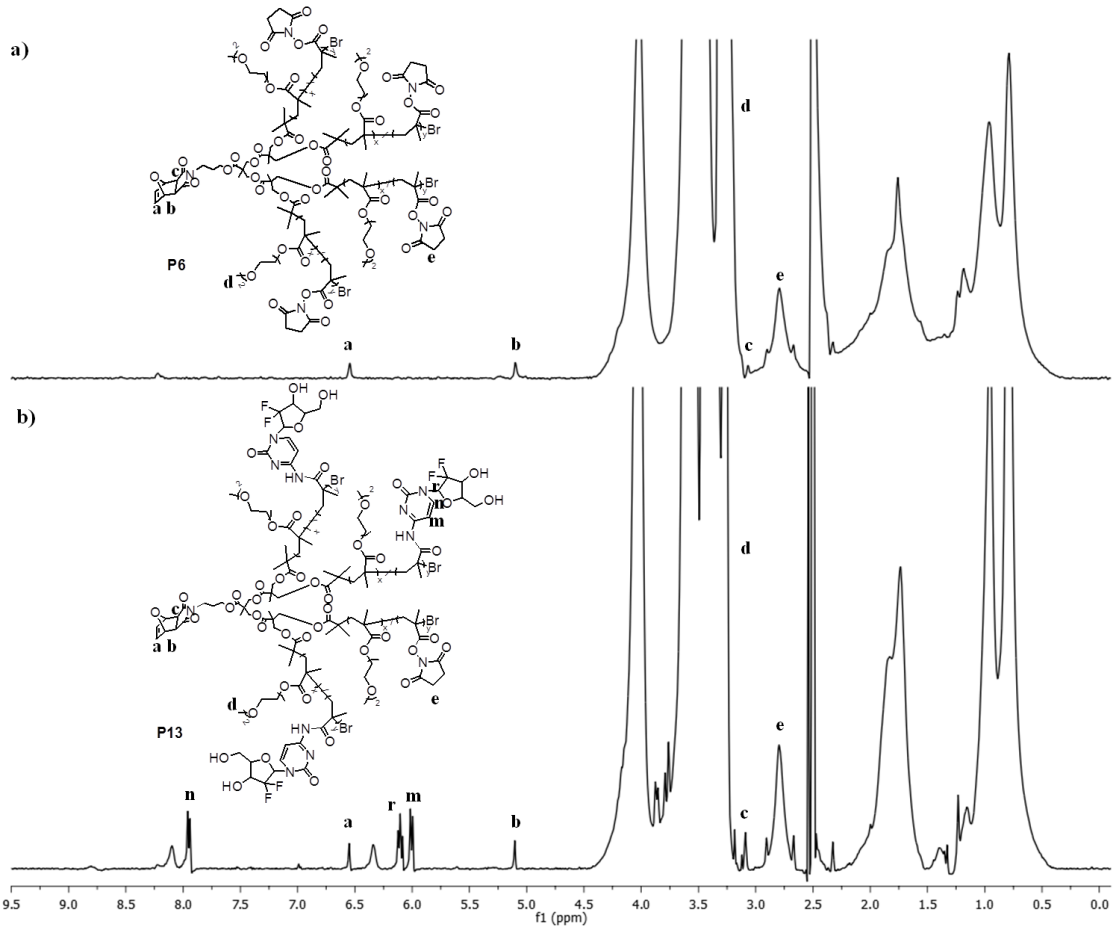

Figure 6. 11. ^{1}H NMR spectra of P6 (a) and P13 (b) in DMSO.

For the dye containing copolymer, multiarm construct was subjected to same reaction conditions as applied to copolymer P6. Bodipy dye located at the core of multiarm star copolymer P12 serves as the imaging agent for these drug carriers, facilitating their localization both in cell internalization and pharmacokinetic studies. Gemcitabine was

conjugated to this orthogonally reactive copolymer replacing NHS functionalities at the side chains (Figures 6.12).

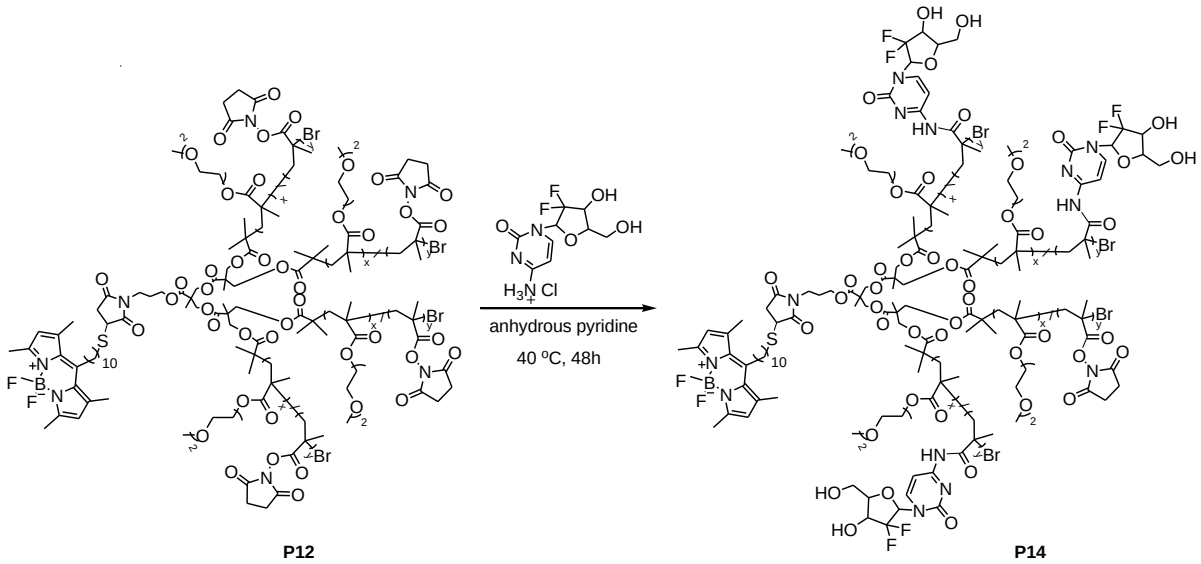

Figure 6. 12. Conjugation of Gemcitabine to multiarm star copolymer P12 via amidation reaction (P14).

Evaluating the ^{1}H NMR spectra of both dye attached multiarm star copolymer and its drug conjugated version (Figure 6.13 a and b respectively), it is obvious that newly emerged doublets at 7.89 and 5.96 ppm (peaks n and m, respectively) and a triplet at 6.11 ppm (peak r) are belong to the drug. Permanence of dye molecule bound to polymer core is verified by the singlet at 6.03 ppm (peak f), representing the hydrogen attached to pyrrole ring in Bodipy structure. Conjugation efficiency and purity of the conjugate was followed by comparison of integration values of peaks for both drug molecule and methoxy protons of polymer chains to conclude that almost 6 drug molecules were successfully conjugated to this multiarm star copolymer that corresponds to. 2.78 % drug content by weight.

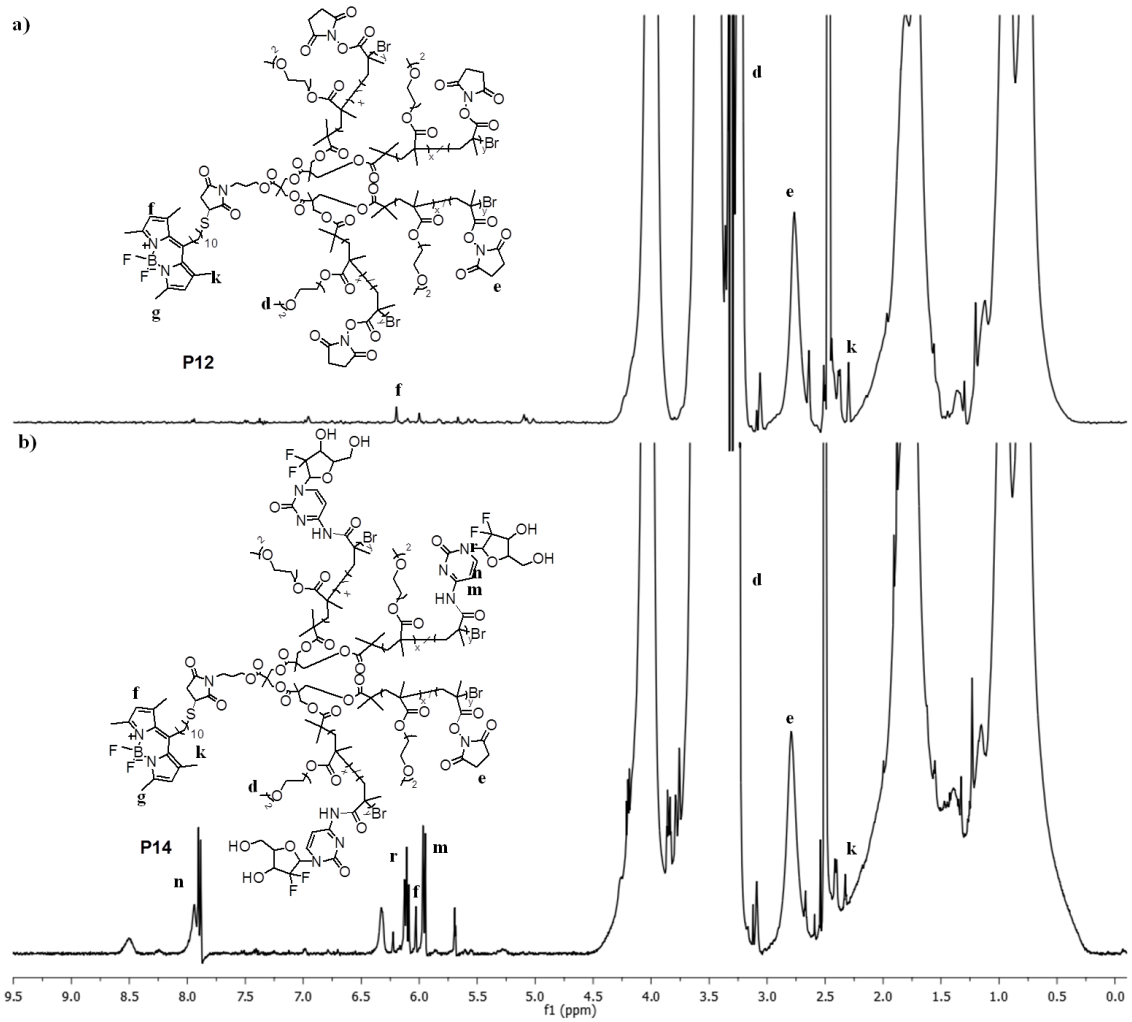

Figure 6. 13. ^{1}H NMR spectra of P12 (a) and P14 (b) in DMSO.

6.3.4. *In vitro* Experiments

6.3.4.1. *In vitro* cytotoxicity assay. Cytotoxicity of synthesized polymer-drug conjugates P13 and P14 were investigated over MDA-MB-231 human breast adenocarcinoma cell lines and compared with that of gemcitabine itself. Copolymers P6 and P11 are the precursor polymers with reactive groups before drug attachment were also evaluated for toxicity. Cells adhered to 96-well plates were treated with drug and polymer-drug samples at 37 ^{o}C for 72h to allow enough time for drug release from the copolymers. Cell viability was evaluated by a colorimetric assay, CCK-8 and obtained absorbance values at 450 nm were processed by GraphPad prism software using non-linear regression curve with a sigmodial dose response equation. By this way, EC_{50} values, concentration at which drug

molecule displaces half of its toxic activity over cells, for drug molecule and conjugates were calculated from the cytoxicity graphs which look like reliable due to the expected “S” shaped pattern with respect to different concentrations of the samples (Figure 6.14). Polymer-drug conjugate P13 devoid of the Bodipy dye was chosen to demonstrate that the presence of dye did not have any added toxicity.

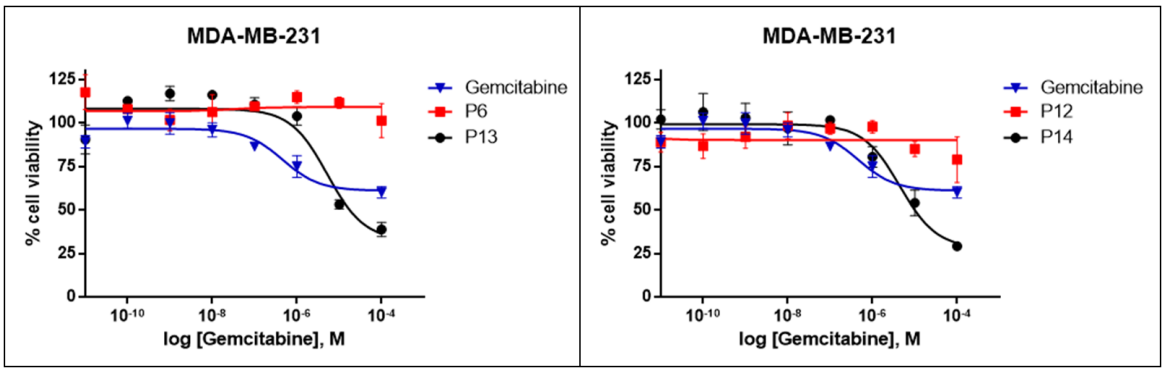

Figure 6. 14. Inhibition of MDA-MB-231 cells proliferation by Gemcitabine itself and Gemcitabine conjugated copolymers P13 and P14, and their reactive precursors P6 and P11, respectively. Cell viability was determined by CCK-8 assay. Results were expressed as mean ± SD (n = 3).

According to growth inhibition studies, drug unbound reactive multiarm polymers did not show significant toxicity over human breast cancer cells, however gemcitabine conjugated polymers P13 and P14 displayed a small compromise (almost 10 times less toxicity) compared to drug itself. Clear shift of cytotoxicity curves (towards higher concentration region) for conjugates proves their reduced activity (Table 6.2).

Table 6. 2. The EC_{50} values for Gemcitabine, its conjugated copolymers P13/P14 and their reactive precursors P6/P12 against human breast cancer cell lines

No	Analyte[a]	Mw or Mn (gr/mol)	Drug Content (% weight)	EC_{50} values/M [b]
1	Gemcitabine	263	-	4.59×10^{-7}
2	P6	57448	0	$>10^{-3}$
3	P12	58604	0	$>10^{-3}$
4	P13	57815	3.25	6.42×10^{-6}
5	P14	58806	2.78	5.06×10^{-6}

[a]Characterization details were given in Tablo 6.1 and Figure 6.11&6.13, [b]evaluated by Graph-Pad prism, non-linear regression mode.

6.3.4.2. *In vitro* internalization assay. Uptake of bodipy conjugated polymers was examined over MDA-MB-231 human adenocarcinoma breast cell lines. Bodipy molecule is fluorescent and can be visualized by green fluorescence filter. However cell nuclei were detected by staining with DAPI, which can be visualized by a blue fluorescence filter. Cultured cells with a density of 10000 cells per well were treated with polymer samples (10^{-5} M) and incubated at 37 ^{o}C for 24 h for efficient internalization. After removal of sample solutions, wells were washed with PBS and DAPI staining was examined. Following the fixation process by formalin, cells were visualized by appropriate fluorescence filters at room temperature. Figure 6.16 displays the fluorescence patterning of internalized polymers from which P11 is the bodipy conjugated multiarm star polymer and P14 bears both Bodipy dye and gemcitabine drug molecules. According to obtained fluorescence images, both polymers were successfully taken up by MDA-MB-231 cells within 24 h in spite of the presense of an anti-biofouling PEG-based composition.

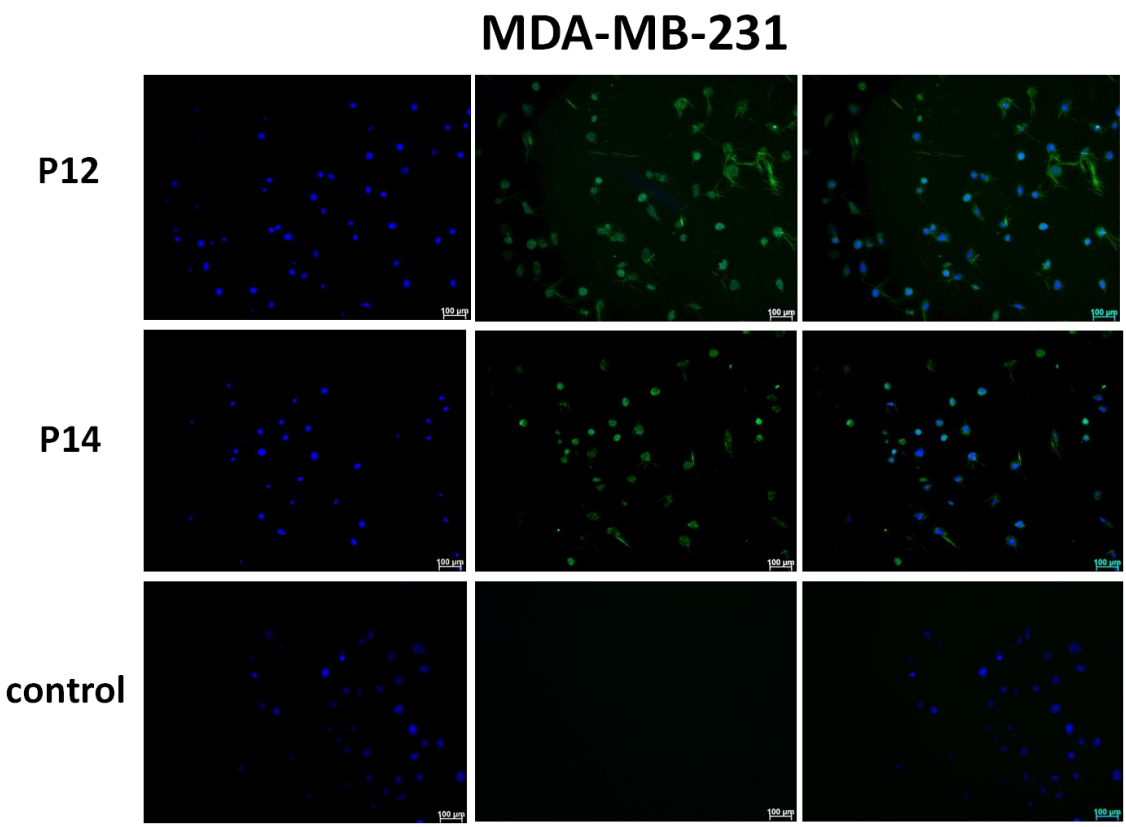

Figure 6. 15. Fluorescence images of MDA-MB-231 cells treated with Bodipy conjugated multiarm star polymers. Cells were incubated at 37 ^{o}C for 24 h and nuclei were stained by DAPI just prior to imaging. (A) shows blue fluorescence of cell nuclei stained by DAPI, (B) shows green fluorescence of internalized Bodipy conjugated polymers, (C) shows the merged images.

6.4. Conclusion

This study describing the synthesis of multifunctional polymeric scaffolds was mainly focused on the design of potential drug delivery systems for a commercially available chemotherapy drug, gemcitabine. Designed as multiarm architectures, obtained polymeric constructs were integrated with orthogonally reactive moieties to facilitate the conjugation of therapeutic and imaging agents of interest. Star polymers obtained by 'core-first' approach obeyed the copolymerization of MMA, DEGMEMA and PEGMEMA monomers with NHS activated ester bearing reactive monomer by the initiators placed at the surface of biodegradable polyester dendrons of three generations. Furan masked maleimide unit was activated by retro Diels/Alder cycloreversion reaction after the copolymerization reactions . These copolymers were conjugated with a hydrophobic dye, BodipyC10SH at their core to play the role of imaging agent. An amine containing drug, gemcitabine was conjugated through the activated esters appended to polymer chains. Results of *in vitro* experiments with these polymer-drug conjugates indicated the efficient uptake of these polymeric systems by breast cancer cell line (MDA-MB-231) with a 10–fold less toxicity.

7. BIODEGRADABLE MULTIARM POLYMERS FOR REVERSIBLE CONJUGATION: SYNTHESIS & FUNCTIONALIZATION

7.1. Introduction

Bioconjugates are of particular interest as attractive pharmaceutical nanocarriers due to their prevalent utility as vehicles for delivery of therapeutic agents, active targeting, gene transfection etc [28], [246, 247]. In recent years a lot of effort has been focused to develop novel polymer architectures for efficient conjugation of peptides, proteins and DNA fragments to serve as polymeric nanomedicine platforms [248, 249].

Recent studies have pointed out that polymer based conjugates and complexes are innovative platforms for improving safety and efficacy of therapeutic peptides and proteins [11], [250]. To enable fabrication of well defined conjugates, polymeric materials have been continuously engineering to possess well-defined biocompatible structures with diverse reactive groups enabling the conjugation of a variety of biomolecules through covalent and bioaffinity bindings [217].

Polymer conjugation addresses the challenge of the stability of therapeutic proteins, poor solubility of chemotherapeutic drugs and tracer dyes, as well as improves their pharmacokinetic behavior. Subjected to proteolytic degradation during circulating in the blood stream, proteins are rapidly eliminated from the kidney resulting in short half-life in the body, which requires frequent administration for sufficient treatment. However high molecular weight polymer chains introduced to protein/peptide assemblies increases the hydrodynamic volume of the resultant macromolecule and provides extended half-life by reducing renal clearance rate [70], [162]. Moreover, modification of protein surface by polymer attachment enhances its stability by emanating a shield for the protein towards proteolytic degradation, the so called “umbrella-like effect” [55].

Today, a number of comprehensively investigated polymer-protein conjugates have passed through all clinical phases successfully and are already in the market for efficient treatment for several diseases. Out of those fascinating constructs, proteins covalently linked to the synthetic polymer poly(ethylene glycol) (PEG) demostrated less immunogenicity due to anti-biofouling property of the polymer. Surrounding the protein surface, PEG chains notably enhance the physical properties of proteins and offer improved pharmacokinetic profiles by eliminating proteolytic degradation [65]. Peg-intron, Somavert and Neulesta are examples of PEGylated proteins in the market routinely administered to the patients with hepatitis C, acromegalia and chemotherapy induced neutropenia, respectively. A novel bioconjugate such as PEG-antiVEGFR-2 fab conjugate named as CDP-791 is in Phase II clinical trials for the treatment of cancer-NSCLC [28].

Discovery of new proteins/peptides conjugates and their evaluation as potential therapeutics has opened the door to design novel polymeric scaffolds [54], [159, 160], [251]. Polymers with various physical properties and chemical functional groups have being synthesized to facilitate the conjugation process in an efficient way. Either physical adsorption or covalent modification routes are followed to obtain complete polymer-protein conjugates [252, 253]. Self-assembled constructs can be designed depending on the association of surface groups of proteins with polymer chains where especially hydrogen bonding and electrostatic interactions are the outstanding ones. However covalent binding of polymers to proteins seems to produce more stable bioconjugates compared to supramolecular assemblies while retaining the protein structure and function intact [254]. So this modification methodology ensures the binding of proteins to polymeric scaffolds in complex biological environments.

Within the diverse range of available conjugation strategies posed by breakthroughs in synthetic chemistry, alternative manipulations to regular reactive amino acid residues on the proteins can be adjusted to a significant extent enabling the design of polymers with complimentary functional groups. Depending on reaction setting and solubility of reagents, polymer-protein conjugates may be prepared by either in situ polymerization over the surface of proteins engineered with required initiation sites or direct modification of

protein with pre-synthesized polymer chains. Generally in situ RAFT and ATRP methods are applied to fabricate desired polymers on protein surface that requires the pre-installation of appropriate initiator groups [60-62]. Mild reaction conditions and controlled nature of these polymerization techniques diminish the possible deteriorations for protein conformation considerably. Regarding the latter one, polymer chains bearing functional groups suitable for reacting with amine and thiol units in protein structure are synthesized in pure form and well-characterized prior the conjugation step. Mostly N-hydroxy succinamide and thiazolidine 2-thione activated esters and dichlorotriazines, thioimidoesters, and aldehydes are preferred for reacting with free lysine residues on the surface of proteins [56], [255]. Since the mentioned reactive groups are randomly located on protein surface, conjugation may not be homogeneous and specific enough to obtain well-defined macromolecules. Instead, thiol groups stem from cystein amino acids or generated by the reduction of disulfide bonds are less frequent in protein structure with known locations and conjugation through these thiol moieties results in site-specific attachment of polymer chains. This challenge is addressed in an amenable manner by polymers with vinyl sulfone, maleimide and activated disulfide end-groups, widely investigated in the literature as popular thiol reactive scaffolds [104], [133-135], [256]. Among those, disulfide exchange reaction is regarded as a powerful tool for composing bioconjugates with biodegradable disulfide bond since after a duration the protein-polymer conjugation breaks and components can be cleared from the body [63], [144], [257].

As mentioned before, polymer architecture has a significant impact on the renal clearance of conjugates where more branched and compact macromolecules are eluted from the kidney at a slower rate, allowing more circulation time in the blood stream to accumulate in the desired part of the body, mostly the tumor tissue due to its leaky morphology. So compared to linear ones, multiarm star polymers provide improved pharmacokinetic behavior for therapeutics like drugs and proteins [258]. In addition, surrounding of these active agents by polymeric arms closely located to each other contributes to the stability of the designed delivery system [259-262].

With the abovementioned characteristics, a reactive disulfide unit containing water soluble multiarm star polymer was synthesized to allow the conjugation of free thiol containing (bio) molecules via disulfide exchange reactions. Periphery of a second generation biodegradable polyester dendron containing a pyridyl disulfide group at the focal point was decorated with suitable initiator moieties to employ ATRP technique for the polymerization of ethylene glycol based monomer, DEGMEMA, to yield water soluble star shaped construct with four polymeric arms. The resultant hydrophilic polymer was utilized to demonstrate solubilization of a hydrophobic dye, BodipyC10SH. The dye-conjugate exhibits fluorescence in water which demonstrates efficient conjugation. The conjugation process was monitored kinetically by recording the UV-Vis absorbance of pyridine 2-thione released as a byproduct from the core of star polymer. Cleavage of the disulfide bond between the polymeric scaffold and conjugated dye molecule was demonstrated by reduction with DTT, where a decrease in the fluorescence was observed over time due to poor solubility of the released dye in aqueous media.

Further implementations of this bioactive star polymer were focused on peptide conjugation. Efficient attachment of a tripeptide, glutathione, to the core of 4-armed star polymer was achieved by reversible disulfide exchange reaction (Figure 7.1). Attempts were focused to demonstrate that this multiarm polymer construct is a potential candidate for protein conjugation that is expected to preserve stability towards proteolytic degradation, slower renal clearance and allow controlled release from the polymer scaffold based on the concentration of free thiol containing molecules in the environment.

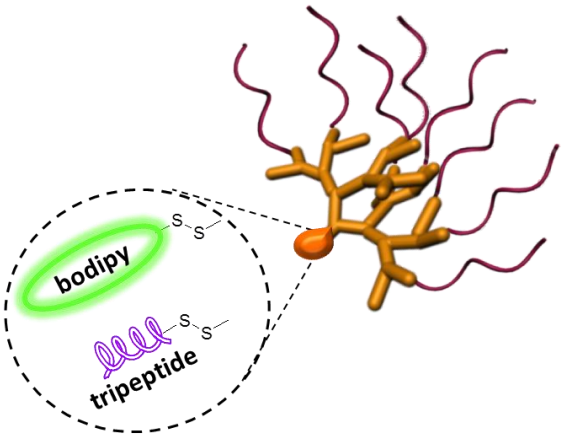

Figure 7. 1. Illustration of a core reactive multiarm star polymer conjugated to an imaging agent and a tripeptide.

7.2. Experimental

7.2.1. Materials

All reagents were obtained from commercial sources and were used as received unless other-wise stated. BodipyC10SH was synthesized according to literature procedures [170]. Di(ethylene glycol) methylether methacrylate (M_n = 188) (DEGMEMA, 99%, Aldrich) was passed through basic alumina column to remove inhibitor prior to use 4,4'-Dinonyl-2,2'-bipyridine (99%, Aldrich) or 2,2'-bipyridine (99%, Aldrich). DMAP, EtN_3 and DTT were obtained from Alfa Aesar and used as received. 2-bromo-2-methyl propionyl bromide (99.9%, Aldrich), L-Reduced Glutathione (98%, Aldrich) and Copper(I)Bromide (CuBr, 99.9%, Aldrich) were used as received. Anhydrous THF was obtained from ScimatCo Purification System. Centrifugal filtration tubes (Spectra/Por® Amicon Ultra-4 Regenerated Cellulose Membranes MWCO 3000 Da) were purchased from Spectrum Labs. All other chemicals were used as received from manufacturer (Merck, Aldrich and Alfa Aesar). Column chromatography was performed using silicagel–

60 (43–60 nm). Thin layer chromatography was performed using silica gel plates (Kiesel gel 60 F254, 0.2mm, Merck).

7.2.2. Instrumentation

7.2.2.1. Nuclear Magnetic Resonance Spectroscopy (NMR). The NMR spectra were recorded using a 400 MHz Varian spectrometer at 25 °C. ^{1}H NMR measurements were made at frequency of 400 MHz, and calibrated with respect to the solvent signal. The measurements were performed in deuterated chloroform ($CDCl_3$) and water (D_2O).

7.2.2.2. Size Exclusion Chromatography (SEC). The molecular weights of the copolymers were estimated by GPC analysis using a Shimadzu PSS-SDV (length/ID 8 × 300 mm, 10 mm particle size) mixed-C column calibrated with polystyrene standards (1–400 kDa) using a refractive-index detector. Tetrahydrofuran (THF) was used as eluent at a flow rate of 1 mL/min at 30 °C.

7.2.2.3. Ultraviolet-Visible Spectroscopy (UV-Vis Spectroscopy). UV-Vis spectra were recorded using a Varian Cary-100 UV-Vis spectrophotometer, centrally controlled by a single dispersion equipped with high performance R928 photomultiplier tube, tungsten halogen visible source with quartz window, deuterium arc ultra violetsource. Wavelength accuracy is ± 0.2 nm.

7.2.3. Synthesis of G2PDS initiator (7)

Pyridyl disulfide containing second generation polyester dendron furnished with four hydroxyl groups at the periphery (**5**) (0.10 g, 0.19 mmol) and DMAP (13.7 mg, 0.11 mmol) were dissolved in THF (15.0 mL) and then triethylamine (0.18 mL, 1.31 mmol) was added onto this solution under nitrogen. The mixture was cooled to 0 °C in an ice bath. On the other side, 2-bromo-isobutyryl bromide (115.0 µL, 0.93 mmol) was diluted in THF (2.0 mL) and added into the former mixture drop wise. The obtained white suspension was stirred for 30 minutes at 0 °C, then warmed to room temperature (25 ^{o}C) and stirred for 6 hours. The ammonium salt formed was filtered off and the residue was concentrated in *vacuo* that was purified by column chromatography on SiO_2 (15 % EtOAc in Hexane) affording the initiator as a pure light yellow solid **(7)** (0.14 g, 67 % yield).

^{1}H NMR ($CDCl_3$, δ, ppm) 8.46 (br s, 1H, C*H*=N), 7.65 (br s, 2H, CH=C*H*-C*H*=N), 7.10 (br s, 1H, N-C-C*H*), 4.42-4.26 (m, 14H, CH_2 ester protons), 3.05 (t, 2H, *J*= 6.0 Hz, SCH_2), 1.59 (s, 24H, CBr(CH_3)), 1.30 (s, 6H, C(CH_3)), 1.27 (s, 3H, C(CH_3)). ^{13}C NMR ($CDCl_3$, δ, ppm) 171.6, 170.9, 149.8, 137.1, 121.0, 120.0, 83.7, 66.0, 63.1, 55.3, 46.8, 36.9, 30.6, 17.9.

7.2.4. Synthesis of 4-arm Multiarm Star Polymer via G2PDS Initiator (P1)

7.2.4.1. Synthesis of G2PDS-DEGMEMA (**P1**). G2PDS-DEGMEMA was prepared by ATRP of DEGMEMA. Pyridyl disulfide containing G2PDS-initiator (**7**) (10.0 mg, 8.84 μmol) dissolved in minimum amount of degassed anisole was introduced into a flask containing Cu(I)Br (5.1 mg, 3.53 μmol), 4,4'-Dinonyl-2,2'-bipyridine (28.9 mg, 70.7 μmol), degassed DEGMEMA (0.65 mL, 3.53 mmol) dissolved in degassed anisole (5.05 mL) under stirring. The flask was then placed in a thermostated oil bath at 80 °C for 120 min. After polymerization, the reaction mixture was cooled down to room temperature, passed through a neutral alumina column to remove the catalyst and precipitated in diethyl ether twice. **P1** was filtered and obtained as a viscous solid (0.15 g). ($[I]_0$:$[M]_0$:[CuBr]:[4,4'-Dinonyl-2,2'-bipyridine]=1:400:4:8, conversion = 23 %, $M_{n,theo}$ = 17560, $M_{n,NMR}$ = 64760, $M_{n,GPC}$ = 27100, M_w/M_n= 1.13, relative to PS).

For polymer **P1**: ^{1}H NMR ($CDCl_3$, δ, ppm) 8.46 (br s, 1H, C*H*=N), 7.67 (br s, 2H, CH=C*H*-C*H*=N), 6.95 (br s, 1H, N-C-C*H*), 4.34-3.90 (m , 16H, CH_2 ester protons), 3.78-3.54 (m, 2H, OCH_2 of DEGMEMA), 3.37 (br s, 3H, OCH_3 of DEGMEMA), 1.89–0.87 (m, 38H, C(CH_3), CBr(CH_3), CH_2 and CH_3 along polymer backbone).

7.2.4.2. Reduction of P1 with Dithiothreitol (DTT). P1 (0.9 mg, 0.014 μmol) was dissolved in a minimal amount of methanol and then diluted with phosphate buffered saline (PBS, pH 7.3) to 5 mL. 1 mL of this solution was mixed with 1 mL of a DTT (dithiothreitol, a reducing agent) solution (1.20 mM in PBS pH 7.3). The absorbance at 379 nm was determined at several time points (0, 10, 30, 60, 90, 120, 180 and 240 min). The concentration of the released pyridine 2-thione was calculated using the reported molar extinction coefficient (8.08 x 10^3 $M^{-1}cm^{-1}$) [256]. Comparison with the total polymer concentration (molecular weight determined from ^{1}H NMR) gave the end group percentage.

7.2.5. Reversible Conjugation of Multiarm Star Polymer with Glutathione and BodipyC10SH

7.2.5.1. Conjugation of Polymer P1 with Glutathione (**P2**). Polymer **P1** (10.0 mg, 0.15 μmol) and Glutathione (0.19 mg, 0.31 μmol) were dissolved in H_2O (0.2 mL) and acetic acid (0.88 μL, 0.015 μmol) was added into the reaction mixture. The reaction was allowed to proceed at room temperature (25 ^oC) for 24 hours. Unreacted tripeptide was removed by centrifugal filtration (MWCO: 3000 Da, 4 times, 7000 rpm, 10 min per time), and the concentrated solution was lyophilized. Glutathione conjugated multiarm star polymer **P2** was obtained as a viscous solid (8.3 mg, 82 % yield).

For polymer **P2**: ^{1}H NMR ($CDCl_3$, δ, ppm) 4.34-3.92 (m , 16H, CH_2 ester protons), 3.78-3.43 (m, 2H, OCH_2 of DEGMEMA), 3.38 (br s, 3H, OCH_3 of DEGMEMA), 2.03–0.86 (m, 38H, C(CH_3), CBr(CH_3), CH_2 and CH_3 along polymer backbone). ^{1}H NMR (D_2O, δ, ppm) 8.41 (s, 2H, N*H* of glutathione), 4.17 (br s, 16H, CH_2 ester protons), 3.76-3.62 (m, 2H, OCH_2 of DEGMEMA), 3.39 (br s, 3H, OCH_3), 2.96-2.90 (m, 2H, SCH_2 of glutathione), 2.49 (br s, 4H, COCH_2CH_2 of glutathione), 2.13-0.86 (m, 38H, C(CH_3), CBr(CH_3), CH_2 and CH_3 along polymer backbone).

7.2.5.2. Conjugation of Polymer P1 with BodipyC10SH (**P3**). Polymer **P1** (20.0 mg, 0.31 μmol) and BodipyC10SH (0.16 mg, 0.37 μmol) were dissolved in THF (0.5 mL) and acetic acid (1.76 μL, 0.031 μmol) was added into the reaction mixture. The reaction was allowed to proceed at room temperature (25 ^oC) for 24 hours. At several time points (0, 1, 2, 3, 4, 5, 6, 7, 8 and 24h) samples were taken from the mixture and THF was removed by a vacuum line. Then samples were dissolved in 3 mL water and analyzed with UV-Vis spectrophotometer to monitor the release of pyridine 2-thione and conjugation of BodipyC10SH with respect to time. At the end of 24h, unreacted dye was removed by washing the conjugate with cold diethyl ether several times. Dye conjugated multiarm star polymer **P3** was obtained as a fluorescent viscous solid (16.3 mg, 81 % yield).

For polymer **P3**: ^{1}H NMR ($CDCl_3$, δ, ppm) 6.03 (s, 2H, *H*C=CCH_3 of Bodipy), 4.32-3.89 (m , 16H, CH_2 ester protons), 3.77-3.53 (m, 2H, OCH_2 of DEGMEMA), 3.37 (br s, 3H,

OCH_3 of DEGMEMA), 2.48 (s, 6H, NCCH_3 of Bodipy), 2.40 (s, 6H, CH_3C=C of Bodipy), 2.30 (t, 2H, J= 8.0 Hz, CCH_2 of Bodipy), 2.02–0.85 (m, 54H, C(CH_3), CBr(CH_3), CH_2 of Bodipy, CH_2 and CH_3 along polymer backbone).

7.2.5.3. Release of BodipyC10SH from P3 with dithiothreitol (DTT). The *in vitro* release of Bodipy dye from polymer P3 was evaluated using DTT (dithiothreitol, a reducing agent). Polymer **P3** (2.0 mg, 0.03 μmol) was dissolved in H_2O (0.5 mL) and then DTT (0.047 mg, 0.3 μmol) was added into this solution. Reaction was allowed to proceed for at room temperature (25 ^oC) for 24 hours. At several time points (0, 0.5, 1, 2, 3, 4, 5, 6, 7, 8 and 24h) samples were taken from the mixture, diluted to 3 mL water and then analyzed with UV-Vis spectrophotometer to monitor the release of BodipyC10SH by time.

7.3. Results and Discussion

Disulfide exchange reaction was utilized as a powerful tool to synthesize bioreactive dendrons and macromolecules for reversible conjugation of proteins, peptides and thiol containing dye molecules. Pyridyl disulfide group bearing a dendritic ATRP initiator was synthesized and DEGMEMA was grown from its periphery to yield water soluble polymeric platform. The following section provides details about the synthesis, functionalization and deattachment of the conjugates from the polymeric scaffolds.

7.3.1. Synthesis of Multiarm Star Polymer with Pyridyl Disulfide Group

Water soluble and biodegradable multiarm star polymer presented in this study was obtained from a dendritic ATRP initiator with a disulfide group placed at the core. Three generations of dendrons were prepared possessing a pyridyl disulfide unit at their focal points was synthesized according to previously established protocols in our laboratory (Figure 7.2) [98]. An alcohol containing a pyridyl disulfide group was utilized to install the desirable disulfide based reactive group at the focal point. Treatment of this alcohol with acetonide-protected bis(hydroxy)propionic anhydride yields an acetal protected first generation dendron. After the removal of acetal groups in acidic media, generated hydroxyl

groups at the periphery of dendrons were treated with acetal-containing anhydride to get second generation dendron. By iterative deprotection of acetal units at the periphery, corresponding hydroxyl group containing polyester dendrons were prepared with pyridyl disulfide group at the focal point.

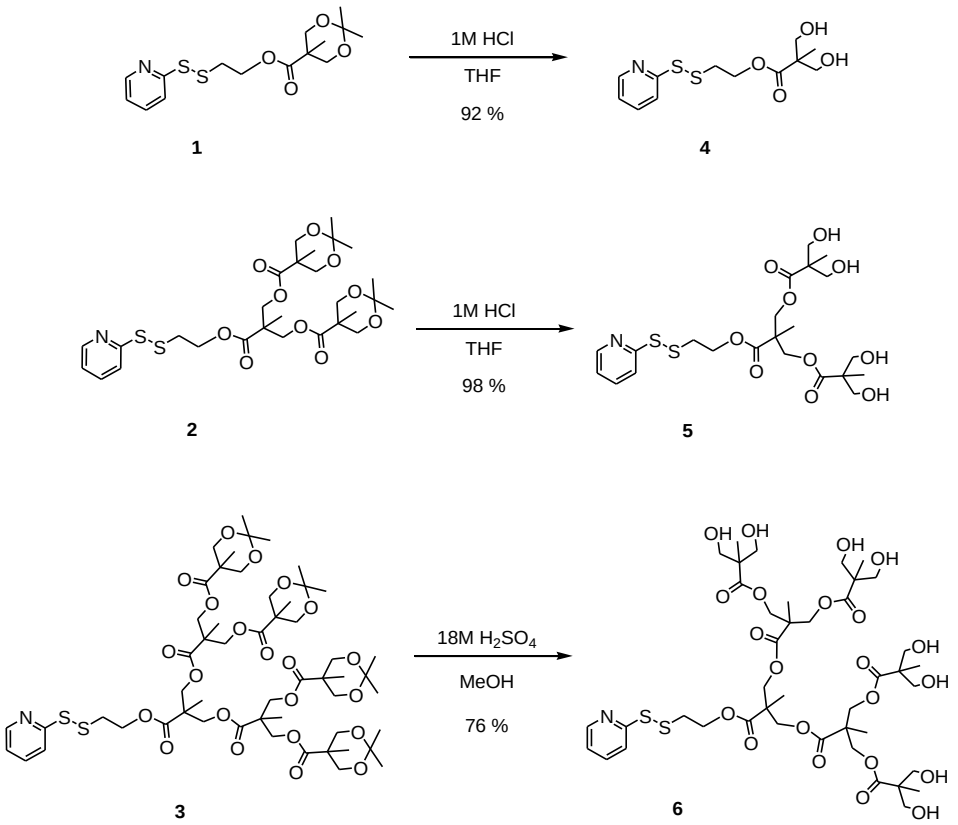

Figure 7. 2. Synthesis of pyridyl disulfide based polyester dendrons G1-3.

Out of these active group containing polyester dendrons, second generation hydroxyl containing dendron (**5**) was chosen for the preparation of polymeric. The hydroxyl groups located at the periphery of the dendron were esterified by 2-bromoisobutyryl bromide in the presence of triethylamine and DMAP to decorate the dendron surface with four initiators to enable the polymerization of a variety of acrylate and methacrylate based monomers (Figure 7.3) [117].

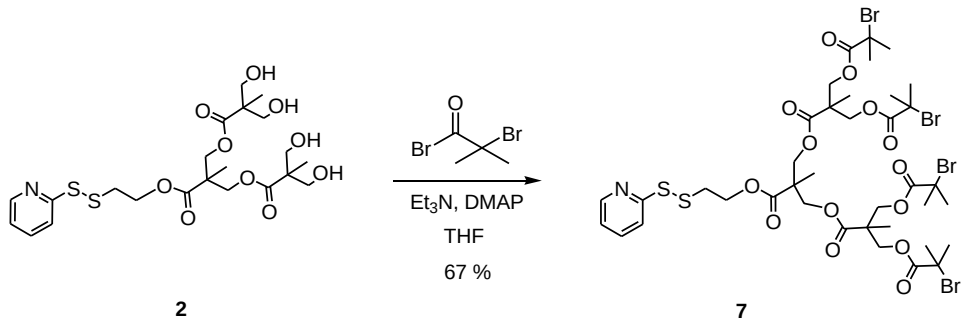

Figure 7. 3. Synthesis of pyridyl disulfide based initiator (7).

Pyridyl disulfide group containing initiator (**7**) was purified by column chromatography and was characterized by ^{1}H and ^{13}C NMR spectroscopy. Presence of pyridyl disulfide unit is clear due to the proton resonances at 8.46, 7.65 and 7.10 ppm (peaks a, b and c respectively, in Figure 7.4a) with the ester protons of dendron at around 4.30 ppm. Complete derivatization of polyester dendron with initiator units was apprehended with the correlated integration values of the singlet at 1.88 ppm belonging to the methyl groups of the initiator part with the ones connected to the tertiary carbon atoms of dendron at 1.30 and 1.27 ppm (peaks m and n respectively, in Figure 7.4a). The carbon NMR gives more information about the structure of the multiarm initiator with newly emerged carbonyl peaks at 171.6 and 170.9 ppm as expected (Figure 7.4b).

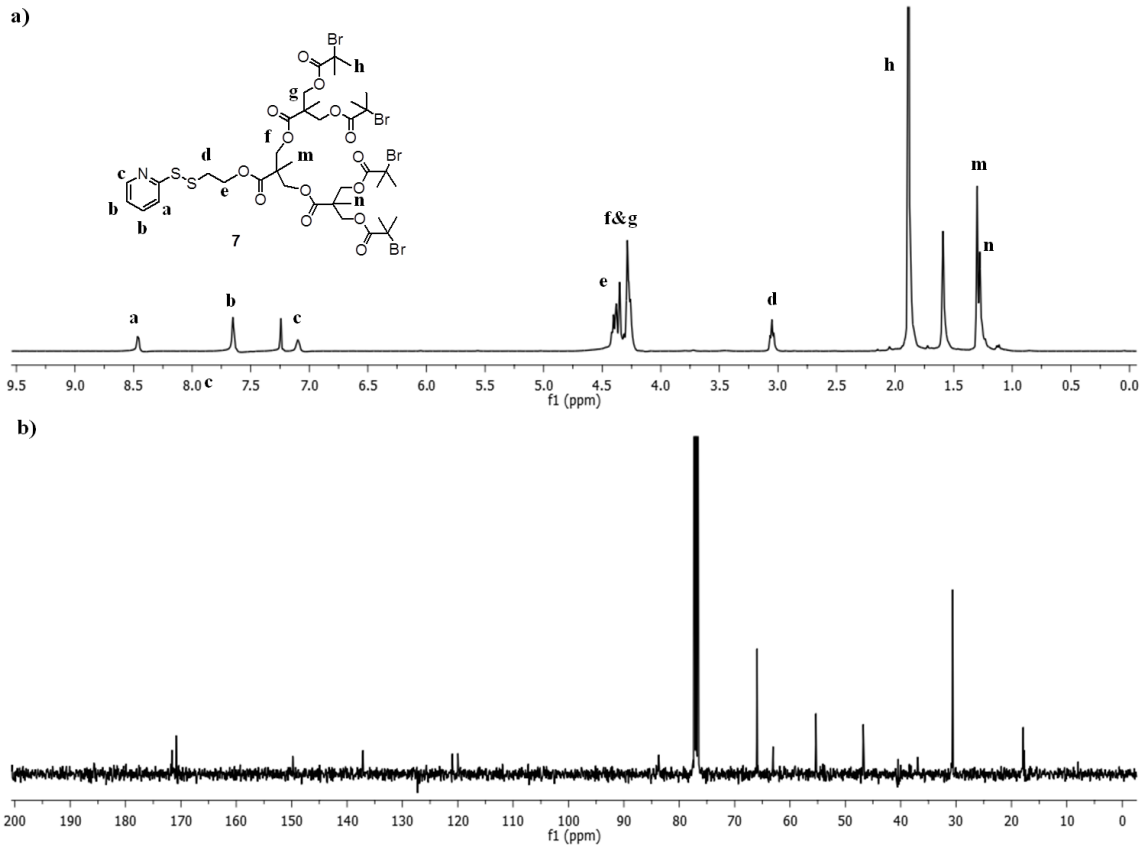

Figure 7. 4. ^{1}H NMR (a) and ^{13}C NMR (b) spectra of pyridyl disulfide based initiator (7) in $CDCl_3$.

Successfully synthesized dendritic initiator (**7**) was then utilized for the growth of methacrylate based DEGMEMA to give rise to water soluble multiarm star polymer **P1**. Suitable with the nature of the initiator groups, ATRP method was applied for the polymerization of this monomer, which is mediated by a catalyst complex of Cu(I)Br with 4,4'-dinonyl-2,2'-bipyridine used as a ligand (Figure 7.5). Polymerization was carried out at 80 ^{o}C to increase the conversion and obtain high molecular weight polymer P1 with pyridyl disulfide group at the core. The multiarm star polymer thus synthesized possessed a high molecular weight, calculated as 64760 g/mol from ^{1}H NMR spectroscopy. This was desirable since the long polymer arms can be expected to protect the protein and increase its stability.

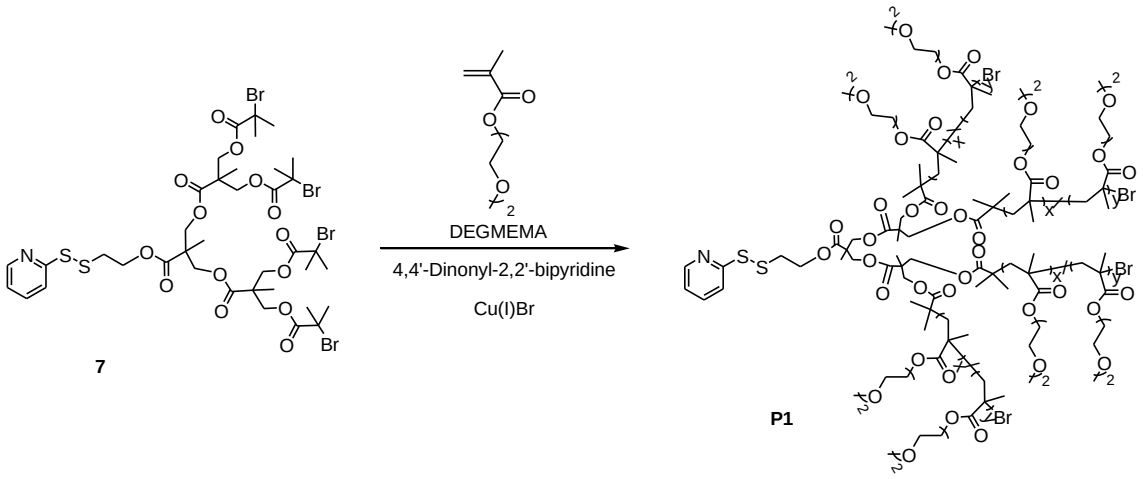

Figure 7. 5. Synthesis of multiarm star polymer with pyridyl disulfide core P1 using the second generation initiator (7).

Structural assignments of the multiarm star polymer P1 was verified by ^{1}H NMR spectroscopy, to ensure the intactness of pyridyl disulfide unit during the polymerization processes. Proton resonances of pyridyl disulfide unit at 8.46, 7.67 and 6.95 ppm (peaks a, b and c respectively, in Figure 7.6) are clearly seen with the expected patterns. Together with ester protons at around 4.08 ppm, methoxy groups appearing at 3.37 ppm confirm the polymerization of DEGMEMA monomer to form the multiarm star polymer.

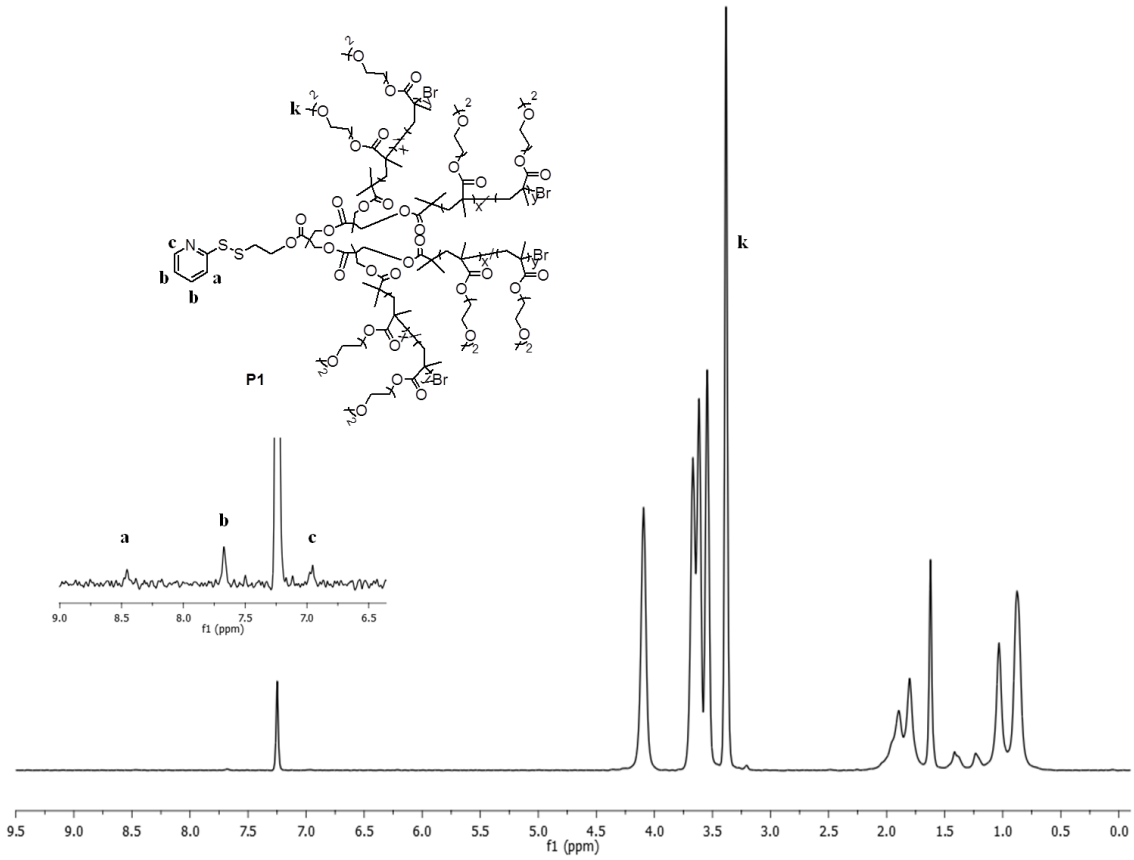

Figure 7. 6. ^{1}H NMR spectrum of G2PDS-DEGMEMA polymer P1.

Presence of the pyridyl disulfide group at the core of the synthesized multiarm star polymer was also quantified via a commonly used functional-group detection methodology. Reduction of this activated disulfide upon treatment with a reducing agent, dithiothreitol (DTT) was performed at room temperature and release of pyridine 2-thione was monitored by UV-Vis spectroscopy. Concentration of the liberated thione from the polymer architecture was determined by measuring the absorbance values at 379 nm with respect to time (Figure 7.7). According to the absorbance value obtained after release gets stabilized, percent of polymers with the activated disulfide group was calculated to be around 84% (unoptimized), which refers to the majority of multiarm star polymers functionalized with pyridyl disulfide unit.

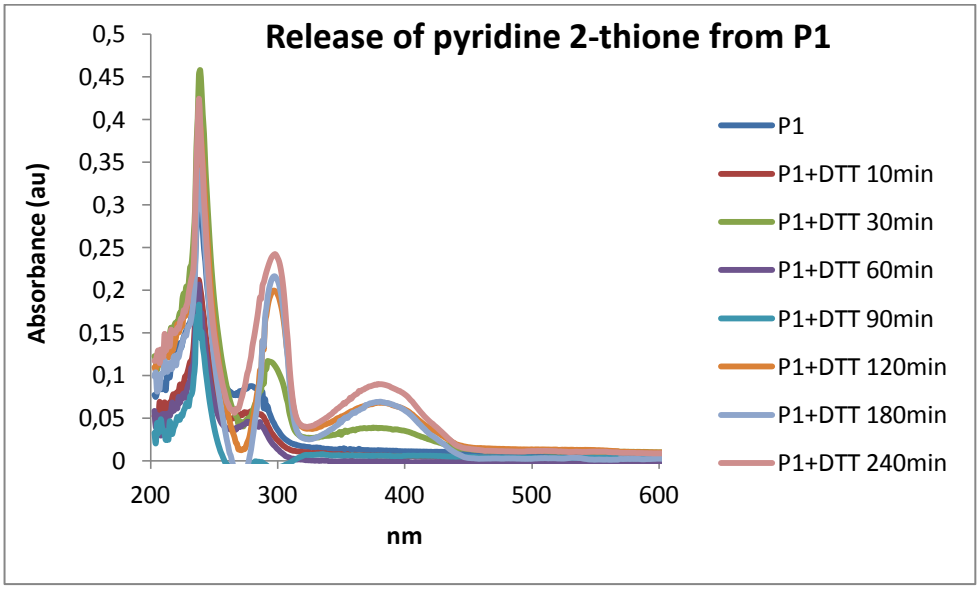

Figure 7. 7. End group content determination for P1.

7.3.2. Conjugation of Multiarm Star Copolymer with Glutathione and BodipyC10SH

Presence of bioactive unit at the core of the polymer enables the reversible conjugation of (bio) molecules via disulfide exchange reaction. In this study, specifically a tripeptide, glutathione, and a hydrophobic dye, Bodipy10CSH, were conjugated to the core of the polymer P1. The free thiol group containing molecules replaces the pyridyl disulfide moiety and forms a disulfide bond with the polymer. Pyridyl disulfide group leaves the system as pyridine 2-thione and can be detected by UV-Vis spectroscopy at around 370 nm. In the case of dye attachment, it is also possible to observe the increasing absorbance of the conjugated dye which becomes soluble in water upon binding to the polymer.

Functionalization of the multiarm star polymer P1 was at first assessed by a tripeptide, glutathione. This free-thiol group containing molecule was conjugated to the core of the polymer via disulfide exchange reaction in the presence of catalytic amount of acetic acid (Figure 7.8). With the addition of excess glutathione to the reaction performed in water due to its hydrophilic nature, complete conjugation was achieved.

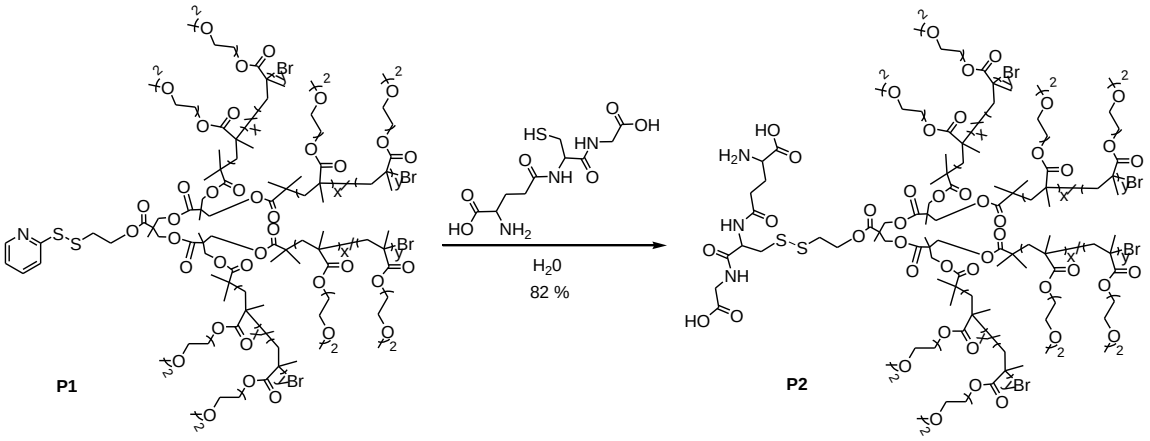

Figure 7. 8. Conjugation of multiarm star polymer P1 with gluthatione via cleavable disulfide linkage (P2).

Peptide conjugated multiarm star polymer P2 was analyzed by ^{1}H NMR spectroscopy. Efficiency of disulfide exchange reaction seems to be quite high upon comparison of the proton spectra of the original polymer P1 to its peptide conjugated version P2. Complete disappearance of proton resonances at 8.46, 7.67 and 6.95 ppm (peaks a, b and c respectively, in Figure 7.9a) point out the removal of pyridyl disulfide unit of P1. Due to hydrophilic nature of glutathione, its characteristic peaks are not visible in NMR spectrum obtained in $CDCl_3$. However, appearance of new peaks at around 2.85 and 2.35 ppm (peaks x and y respectively, in Figure 7.9c) for the proton NMR spectrum performed in D_2O confirms the presence of peptide molecule attached to the polymer core.

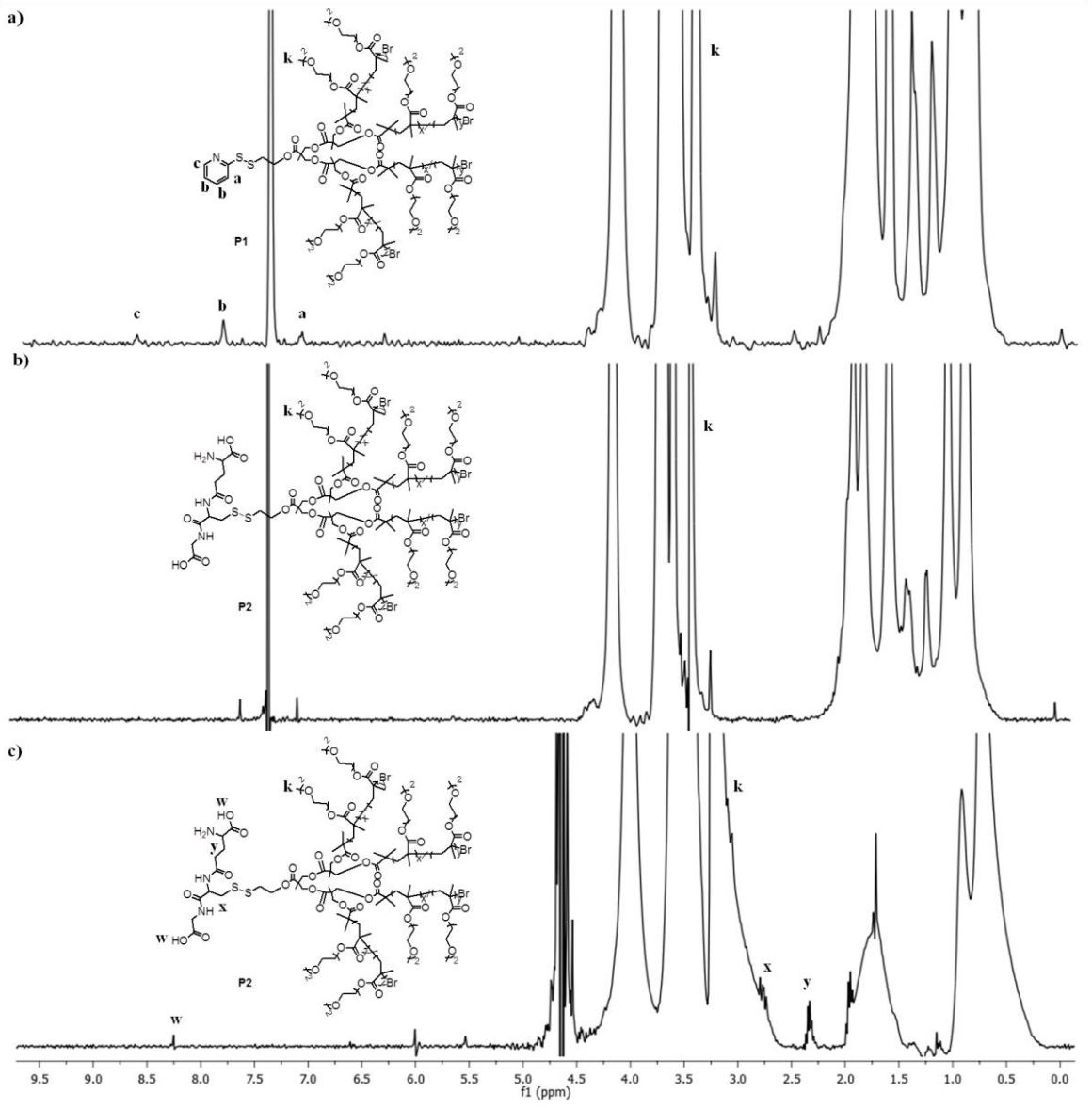

Figure 7. 9. ^{1}H NMR spectra of P1 (a) in $CDCl_3$, P2 (b) in $CDCl_3$ and (c) in D_2O.

Peptide conjugation to the core of multiarm star polymer was verified by monitoring the release of pyridine 2-thione from the polymer as a byproduct during the disulfide exchange reaction (Figure 7.10). The absorption peak detected after the conjugation reaction was thought to be the characteristic peak of the generated thione at 353 nm for the measurements taken in THF. This newly appeared peak clearly points out the successful attachment of glutathione to the core of polymer scaffold that originally does not show any absorption behaviour around this wavelenght.

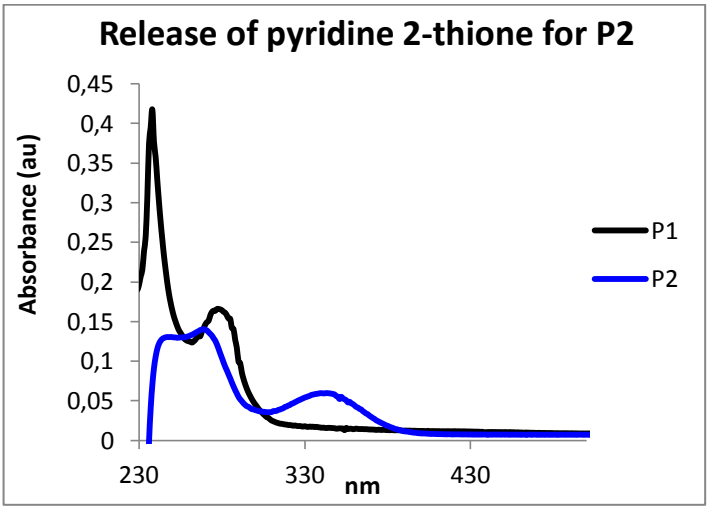

Figure 7. 10. UV-Vis absorption spectra for glutathione with Pyridyl disulfide group containing 4-armed star polymer P1.

Other reported conjugation experiment was examined by a thiol modified hydrophobic dye, BodipyC10SH, synthesized according to literature procedures and purified by column chromatography [170]. Disulfide exchange reaction took place between the free thiol group of dye and pyridyl disulfide group at the core of the multiarm star polymer P1 resulted in the attachment of fluorescent dye to water soluble polymeric platform. Although this reaction was carried out in THF to solubilize the dye, its attachment to polymer makes it water soluble and still possessing its fluorescence property in water medium. Efficient functionalization was ensured by the utilization of the dye with higher stoichiometric ratios (Figure 7.11).

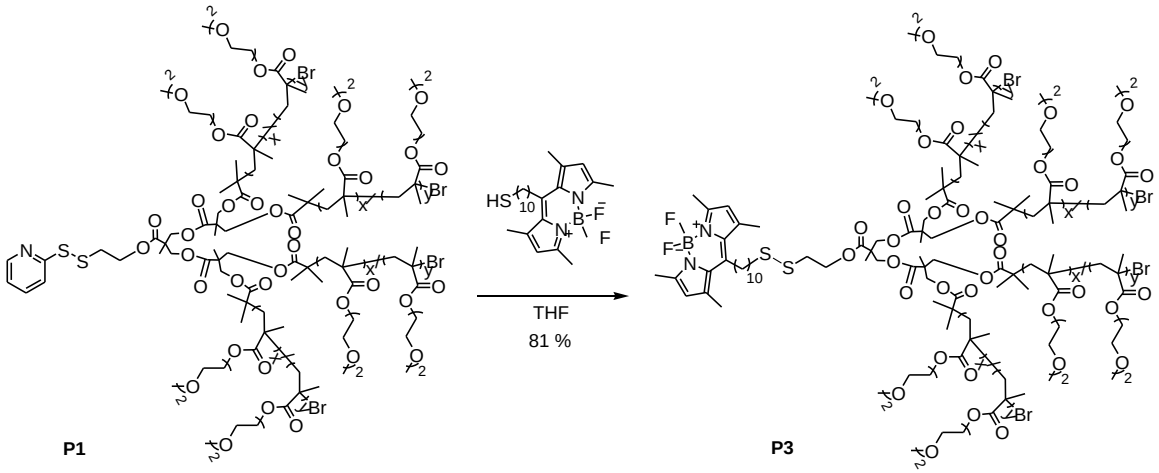

Figure 7. 11. Conjugation of multiarm star polymer P1 with BodipyC10SH via cleavable disulfide linkage (P3).

Additionally, conjugation with a thiol modified hydrophobic dye, namely BodipyC10SH, was undertaken. Although this reaction was carried out in THF to solubilize the dye, its attachment to the polymer makes it water soluble. Efficient functionalization was ensured by the utilization of the dye with higher stoichiometric ratios (Figure 7.11).

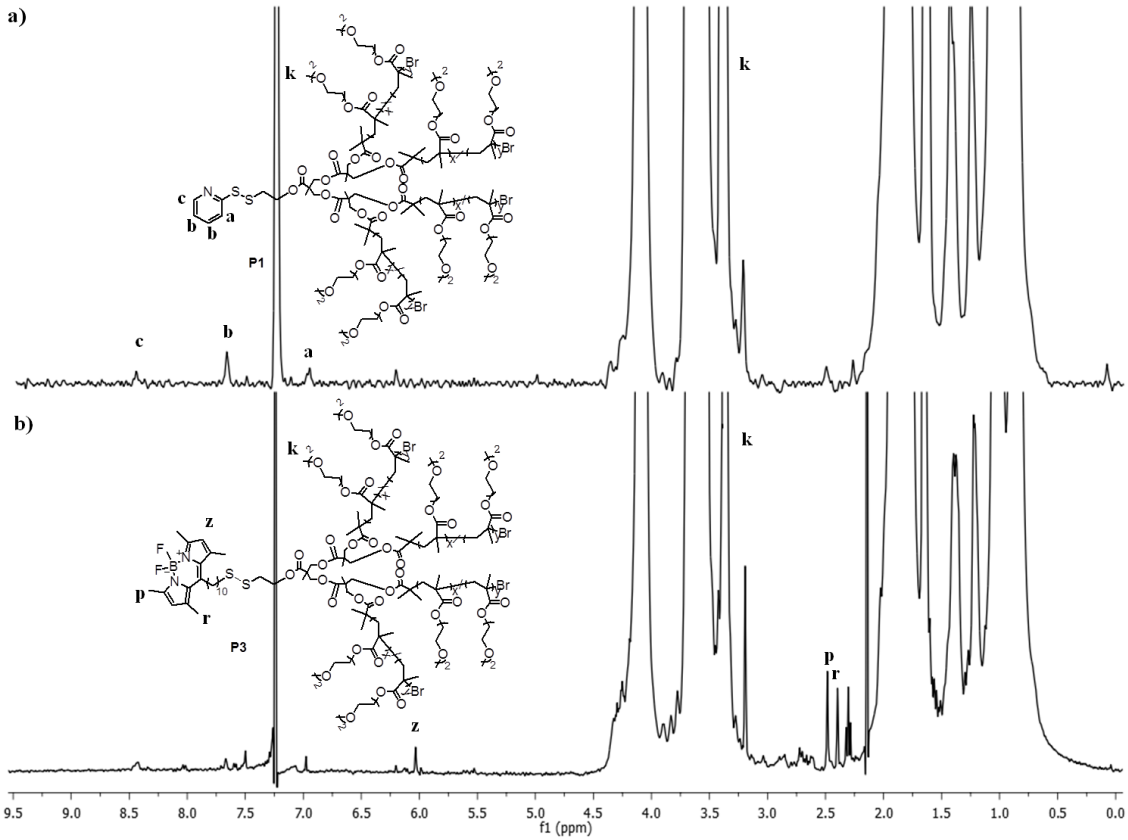

Figure 7. 12. ^{1}H NMR spectra of P1 (a) and P3 (b) in $CDCl_3$.

Conjugation of the Bodipy dye molecule to the ethylene glycol based polymer scaffold provides the expected water solubility to this hydrophobic dye which enlarges its use in aqueous media especially for imaging applications. It is clearly visible from the photograph displayed in Figure 7.13 that the non-conjugated dye molecule is insoluble in 5% methanol containing aqueous solution, whereas the polymer conjugated dye is freely soluble and the solution is fluorescent. Cleavage of disulfide linkage placed between Bodipy and the polymer core was achieved upon reduction by DTT that results in the liberation of free dye molecule that precipitates due to its insolubility in aqueous media and accumulates on the stirrer bar and the solution losses its fluorescence to a large extent.

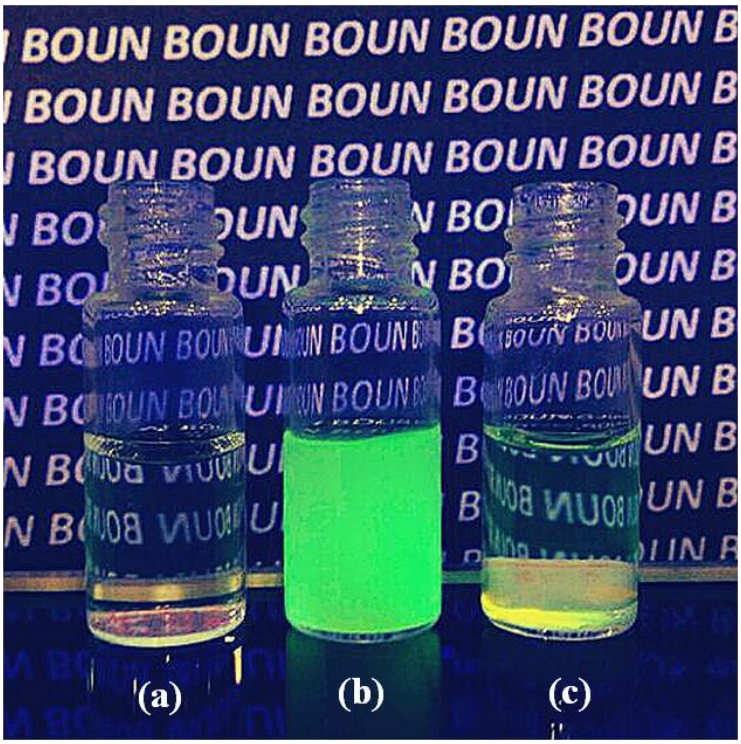

Figure 7. 13. 5 % methanol containing aqueous solutions of free BodipyC10SH (a), polymer conjugated BodipyC10SH (b) and liberated BodipyC10SH from the polymer via DTT treatment (c).

Regarding the disulfide exchange reaction performed for the conjugation of bodipy molecule to the multiarm star polymer, UV-Vis absorbance measurements were taken in aqueous medium where solely the polymer bound dye could give absorbance signal in the reaction mixture. Tracking of conjugated dye was accomplished by taking aliquots from the reaction mixture and removing all volatiles under vacuum, followed by analyzing for absorption profiles. As expected, the increasing absorbance value of the peak at 497 nm by time demonstrates that the dye molecule gets conjugated to water soluble polymer (Figure 7.14).

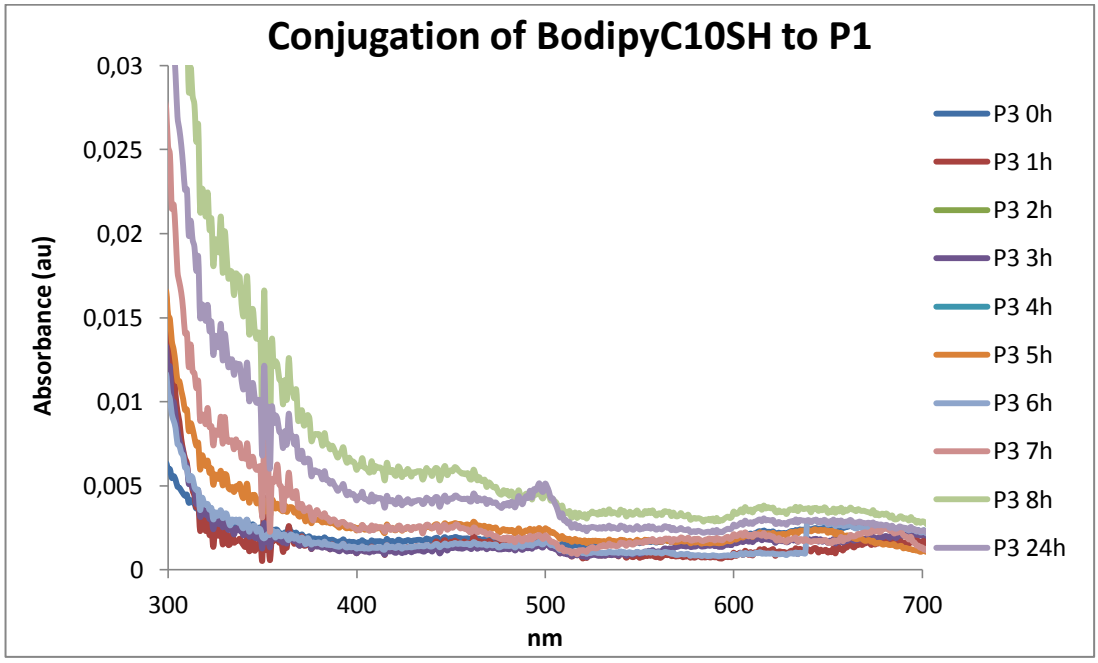

Figure 7. 14. UV-Vis absorption spectra for time-dependent conjugation of BodipyC10SH to P1.

Likewise, the reversibility of disulfide exchange reaction was examined by the reducing agent driven release of Bodipy dye conjugated to water soluble polymer. Upon cleavage of disulfide bond between dye and polymer core, the concentration of the dye molecule bound to polymer scaffold decreases and the absorbance intensity observed at 497 nm in aqueous medium diminishes accordingly, which is remarkable in UV-Vis spectra of the samples taken from the reaction mixture at certain time points (Figure 7.15). After 24 hours, more than 95% of the Bodipy conjugated to the core of the multiarm star polymer seems to be released and hydrophobic dye was recovered in its pure form, detected as single spot on TLC plate. Deterioration in baseline of the obtained absorbance spectra was estimated to be originated from the turbidity increased with time due to gradually increasing release of water insoluble dye molecule in aqueous medium.

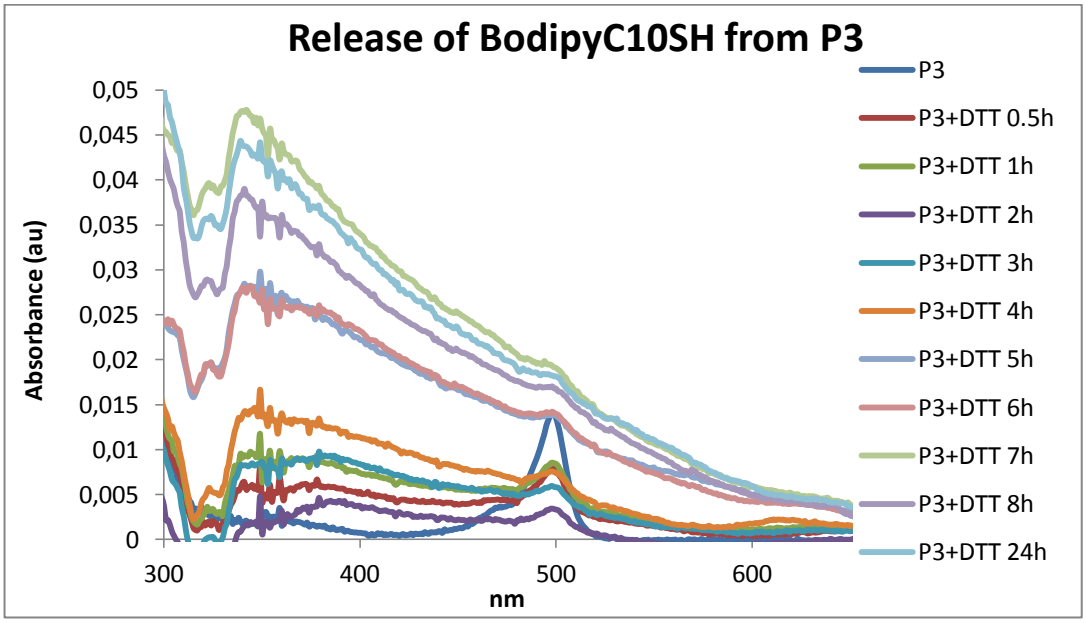

Figure 7. 15. UV-Vis absorption spectra for time-dependent release of BodipyC10SH from P3 upon treatment with DTT.

7.4. Conclusion

Overall, this part of the thesis discloses the synthesis of a promising polymeric platform for the design of peptide and protein conjugation. Pyridyl disulfide functionality placed at the core of dendrons and star polymer enables reversible conjugation of free thiol containing biomolecules. Periphery of bioactive group containing second generation bis-MPA based polyester dendron was modified by initiator groups allowing polymerization of DEGMEMA monomer by ATRP method to conclude with a water soluble 4-armed star polymer. Upon disulfide exchange reaction of pyridyl disulfide group at the polymer core with reactive thiol unit of hydrophobic dye, BodipyC10SH, pyridine 2-thione was liberated as a byproduct, whose absorbance is monitored to determine the conjugation. Bioconjugation was performed by efficient conjugation of a tripeptide (glutathione) to the core of water soluble multiarm star polymer. Synthesized polymer-peptide conjugate can be expected to serve as a promising candidate for increasing the stability and improving the efficacy of peptides and proteins *in vivo* due to the shielding from the protective polymeric arms.

8. CONCLUSIONS

This thesis covers the design and synthesis of reactive polymeric materials that can act as supports for therapeutic agents. Macromolecules conjugated to drugs contribute to an increase in its blood circulation time by slowing down the renal filtration. Based on this approach, polymeric scaffolds with different architectures were designed to possess various reactive groups. Both linear and multiarm star polymers were obtained by employing radical polymerization techniques and evaluated as supports for drug conjugation. Efficient conjugations were performed via thiol and amine reactive groups. Loading capacity was increased with the insertion of dendrons to polymer architecture to obtain dendron-polymer conjugates. Dendrons were also evaluated as initiators to synthesize multiarm star polymers as more compact and globular macromolecules.

First project described in this thesis is related to the design of thiol reactive linear polymers and their use in bio-conjugations. Furan protected maleimide group containing monomer was copolymerized by PEG-based methacrylate monomer by ATRP and the resultant polymer was activated by removal of furan groups via retro-Diels/Alder reaction. Efficiency of functionalization was achieved by sequential conjugation of first Bodipy-SH, a hydrophobic dye, and then cRGD, targeting group. In vitro cytotoxicity data and internalization verified their non-toxicity towards both cancerous and healthy cells, and efficient uptake for the targeting group containing polymers.

Second project involved the synthesis of polymer-drug conjugates and their both *in vitro* and *in vivo* evaluations. Drug containing monomers were successfully synthesized and copolymerized to give water soluble linear polymer-drug conjugates. Different linkers were utilized for the attachment of drug to polymer backbone: ester, amide and peptide linkers. Polymer-drug conjugates were examined for their in vitro cytotoxicity and in vivo pharmacokinetic profiles. Results demonstrate the reduced toxicity and prolonged circulation of drug when conjugated to polymer scaffold.

Third project is related to the synthesis of a novel polymer-dendron conjugate with functional cluster along the polymer chain. Active maleimide group containing polyester dendrons were copolymerized by styrene via NMP and the sequence controlled nature of the polymerization of styrene and maleimide resulted in dendrons appended to linear styrene based backbone at precise locations. Functionalization efficiency of dendrons were determined by conjugation of a free thiol containing molecule to alkene decorated periphery of dendrons via photo-induced thiol-ene chemistry.

The fourth project extends the use of dendrons as initiators for star polymer synthesis. Peripheral groups of polyester dendrons were decorated with initiators to copolymerize various methacrylate monomers with a reactive group bearing monomer. NHS functionality was inserted into the polymerization as its methacrylate monomer and together with furan masked maleimide unit at the core, obtained multiarm polymers exhibited orthogonal reactivity. Then, conjugation of an imaging agent (Bodipy-SH) to the core via 1,4-Michael addition reaction was followed by drug (gemcitabine) attachment to side chains via activated esters. Obtained drug conjugates were evaluated in cytotoxicity and internalization assay and *in vitro* experimental results indicates almost 10 fold decrease in toxicity of drug upon polymer conjugation.

The final study related to design of multiarm star polymers for peptide and protein conjugations. Pyridyl disulfide group containing polyester dendrons were furnished with ATRP initiators and then utilized to yield core reactive multiarm polymer. Free thiol containing dye molecule (Bodipy-SH) was conjugated to the core via disulfide exchange reaction and as a model protein, reduced glutathione was conjugated to the core via reversible disulfide bond, which verifies the potential of this polymeric scaffold in bio-molecule conjugation.

In general, this thesis involves the design of novel polymeric platforms that possess multifunctional groups for efficient conjugation of chemotherapy agents, imaging and targeting groups. Synthesis and preliminary biological evaluations of some of these polymeric conjugates suggest their utility as suitable carriers in drug delivery systems.

9. APPENDIX A: SPECTROSCOPY DATA

^{1}H NMR, ^{13}C NMR, FT-IR and GPC spectra of the synthesized products are included.

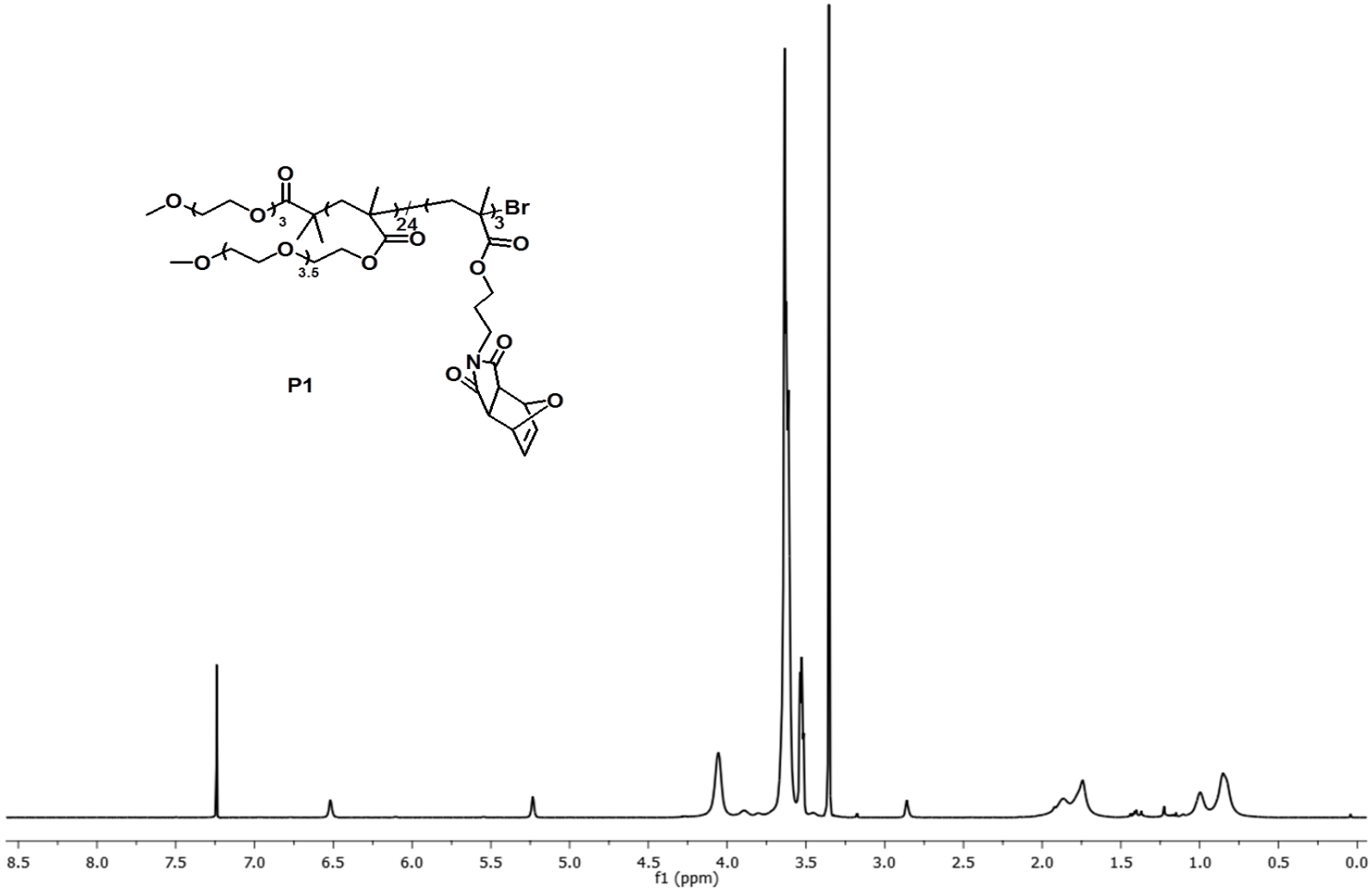

Figure 3A. 1. ^{1}H NMR spectrum of the copolymer P1 in $CDCl_3$

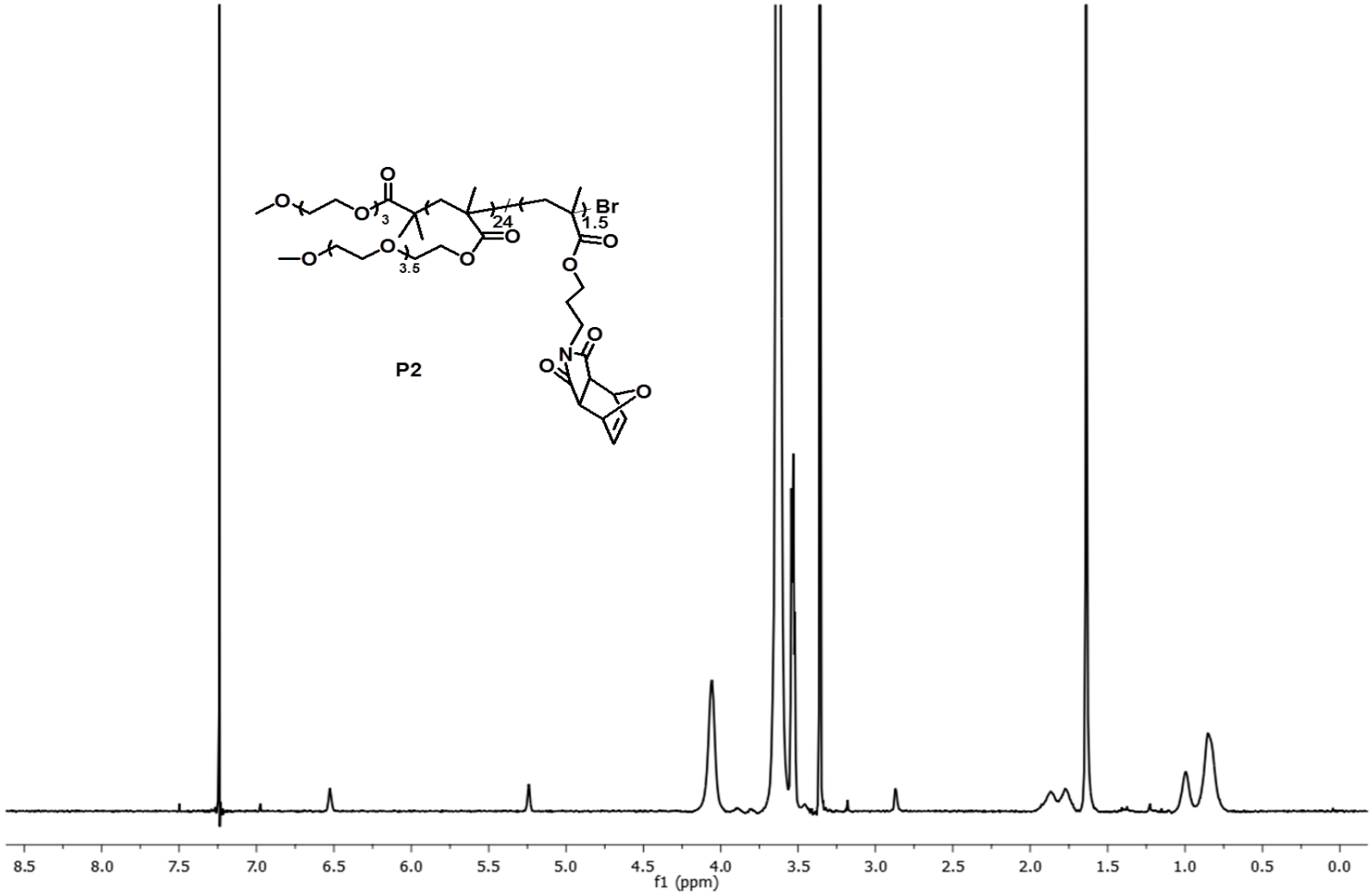

Figure 3A. 2. ^{1}H NMR spectrum of the copolymer P2 in $CDCl_3$

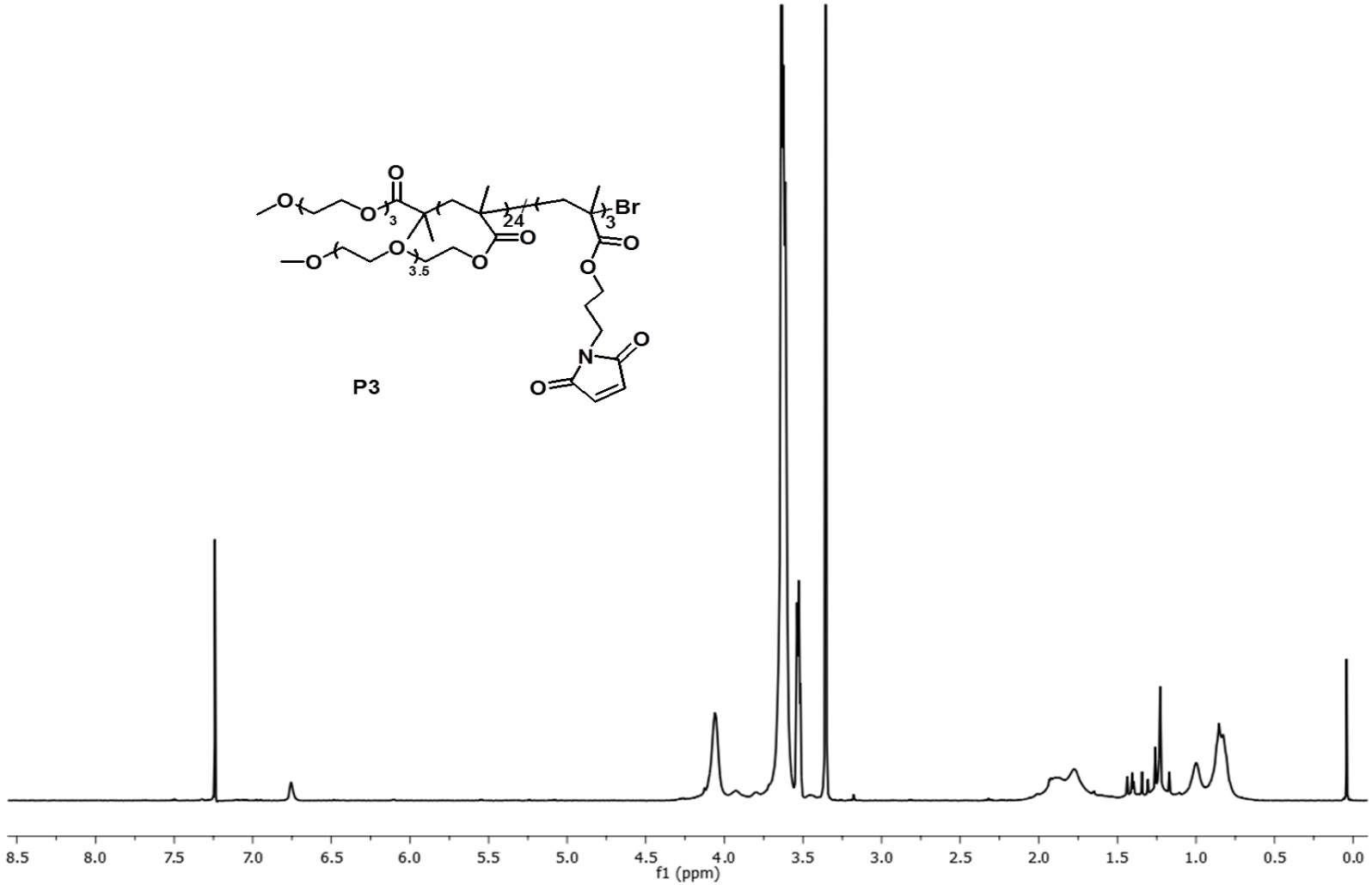

Figure 3A. 3. ^{1}H NMR spectrum of the copolymer P3 in $CDCl_3$

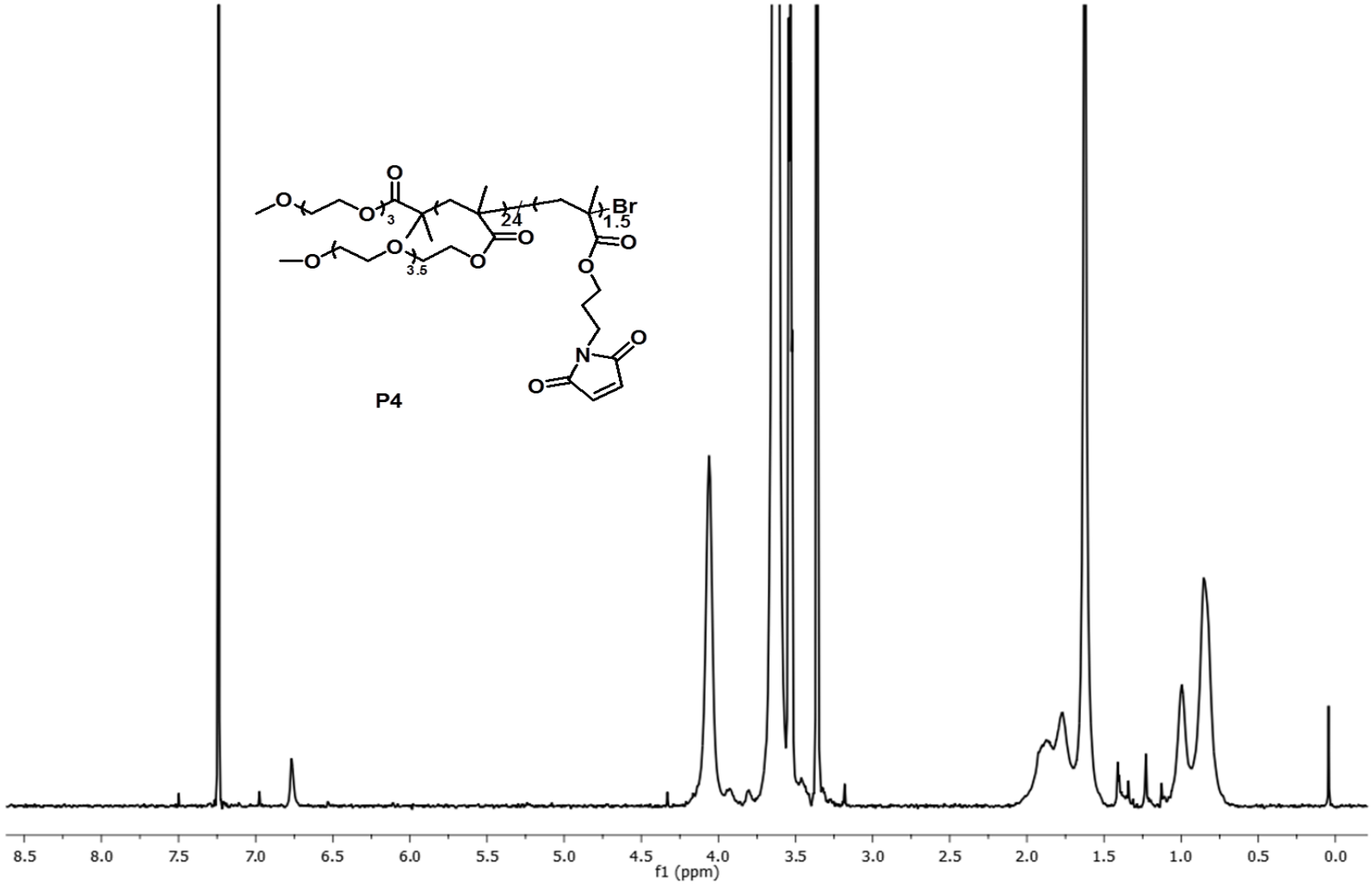

Figure 3A. 4. ^{1}H NMR spectrum of the copolymer P4 in $CDCl_3$

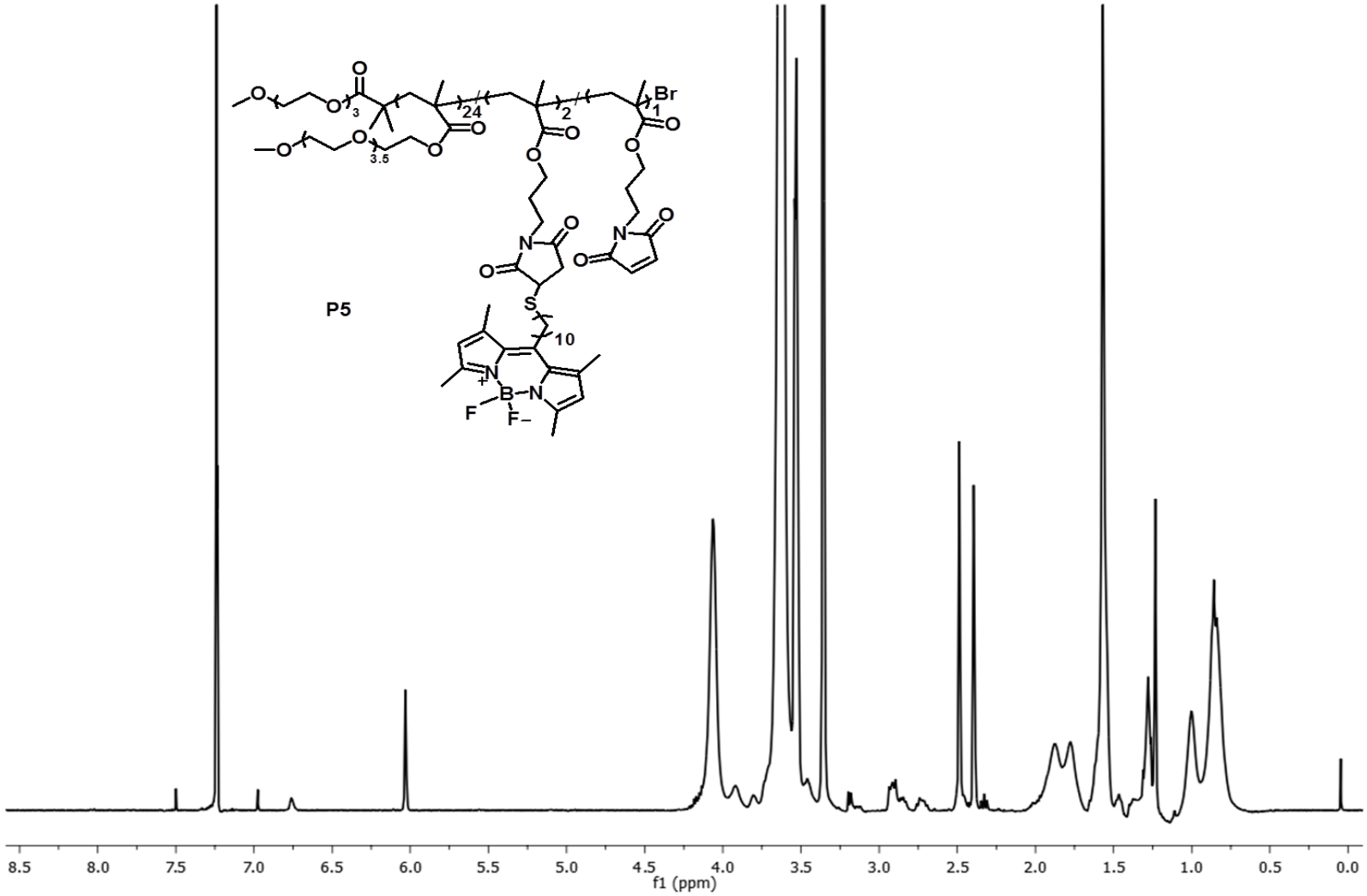

Figure 3A. 5. ^{1}H NMR spectrum of the copolymer P5 in $CDCl_3$

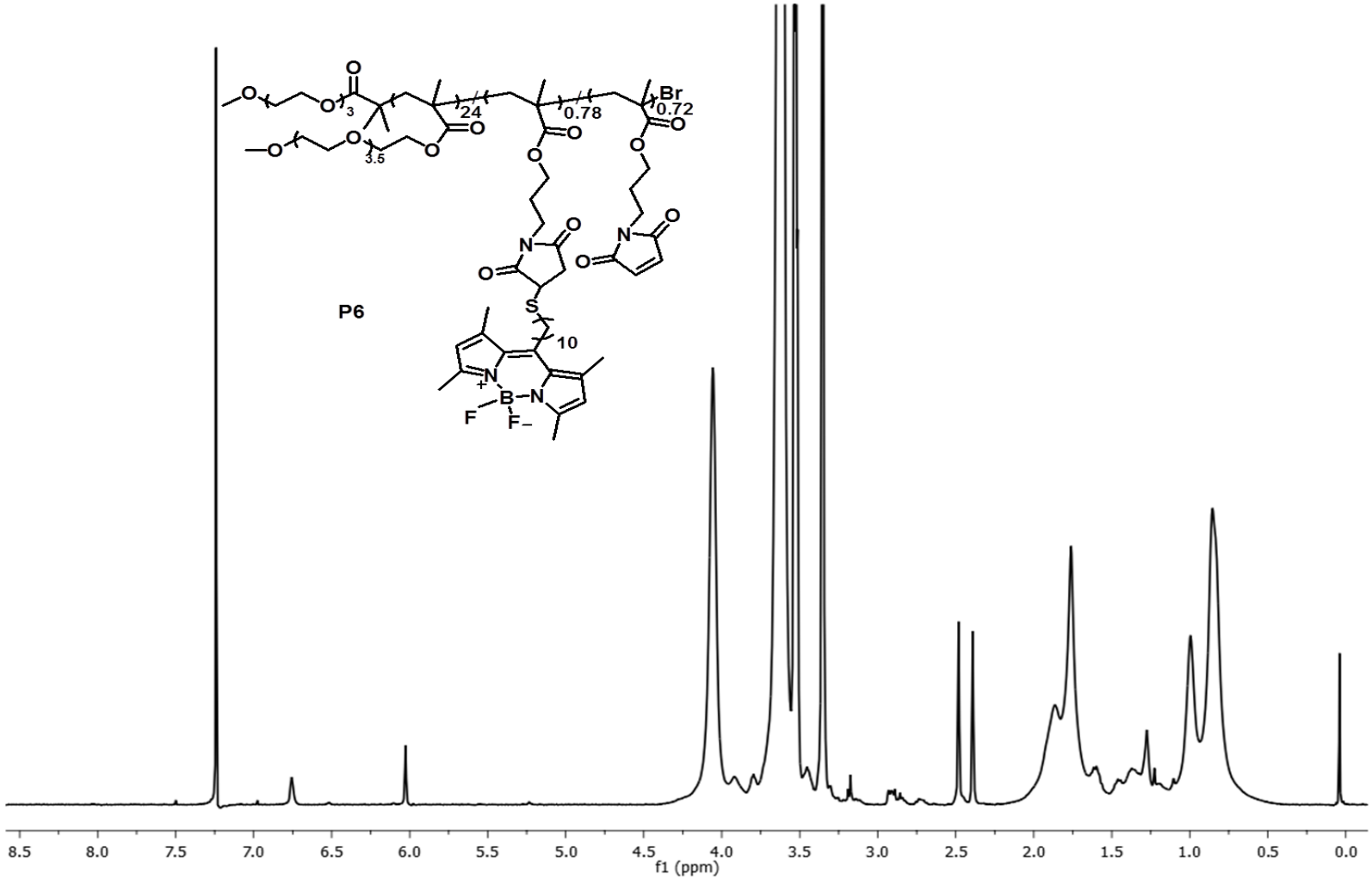

Figure 3A. 6. ^{1}H NMR spectrum of the copolymer P6 in $CDCl_3$

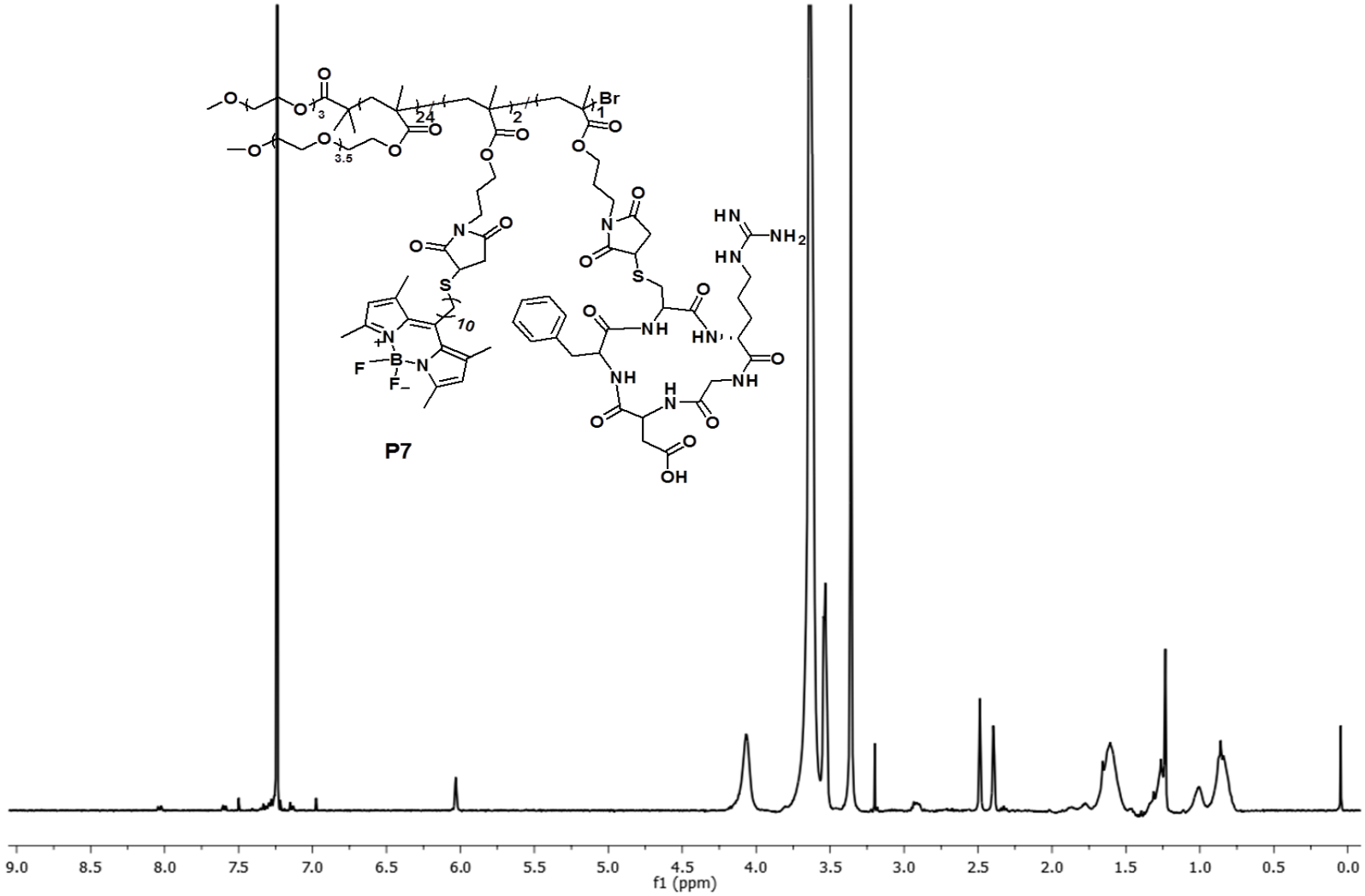

Figure 3A. 7. ^{1}H NMR spectrum of the copolymer P7 in $CDCl_3$

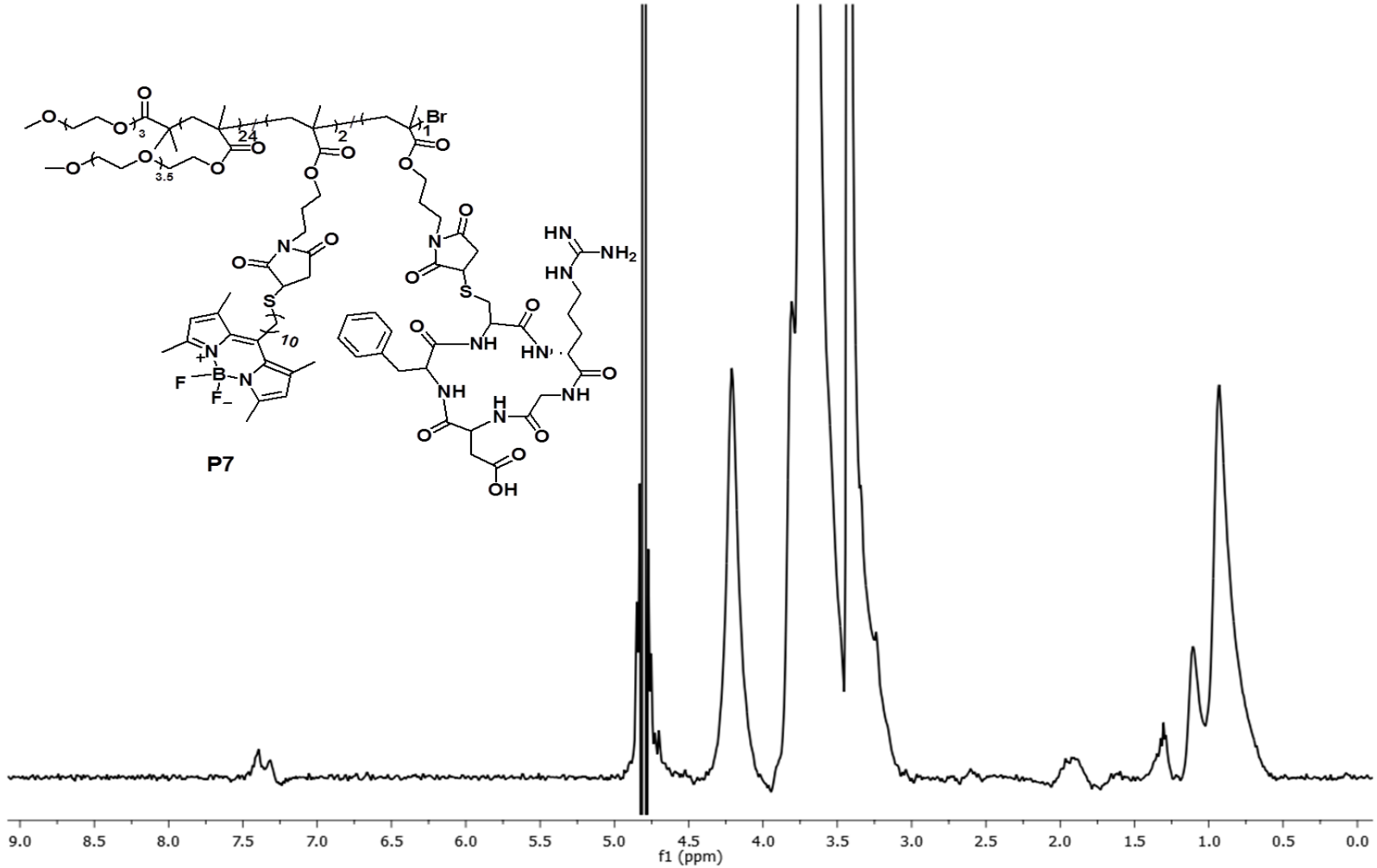

Figure 3A. 8. ^{1}H NMR spectrum of the copolymer P7 in D_2O

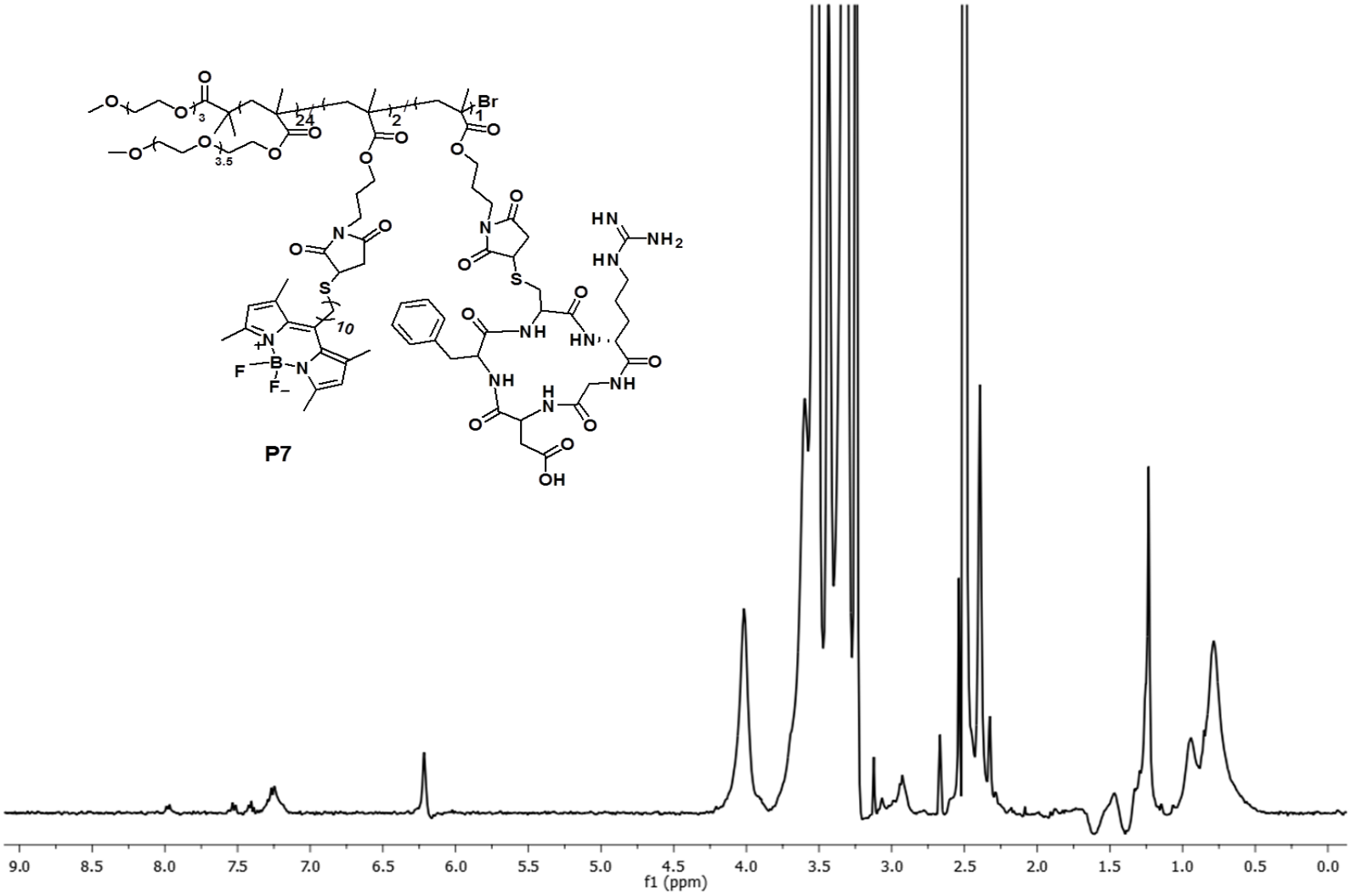

Figure 3A. 9. ^{1}H NMR spectrum of the copolymer P7 in DMSO

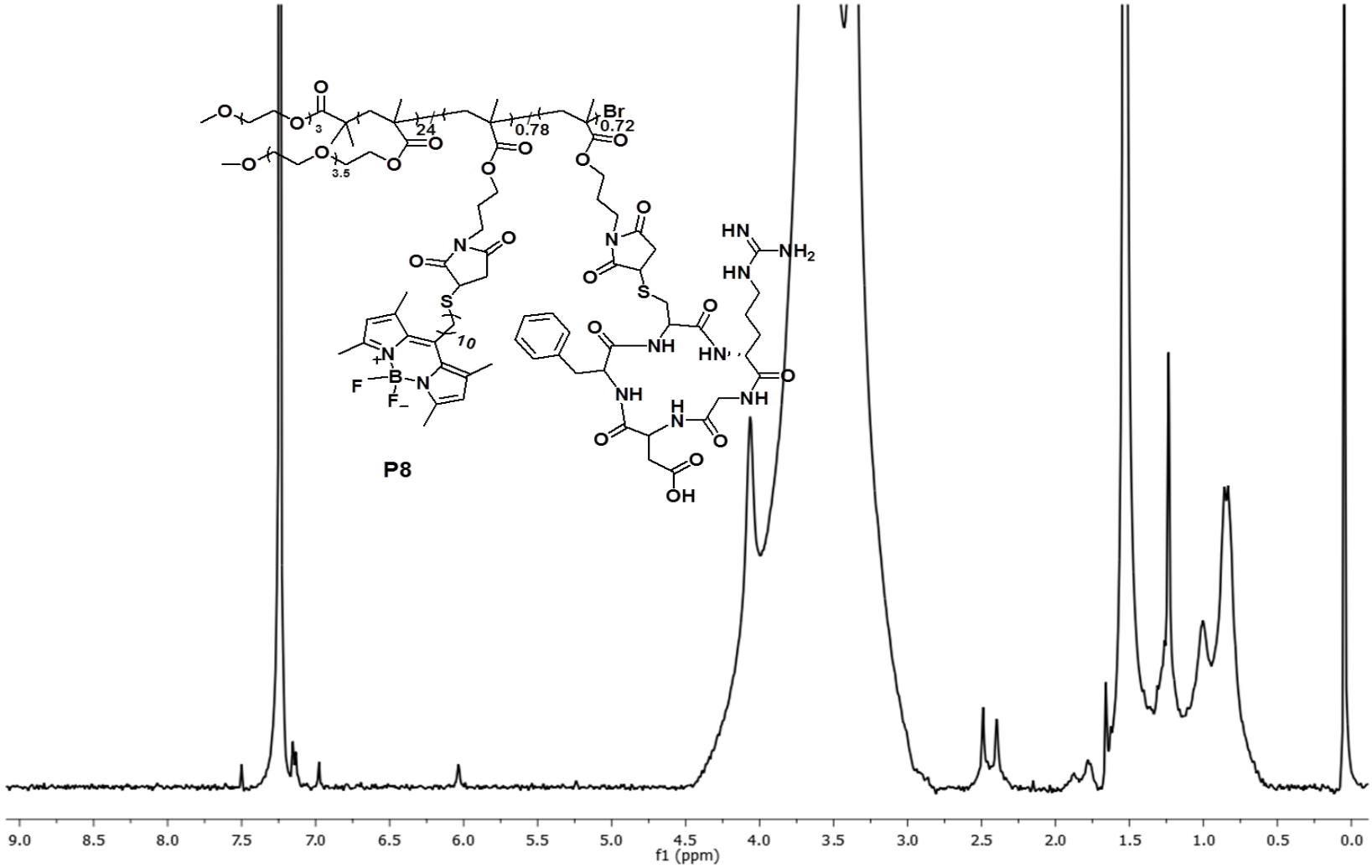

Figure 3A. 10. ^{1}H NMR spectrum of the copolymer P8 in $CDCl_3$

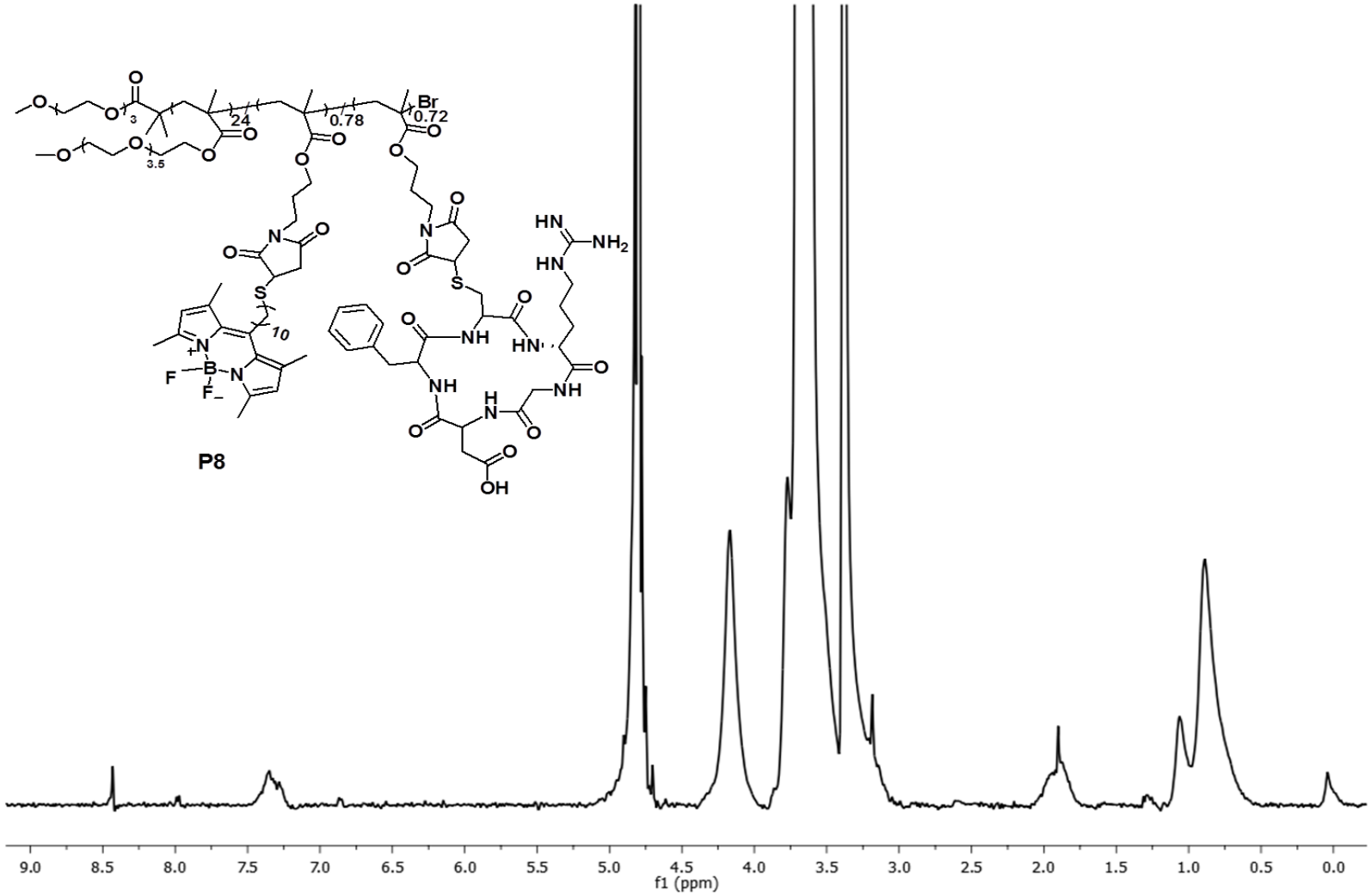

Figure 3A. 11. ^{1}H NMR spectrum of the copolymer P8 in D_2O

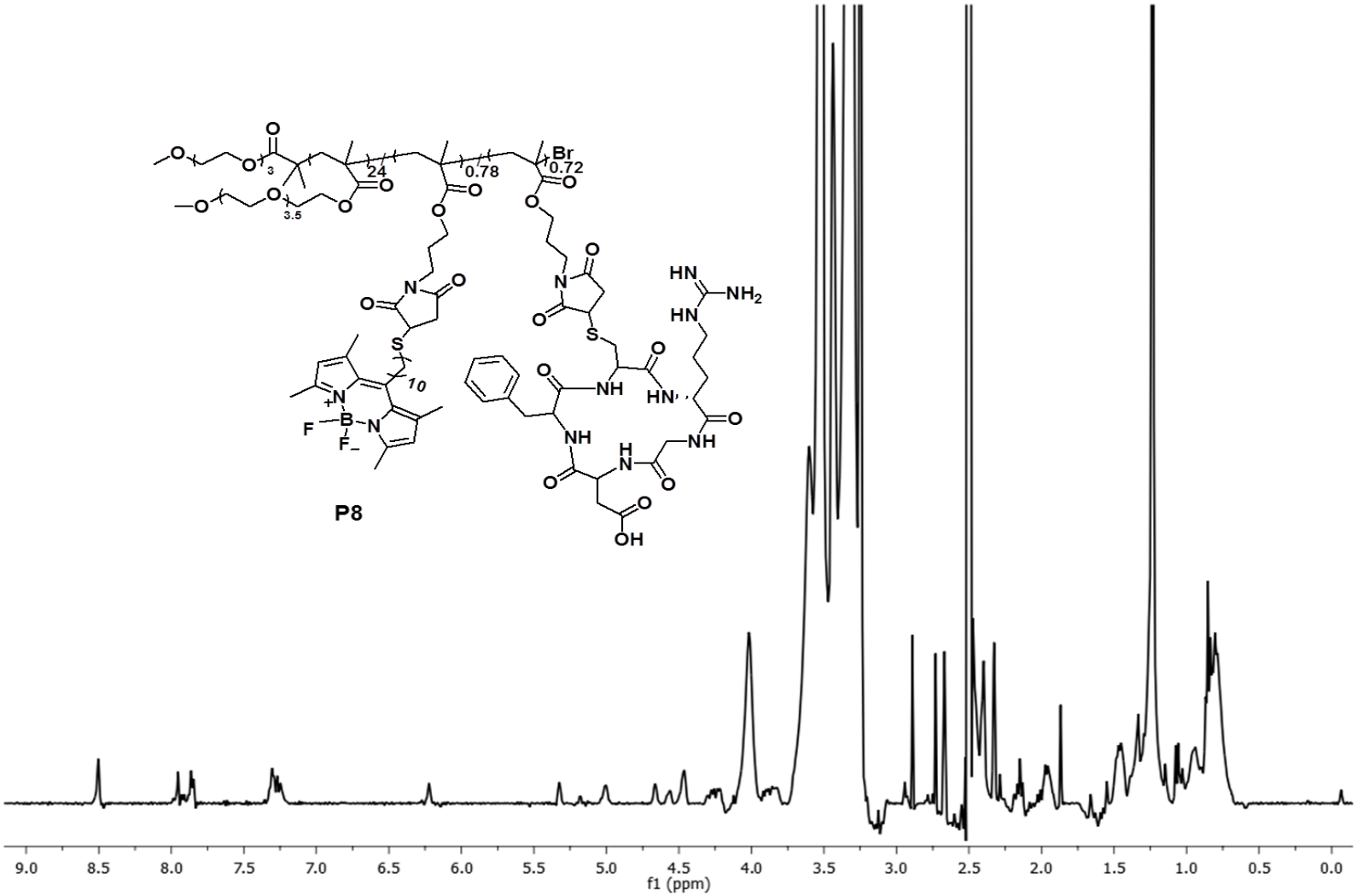

Figure 3A. 12. ^{1}H NMR spectrum of the copolymer P8 in DMSO

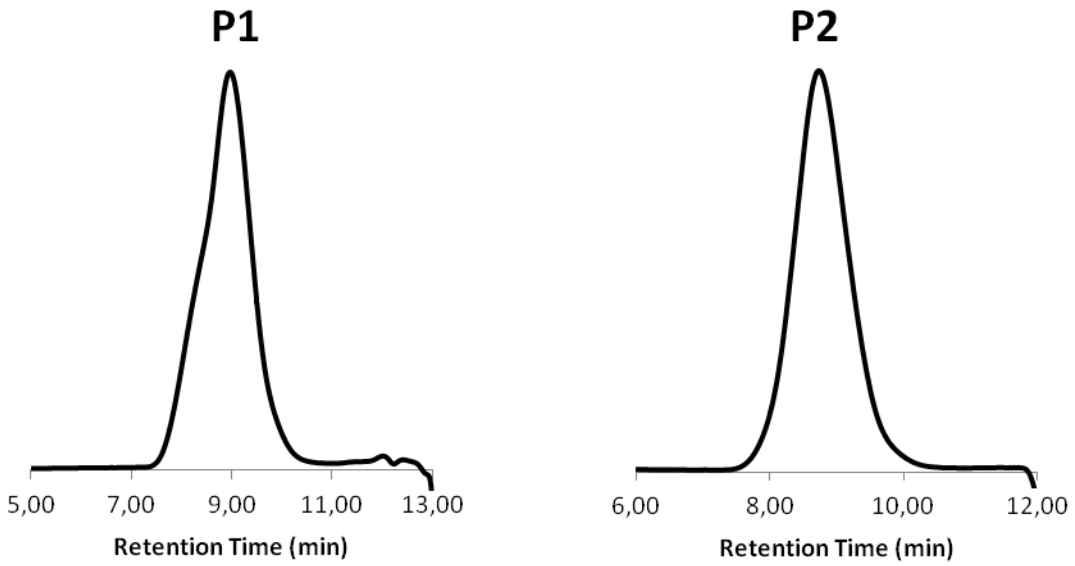

Figure 3A. 13. GPC traces of copolymers P1 and P2 in THF

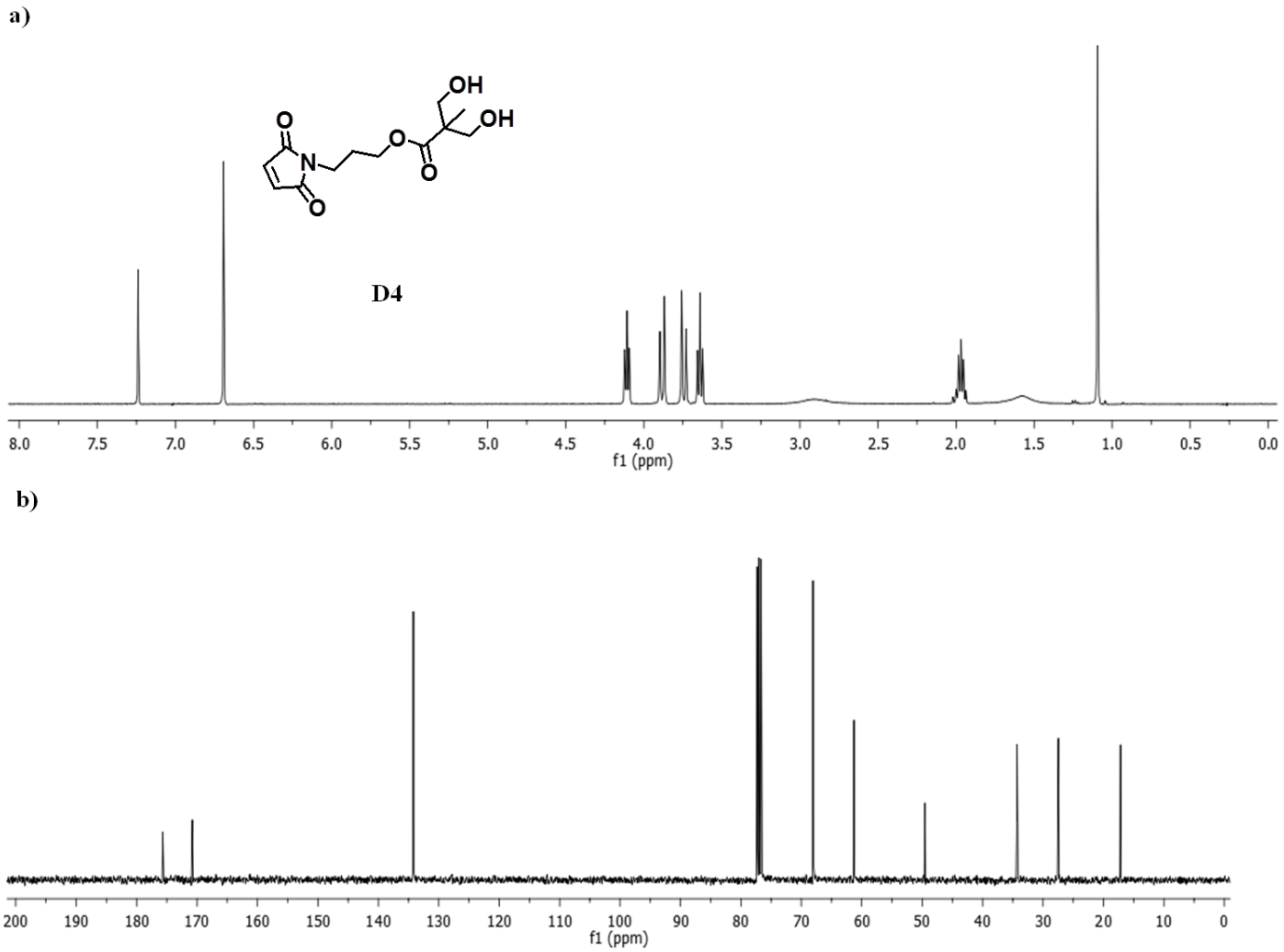

Figure 5A. 1. ^{1}H NMR (a) and ^{13}C NMR (b) spectra of R-G1M-OH (D4)

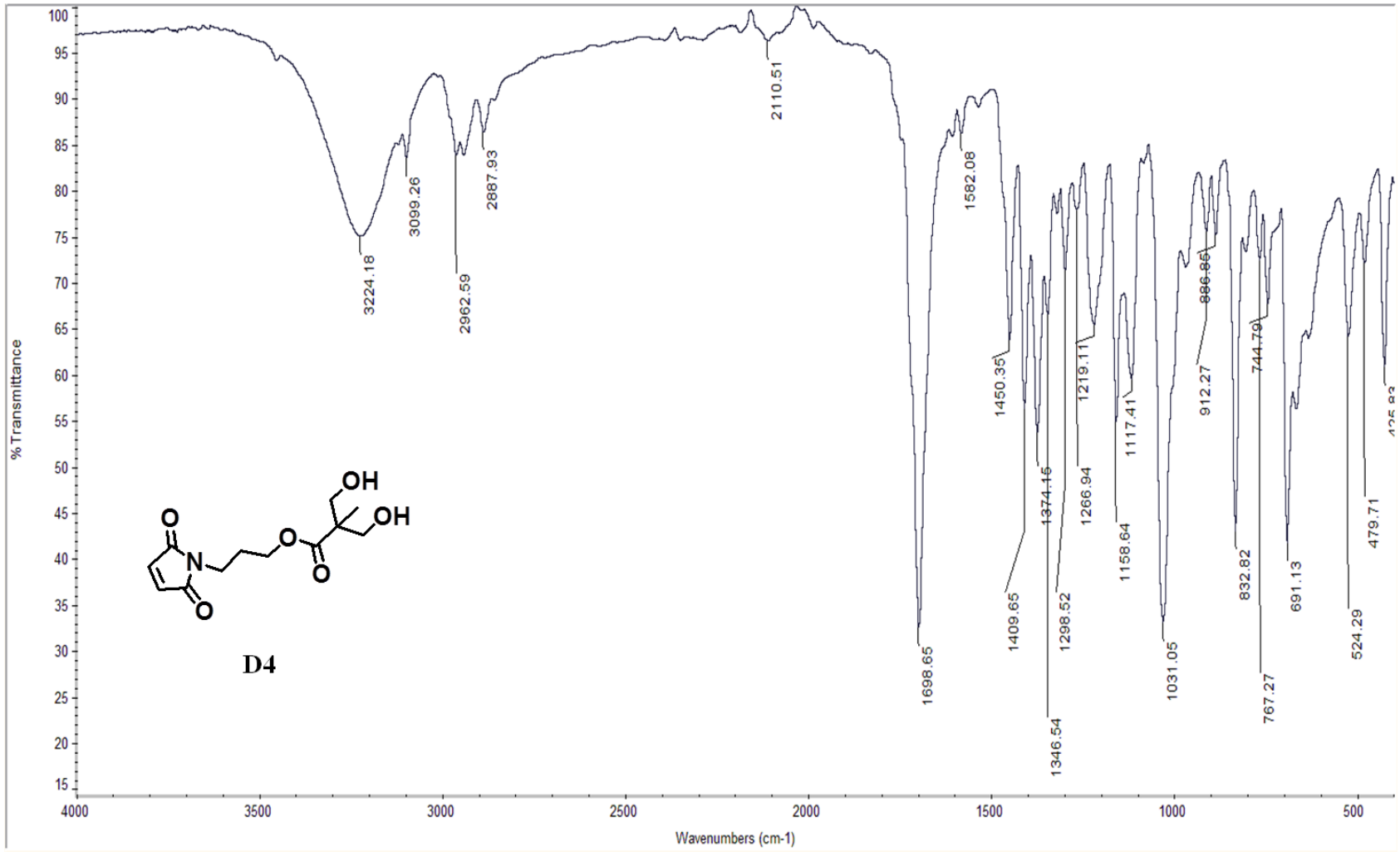

Figure 5A. 2. FTIR spectrum of R-G1M-OH (D4)

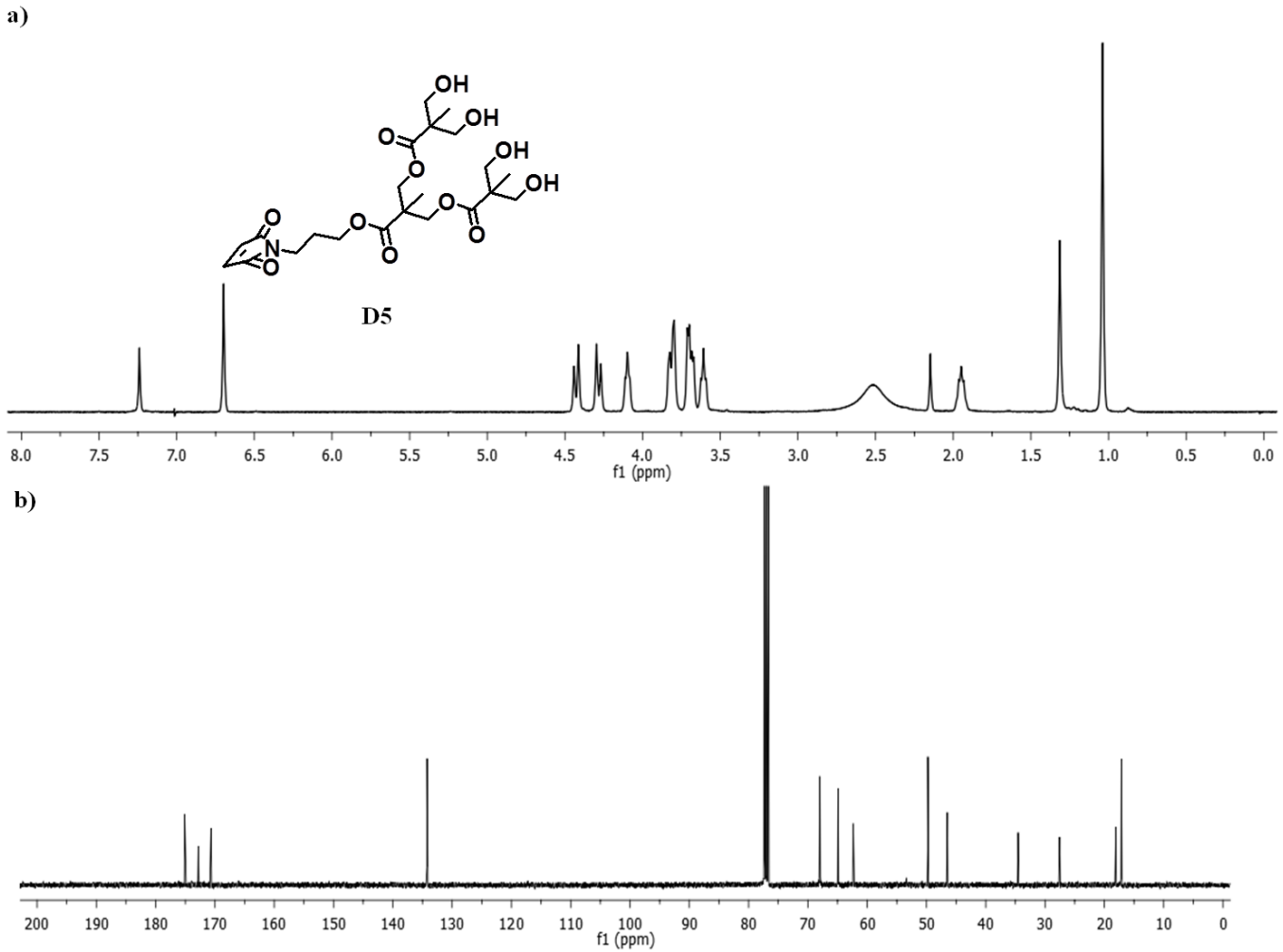

Figure 5A. 3. ^{1}H NMR (a) and ^{13}C NMR (b) spectra of R-G2M-OH (D5)

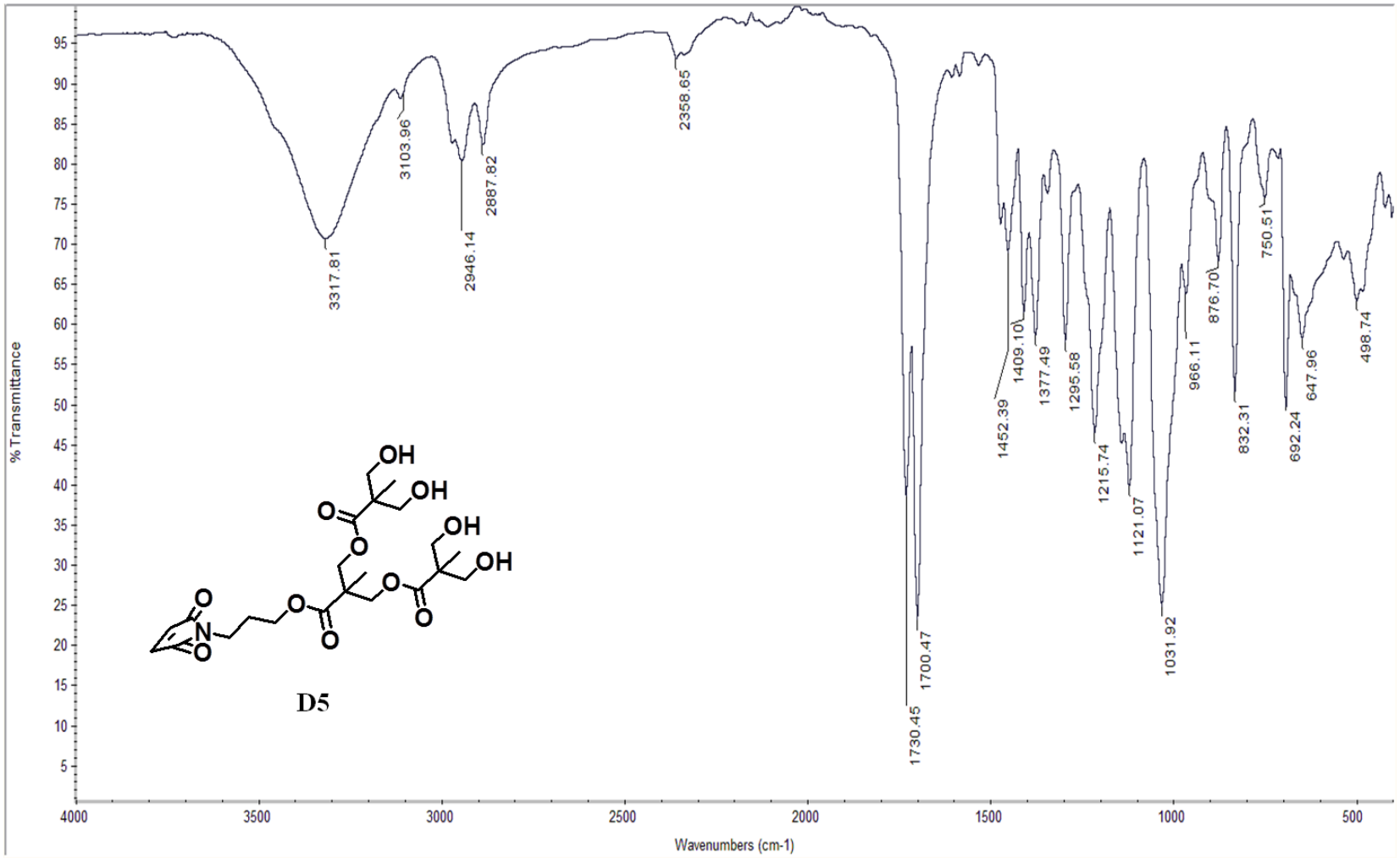

Figure 5A. 4. FTIR spectrum of R-G2M-OH (D5)

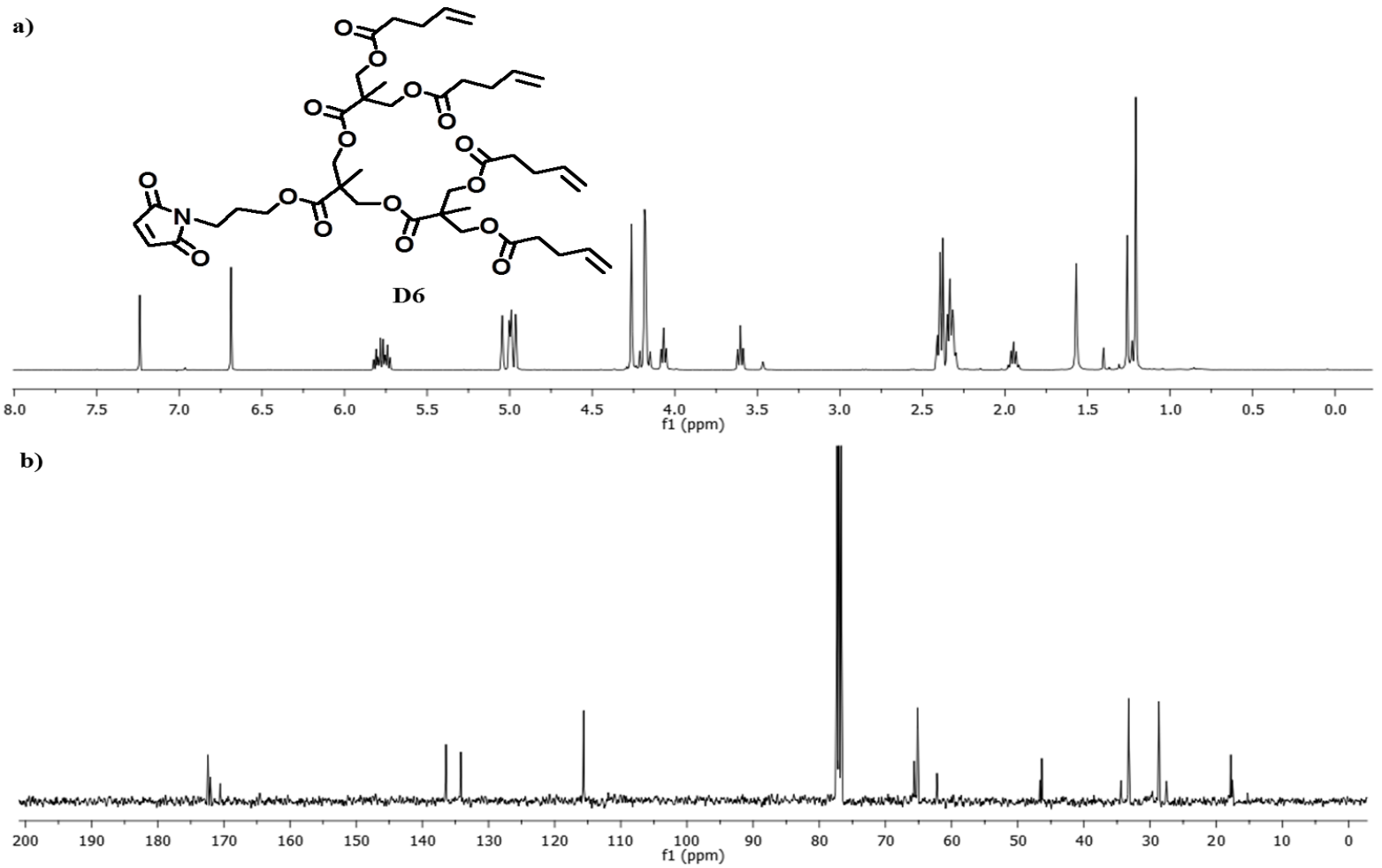

Figure 5A. 5. ^{1}H NMR (a) and ^{13}C NMR (b) spectra of R-G2M-alkene (D6)

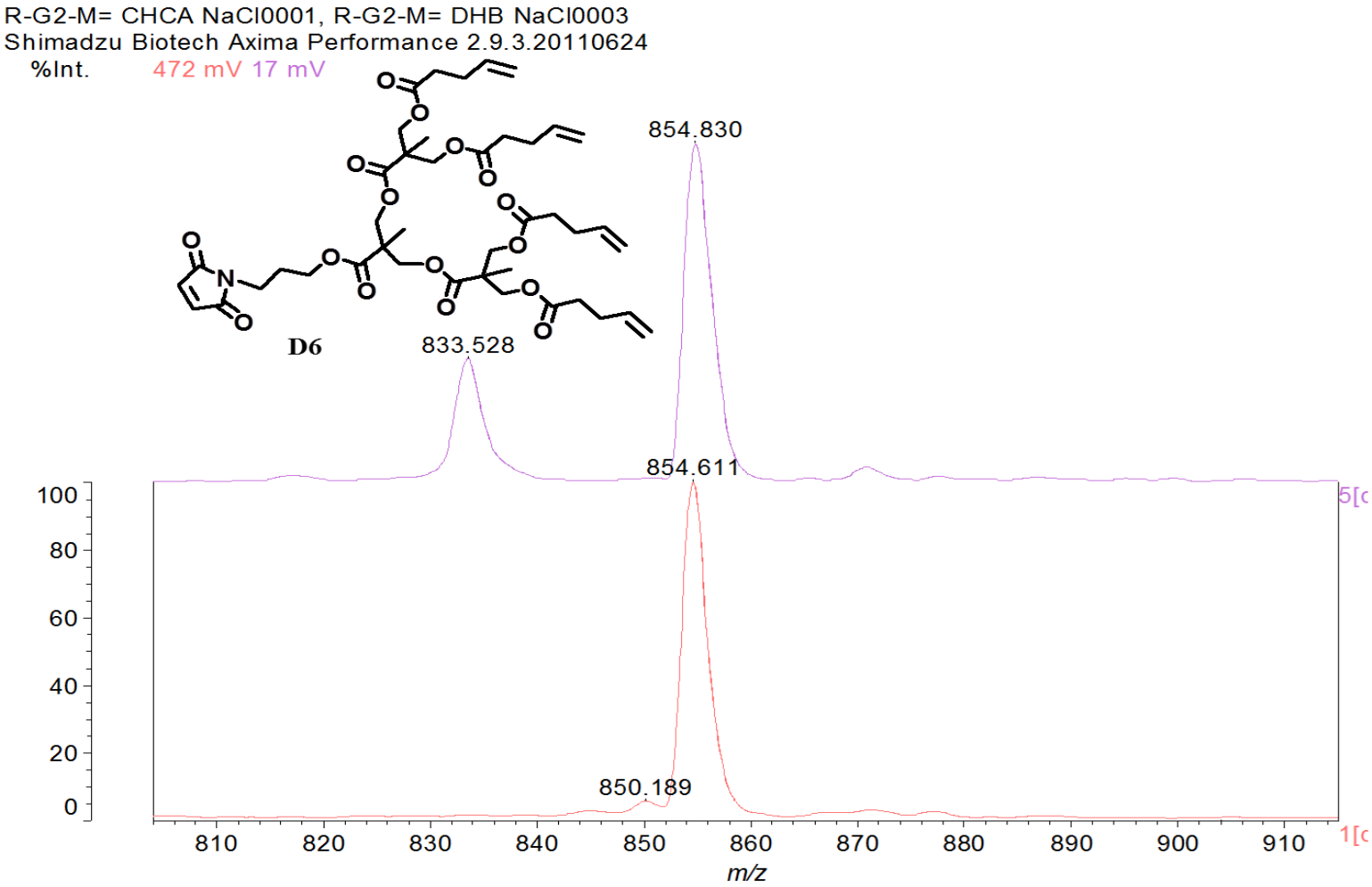

Figure 5A. 6. Maldi-TOF result of R-G2M-alkene (D6)

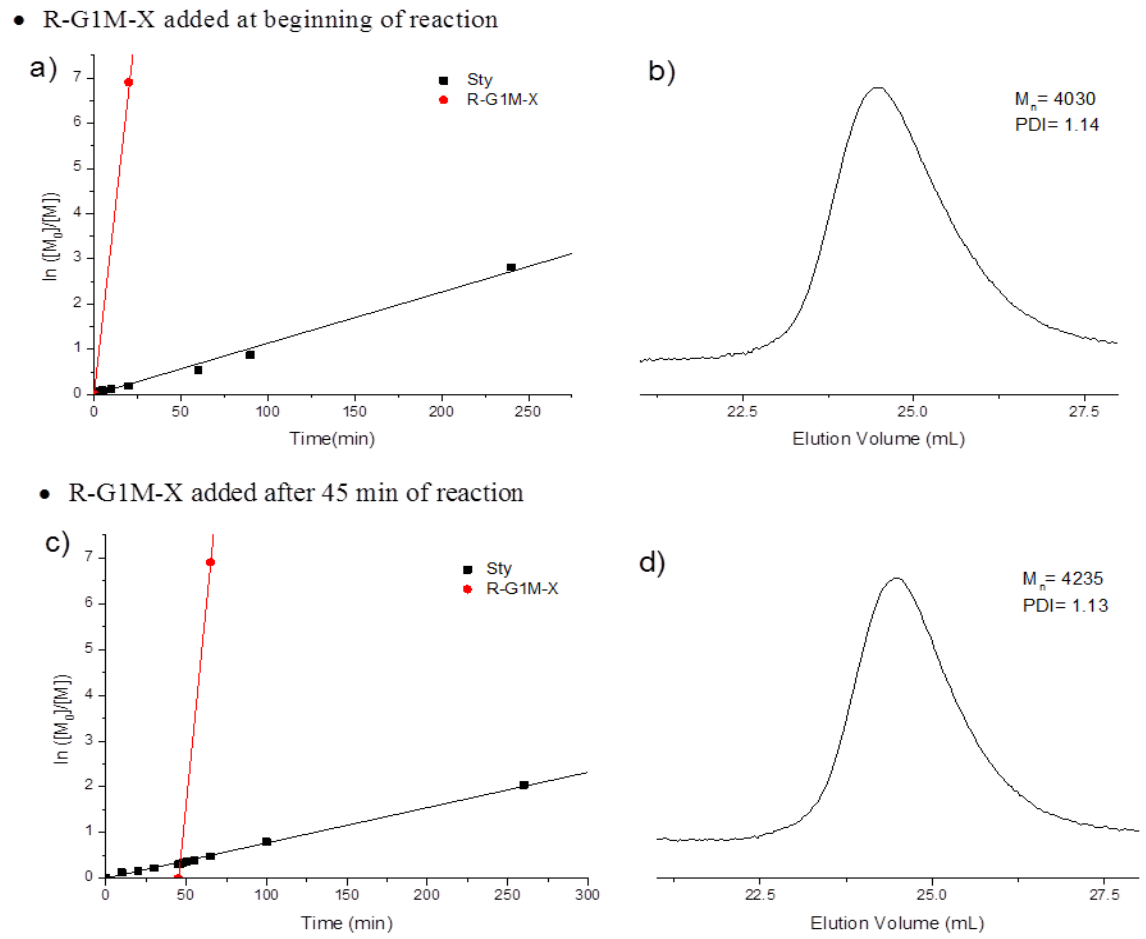

Figure 5A. 7. (a) and (c) Semi-logarithmic plots of monomers conversion versus time for nitroxide-mediated copolymerization of styrene (Sty, 50 equiv.) (black squares) with D1 (R-G1M-X, 1 equiv.) (red dots) added at beginning or after 45 minutes of reaction. Experimental conditions: bulk, 120 °C, Sty/MI/BlocBuilder=50/1/1. (b) and (d) Size exclusion chromatograms of the isolated copolymers

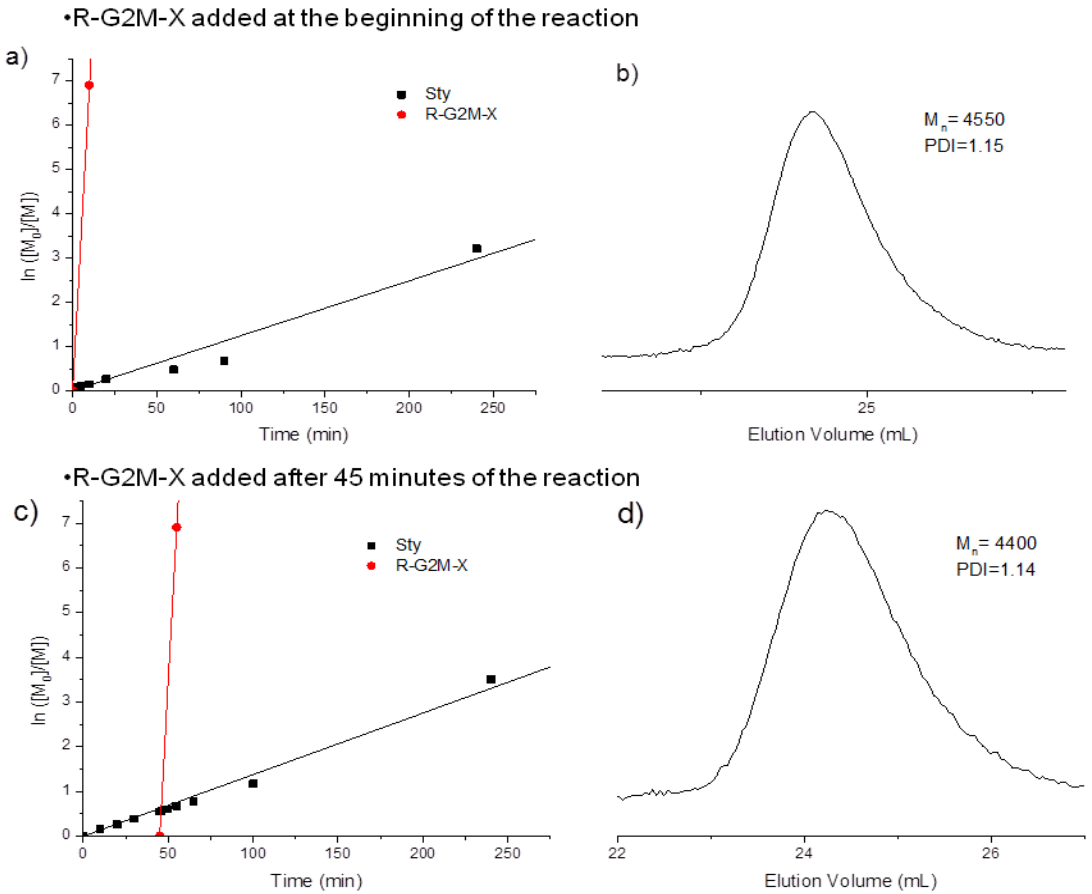

Figure 5A. 8. (a) and (c) Semi-logarithmic plots of monomers conversion versus time for nitroxide-mediated copolymerization of styrene (Sty, 50 equiv.) (black squares) with D2 (R-G2M-X, 1 equiv.) (red dots) added at beginning or after 45 minutes of reaction. Experimental conditions: bulk, 120 °C, Sty/MI/BlocBuilder=50/1/1. (b) and (d) Size exclusion chromatograms of the isolated copolymers

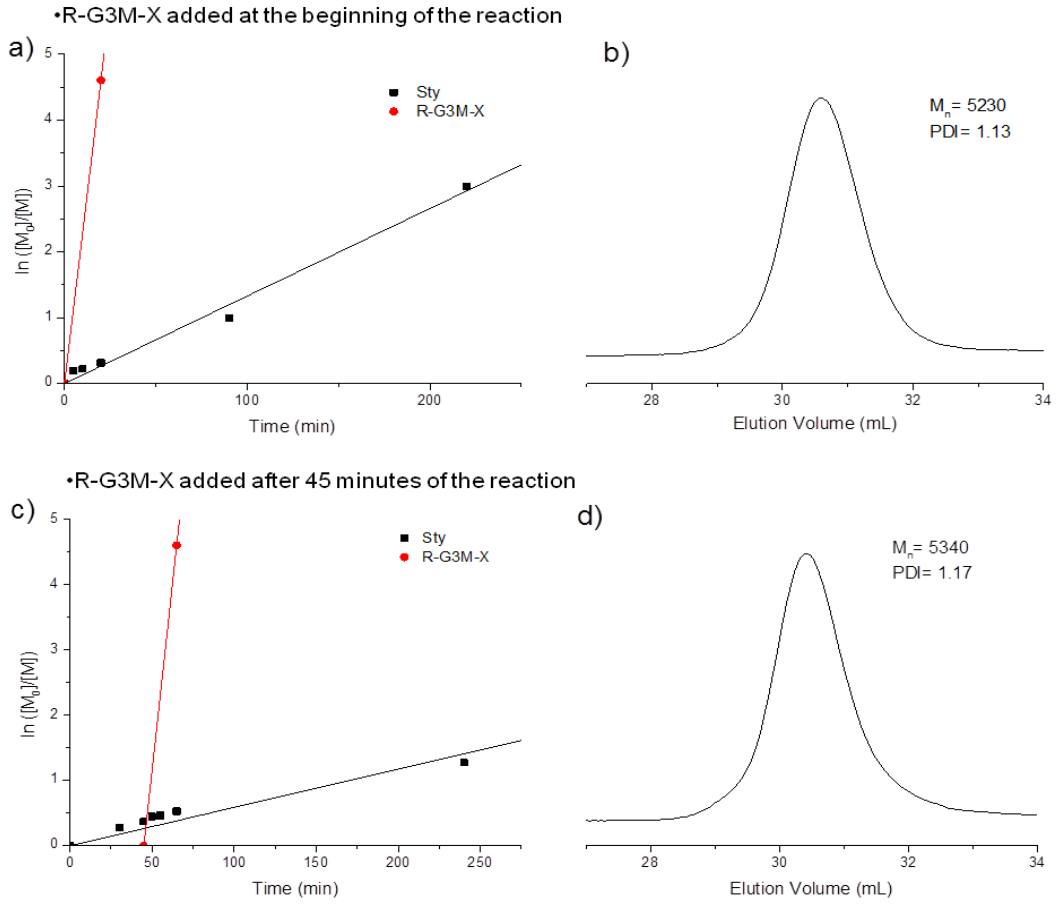

Figure 5A. 9. (a) and (c) Semi-logarithmic plots of monomers conversion versus time for nitroxide-mediated copolymerization of styrene (Sty, 50 equiv.) (black squares) with D3 (R-G3M-X, 1 equiv.) (red dots) added at beginning or after 45 minutes of reaction. Experimental conditions: bulk, 120 °C, Sty/MI/BlocBuilder=50/1/1. (b) and (d) Size exclusion chromatograms of the isolated copolymers

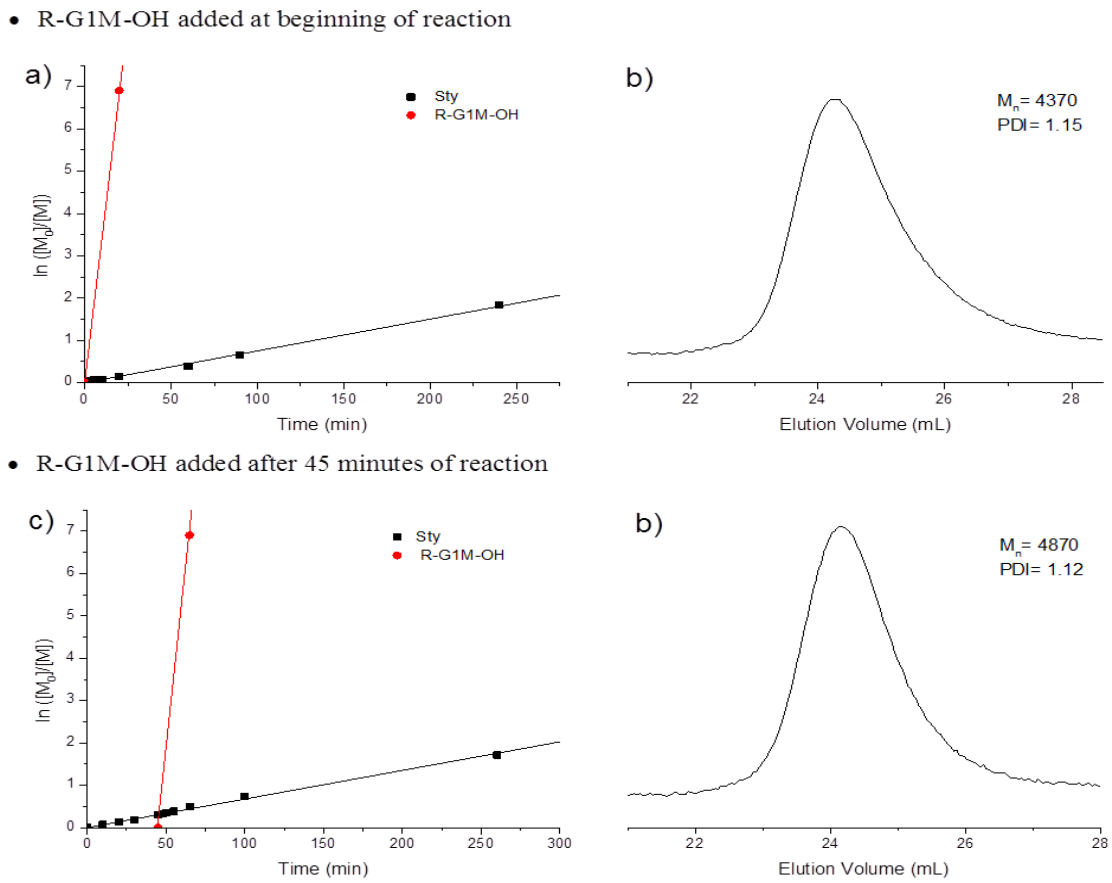

Figure 5A. 10. (a) and (c) Semi-logarithmic plots of monomers conversion versus time for nitroxide-mediated copolymerization of styrene (Sty, 50 equiv.) (black squares) with D4 (R-G1M-OH, 1 equiv.) (red dots) added at beginning or after 45 minutes of reaction. Experimental conditions: bulk, 120 °C, Sty/MI/BlocBuilder=50/1/1. (b) and (d) Size exclusion chromatograms of the isolated copolymers

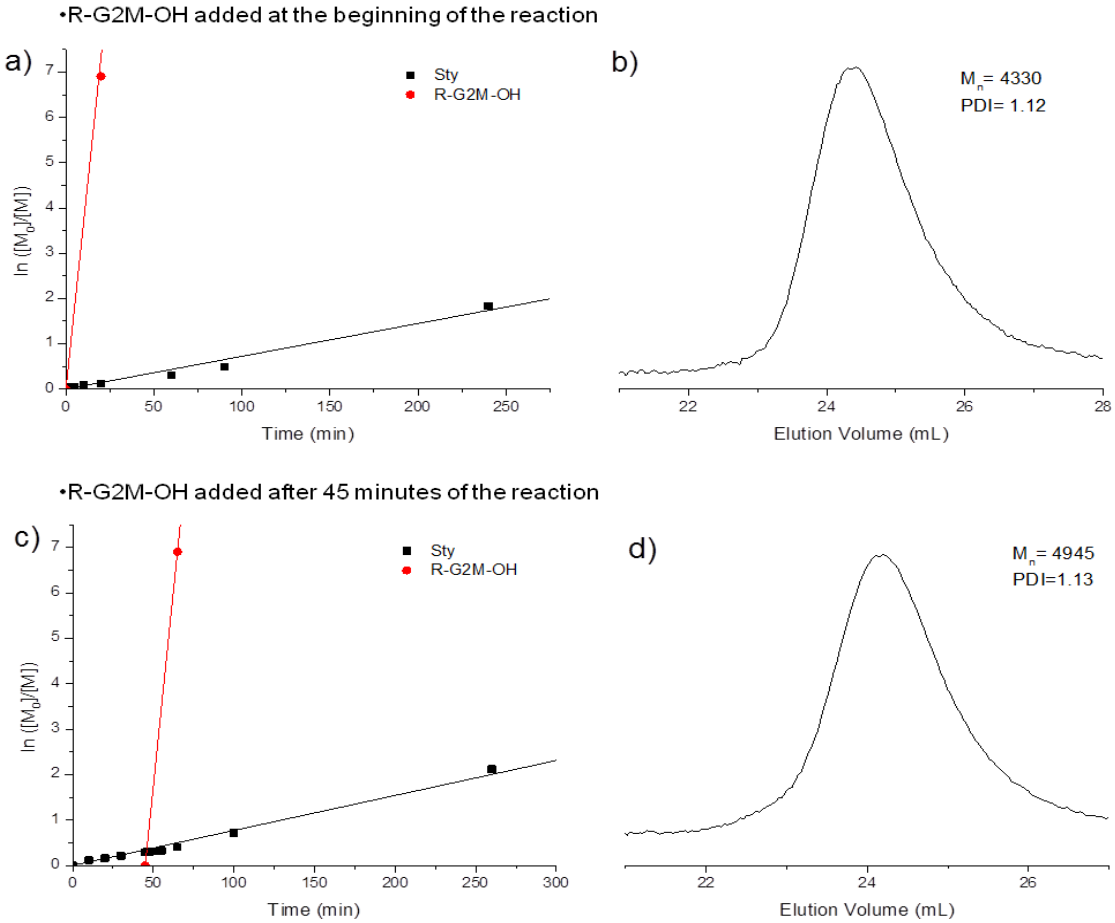

Figure 5A. 11. (a) and (c) Semi-logarithmic plots of monomers conversion versus time for nitroxide-mediated copolymerization of styrene (Sty, 50 equiv.) (black squares) with D5 (R-G2M-OH, 1 equiv.) (red dots) added at beginning or after 45 minutes of reaction. Experimental conditions: bulk, 120 °C, Sty/MI/BlocBuilder=50/1/1. (b) and (d) Size exclusion chromatograms of the isolated copolymer

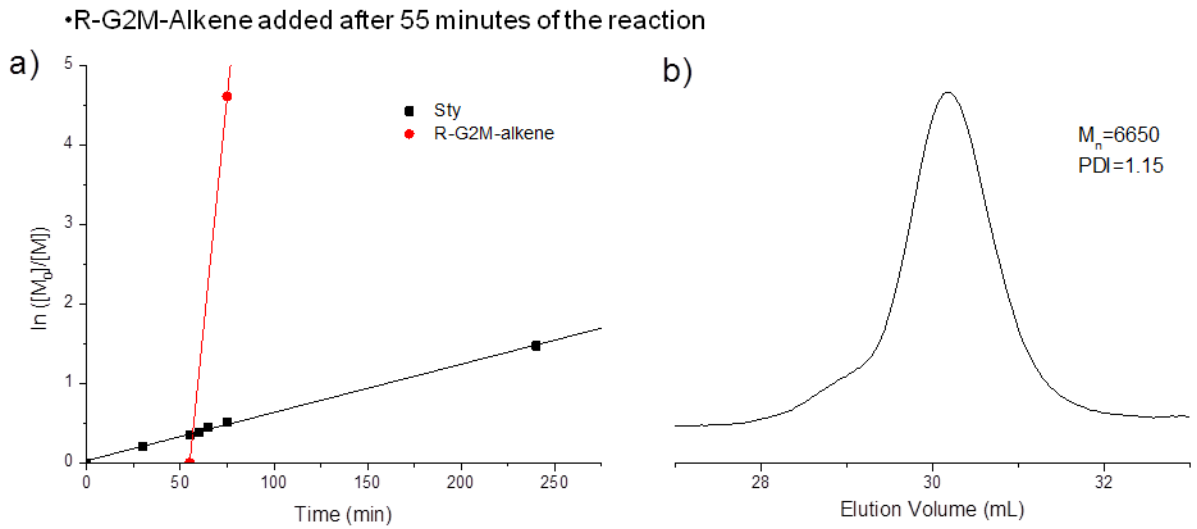

Figure 5A. 12. (a) Semi-logarithmic plot of monomers conversion versus time for nitroxide-mediated copolymerization of styrene (Sty, 50 equiv.) (black squares) with D6 (R-G2M-alkene, 1 equiv.) (red dots) added after 55 minutes of reaction. Experimental conditions: bulk, 120 °C, Sty/MI/BlocBuilder=50/1/1. (b) Size exclusion chromatogram of the isolated copolymer

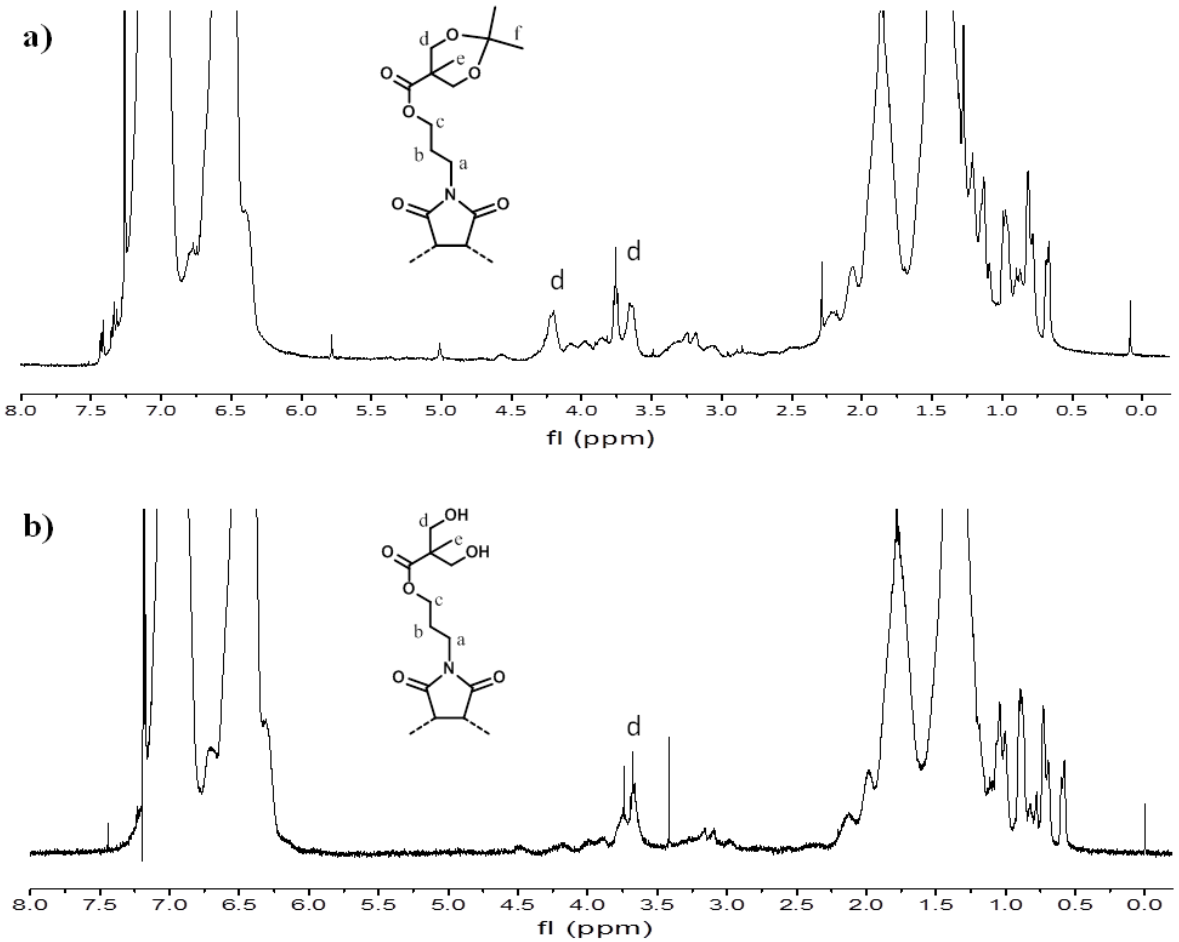

Figure 5A. 13. ^{1}H NMR spectra of copolymers P(S-*co*-D1) (a) and P(S-*co*-D4) (b) recorded at RT in $CDCl_3$

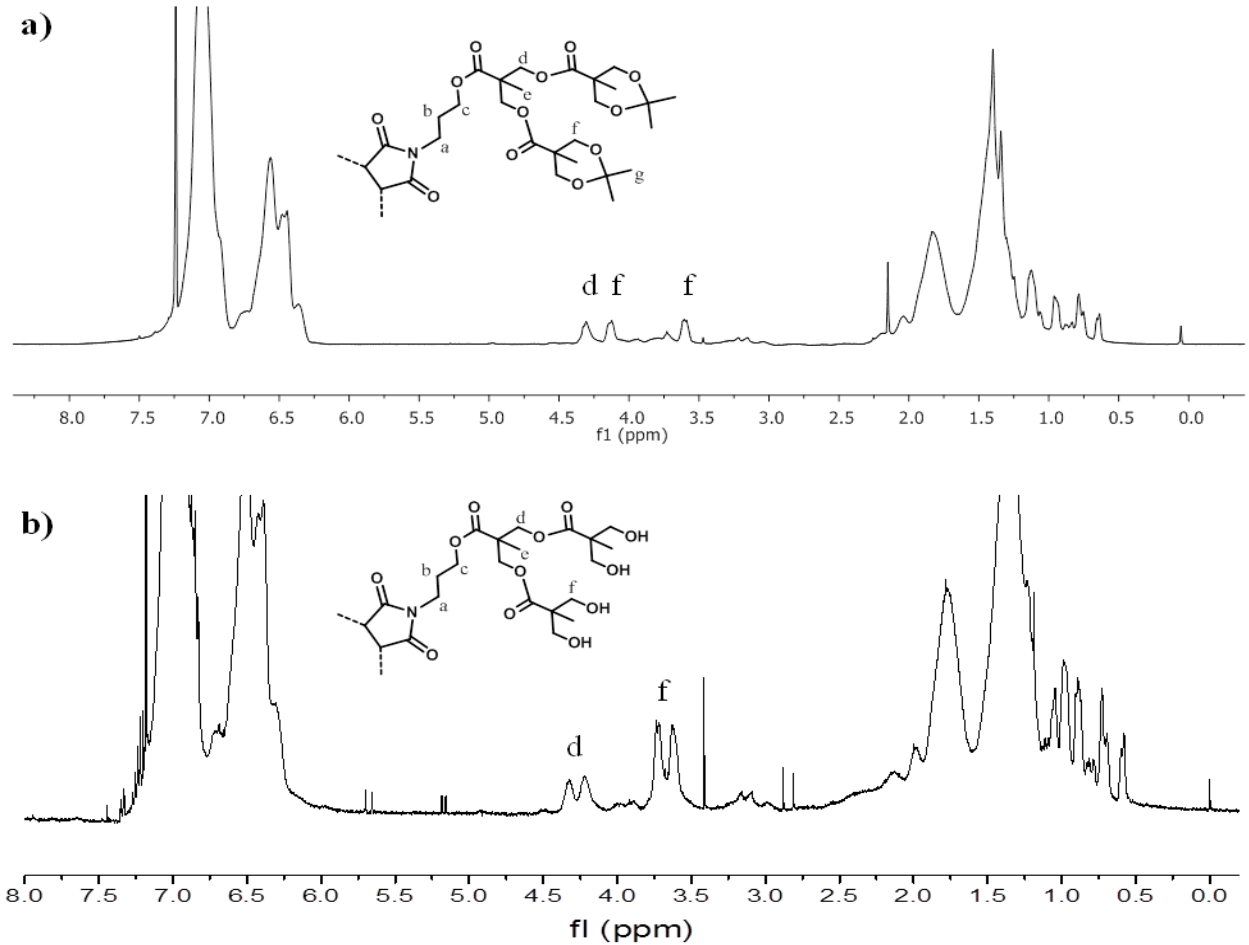

Figure 5A. 14. ^{1}H NMR spectra of copolymers P(S-*co*-D2) (a) and P(S-*co*-D5) (b) recorded at RT in $CDCl_3$

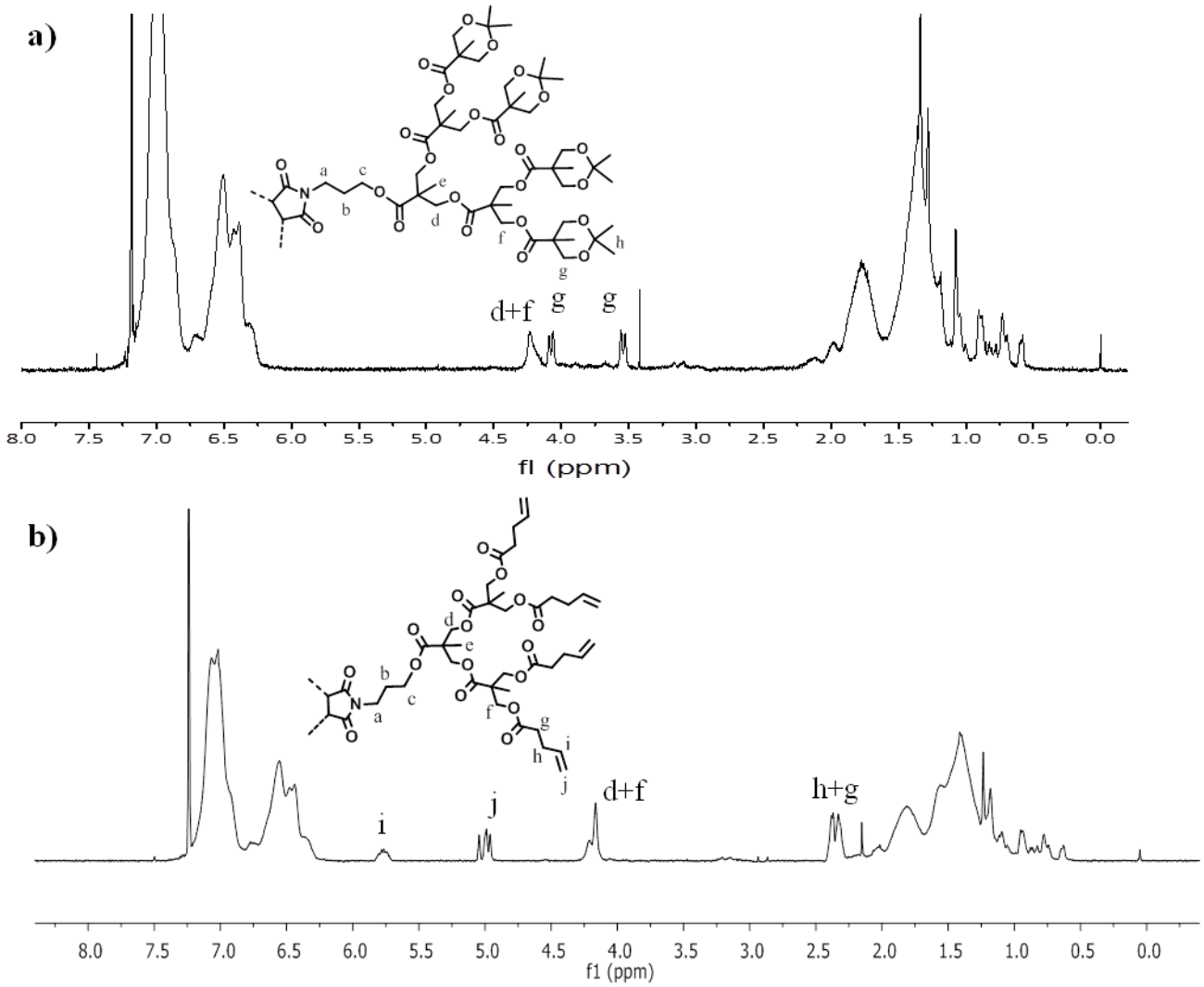

Figure 5A. 15. ^{1}H NMR spectra of copolymers P(S-*co*-D3) (a) and P(S-*co*-D6) (b) recorded at RT in $CDCl_3$

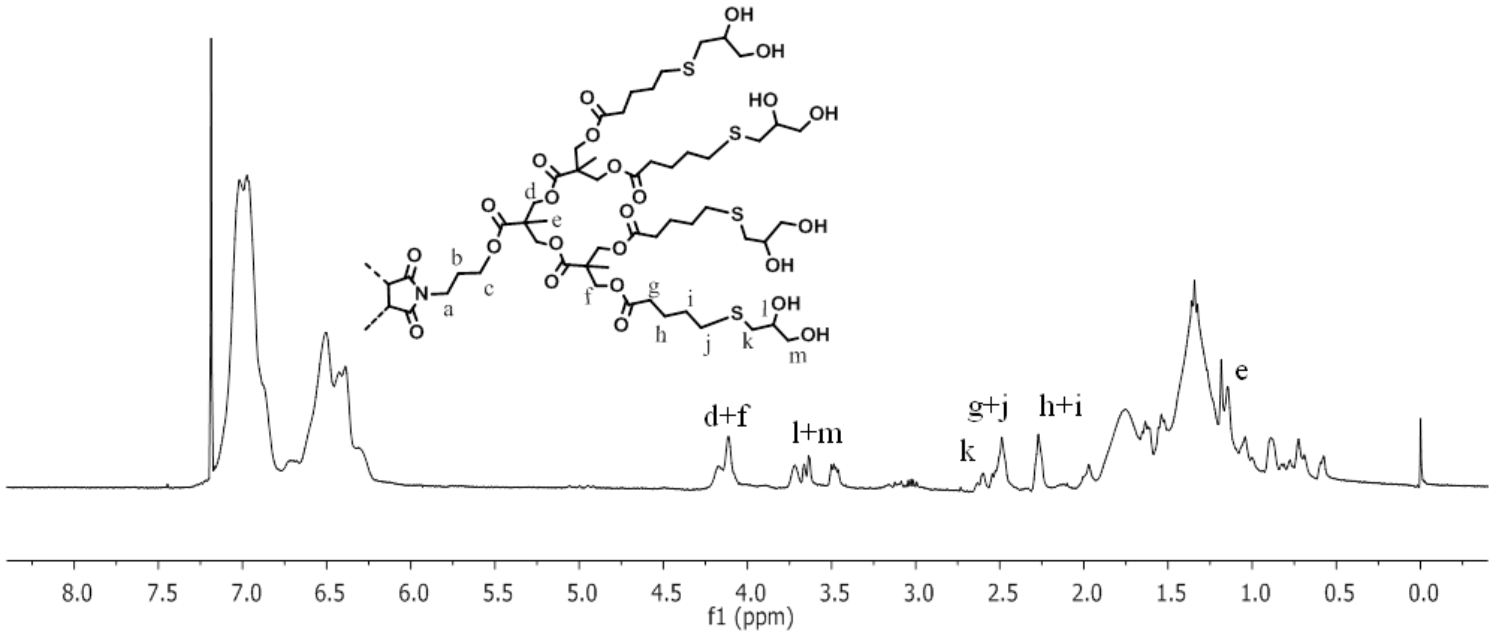

Figure 5A. 16. ^{1}H NMR spectrum of the copolymer P(S-*co*-D6') recorded at RT in $CDCl_3$

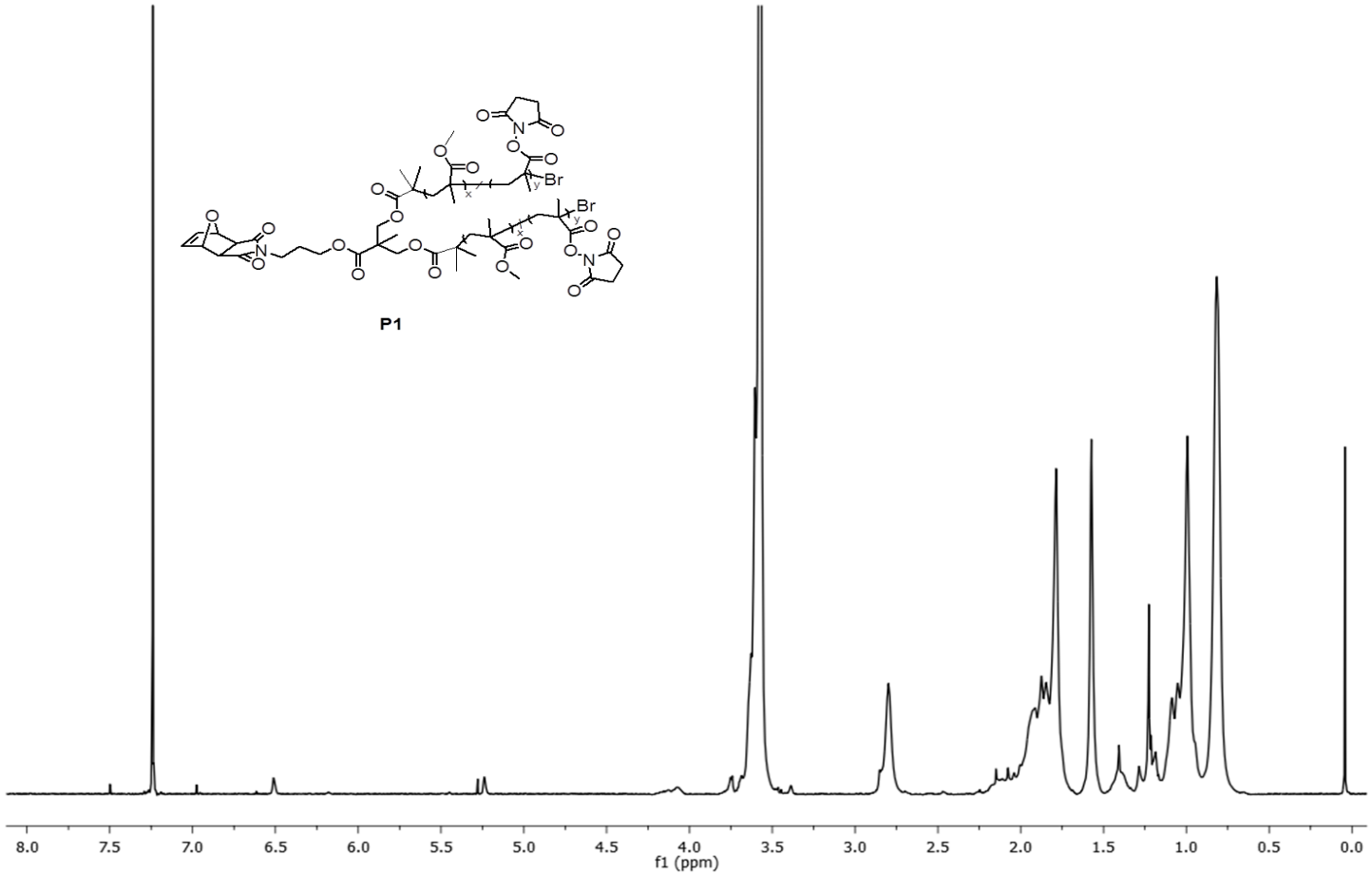

Figure 6A. 1. ^{1}H NMR spectrum of G1M-(PMMA-*co*-NHSMA) (P1) in $CDCl_3$

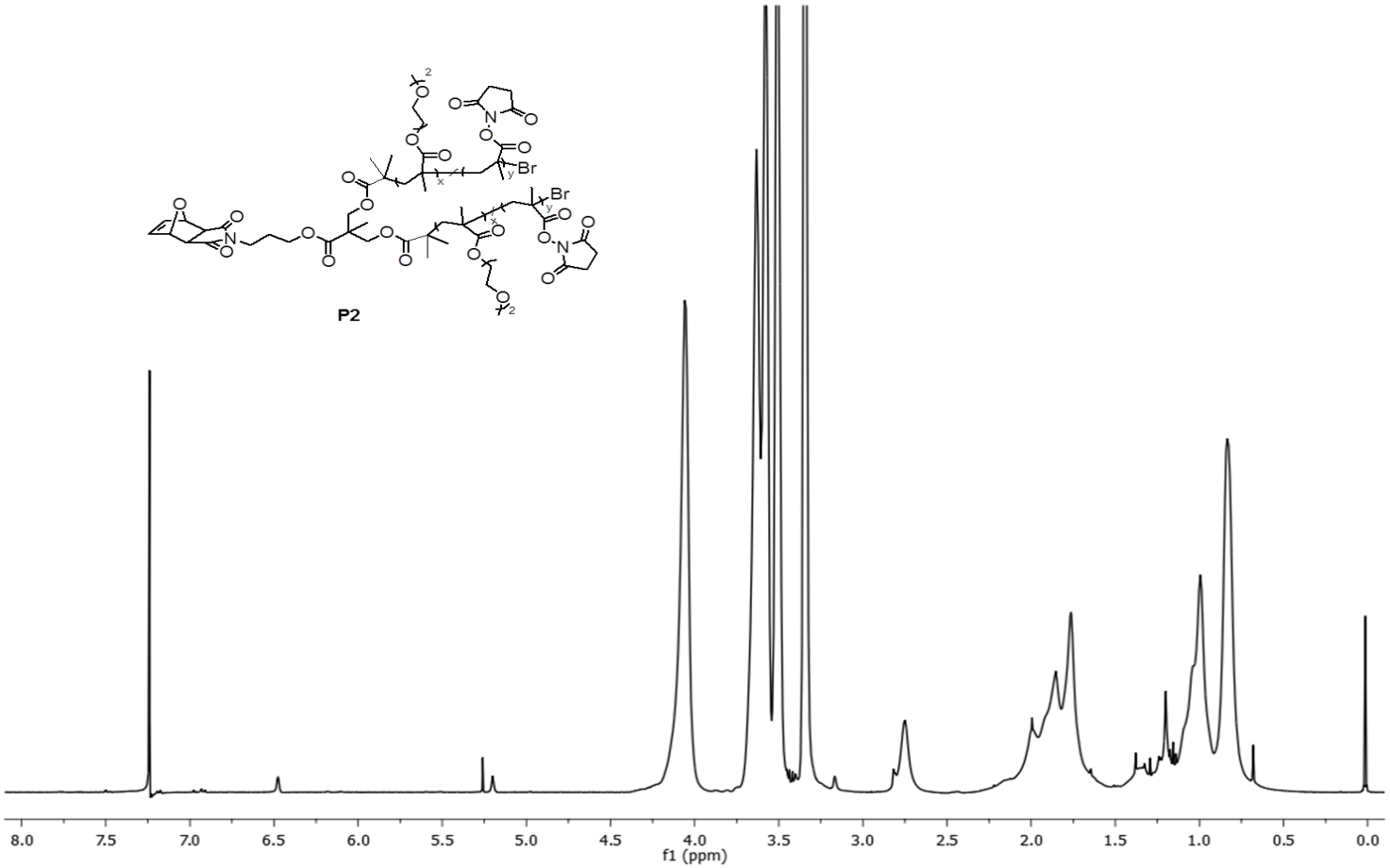

Figure 6A. 2. ^{1}H NMR spectrum of G1M-(DEGMEMA-*co*-NHSMA) (P2) in $CDCl_3$

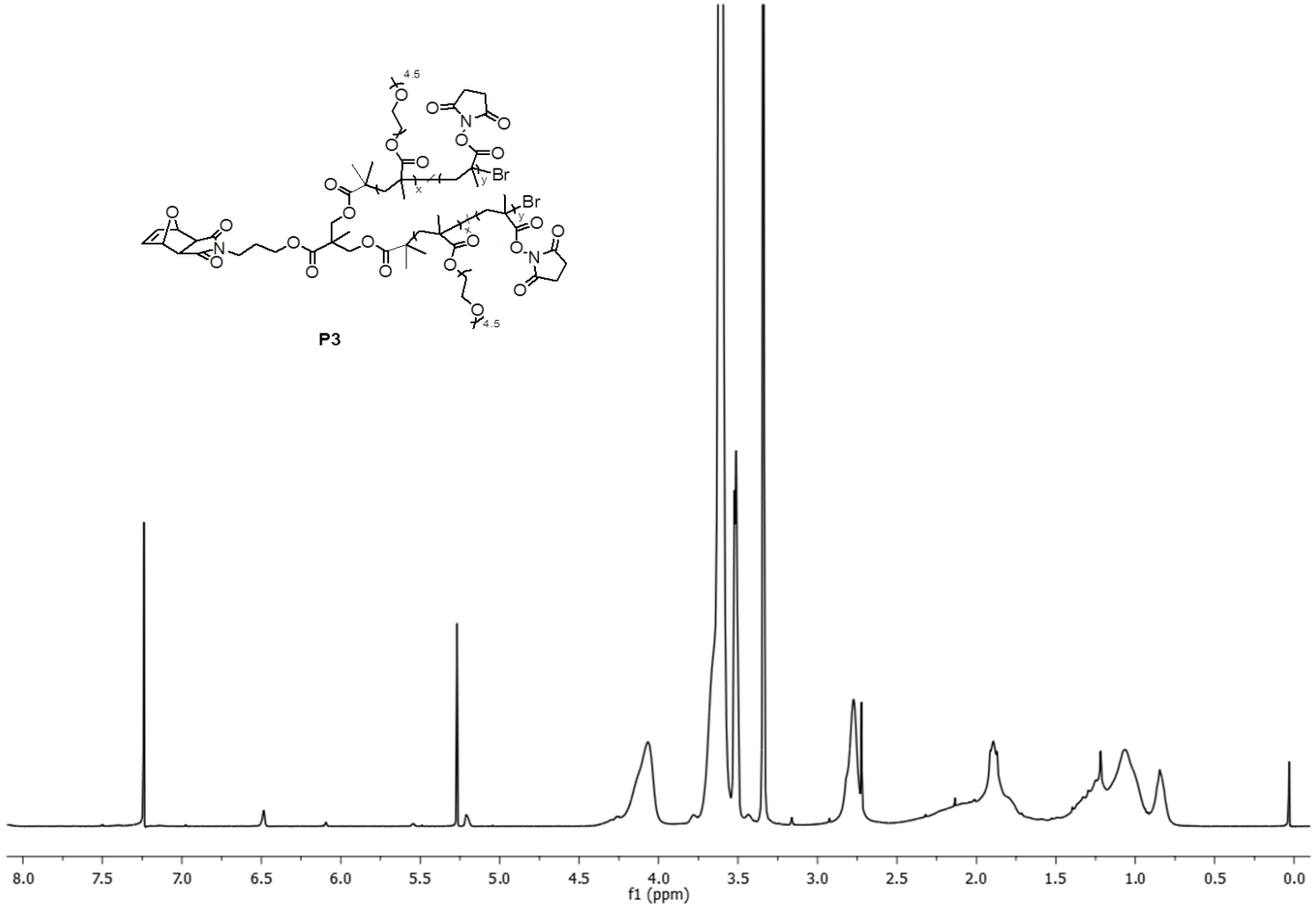

Figure 6A. 3. ^{1}H NMR spectrum of G1M-(PEGMEMA-*co*-NHSMA) (P3) in $CDCl_3$

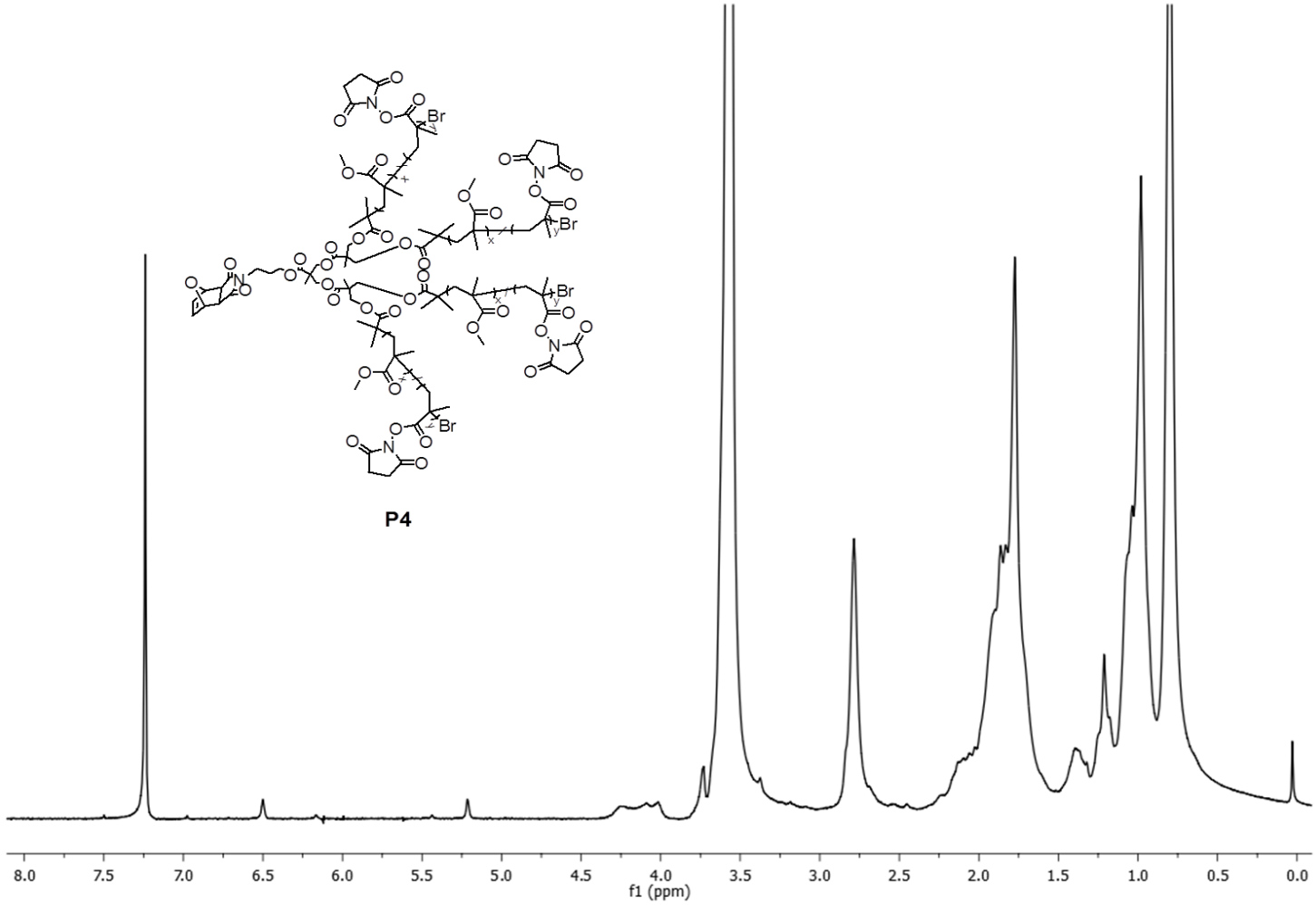

Figure 6A. 4. ^{1}H NMR spectrum of G2M-(PMMA-*co*-NHSMA) (P4) in $CDCl_3$

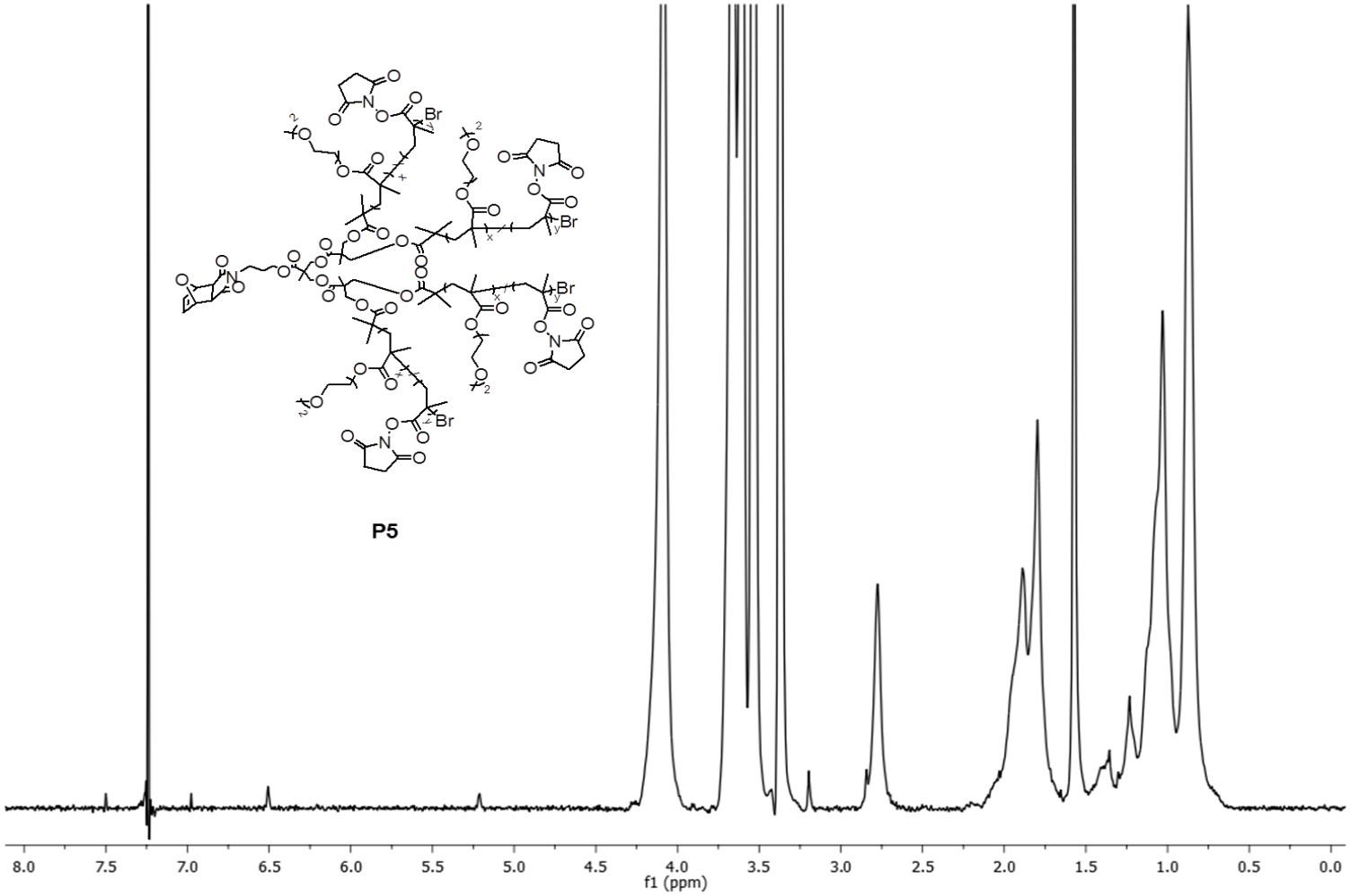

Figure 6A. 5. ^{1}H NMR spectrum of G2M-(DEGMEMA-*co*-NHSMA) (P5) in $CDCl_3$

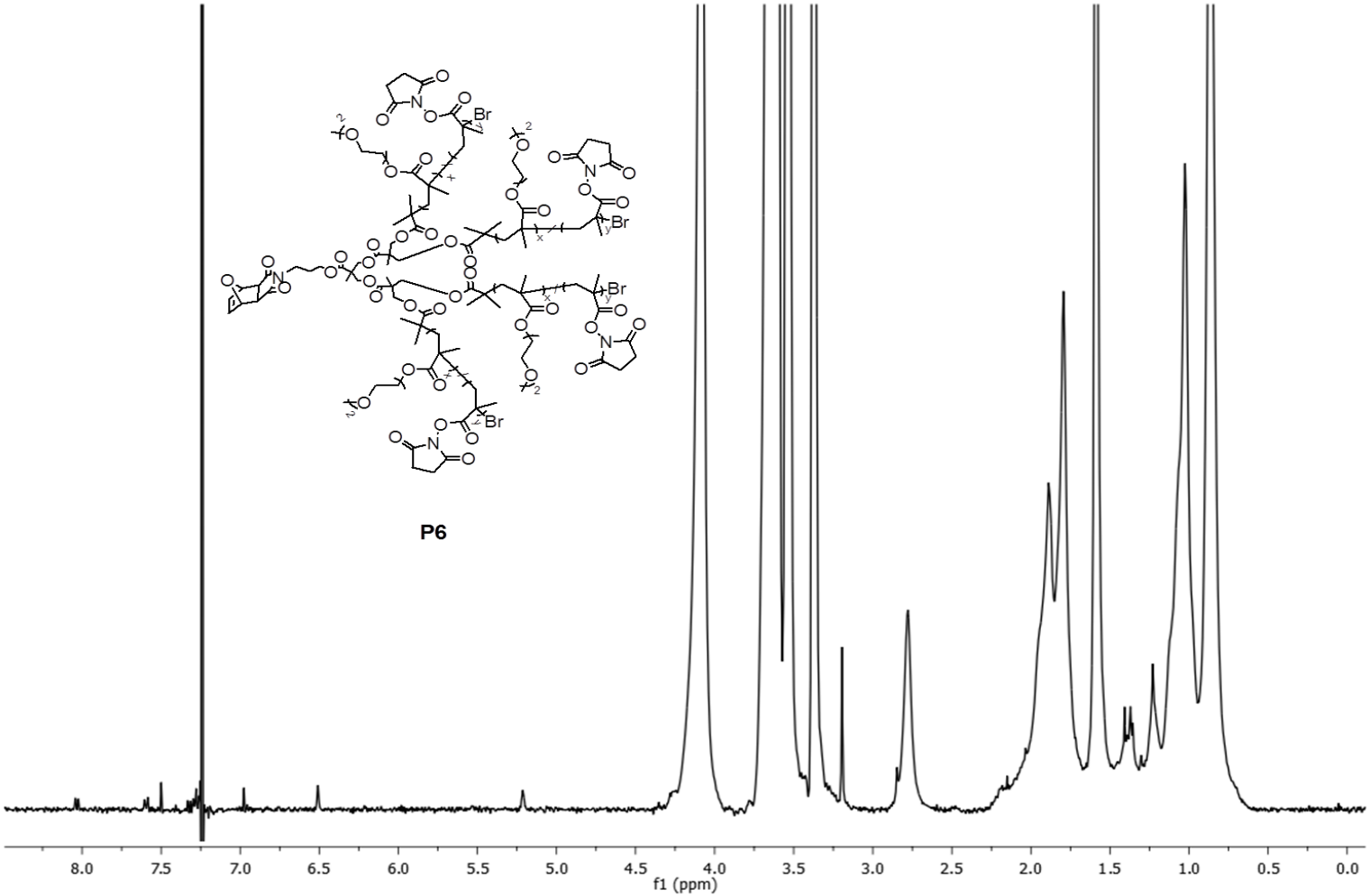

Figure 6A. 6. ^{1}H NMR spectrum of G2M-(DEGMEMA-*co*-NHSMA) (P6) in $CDCl_3$

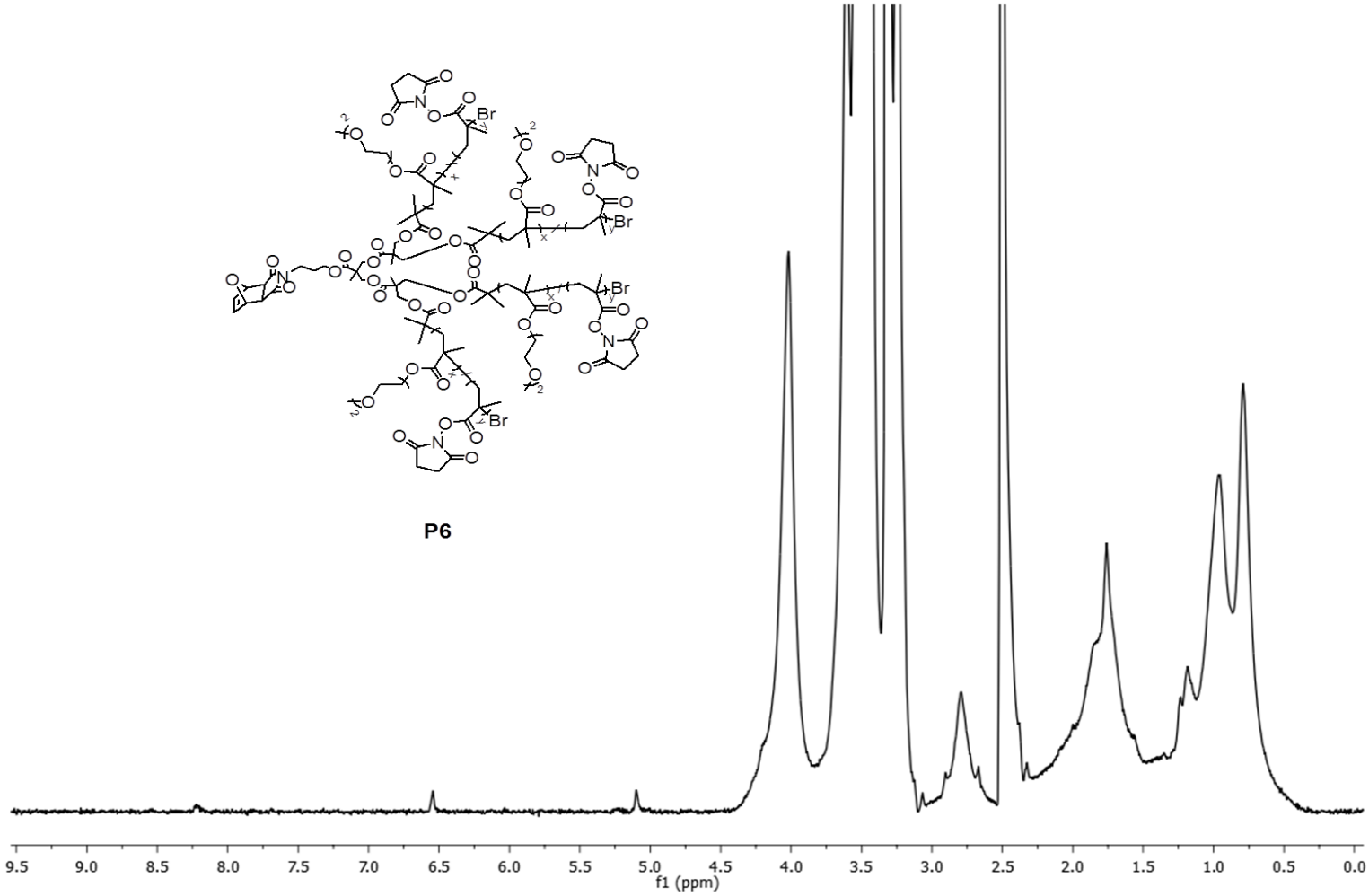

Figure 6A. 7. ^{1}H NMR spectrum of G2M-(DEGMEMA-*co*-NHSMA) (P6) in DMSO

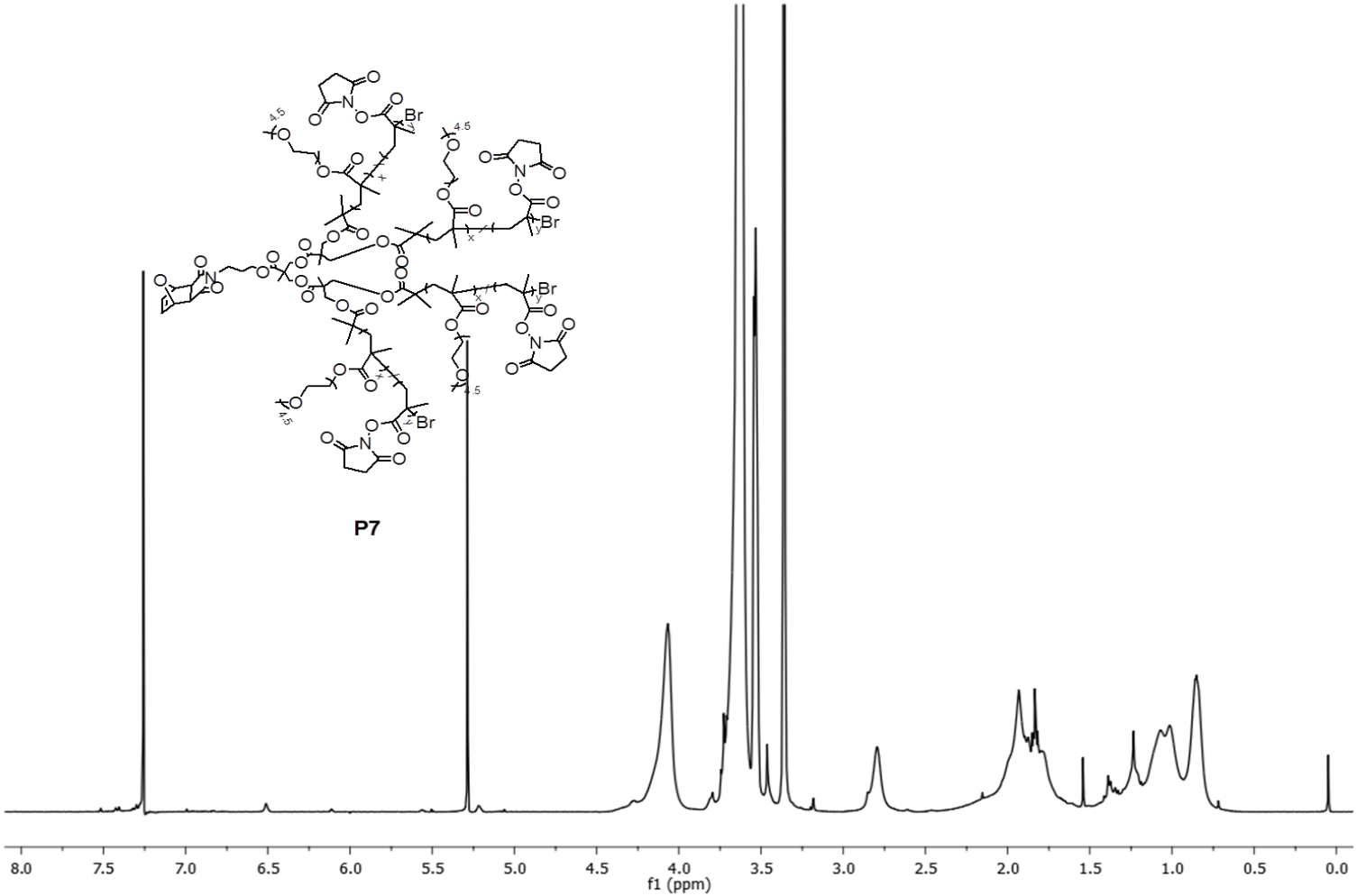

Figure 6A. 8. ^{1}H NMR spectrum of G2M-(PEGMEMA-*co*-NHSMA) (P7) in $CDCl_3$

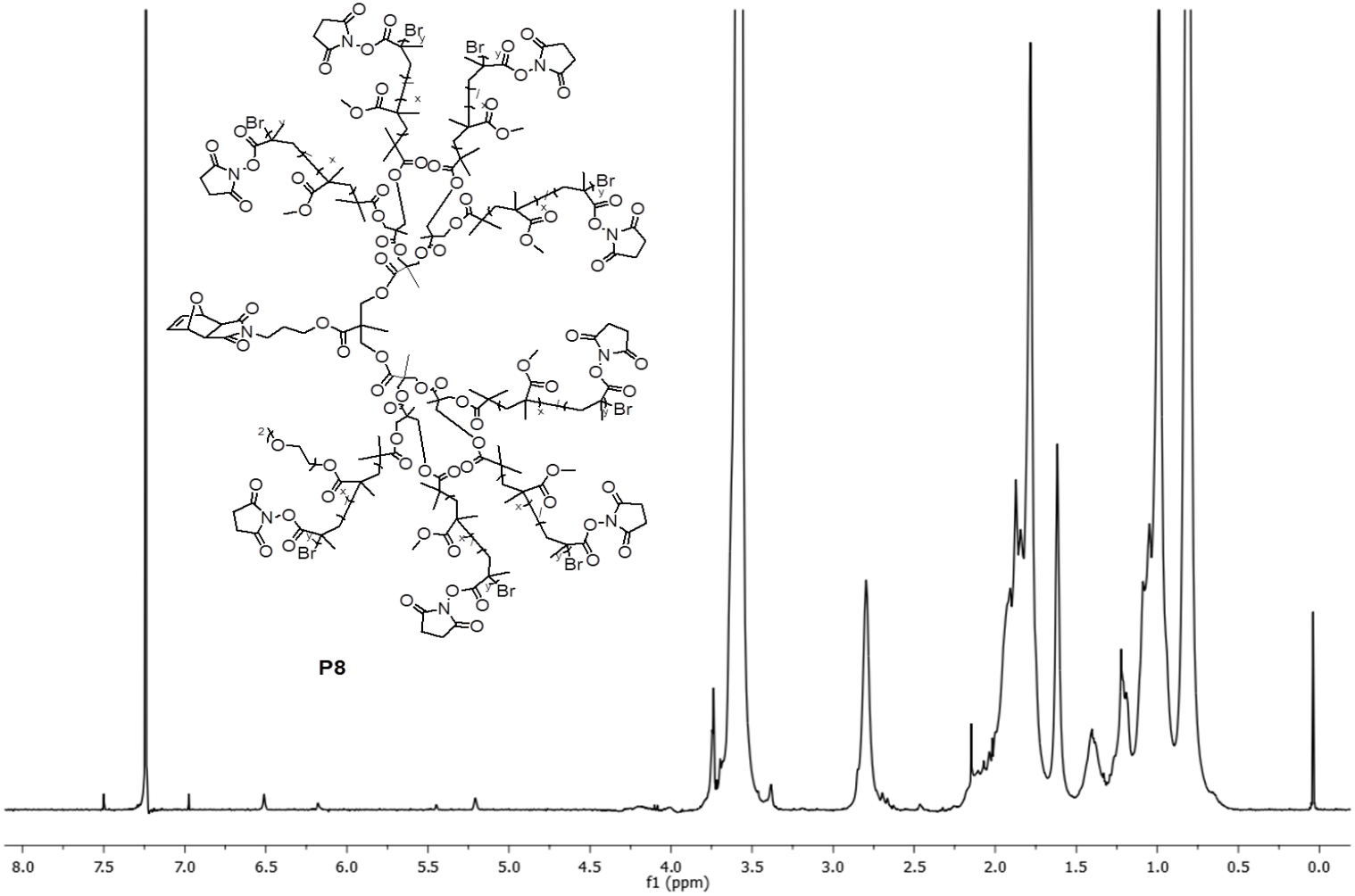

Figure 6A. 9. ^{1}H NMR spectrum of G3M-(PMMA-*co*-NHSMA) (P8) in $CDCl_3$

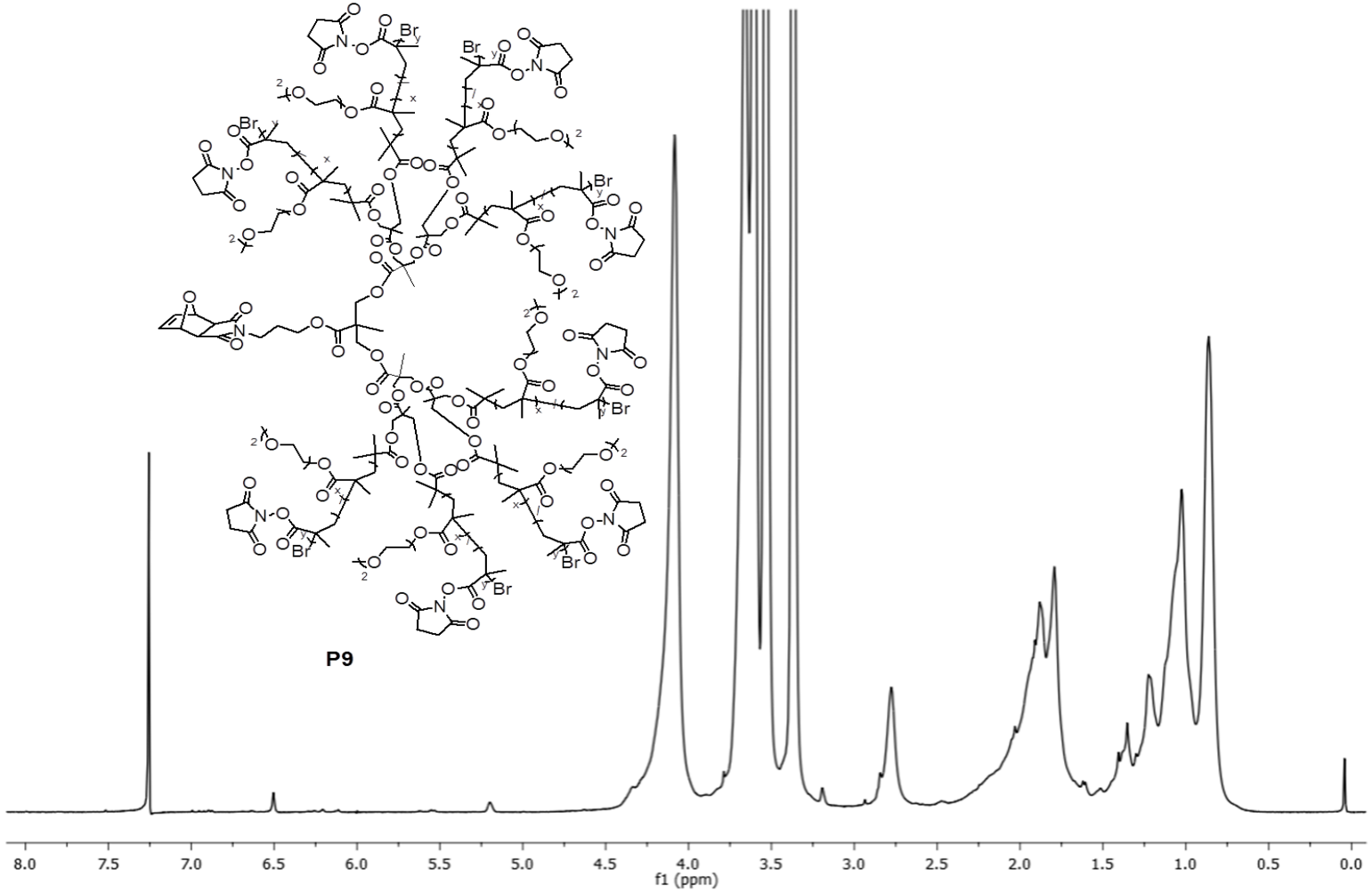

Figure 6A. 10. ^{1}H NMR spectrum of G3M-(DEGMEMA-*co*-NHSMA) (P9) in $CDCl_3$

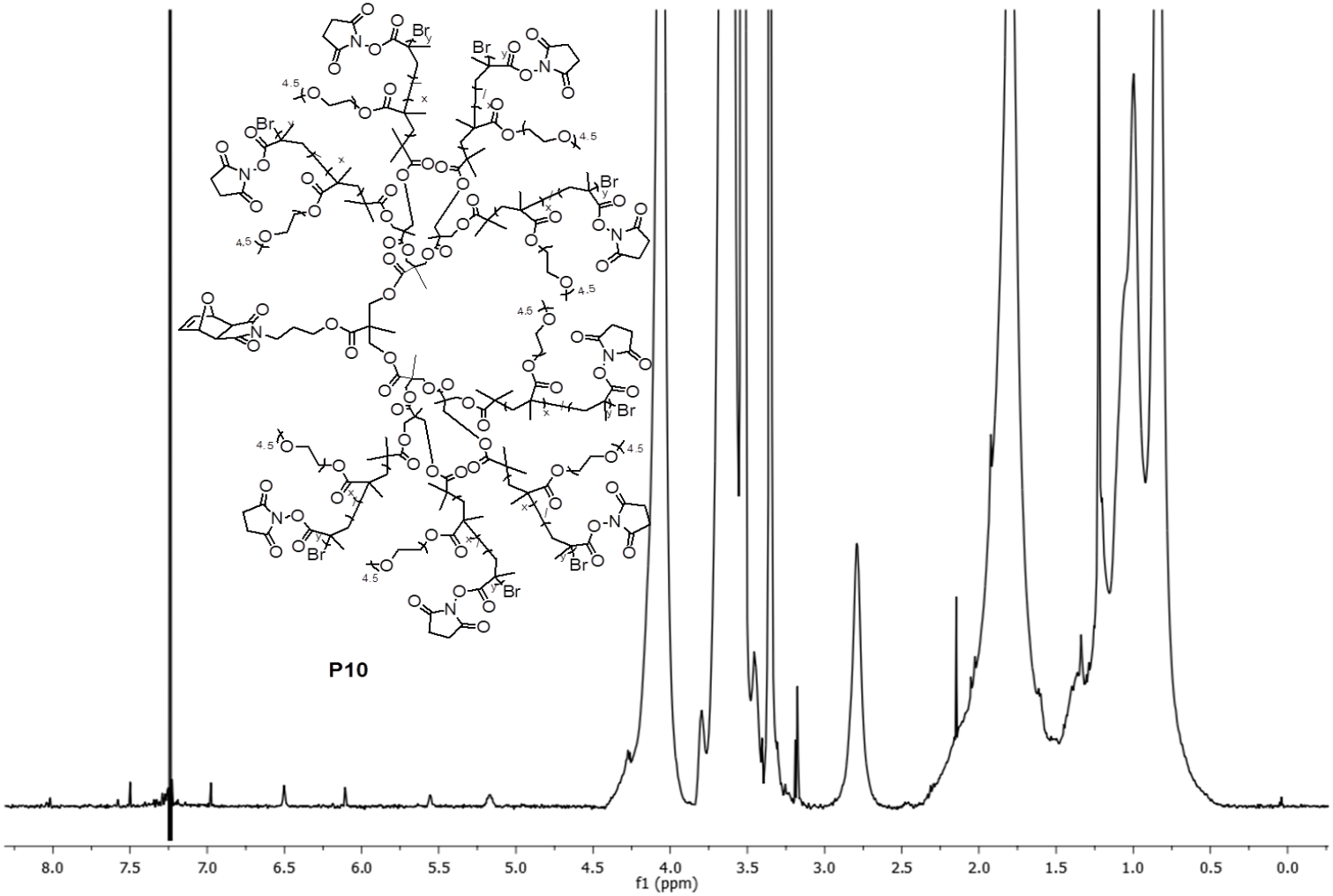

Figure 6A. 11. ^{1}H NMR spectrum of G2M-(PEGMEMA-*co*-NHSMA) (P10) in $CDCl_3$

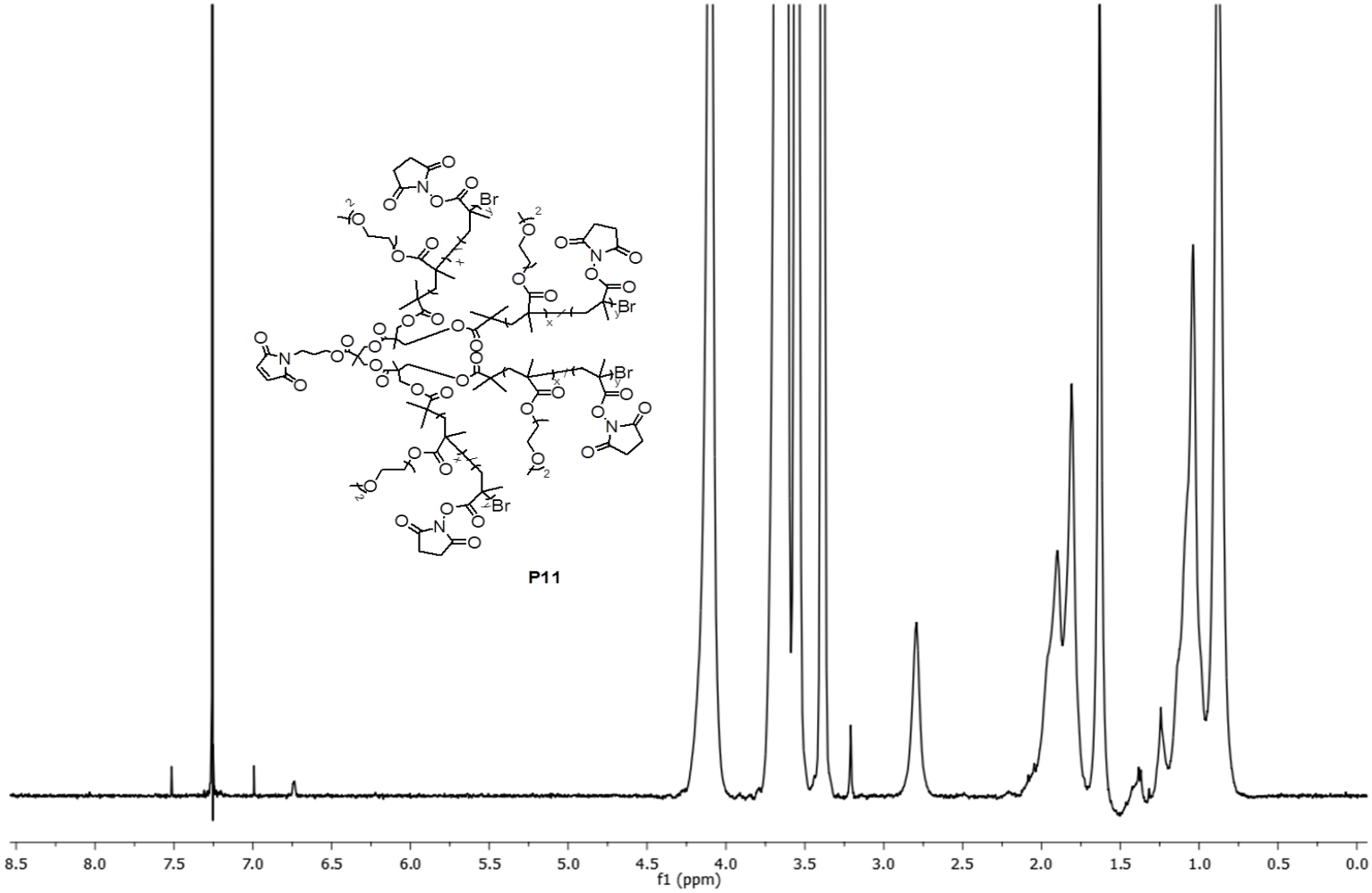

Figure 6A. 12. ^{1}H NMR spectrum of activated G2M-(DEGMEMA-*co*-NHSMA) (P11) in $CDCl_3$

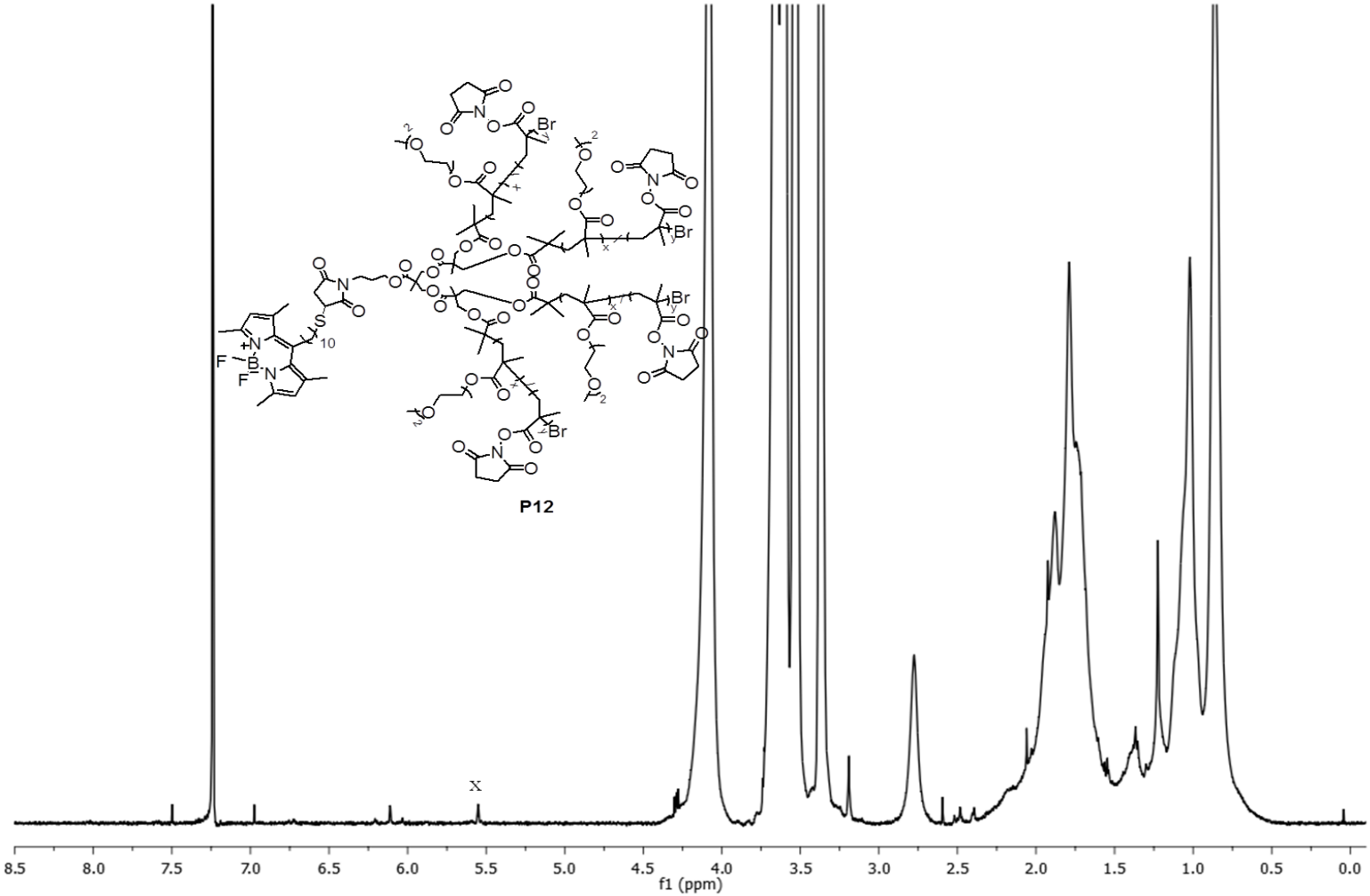

Figure 6A. 13. ^{1}H NMR spectrum of Bodipy10CS-G2M-(DEGMEMA-*co*-NHSMA) (P12) in $CDCl_3$

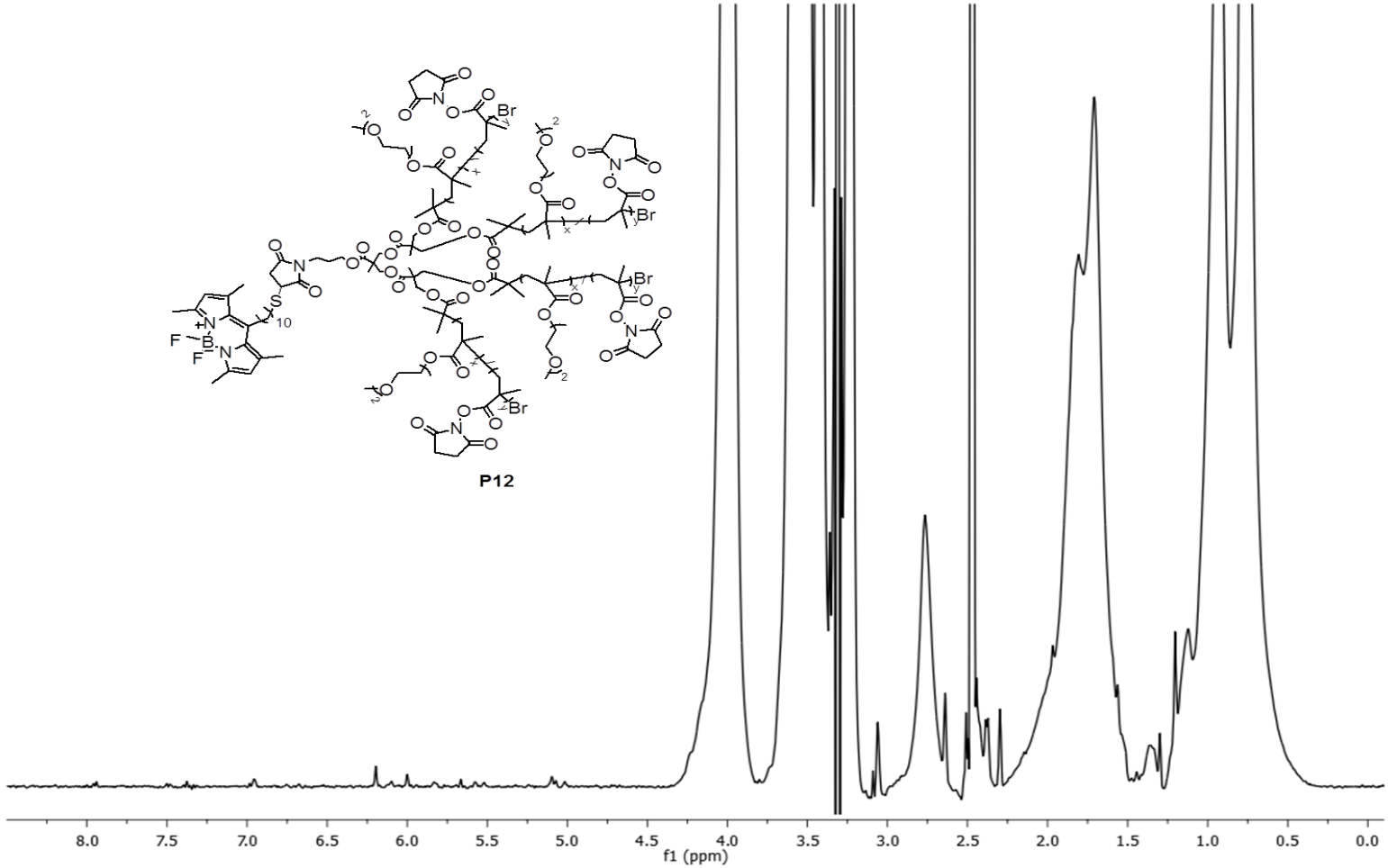

Figure 6A. 14. ^{1}H NMR spectrum of Bodipy10CS-G2M-(DEGMEMA-*co*-NHSMA) (P12) in DMSO

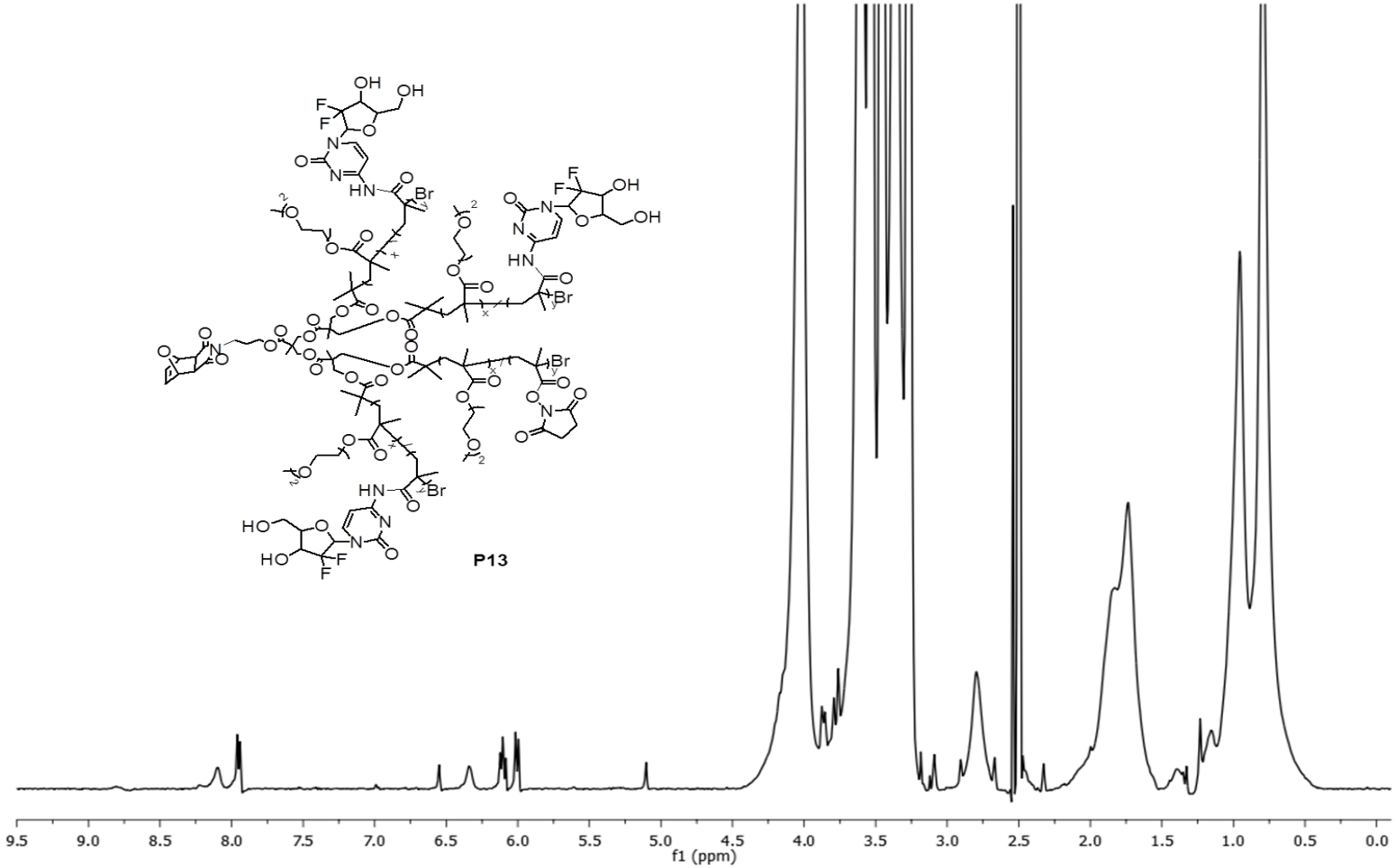

Figure 6A. 15. ^{1}H NMR spectrum of GEMC conjugated G2(DEGMEMA-*co*-NHSMA) (P13) in DMSO

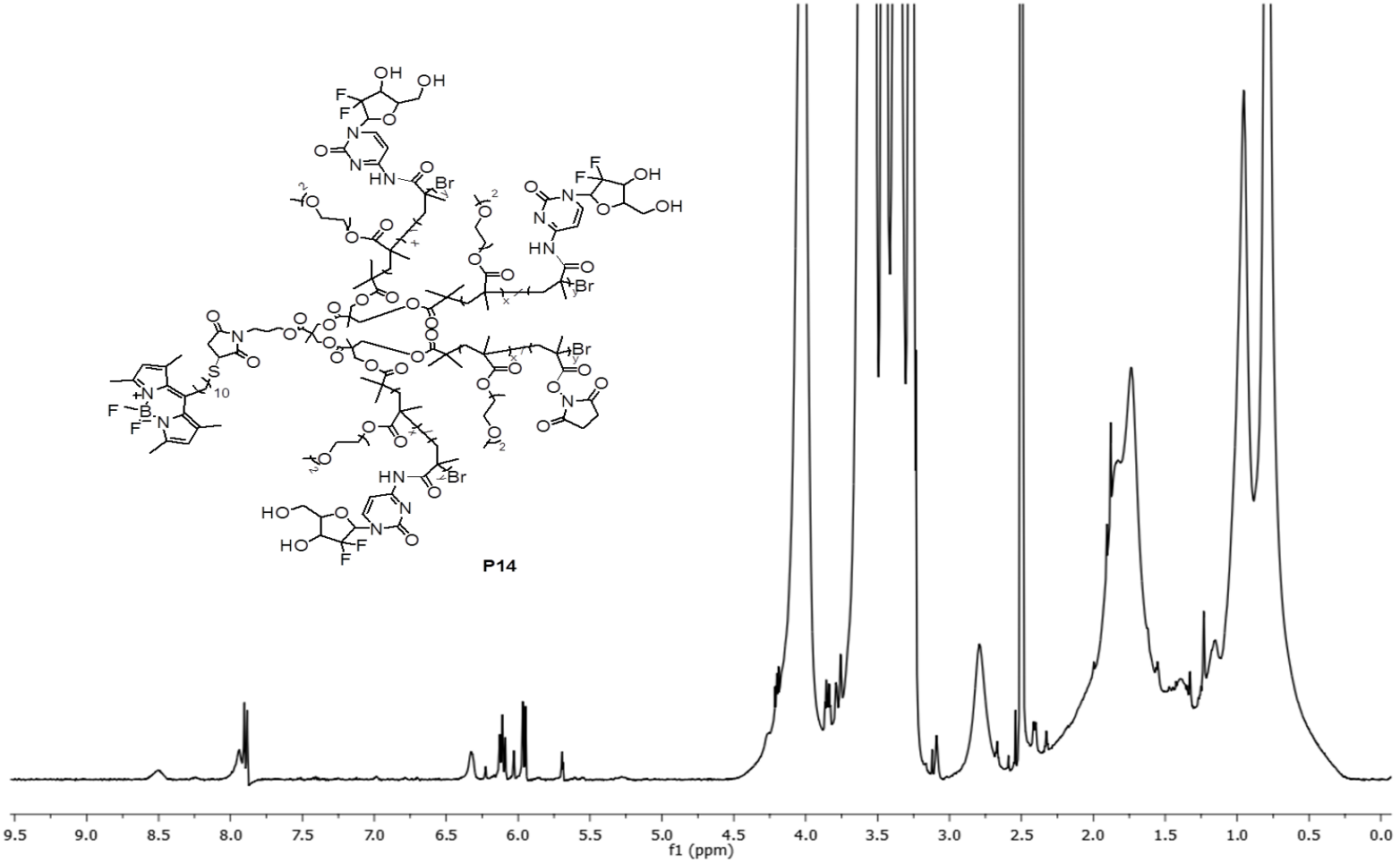

Figure 6A. 16. ^{1}H NMR spectrum of Bodipy10CSH and GEMC conjugated G2M-(DEGMEMA-*co*-NHSMA) (P14) in DMSO

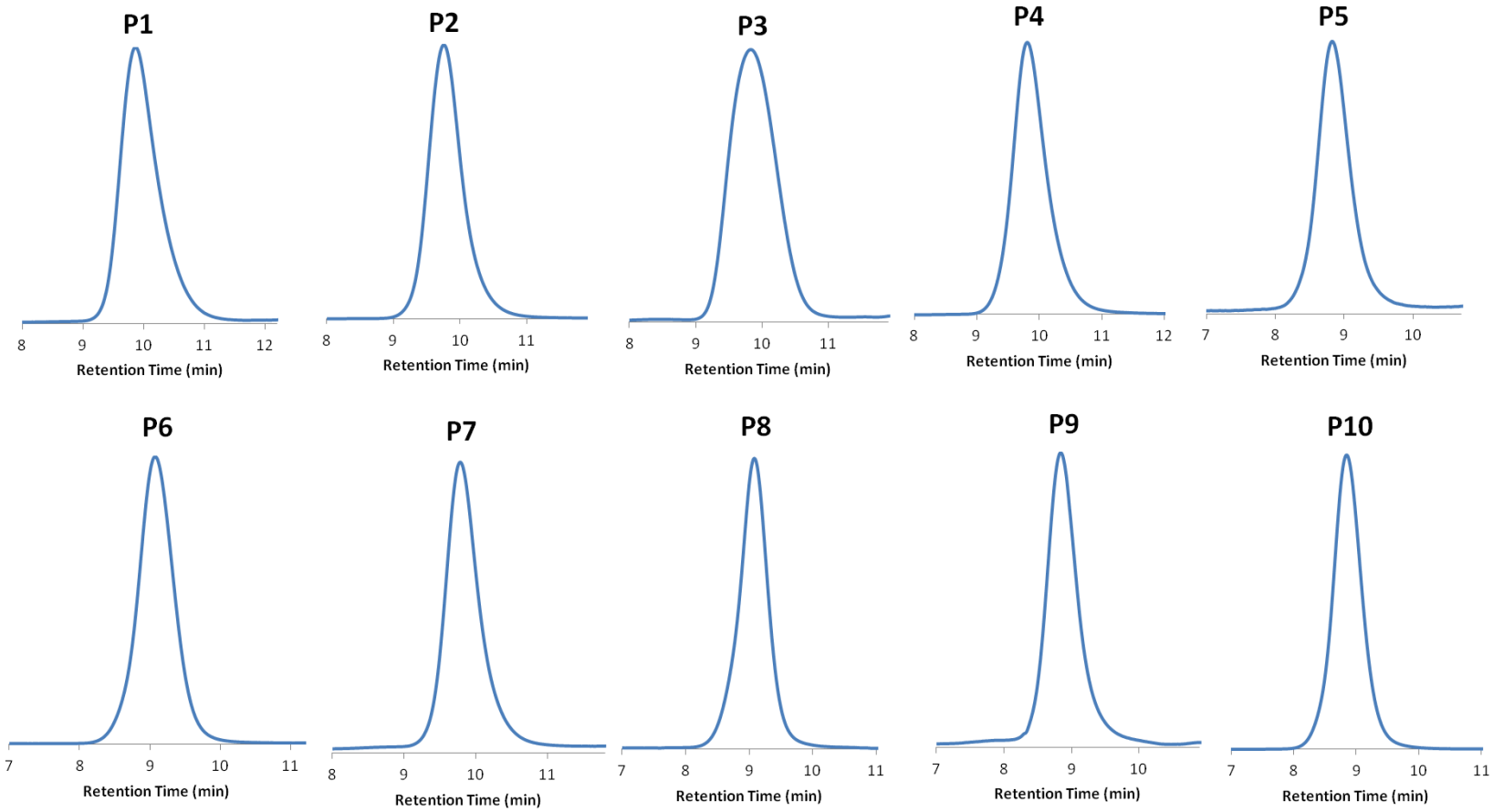

Figure 6A. 17. GPC traces of copolymers P1-10 in THF

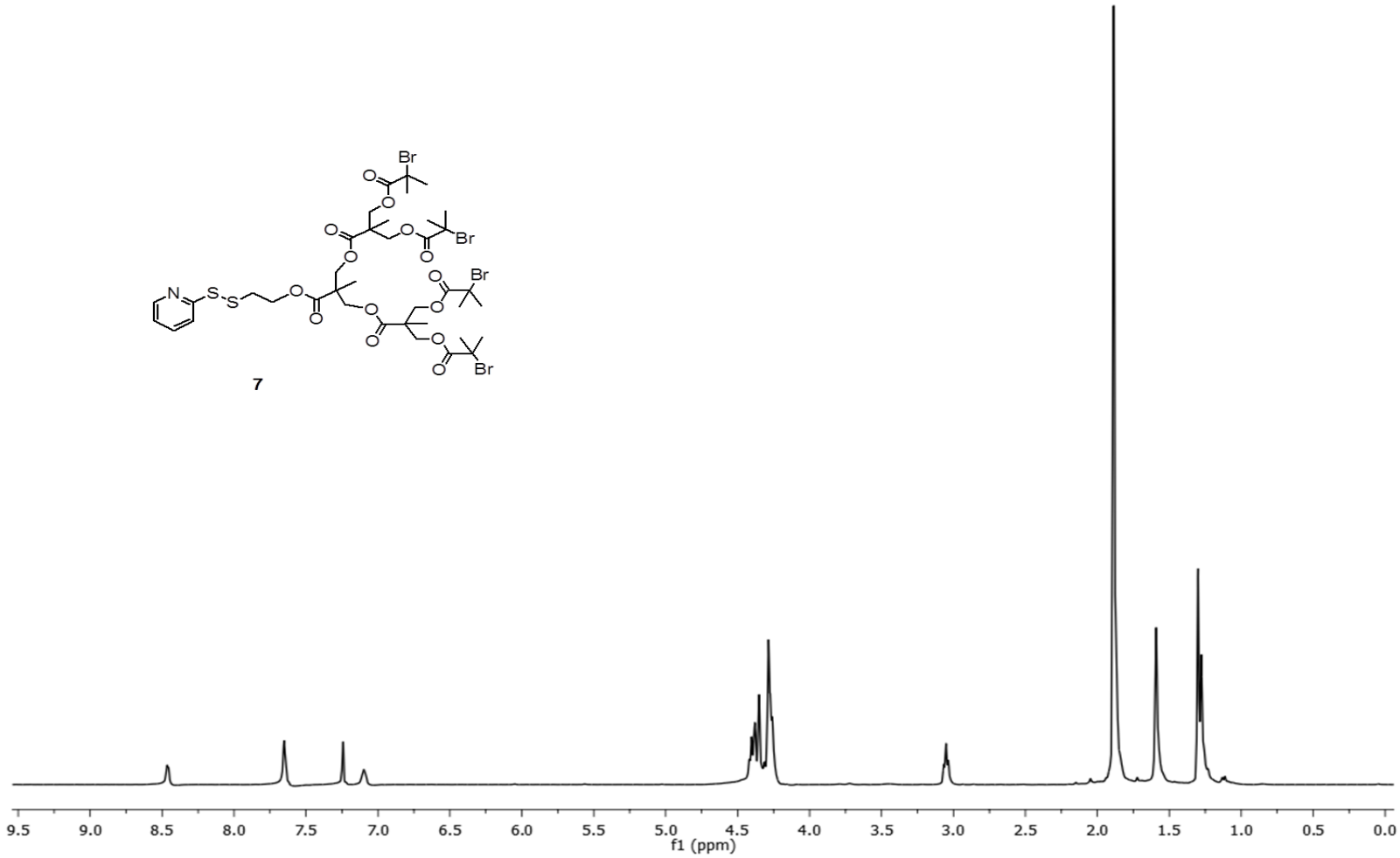

Figure 7A. 1. ^{1}H NMR spectrum of G2PDS initiator (7) in $CDCl_3$

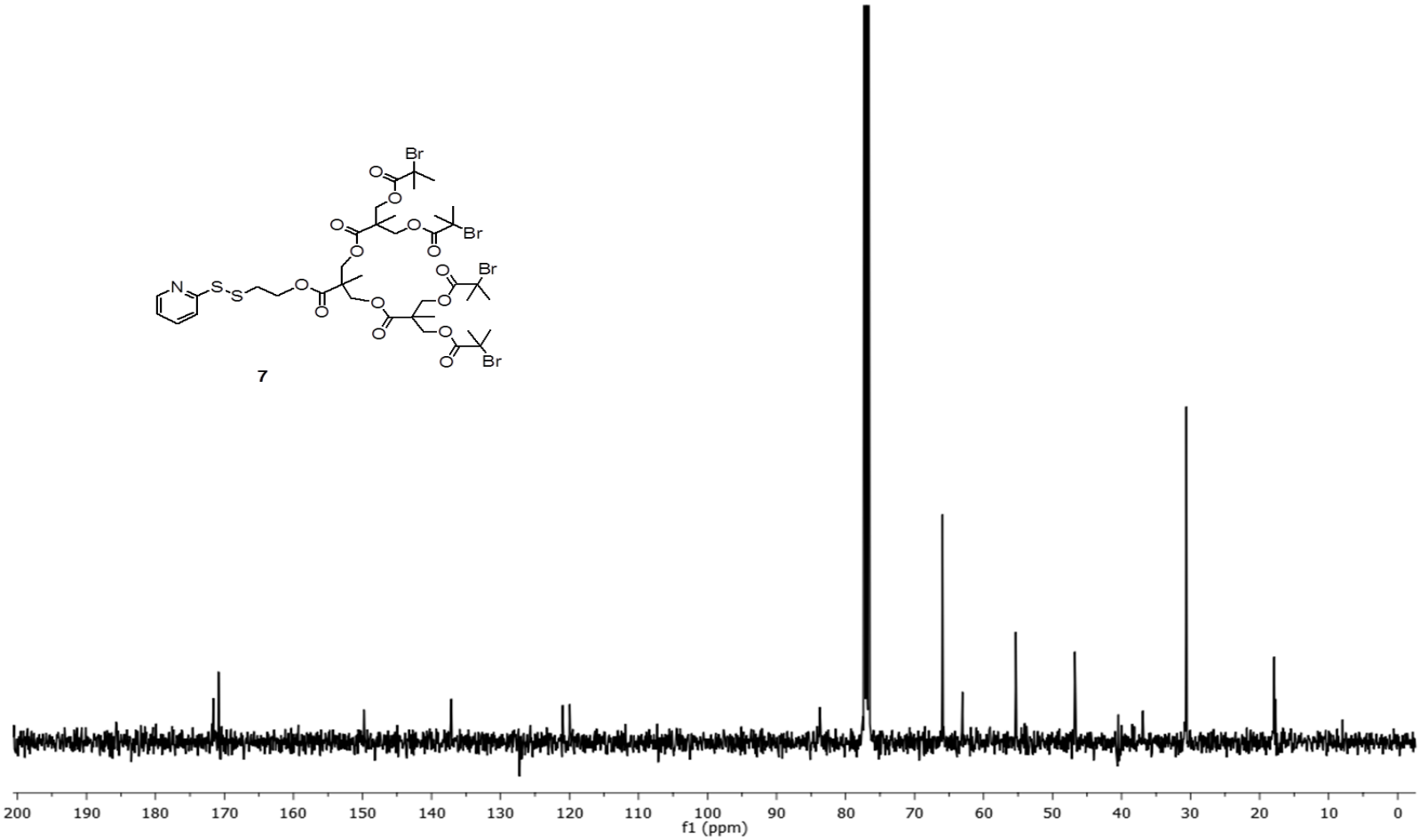

Figure 7A. 2. ^{13}C NMR spectrum of G2PDS initiator (7) in $CDCl_3$

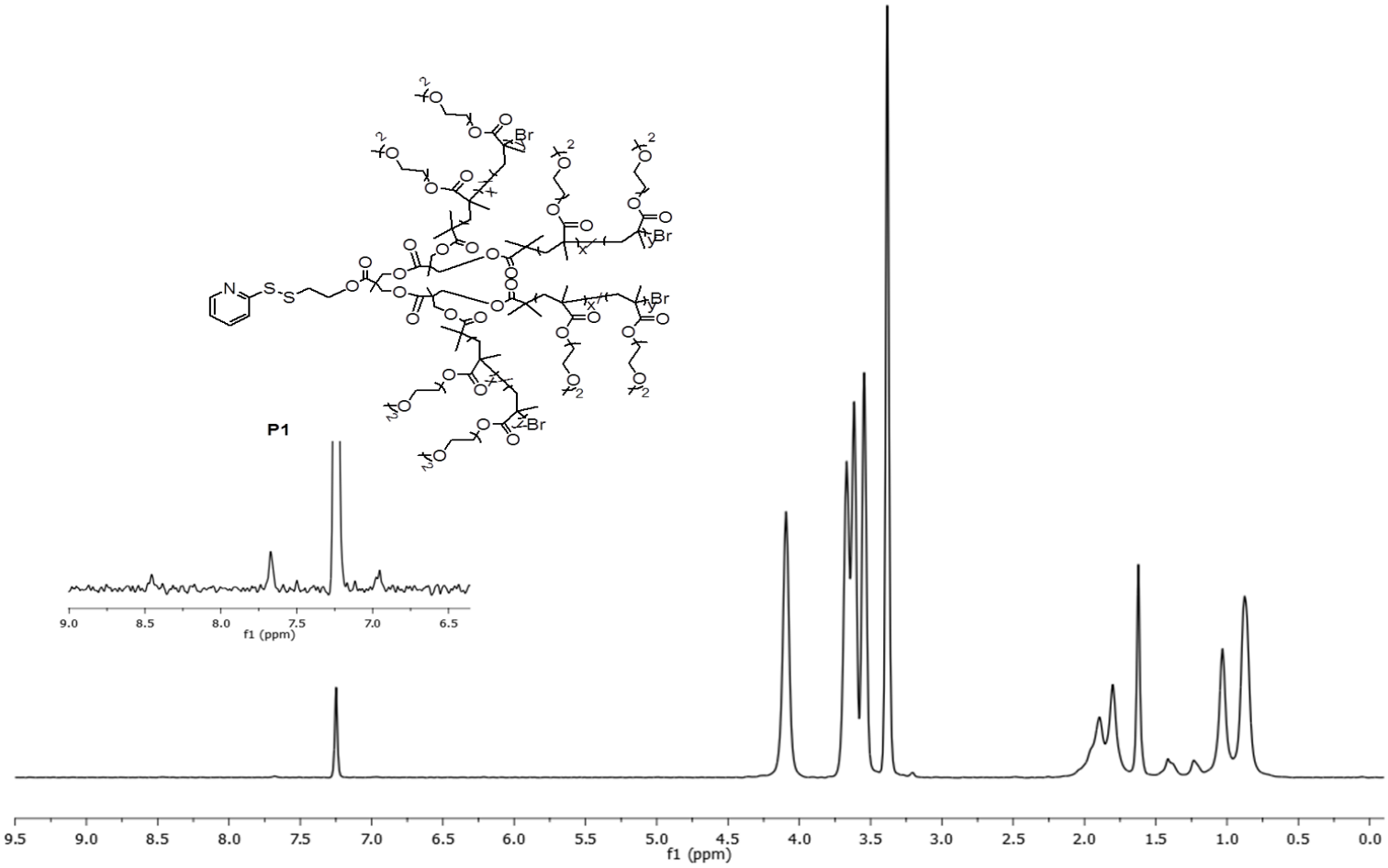

Figure 7A. 3. ^{1}H NMR spectrum of G2PDS-DEGMEMA (P1) in $CDCl_3$

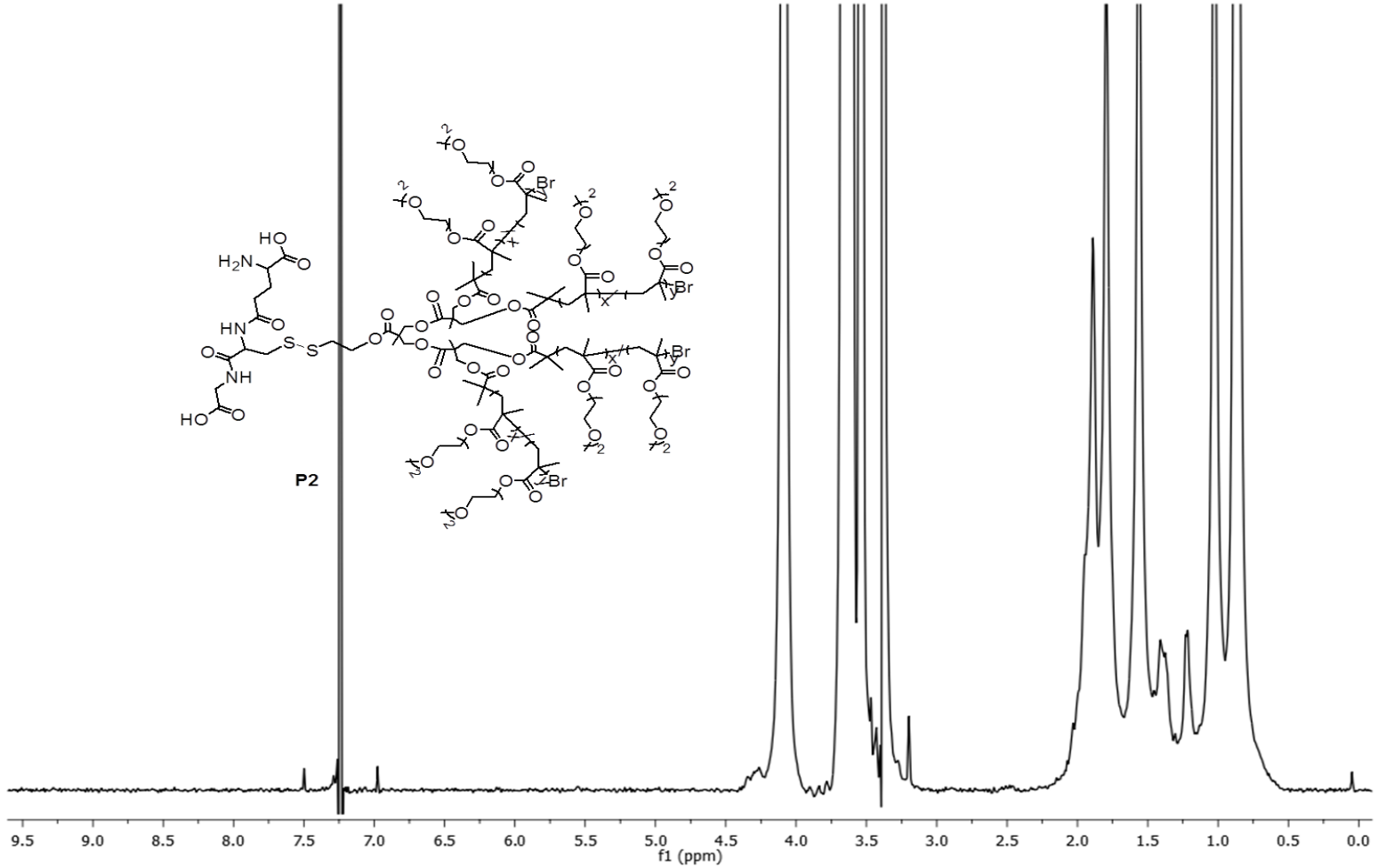

Figure 7A. 4. ^{1}H NMR spectrum of Glutathione-G2-DEGMEMA (P2) in $CDCl_3$

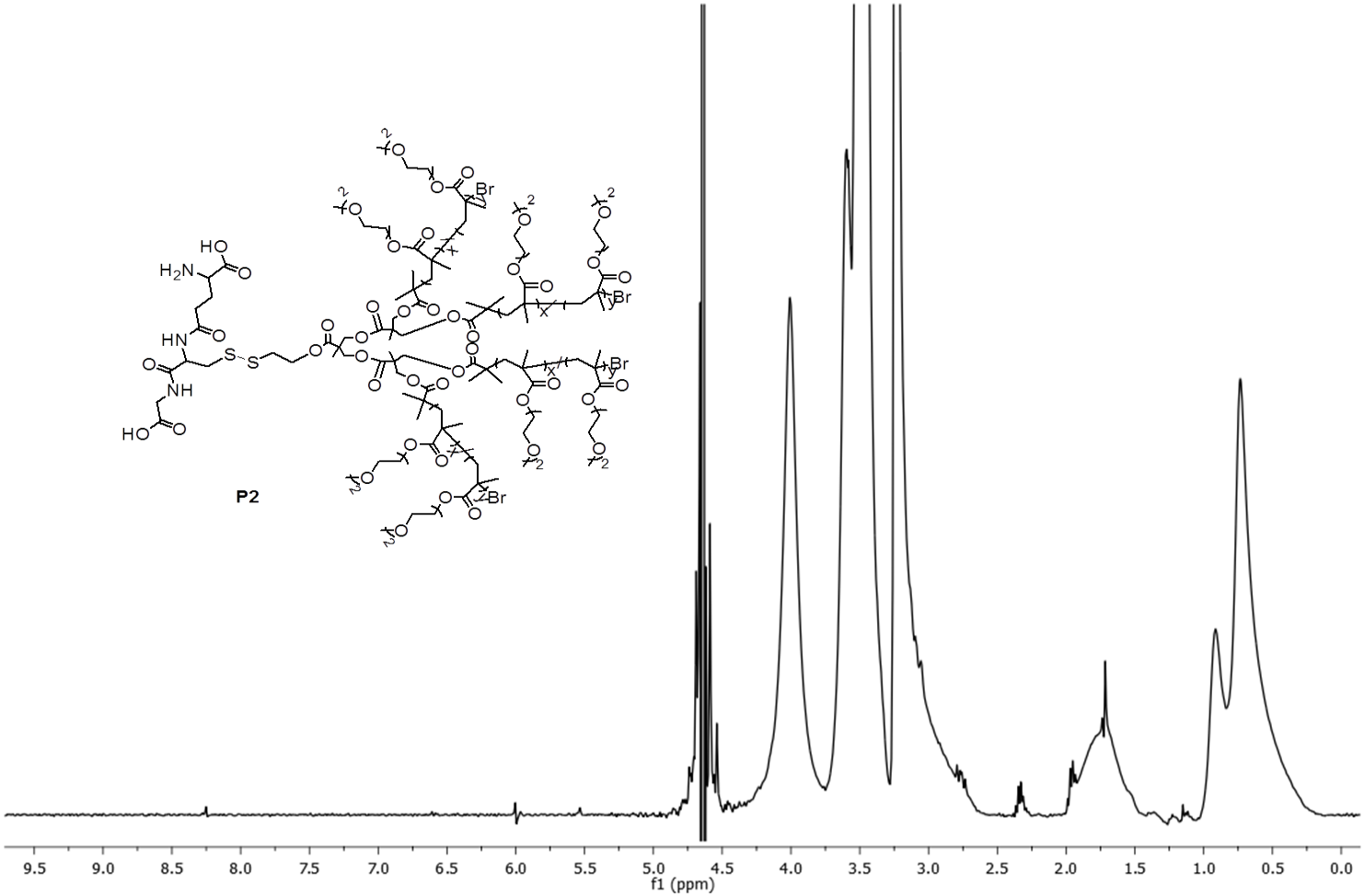

Figure 7A. 5. ^{1}H NMR spectrum of Glutathione-G2-DEGMEMA (P2) in DMSO

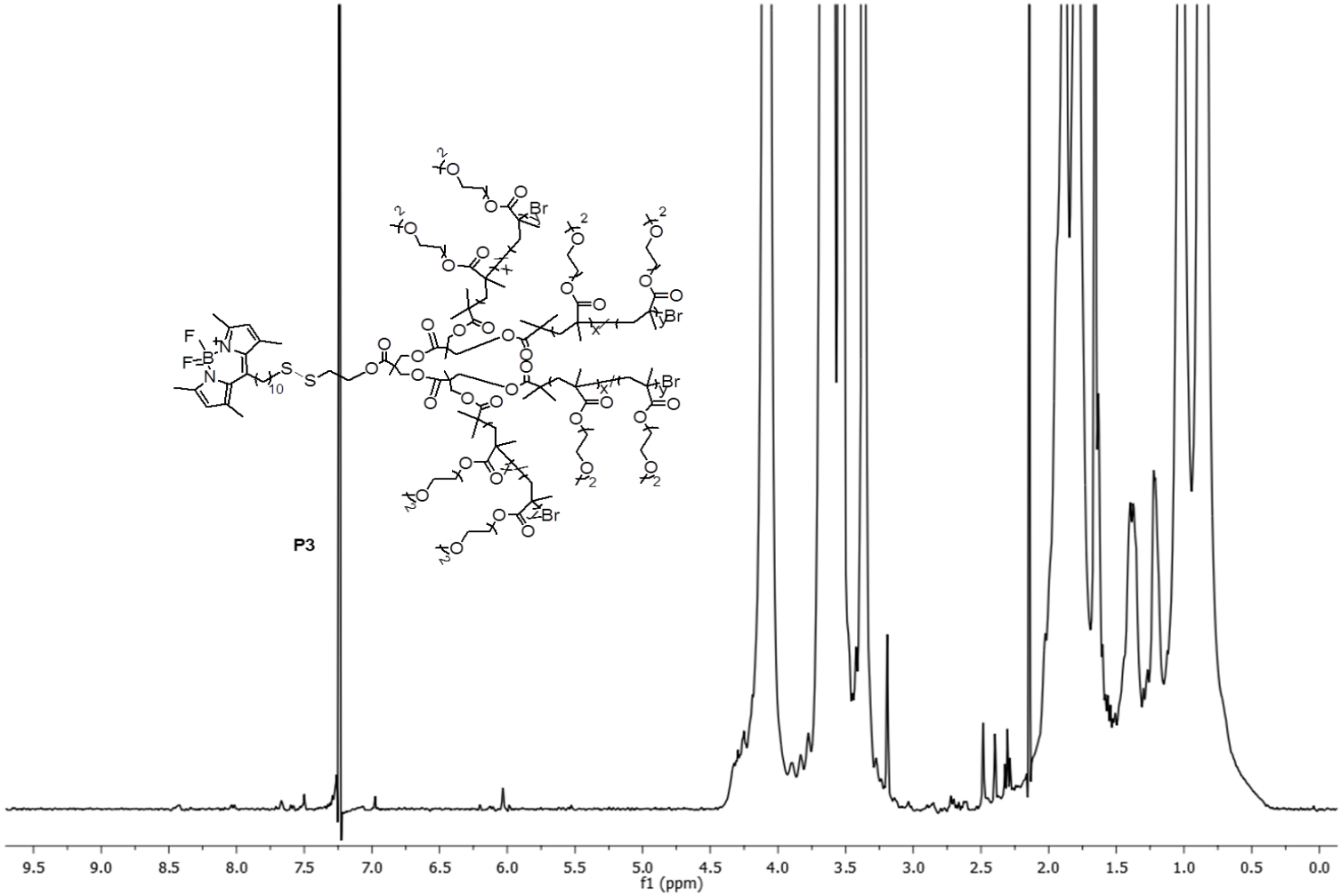

Figure 7A. 6. ^{1}H NMR spectrum of BodipyC10S-G2-DEGMEMA (P3) in $CDCl_3$

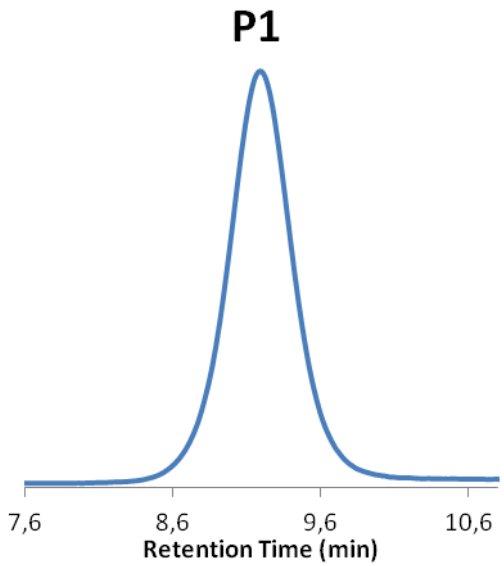

Figure 7A. 7. GPC trace of polymer P1 in THF

REFERENCES

1. Siegel, R., J. Ma, Z. Zou, and A. Jemal, "Cancer statistics, 2014", *CA: A Cancer Journal for Clinicians.*, Vol. 64, pp. 9–29, 2014.

2. Stewart, B. W., and C. P. Wild, "World Cancer Report 2014", 2014.

3. Klaner, P., "Chemotherapy side effects profile", *Lung cancer guide book*, 2005, http://www.lungcancerguidebook.org/lcguidebook_a05/appendix_cxtx_side_effects.pdf, [Accessed August 2013].

4. Verhoef, M. J., R. J. Hilsden, and M. O'Beirne, "Complementary therapies and cancer care: An overview", *Patient Education and Counseling*, Vol. 38. pp. 93–100, 1999.

5. Decker, G. M., "The Marriage of Conventional Cancer Treatments and Alternative Cancer Therapies", *Revista Espanola de Cirugia Ortopedica y Traumatologia*, Vol. 52, pp. 221–241, 2008.

6. Feyer, P., U. R. Kleeberg, M. Steingräber, W. Günther, and M. Behrens, "Frequency of side effects in outpatient cancer care and their influence on patient satisfaction--a prospective survey using the PASQOC questionnaire", *Supportive Care Cancer*, Vol. 16, pp. 567–575, 2008.

7. Partridge, A. H., H. J. Burstein, and E. P. Winer, "Side effects of chemotherapy and combined chemohormonal therapy in women with early-stage breast cancer", *Journal of the National Cancer Institute Monographs*, pp. 135–142, 2001.

8. Low, K. H., K. F. Leong, C. K. Chua, Z. H. Du, and C. M. Cheah, "Characterization of SLS parts for drug delivery devices", *Rapid Prototyping Journal*, Vol. 7, pp. 262-267, 2001.

9. Rathi, R. C., P. Kopeckova, B. Rihova, and J. Kopecek, "Containing Pendant Saccharide Moieties : Synthesis and Bioadhesive Properties", *Journal of Polymer Science: Part A: Polymer Chemistry*, Vol. 29, No. 13, pp. 1895–1902, 1991.

10. Batz, H. G., G. Franzmann, and H. Ringsdorf, "Model reactions for synthesis of pharmacologically active polymers by way of monomeric and polymeric reactive esters", *Angewandte Chemie International Edition English*, Vol. 11, pp. 1103–1104, 1972.

11. Canal, F., J. Sanchis, and M. J. Vicent, "Polymer--drug conjugates as nano-sized medicines", *Current Opinions in Biotechnology*, Vol. 22, No. 6, pp. 894–900, 2011.

12. Larson, N., and H. Ghandehari, "Polymeric conjugates for drug delivery", *Chemistry of Materials*, Vol. 24, No. 5, pp. 840–853, 2012.

13. Lammers, T., and K. Ulbrich, "HPMA copolymers: 30 years of advances", *Advanced Drug Delivery Reviews*, Vol. 62, No. 2, pp. 119–21, 2010.

14. Pasut, G., and F. M. Veronese, "State of the art in PEGylation: The great versatility achieved after forty years of research", *Journal of Controlled Release*, Vol. 161. pp. 461–472, 2012.

15. Torchilin, V., "Multifunctional and stimuli-sensitive pharmaceutical nanocarriers", *European Journal of Pharmaceutics and Biopharmaceutics*, Vol. 71. pp. 431–444, 2009.

16. Leriche, G., L. Chisholm, and A. Wagner, "Cleavable linkers in chemical biology", *Bioorganic Medicinal Chemistry*, Vol. 20, pp. 571–582, 2012.

17. Torchilin, V., "Tumor delivery of macromolecular drugs based on the EPR effect", *Advanced Drug Delivery Reviews*, Vol. 63, No. 3, pp. 131–135, 2011.

18. Maeda, H., "Macromolecular therapeutics in cancer treatment: The EPR effect and beyond", *Journal of Controlled Release*, Vol. 164. pp. 138–144, 2012.

19. Greish, K., "Enhanced permeability and retention (EPR) effect for anticancer nanomedicine drug targeting", *Methods in Molecular Biology*, Vol. 624, pp. 25–37, 2010.

20. Fox, M. E., F. C. Szoka, and J. M. J. Fréchet, "Soluble polymer carriers for the treatment of cancer: the importance of molecular architecture", *Accounts of Chemical Research*, Vol. 42, No. 8, pp. 1141–1151, 2009.

21. Lee, C. C., E. R. Gillies, M. E. Fox, S. J. Guillaudeu, J. M. J. Fréchet, E. E. Dy, and F. C. Szoka, "A single dose of doxorubicin-functionalized bow-tie dendrimer cures mice bearing C-26 colon carcinomas", *Proc. Natl. Acad. Sci. U. S. A.*, Vol. 103, No. 45, pp. 16649–16654, 2006.

22. Gillies, E. R., and J. M. J. Fréchet, "pH-Responsive copolymer assemblies for controlled release of doxorubicin", *Bioconjugate Chemistry*, Vol. 16, No. 2, pp. 361–368, 2005.

23. Lee, C. C., J. MacKay, J. M. J. Fréchet, and F. C. Szoka, "Designing dendrimers for biological applications", *Nature Biotechnology*, Vol. 23, No. 12, pp. 1517–1526, 2005.

24. Aggarwal, S., "Targeted cancer therapies", *Nature Reviews Drug Discovery*, Vol. 9, pp. 427–428, 2010.

25. Zhang, Z., J. Jia, Y. Lai, Y. Ma, J. Weng, and L. Sun, "Conjugating folic acid to gold nanoparticles through glutathione for targeting and detecting cancer cells", *Bioorganic Medicinal Chemisry*, Vol. 18, pp. 5528–5534, 2010.

26. Pike, D. B., and H. Ghandehari, "HPMA copolymer-cyclic RGD conjugates for tumor targeting", *Advanced Drug Delivery Reviews*, Vol. 62. pp. 167–183, 2010.

27. Duncan, R., "The dawning era of polymer therapeutics", *Nature Reviews Drug Discovery*, Vol. 2, pp. 347–360, 2003.

28. Duro-Castano, A., I. Conejos-Sánchez, and M. Vicent, "Peptide-Based Polymer Therapeutics", *Polymers (Basel)*, Vol. 6, No. 2, pp. 515–551, 2014.

29. Dong, S., S. Shang, J. Li, Z. Tan, T. Dean, A. Maeda, T. J. Gardella, and S. J. Danishefsky, "Engineering of therapeutic polypeptides through chemical synthesis:

Early lessons from human parathyroid hormone and analogues", *Journal of American Chemical Society*, Vol. 134, pp. 15122–15129, 2012.

30. Deming, T. J., "Synthetic polypeptides for biomedical applications", *Progress in Polymer Science (Oxford)*, Vol. 32. pp. 858–875, 2007.

31. De Stefano, N., M. Filippi, C. Confavreux, P. Vermersch, M. Simu, C. Sindic, R. Hupperts, O. Bajenaru, G. Edan, L. Grimaldi, I. Marginean, R. Medaer, G. Orefice, I. Pascu, J. Pelletier, E. Sanders, E. Scarpini, and G. L. Mancardi, "The results of two multicenter, open-label studies assessing efficacy, tolerability and safety of protiramer, a high molecular weight synthetic copolymeric mixture, in patients with relapsing-remitting multiple sclerosis", *Multiple Sclerosis*, Vol. 00, pp. 1-6, 2008.

32. Tsareva, E. I., O. G. Kulakova, O. I. Makarycheva, A. N. Boĭko, S. G. Shchur, N. I. Lashch, N. F. Popova, E. I. Gusev, V. V Bashinskaia, D. V L'vov, A. V Favorov, M. F. Ochs, and O. O. Favorova, "Pharmacogenomics of multiple sclerosis: association of immune response genes polymorphism with copaxone treatment efficacy", *Molecular Biology (Mosk).*, Vol. 45, pp. 963–972, 2011.

33. Moscicki, A.-B., R. Kaul, Y. Ma, M. E. Scott, I. I. Daud, E. A. Bukusi, S. Shiboski, A. Rebbapragada, S. Huibner, and C. R. Cohen, "Measurement of Mucosal Biomarkers in a Phase 1 Trial of Intravaginal 3% StarPharma LTD 7013 Gel (VivaGel) to Assess Expanded Safety", *JAIDS Journal of Acquired Immune Deficiency Syndromes*, Vol. 59. pp. 134–140, 2012.

34. Tros, I., C., Y. Sun, and N. Düzgüneş, "Gene delivery by lipoplexes and polyplexes", *European Journal of Pharmaceutical Sciences*, Vol. 40. pp. 159–170, 2010.

35. Dai, J., S. Zou, Y. Pei, D. Cheng, H. Ai, and X. Shuai, "Polyethylenimine-grafted copolymer of poly(l-lysine) and poly(ethylene glycol) for gene delivery", *Biomaterials*, Vol. 32, pp. 1694–1705, 2011.

36. Yamagata, M., T. Kawano, K. Shiba, T. Mori, Y. Katayama, and T. Niidome, "Structural advantage of dendritic poly(l-lysine) for gene delivery into cells", *Bioorganic Medicinal Chemistry*, Vol. 15, pp. 526–532, 2007.

37. Kedar, U., P. Phutane, S. Shidhaye, and V. Kadam, "Advances in polymeric micelles for drug delivery and tumor targeting", *Nanomedicine: Nanotechnology, Biology and Medicine*, Vol. 6. pp. 714–729, 2010.

38. Miyata, K., R. J. Christie, and K. Kataoka, "Polymeric micelles for nano-scale drug delivery", *Reactive and Functional Polymers*, Vol. 71, pp. 227–234, 2011.

39. Wu, H., H. Cabral, K. Toh, P. Mi, Y. C. Chen, Y. Matsumoto, N. Yamada, X. Liu, H. Kinoh, Y. Miura, M. R. Kano, H. Nishihara, N. Nishiyama, and K. Kataoka, "Polymeric micelles loaded with platinum anticancer drugs target preangiogenic micrometastatic niches associated with inflammation", *Journal of Controlled Release*, Vol. 189, pp. 1–10, 2014.

40. Oe, Y., R. J. Christie, M. Naito, S. A. Low, S. Fukushima, K. Toh, Y. Miura, Y. Matsumoto, N. Nishiyama, K. Miyata, and K. Kataoka, "Actively-targeted polyion complex micelles stabilized by cholesterol and disulfide cross-linking for systemic delivery of siRNA to solid tumors", *Biomaterials*, Vol. 35, pp. 7887–7895, 2014.

41. Matsumura, Y., "Preclinical and clinical studies of NK012, an SN-38-incorporating polymeric micelles, which is designed based on EPR effect", *Advanced Drug Delivery Reviews*, Vol. 63, No. 3, pp. 184–92, 2011.

42. Vilar, G., J. Tulla-Puche, and F. Albericio, "Polymers and drug delivery systems", *Current Drug Delivery*, Vol. 9, pp. 367–94, 2012.

43. Nowotnik, D. P., and E. Cvitkovic, "ProLindac (AP5346): a review of the development of an HPMA DACH platinum Polymer Therapeutic", *Advanced Drug Delivery Reviews*, Vol. 61, No. 13, pp. 1214–9, 2009.

44. Zhou, Y., J. Yang, and J. Kopeček, "Selective inhibitory effect of HPMA copolymer-cyclopamine conjugate on prostate cancer stem cells", *Biomaterials*, Vol. 33, No. 6, pp. 1863–72, 2012.

45. Duncan, R., and M. J. Vicent, "Do HPMA copolymer conjugates have a future as clinically useful nanomedicines? A critical overview of current status and future opportunities", *Advanced Drug Delivery Reviews*, Vol. 62, pp. 272–282, 2010.

46. Greish, K., A. Ray, H. Bauer, N. Larson, A. Malugin, D. Pike, M. Haider, and H. Ghandehari, "Anticancer and antiangiogenic activity of HPMA copolymer-aminohexylgeldanamycin-RGDfK conjugates for prostate cancer therapy", *Journal of Controlled Release*, Vol. 151, No. 3, pp. 263–70, 2011.

47. Duncan, R., "Polymer therapeutics as nanomedicines: New perspectives", *Current Opinion in Biotechnology*, Vol. 22. pp. 492–501, 2011.

48. Chipman, S. D., F. B. Oldham, G. Pezzoni, and J. W. Singer, "Biological and clinical characterization of paclitaxel poliglumex (PPX, CT-2103), a macromolecular polymer-drug conjugate", *International Journal of. Nanomedicine*, Vol. 1, No. 4, pp. 375–83, 2006.

49. Harris, J. M., and R. B. Chess, "Effect of pegylation on pharmaceuticals", *Nature Reviews Drug Discovery*, Vol. 2, pp. 214–221, 2003.

50. Zhu, S., M. Hong, G. Tang, L. Qian, J. Lin, Y. Jiang, and Y. Pei, "Partly PEGylated polyamidoamine dendrimer for tumor-selective targeting of doxorubicin: the effects of PEGylation degree and drug conjugation style", *Biomaterials*, Vol. 31, No. 6, pp. 1360–71, 2010.

51. Sapra, P., H. Zhao, M. Mehlig, J. Malaby, P. Kraft, C. Longley, L. M. Greenberger, and I. D. Horak, "Novel delivery of SN38 markedly inhibits tumor growth in xenografts, including a camptothecin-11-refractory model", *Clinical Cancer Research*, Vol. 14, No. 6, pp. 1888–96, 2008.

52. Duncan, R., "Polymer conjugates as anticancer nanomedicines", *Nature Reviews Cancer*, Vol. 6, pp. 688–701, 2006.

53. Lammers, T., V. Subr, K. Ulbrich, P. Peschke, P. E. Huber, W. E. Hennink, and G. Storm, "Simultaneous delivery of doxorubicin and gemcitabine to tumors in vivo using prototypic polymeric drug carriers", *Biomaterials*, Vol. 30, No. 20, pp. 3466–75, 2009.

54. Gauthier, M. A., and H.-A. Klok, "Peptide/protein-polymer conjugates: synthetic strategies and design concepts", *Chemical Commununications (Camb).*, pp. 2591–2611, 2008.

55. Tao, L., J. Liu, and T. P. Davis, "Branched polymer-protein conjugates made from mid-chain-functional P(HPMA)", *Biomacromolecules*, Vol. 10, No. 10, pp. 2847–51, 2009.

56. Tao, L., J. Liu, J. Xu, and T. P. Davis, "Synthesis and bioactivity of poly(HPMA)-lysozyme conjugates: the use of novel thiazolidine-2-thione coupling chemistry", *Organic&Biomolecular Chemistry*, Vol. 7, No. 17, pp. 3481–5, 2009.

57. Jevševar, S., M. Kunstelj, and V. G. Porekar, "PEGylation of therapeutic proteins", *Biotechnology Journal*, Vol. 5, pp. 113–128, 2010.

58. Bontempo, D., K. L. Heredia, B. A. Fish, and H. D. Maynard, "Cysteine-reactive polymers synthesized by atom transfer radical polymerization for conjugation to proteins", *Journal of Polymer Science: Part A: Polymer Chemistry*, Vol. 126, No. 47, pp. 15372-15373, 2004.

59. Zhao, H., K. Yang, A. Martinez, A. Basu, R. Chintala, H. C. Liu, A. Janjua, M. Wang, and D. Filpula, "Linear and branched bicin linkers for releasable PEGylation of macromolecules: Controlled release in vivo and in vitro from mono- and multi-PEGylated proteins", *Bioconjugate Chemistry*, Vol. 17, pp. 341–351, 2006.

60. Averick, S., A. Simakova, S. Park, D. Konkolewicz, A. J. D. Magenau, R. A. Mehl, and K. Matyjaszewski, "ATRP under Biologically Relevant Conditions: Grafting from a Protein", *ACS Macro Letters*, Vol. 1, No. 1, pp. 6–10, 2012.

61. Averick, S. E., C. G. Bazewicz, B. F. Woodman, A. Simakova, R. A. Mehl, and K. Matyjaszewski, "Protein-polymer hybrids: Conducting ARGET ATRP from a genetically encoded cleavable ATRP initiator", *European Polymer Journal*, Vol. 49, pp. 2919–2924, 2013.

62. Liu, J., V. Bulmus, D. L. Herlambang, C. Barner-Kowollik, M. H. Stenzel, and T. P. Davis, "In situ formation of protein-polymer conjugates through reversible addition fragmentation chain transfer polymerization", *Angewandte Chemie International Edition English*, Vol. 46, No. 17, pp. 3099–103, 2007.

63. Boyer, C., J. Liu, L. Wong, M. Tippett, V. Bulmus, and T. P. Davis, "Stability and Utility of Pyridyl Disulfide Functionality in RAFT and Conventional Radical Polymerizations", *Journal of Polymer Science: Part A: Polymer Chemistry*, Vol. 46, No. 21, pp. 7207–7224, 2008.

64. Liu, J., H. Liu, V. Bulmus, L. Tao, C. Boyer, and T. P. Davis, "A simple methodology for the synthesis of heterotelechelic protein-polymer-biomolecule conjugates", *Journal of Polymer Science: Part A: Polymer Chemistry*, Vol. 48, pp. 1399–1405, 2010.

65. Yang, B., Y. Zhao, S. Wang, Y. Zhang, C. Fu, Y. Wei, and L. Tao, "Synthesis of Multifunctional Polymers through the Ugi Reaction for Protein Conjugation", *Macromolecules*, Vol. 47, No. 16, pp. 5607–5612, 2014.

66. Boyer, C., J. Liu, V. Bulmus, T. P. Davis, C. Barner-Kowollik, and M. H. Stenzel, "Direct Synthesis of Well-Defined Heterotelechelic Polymers for Bioconjugations", *Macromolecules*, Vol. 41, No. 15, pp. 5641–5650, 2008.

67. González-Toro, D. C., and S. Thayumanavan, "Advances in polymer and polymeric nanostructures for protein conjugation", *Eurepean Polymer Journal*, Vol. 49, pp. 2906–2918, 2013.

68. Marcellin, P., T.-T. Chang, S. G. Lim, M. J. Tong, W. Sievert, M. L. Shiffman, L. Jeffers, Z. Goodman, M. S. Wulfsohn, S. Xiong, J. Fry, and C. L. Brosgart, "Adefovir dipivoxil for the treatment of hepatitis B e antigen-positive chronic hepatitis B", *The New England Journal of Medicine*, Vol. 348, pp. 808-816, 2003.

69. Bailon, P., A. Palleroni, C. A. Schaffer, C. L. Spence, W.-J. Fung, J. E. Porter, G. K. Ehrlich, W. Pan, Z.-X. Xu, M. W. Modi, A. Farid, and W. Berthold, "Rational Design of a Potent, Long-Lasting Form of Interferon: A 40 kDa Brached Polythylene Glycol-Conjugated Interferon a-2a for the Treatment of Hepatitis C", *Bioconjugate Chemistry*, Vol. 12, pp. 195–202, 2001.

70. Duncan, R., and M. J. Vicent, "Polymer therapeutics-prospects for 21st century: the end of the beginning", *Advanced Drug Delivery Reviews*, Vol. 65, No. 1, pp. 60–70, 2013.

71. Wang, J., and K. Matyjaszewski, "Controlled/“living” radical polymerization. atom transfer radical polymerization in the presence of transition-metal complexes", *Journal of Polymer Science: Part A: Polymer Chemistry*, Vol. 117, pp. 5614–5615, 1995.

72. Matyjaszewski, K., "Atom Transfer Radical Polymerization (ATRP): Current status and future perspectives", *Macromolecules*, Vol. 45, pp. 4015–4039, 2012.

73. Von Natzmer, P., D. Bontempo, and N. Tirelli, "Supported ATRP and giant polymers", *Chemical Communications*, p. 1600, 2003.

74. Matyjaszewski, K., and J. Xia, "Atom Transfer Radical Polymerization", *Chemical Reviews*, Vol. 101, pp. 2921–2990, 2001.

75. Grubbs, R. B., "Nitroxide-Mediated Radical Polymerization: Limitations and Versatility", *Polymer Reviews*, Vol. 51. pp. 104–137, 2011.

76. Nicolas, J., Y. Guillaneuf, D. Bertin, D. Gigmes, and B. Charleux, "Nitroxide-Mediated Polymerization", *Polymer Science: A Comprehensive Reference*, Vol. 3, pp. 277–350, 2012.

77. Tang, W., T. Fukuda, and K. Matyjaszewski, "Reevaluation of persistent radical effect in NMP", *Macromolecules*, Vol. 39, pp. 4332–4337, 2006.

78. Tomoeda, S., Y. Kitayama, J. Wakamatsu, H. Minami, P. B. Zetterlund, and M. Okubo, "Nitroxide-mediated radical polymerization in microemulsion (microemulsion NMP) of n -butyl acrylate", *Macromolecules*, Vol. 44, pp. 5599–5604, 2011.

79. Badi, N., and J.-F. Lutz, "Sequence control in polymer synthesis", *Chemical Society Reviews*, Vol. 38, pp. 3383–3390, 2009.

80. Glatzel, S., N. Badi, M. Päch, A. Laschewsky, and J.-F. Lutz, "Well-defined synthetic polymers with a protein-like gelation behavior in water", *Chemical Communications (Camb).*, Vol. 46, pp. 4517–4519, 2010.

81. Lutz, J.-F., M. Ouchi, D. R. Liu, and M. Sawamoto, "Sequence-controlled polymers", *Science*, Vol. 341, p. 1238149, 2013.

82. Tomalia, D. A., H. Baker, J. Dewald, M. Hall, G. Kallos, S. Martin, J. Roeck, J. Ryder, and P. Smith, "A new class of polymers: Starburst-dendritic macromolecules", *Polymer Journal*, Vol. 17. pp. 117–132, 1985.

83. Generations, F., and F. Groups, "Dendrimers : From Generations and Functional Groups to Functions", *Angewante Chemie International Edition English*, Vol. 33, pp. 2413–2420, 1994.

84. Menjoge, A. R., R. M. Kannan, and D. A. Tomalia, "Dendrimer-based drug and imaging conjugates: design considerations for nanomedical applications", *Drug Discovery Today*, Vol. 15. pp. 171–185, 2010.

85. Tomalia, D. A., "Birth of a new macromolecular architecture: Dendrimers as quantized building blocks for nanoscale synthetic polymer chemistry", *Progress in Polymer Science (Oxford)*, Vol. 30. pp. 294–324, 2005.

86. Svenson, S., "Dendrimers as versatile platform in drug delivery applications", *European Journal of Pharmaceutics and Biopharmaceutics*, Vol. 71. pp. 445–462, 2009.

87. Kofoed, J., and J. L. Reymond, "Dendrimers as artificial enzymes", *Current Opinion in Chemical Biology*, Vol. 9. pp. 656–664, 2005.

88. Amis, E., R. C. Hedden, B. J. Bauer, A. P. Smith, and F. Gro, "Templating of inorganic nanoparticles by PAMAM / PEG dendrimer – star polymers", *Polymer*, Vol. 43, pp. 5473–5481, 2002.

89. Balzani, V., P. Ceroni, M. Maestri, and V. Vicinelli, "Light-harvesting dendrimers", *Current Opinion in Chemical Biology*, Vol. 7. pp. 657–665, 2003.

90. Bhatnagar, P., S. S. Mark, I. Kim, H. Chen, B. Schmidt, M. Lipson, and C. a. Batt, "Dendrimer-Scaffold-Based Electron-Beam Patterning of Biomolecules", *Advanced Materials*, Vol. 18, No. 3, pp. 315–319, 2006.

91. Söntjens, S. H. M., D. L. Nettles, M. A. Carnahan, L. A. Setton, and M. W. Grinstaff, "Biodendrimer-based hydrogel scaffolds for cartilage tissue repair", *Biomacromolecules*, Vol. 7, pp. 310–316, 2006.

92. Grayson, S. M., and J. M. J. Fréchet, "Convergent dendrons and dendrimers: From synthesis to applications", *Chemical Reviews*, Vol. 101. pp. 3819–3867, 2001.

93. Newkome, G. R., and C. D. Shreiner, "Poly(amidoamine), polypropylenimine, and related dendrimers and dendrons possessing different branching motifs: An overview of the divergent procedures", *Polymer*, Vol. 49. pp. 1–173, 2008.

94. Hadjichristidis, N., M. Pitsikalis, and H. Iatrou, "Synthesis of block copolymers", *Advances in Polymer Science*, Vol. 189. pp. 1–124, 2005.

95. Jean, M., "Unusual Macromolecula Architectures: The Convergent Growth Approach to Dendritic Polyesters and Novel Block Copolymers", *Journal of Polymer Science: Part A: Polymer Chemistry*, Vol. 3, No. 9, pp. 8405–8413, 1992.

96. Iha, R. K., K. L. Wooley, A. M. Nyström, D. J. Burke, M. J. Kade, and C. J. Hawker, "Applications of orthogonal "click" chemistries in the synthesis of functional soft materials", *Chemical Reviews*, Vol. 109, No. 11, pp. 5620–86, 2009.

97. Aoi, K., K. Itoh, and M. Okada, "Divergent/Convergent Joint Approach with a Half-Protected Initiator Core to Synthesize Surface-Block Dendrimers", *Macromolecules*, Vol. 30, No. 25, pp. 8072–8074, 1997.

98. Kose, M. M., G. Yesilbag, and A. Sanyal, "Segment block dendrimers via diels-alder cycloaddition", *Organic Letters*, Vol. 10, pp. 2353–2356, 2008.

99. Borman, S., "Multivalency: Strength in Numbers", *Chemical& Engineering News*, Vol. 78, pp. 48–53, 2000.

100. Hong, S., P. R. Leroueil, I. J. Majoros, B. G. Orr, J. R. Baker, and M. M. Banaszak Holl, "The binding avidity of a nanoparticle-based multivalent targeted drug delivery platform", *Chemical Biology*, Vol. 14, No. 1, pp. 107–15, 2007.

101. Rolland, O., C.-O. Turrin, A.-M. Caminade, and J.-P. Majoral, "Dendrimers and nanomedicine: multivalency in action", *New Journal of Chemistry*, Vol. 33. p. 1809, 2009.

102. Gaertner, H. F., F. Cerini, A. Kamath, A. F. Rochat, C. A. Siegrist, L. Menin, and O. Hartley, "Efficient orthogonal bioconjugation of dendrimers for synthesis of bioactive nanoparticles", *Bioconjugate Chemistry*, Vol. 22, pp. 1103–1114, 2011.

103. Goyal, P., K. Yoon, and M. Weck, "Multifunctionalization of dendrimers through orthogonal transformations", *Chemistry-A European Journal*, Vol. 13, pp. 8801–8810, 2007.

104. Kose, M. M., S. Onbulak, I. I. Yilmaz, and A. Sanyal, "Orthogonally “clickable” biodegradable dendrons", *Macromolecules*, Vol. 44, pp. 2707–2714, 2011.

105. Frauenrath, H., "Dendronized polymers - Building a new bridge from molecules to nanoscopic objects", *Progress in Polymer Science (Oxford)*, Vol. 30. pp. 325–384, 2005.

106. Kröger, M., O. Peleg, and A. Halperin, "From dendrimers to dendronized polymers and forests: Scaling theory and its limitations", *Macromolecules*, Vol. 43, pp. 6213–6224, 2010.

107. Calderón, M., M. Martinelli, P. Froimowicz, A. Leiva, L. Gargallo, D. Radić, and M. C. Strumía, "Synthesis and characterization of dendronized polymers", *Macromolecular Symposia*, Vol. 258, pp. 53–62, 2007.

108. Nyström, A., and A. Hult, "Dendronized polymers with tailored surface groups", *Journal of Polymer Science: Part A: Polymer Chemistry*, Vol. 43, pp. 3852–3867, 2005.

109. Ihre, H., O. L. Padilla De Jesús, and J. M. J. Fréchet, "Fast and convenient divergent synthesis of aliphatic ester dendrimers by anhydride coupling", *Journal of American Chemical Society*, Vol. 123, pp. 5908–5917, 2001.

110. Gok, O., S. Yigit, M. Merve Kose, R. Sanyal, and A. Sanyal, "Dendron-polymer conjugates via the diels-alder “click” reaction of novel anthracene-based dendrons", *Journal of Polymer Science: Part A: Polymer Chemistry*, Vol. 51, pp. 3191–3201, 2013.

111. Daoud, M., and J. P. Cotton, "Star shaped polymers : a model for the conformation and its concentration dependence", *Journal de Physique*, Vol. 43. pp. 531–538, 1982.

112. Hirao, A., M. Hayashi, S. Loykulnant, K. Sugiyama, S. W. Ryu, N. Haraguchi, A. Matsuo, and T. Higashihara, "Precise syntheses of chain-multi-functionalized polymers, star-branched polymers, star-linear block polymers, densely branched

polymers, and dendritic branched polymers based on iterative approach using functionalized 1,1-diphenylethylene derivatives", *Progress in Polymer Science (Oxford)*, Vol. 30. pp. 111–182, 2005.

113. Khanna, K., S. Varshney, and A. Kakkar, "Miktoarm star polymers: advances in synthesis, self-assembly, and applications", *Polymer Chemistry*, Vol. 1. p. 1171, 2010.

114. Miura, Y., A. Narumi, S. Matsuya, T. Satoh, Q. Duan, H. Kaga, and T. Kakuchi, "Synthesis of well-defined AB20-type star polymers with cyclodextrin-core by combination of NMP and ATRP", *Journal of Polymer Science: Part A: Polymer Chemistry*, Vol. 43, pp. 4271–4279, 2005.

115. Cho, H. Y., H. Gao, A. Srinivasan, J. Hong, S. A. Bencherif, D. J. Siegwart, H. J. Paik, J. O. Hollinger, and K. Matyjaszewski, "Rapid cellular internalization of multifunctional star polymers prepared by atom transfer radical polymerization", *Biomacromolecules*, Vol. 11, pp. 2199–2203, 2010.

116. Georgiou, T. K., "Star polymers for gene delivery", *Polymer International*, Vol. 63, No. 7, pp. 1130–1133, 2014.

117. Gok, O., H. Durmaz, E. S. Ozdes, G. Hizal, U. Tunca, and A. Sanyal, "Maleimide-based thiol reactive multiarm star polymers via diels-alder/retro diels-alder strategy", *Journal of Polymer Science: Part A: Polymer Chemistry*, Vol. 48, pp. 2546–2556, 2010.

118. Nicolaou, K. C., S. A. Snyder, T. Montagnon, and G. Vassilikogiannakis, "The Diels--Alder reaction in total synthesis", *Angewante Chemie International Edition English*, Vol. 41, pp. 1668–1698, 2002.

119. Durmaz, H., A. Dag, C. Onen, O. Gok, A. Sanyal, G. Hizal, and U. Tunca, "Multiarm star polymers with peripheral dendritic PMMA arms through Diels-Alder click reaction", *Journal of Polymer Science: Part A: Polymer Chemistry*, Vol. 48, pp. 4842–4846, 2010.

120. Shi, M., J. H. Wosnick, K. Ho, A. Keating, and M. S. Shoichet, "Immuno-Polymeric Nanoparticles by Diels–Alder Chemistry", *Angewante Chemie*, Vol. 119, No. 32, pp. 6238–6243, 2007.

121. Tasdelen, M. A., "Diels–Alder "click" reactions: recent applications in polymer and material science", *Polymer Chemistry*, Vol. 2, p. 2133, 2011.

122. Liu, Y. L., C. Y. Hsieh, and Y. W. Chen, "Thermally reversible cross-linked polyamides and thermo-responsive gels by means of Diels-Alder reaction", *Polymer (Guildf).*, Vol. 47, pp. 2581–2586, 2006.

123. Koehler, K. C., K. S. Anseth, and C. N. Bowman, "Diels-alder mediated controlled release from a poly(ethylene glycol) based hydrogel", *Biomacromolecules*, Vol. 14, pp. 538–547, 2013.

124. Gousse, C., and A. Gandini, "Diels-Alder polymerization of difurans with bismaleimides", *Polymer International*, Vol. 48, pp. 723–731, 1999.

125. Winkler, J. D., "Tandem Diels-Alder cycloadditions in organic synthesis", *Chemistry Reviews*, Vol. 96, pp. 167–176, 1996.

126. Kade, M. J., D. J. Burke, and C. J. Hawker, "The power of thiol-ene chemistry", *Journal of Polymer Science: Part A: Polymer Chemistry*, Vol. 48, pp. 743–750, 2010.

127. Dondoni, A., "The emergence of thiol-ene coupling as a click process for materials and bioorganic chemistry", *Angewandte Chemie - International Edition*, Vol. 47. pp. 8995–8997, 2008.

128. Connal, L. A., C. R. Kinnane, A. N. Zelikin, and F. Caruso, "Stabilization and functionalization of polymer multilayers and capsules via thiol-ene click chemistry", *Chemistry of Materials*, Vol. 21, pp. 576–578, 2009.

129. Killops, K. L., L. M. Campos, and C. J. Hawker, "Robust, efficient, and orthogonal synthesis of dendrimers via thiol-ene “click” chemistry", *Journal of American Chemistry Society*, Vol. 130, pp. 5062–5064, 2008.

130. Chan, J. W., C. E. Hoyle, A. B. Lowe, and M. Bowman, "Nucleophile-initiated thiol-michael reactions: Effect of organocatalyst, thiol, and Ene", *Macromolecules*, Vol. 43, pp. 6381–6388, 2010.

131. Mather, B. D., K. Viswanathan, K. M. Miller, and T. E. Long, "Michael addition reactions in macromolecular design for emerging technologies", *Progress in Polymer Science (Oxford)*, Vol. 31. pp. 487–531, 2006.

132. Arslan, M., T. N. Gevrek, J. Lyskawa, S. Szunerits, R. Boukherroub, R. Sanyal, P. Woisel, and A. Sanyal, "Bioinspired Anchorable Thiol-Reactive Polymers: Synthesis and Applications Toward Surface Functionalization of Magnetic Nanoparticles", *Macromolecules*, Vol. 47, No. 15, pp. 5124–5134, 2014.

133. Billiet, L., O. Gok, A. P. Dove, A. Sanyal, L.-T. T. Nguyen, and F. E. Du Prez, "Metal-Free Functionalization of Linear Polyurethanes by Thiol-Maleimide Coupling Reactions", *Macromolecules*, Vol. 44, No. 20, pp. 7874–7878, 2011.

134. Dispinar, T., R. Sanyal, and A. Sanyal, "A Diels-Alder/retro Diels-Alder strategy to synthesize polymers bearing maleimide side chains", *Journal of Polymer Science: Part A: Polymer Chemistry*, Vol. 45, pp. 4545–4551, 2007.

135. Onbulak, S., S. Tempelaar, R. J. Pounder, O. Gok, R. Sanyal, A. P. Dove, and A. Sanyal, "Synthesis and Functionalization of Thiol-Reactive Biodegradable Polymers", *Macromolecules*, Vol. 2, pp. 1715-1722, 2012.

136. Uysal, B. B., U. S. Gunay, G. Hizal, and U. Tunca, "Orthogonal multifunctionalization of aliphatic polycarbonate via sequential Michael addition and radical-thiol-ene click reactions", *Journal of Polymer Science: Part A: Polymer Chemistry*, Vol. 52, No. 11, pp. 1581–1587, 2014.

137. Yilmaz, I. I., M. Arslan, and A. Sanyal, "Design and synthesis of novel “orthogonally” functionalizable maleimide-based styrenic copolymers", *Macromolecular Rapid Communications*, Vol. 33, pp. 856–862, 2012.

138. Messens, J., and J.-F. Collet, "Thiol-disulfide exchange in signaling: disulfide bonds as a switch", *Antioxidants&Redox Signaling*, Vol. 18, pp. 1594–1596, 2013.

139. Gilbert, H. F., "Thiol/disulfide exchange equilibria and disulfidebond stability", *Methods in Enzymology*, Vol. 251, pp. 8–28, 1995.

140. Boyer, C., A. H. Soeriyadi, P. J. Roth, M. R. Whittaker, and T. P. Davis, "Post-functionalization of ATRP polymers using both thiol/ene and thiol/disulfide exchange chemistry", *Chemical Communications (Camb).*, Vol. 47, pp. 1318–1320, 2011.

141. Vázquez-Dorbatt, V., Z. P. Tolstyka, C. W. Chang, and H. D. Maynard, "Synthesis of a pyridyl disulfide end-functionalized glycopolymer for conjugation to biomolecules and patterning on gold surfaces", *Biomacromolecules*, Vol. 10, pp. 2207–2212, 2009.

142. Liu, J., V. Bulmus, C. Barner-Kowollik, M. H. Stenzel, and T. P. Davis, "Direct synthesis of pyridyl disulfide-terminated polymers by RAFT polymerization", *Macromolecular Rapid Communications*, Vol. 28, pp. 305–314, 2007.

143. Van Der Vlies, A. J., C. P. Oneil, U. Hasegawa, N. Hammond, and J. A. Hubbell, "Synthesis of pyridyl disulfide-functionalized nanoparticles for conjugating thiol-containing small molecules, peptides, and proteins", *Bioconjugate Chemistry*, Vol. 21, pp. 653–662, 2010.

144. Matsumoto, N. M., D. C. Gonzalez-Toro, R. T. Chacko, H. D. Maynard, and S. Thayumanavan, "Synthesis of Nanogel-Protein Conjugates", *Polymer Chemistry*, Vol. 4, pp. 2464–2469, 2013.

145. Deng, X., C. Friedmann, and J. Lahann, "Bio-orthogonal “double-click” chemistry based on multifunctional coatings", *Angewante Chemie International Edition*, Vol. 50, pp. 6522–6526, 2011.

146. Goldmann, A. S., M. Glassner, A. J. Inglis, and C. Barner-Kowollik, "Post-functionalization of polymers via orthogonal ligation chemistry", *Macromolecular Rapid Communications*, Vol. 34. pp. 810–849, 2013.

147. Borchmann, D. E., N. Brummelhuis, and M. Weck, "GRGDS-Functionalized Poly(lactide)- graft -poly(ethylene glycol) Copolymers: Combining Thiol − Ene Chemistry with Staudinger Ligation", *Macromolecules*, Vol. 46, No. 11, pp. 4426-4431, 2013.

148. Beal, D. M., V. E. Albrow, G. Burslem, L. Hitchen, C. Fernandes, C. Lapthorn, L. R. Roberts, M. D. Selby, and L. H. Jones, "Click-enabled heterotrifunctional template for sequential bioconjugations", *Organic & Biomolecular Chemistry*, Vol. 10, p. 548, 2012.

149. Cengiz, N., H. Kabadayioglu, and R. Sanyal, "Orthogonally functionalizable copolymers based on a novel reactive carbonate monomer", *Journal of Polymer Science: Part A: Polymer Chemistry*, Vol. 48, pp. 4737–4746, 2010.

150. Chan, D. P. Y., S. C. Owen, and M. S. Shoichet, "Double click: dual functionalized polymeric micelles with antibodies and peptides", *Bioconjugate Chemistry*, Vol. 24, No. 1, pp. 105–13, 2013.

151. Ghosh, S., S. Basu, and S. Thayumanavan, "Simultaneous and Reversible Functionalization of Copolymers for Biological Applications", *Macromolecules*, Vol. 39, pp. 5595–5597, 2006.

152. Van Dijkhuizen-Radersma, R., L. Moroni, A. van Apeldoorn, Z. Zhang, and D. Grijpma, "Degradable Polymers for Tissue Engineering", *Tissue Engineering*, pp. 193–221, 2008.

153. Jeong, J. H., S. W. Kim, and T. G. Park, "Molecular design of functional polymers for gene therapy", *Progress in Polymer Science*, Vol. 32. pp. 1239–1274, 2007.

154. Gracia, R., and D. Mecerreyes, "Polymers with redox properties: materials for batteries, biosensors and more", *Polymer Chemistry*, Vol. 4, pp. 2206–2214, 2013.

155. Park, J. H., M. Ye, and K. Park, "Biodegradable polymers for microencapsulation of drugs", *Molecules*, Vol. 10, pp. 146–161, 2005.

156. Mok, H., and T. G. Park, "Functional polymers for targeted delivery of nucleic acid drugs", *Macromolecular Bioscience*, Vol. 9. pp. 731–743, 2009.

157. Shim, M. S., and Y. J. Kwon, "Stimuli-responsive polymers and nanomaterials for gene delivery and imaging applications", *Advanced Drug Delivery Reviews*, Vol. 64. pp. 1046–1059, 2012.

158. Nair, L. S., and C. T. Laurencin, "Biodegradable polymers as biomaterials", *Progress in Polymer Science (Oxford)*, Vol. 32. pp. 762–798, 2007.

159. Heredia, K. L., and H. D. Maynard, "Synthesis of protein-polymer conjugates", *Organic&Biomolecular Chemistry*, Vol. 5, pp. 45–53, 2007.

160. Lele, B. S., H. Murata, K. Matyjaszewski, and A. J. Russell, "Synthesis of uniform protein-polymer conjugates", *Biomacromolecules*, Vol. 6, pp. 3380–3387, 2005.

161. Tian, H., Z. Tang, X. Zhuang, X. Chen, and X. Jing, "Biodegradable synthetic polymers: Preparation, functionalization and biomedical application", *Progress in Polymer Science*, Vol. 37, pp. 237–280, 2012.

162. Sato, A. K., M. Viswanathan, R. B. Kent, and C. R. Wood, "Therapeutic peptides: technological advances driving peptides into development", *Current Opinion in Biotechnology*, Vol. 17. pp. 638–642, 2006.

163. Pasut, G., and F. M. Veronese, "Polymer-drug conjugation, recent achievements and general strategies", *Progress in Polymer Science (Oxford)*, Vol. 32. pp. 933–961, 2007.

164. Lecolley, F., L. Tao, G. Mantovani, I. Durkin, S. Lautru, and D. M. Haddleton, "A new approach to bioconjugates for proteins and peptides (“pegylation”) utilising living radical polymerisation", *Chemical Communications (Camb)*, pp. 2026–2027, 2004.

165. Kim, Y., S. O. Ho, N. R. Gassman, Y. Korlann, E. V. Landorf, F. R. Collart, and S. Weiss, "Efficient site-specific labeling of proteins via cysteines", *Bioconjugate Chemistry*, Vol. 19, pp. 786–791, 2008.

166. Hall, D. J., H. M. Van Den Berghe, and A. P. Dove, "Synthesis and post-polymerization modification of maleimide-containing polymers by ‘thiol-ene’ click and Diels-Alder chemistries", *Polymer International*, Vol. 60. pp. 1149–1157, 2011.

167. Durmaz, H., B. Colakoglu, U. Tunca, and G. Hizal, "Preparation of block copolymers via Diels Alder reaction of maleimide- and anthracene-end functionalized polymers", *Journal of Polymer Science: Part A: Polymer Chemistry*, Vol. 44, pp. 1667–1675, 2006.

168. Mantovani, G., F. Lecolley, L. Tao, D. M. Haddleton, J. Clerx, J. J. L. M. Cornelissen, and K. Velonia, "Design and synthesis of N-maleimido-functionalized hydrophilic polymers via copper-mediated living radical polymerization: A suitable alternative to pegylation chemistry", *Journal of American Chemical Society*, Vol. 127, pp. 2966–2973, 2005.

169. Nair, D. P., M. Podgrski, S. Chatani, T. Gong, W. Xi, C. R. Fenoli, and C. N. Bowman, "The Thiol-Michael addition click reaction: A powerful and widely used tool in materials chemistry", *Chemistry of Materials*, Vol. 26. pp. 724–744, 2014.

170. Heisig, F., S. Gollos, S. J. Freudenthal, A. El-Tayeb, J. Iqbal, and C. E. Müller, "Synthesis of BODIPY derivatives substituted with various bioconjugatable linker

groups: a construction kit for fluorescent labeling of receptor ligands", *Journal of Fluorescence*, Vol. 24, No. 1, pp. 213–30, 2014.

171. Gheneim, R., C. Perez-Berumen, and A. Gandini, "Diels-Alder reactions with novel polymeric dienes and dienophiles: Synthesis of reversibly cross-linked elastomers", *Macromolecules*, Vol. 35, pp. 7246–7253, 2002.

172. Kosif, I., E. J. Park, R. Sanyal, and A. Sanyal, "Fabrication of maleimide containing thiol reactive hydrogels via diels-alder/retro-diels-alder strategy", *Macromolecules*, Vol. 43, pp. 4140–4148, 2010.

173. McCusker, C. F., P. J. Kocienski, F. T. Boyle, and A. G. Schitzlein, "Solid-phase synthesis of c(RGDfK) derivatives: On-resin cyclisation and lysine functionalisation", *Bioorganic Medicinal Chemistry Letters*, Vol. 12, pp. 547–549, 2002.

174. Bouilhac, C., E. Cloutet, H. Cramail, A. Deffieux, and D. Taton, "Functionalized Star-Like Polystyrenes as Organic Supports of a Tridentate Bis(imino)pyridinyliron/Aluminic Derivative Catalytic System for Ethylene Polymerization", *Macromolecular Rapid Commununications*, Vol. 26, No. 20, pp. 1619–1625, 2005.

175. Julio, B., S. Roman, A. Gallardo, and B. Levenfeld, "Polymeric Drug Delivery Systems", *Advanced Materials*, Vol. 7, pp. 203–208, 1995.

176. Yoo, J.-W., D. J. Irvine, D. E. Discher, and S. Mitragotri, "Bio-inspired, bioengineered and biomimetic drug delivery carriers", *Natural Reviews in Drug Discovery*, Vol. 10, pp. 521–535, 2011.

177. Gong, J., M. Chen, Y. Zheng, S. Wang, and Y. Wang, "Polymeric micelles drug delivery system in oncology", *Journal of Controlled Release*, Vol. 159. pp. 312–323, 2012.

178. Koren, E., and V. P. Torchilin, "Drug carriers for vascular drug delivery", *International Union of Biochemistry and Molecular Biology Life*, Vol. 63. pp. 586–595, 2011.

179. Stolnik, S., L. Illum, and S. S. Davis, "Long circulating microparticulate drug carriers", *Advanced Drug Delivery Reviews*, Vol. 64. pp. 290–301, 2012.

180. Patri, A. K., I. J. Majoros, and J. R. Baker, "Dendritic polymer macromolecular carriers for drug delivery", *Current Opinion in Chemical Biology*, Vol. 6, pp. 466–471, 2002.

181. Moses, M. a, H. Brem, and R. Langer, "Advancing the field of drug delivery: taking aim at cancer", *Cancer Cell*, Vol. 4, No. 5, pp. 337–41, 2003.

182. Mbeunkui, F., and D. J. Johann, "Cancer and the tumor microenvironment: A review of an essential relationship", *Cancer Chemotherapy and Pharmacology*, Vol. 63. pp. 571–582, 2009.

183. Kim, M. Y., T. Oskarsson, S. Acharyya, D. X. Nguyen, X. H. F. Zhang, L. Norton, and J. Massagu, "Tumor Self-Seeding by Circulating Cancer Cells", *Cell*, Vol. 139, pp. 1315–1326, 2009.

184. Jones, R. G., and C. B. Thompson, "Tumor suppressors and cell metabolism: a recipe for cancer growth", *Genes & Development*, Vol. 23, pp. 537–548, 2009.

185. Klener, P., "Chemotherapy side effects and their management", *Basic Clinical Oncology*, Vol. 19, pp. 279–295, 1999.

186. Klaner, P., "Chemotherapy side effects profile", *Lung cancer guide book*, 2005, http://www.lungcancerguidebook.org/lcguidebook_aug05/appendix_cxtx_side_effects.pdf, 2013.

187. Liu, S., R. Maheshwari, and K. L. Kiick, "Polymer-Based Therapeutics", *Macromolecules*, Vol. 42, No. 1, pp. 3–13, 2009.

188. Blanco, E., C. W. Kessinger, B. D. Sumer, and J. Gao, "Multifunctional micellar nanomedicine for cancer therapy", *Experimental Biology and Medicine (Maywood)*, Vol. 234, No. 2, pp. 123–31, 2009.

189. Sutton, D., N. Nasongkla, E. Blanco, and J. Gao, "Functionalized micellar systems for cancer targeted drug delivery", *Pharmaceutical Research*, Vol. 24, No. 6, pp. 1029–46, 2007.

190. Haag, R., "Supramolecular drug-delivery systems based on polymeric core-shell architectures", *Angewante Chemie International Edition English*, Vol. 43, No. 3, pp. 278–82, 2004.

191. Maeda, H., "Tumor-selective delivery of macromolecular drugs via the EPR effect: Background and future prospects", *Bioconjugate Chemistry*, Vol. 21. pp. 797–802, 2010.

192. Tanaka, T., S. Shiramoto, M. Miyashita, Y. Fujishima, and Y. Kaneo, "Tumor targeting based on the effect of enhanced permeability and retention (EPR) and the mechanism of receptor-mediated endocytosis (RME)", *International Journal of Pharmaceutics*, Vol. 277, pp. 39–61, 2004.

193. Schoenmakers, R. G., P. Van De Wetering, D. L. Elbert, and J. A. Hubbell, "The effect of the linker on the hydrolysis rate of drug-linked ester bonds", *Journal of Controlled Release*, Vol. 95, pp. 291–300, 2004.

194. Gondi, C. S., and J. S. Rao, "Cathepsin B as a cancer target", *Expert Opinions on Therapeutic Targets*, Vol. 17, pp. 281–291, 2013.

195. Green, M., and M. A. Stahmann, "ARTICLE : Synthesis and Enzymatic Hydrolysis of Glutamic Acid Polypeptides", *Journal of Biological Chemistry*, Vol. 197, pp. 771-782, 1952.

196. Matyjaszewski, K., and N. V Tsarevsky, "Nanostructured functional materials prepared by atom transfer radical polymerization", *Natural Chemistry*, Vol. 1, pp. 276–288, 2009.

197. Matyjaszewski, K., "Controlled Radical Polymerization: State-of-the-Art in 2011", in *Progress in Controlled Radical Polymerization: Mechanisms and Techniques*, Vol. 1100, pp. 1–13, 2012.

198. Tomalia, D. A., A. M. Naylor, and W. A. Goddard, "Starburst Dendrimers: Molecular-Level Control of Size, Shape, Surface Chemistry, Topology, and Flexibility from Atoms to Macroscopic Matter", *Angewante Chemie International Edition*, Vol. 29, pp. 138–175, 1990.

199. Rinker, S., Y. Ke, Y. Liu, R. Chhabra, and H. Yan, "Self-assembled DNA nanostructures for distance-dependent multivalent ligand-protein binding", *Natural Nanotechnoogy*., Vol. 3, pp. 418–422, 2008.

200. Hong, S., P. R. Leroueil, I. J. Majoros, B. G. Orr, J. R. Baker, and M. M. Banaszak Holl, "The Binding Avidity of a Nanoparticle-Based Multivalent Targeted Drug Delivery Platform", *Chemical Biology*, Vol. 14, pp. 107–115, 2007.

201. Cabane, E., X. Zhang, K. Langowska, C. G. Palivan, and W. Meier, "Stimuli-responsive polymers and their applications in nanomedicine", *Biointerphases*, Vol. 7. pp. 1–27, 2012.

202. Hawker, C. J., and J. M. J. Fréchet, "The synthesis and polymerization of a hyperbranched polyether macromonomer", *Polymer*, Vol. 33, pp. 1507–1511, 1992.

203. Chen, Y., and X. Xiong, "Tailoring dendronized polymers", *Chemical Communucations (Camb)*, Vol. 46, pp. 5049–5060, 2010.

204. Schlüter, A., and J. Rabe, "Dendronized Polymers: Synthesis, Characterization, Assembly at Interfaces, and Manipulation", *Angewante Chemie International Edition English*, Vol. 39, pp. 864–883, 2000.

205. Shu, L., A. D. Schlüter, C. Ecker, N. Severin, and J. P. Rabe, "Extremely long dendronized polymers: Synthesis, quantification of structure perfection, individualization, and SFM manipulation", *Angewante Chemie International Edition*, Vol. 40, pp. 4666–4669, 2001.

206. Tonga, M., N. Cengiz, M. Merve Kose, T. Dede, and A. Sanyal, "Dendronized polymers via diels-alder “click” reaction", *Journal of Polymer Science: Part A: Polymer Chemistry*, Vol. 48, pp. 410–416, 2010.

207. Ouchi, M., N. Badi, J.-F. Lutz, and M. Sawamoto, "Single-chain technology using discrete synthetic macromolecules", *Nature Chemistry*, Vol. 3. pp. 917–924, 2011.

208. Lutz, J.-F., M. Ouchi, D. R. Liu, and M. Sawamoto, "Sequence-controlled polymers", *Science*, Vol. 341, p. 1238149, 2013.

209. Pfeifer, S., and J. F. Lutz, "Development of a library of N-substituted maleimides for the local functionalization of linear polymer chains", *Chemistry: A European Journal*, Vol. 14, pp. 10949–10957, 2008.

210. Srichan, S., N. Kayunkid, L. Oswald, B. Lotz, and J.-F. Lutz, "Synthesis and Characterization of Sequence-Controlled Semicrystalline Comb Copolymers: Influence of Primary Structure on Materials Properties", *Macromolecules*, Vol. 47, pp. 1570–1577, 2014.

211. Lutz, J.-F., "Sequence-controlled polymerizations: the next Holy Grail in polymer science", *Polymer Chemistry*, Vol. 1. p. 55, 2010.

212. Schmidt, B. V. K. J., N. Fechler, J. Falkenhagen, and J.-F. Lutz, "Controlled folding of synthetic polymer chains through the formation of positionable covalent bridges", *Natural Chemistry*, Vol. 3, pp. 234–238, 2011.

213. Hoyle, C. E., and C. N. Bowman, "Thiol-ene click chemistry", *Angewandte Chemie International Edition*, Vol. 49. pp. 1540–1573, 2010.

214. Malkoch, M., E. Malmstrm, and A. Hult, "Rapid and efficient synthesis of aliphatic ester dendrons and dendrimers", *Macromolecules*, Vol. 35, pp. 8307–8314, 2002.

215. Ihre, H., A. Hult, J. M. J. Fréchet, and I. Gitsov, "Double-Stage Convergent Approach for the Synthesis of Functionalized Dendritic Aliphatic Polyesters Based

on 2,2-Bis(hydroxymethyl)propionic Acid", *Macromolecules*, Vol. 31, pp. 4061–4068, 1998.

216. Zhang, Y., H. F. Chan, and K. W. Leong, "Advanced materials and processing for drug delivery: the past and the future", *Advanced Drug Delivery Reviews*, Vol. 65, No. 1, pp. 104–20, 2013.

217. Du, A. W., and M. H. Stenzel, "Drug carriers for the delivery of therapeutic peptides", *Biomacromolecules*, Vol. 15, pp. 1097–114, 2014.

218. Danquah, M. K., X. a Zhang, and R. I. Mahato, "Extravasation of polymeric nanomedicines across tumor vasculature", *Advanced Drug Delivery Reviews*, Vol. 63, No. 8, pp. 623–39, 2011.

219. Torchilin, V. P., "Multifunctional nanocarriers", *Advanced Drug Delivery Reviews*, Vol. 64, pp. 302–315, 2012.

220. Nazemi, A., R. C. Amos, C. V. Bonduelle, and E. R. Gillies, "Dendritic surface functionalization of biodegradable polymer assemblies", *Journal of Polymer Science: Part A: Polymer Chemistry*, Vol. 49, No. 12, pp. 2546–2559, 2011.

221. Altin, H., I. Kosif, and R. Sanyal, "Fabrication of “Clickable” Hydrogels via Dendron−Polymer Conjugates", *Macromolecules*, Vol. 43, No. 8, pp. 3801–3808, 2010.

222. Abraham, S., J. H. Choi, C. S. Ha, and I. Kim, "Synthesis of star polymers via nitroxide mediated free-radical polymerization: A “core-first” approach using resorcinarene-based alkoxyamine initiators", *Journal of Polymer Science: Part A: Polymer Chemistry*, Vol. 45, pp. 5559–5572, 2007.

223. Altintas, O., A. P. Vogt, C. Barner-Kowollik, and U. Tunca, "Constructing star polymers via modular ligation strategies", *Polymer Chemistry*, Vol. 3. p. 34, 2012.

224. Saha, A., and S. Ramakrishnan, "Single step synthesis of peripherally “clickable” hyperbranched polyethers", *Macromolecules*, Vol. 42, pp. 4956–4959, 2009.

225. Chen, Y., Z. Shen, E. Barriau, H. Kautz, and H. Frey, "Synthesis of multiarm star poly(glycerol)-block-poly(2-hydroxyethyl methacrylate)", *Biomacromolecules*, Vol. 7, No. 3, pp. 919–26, 2006.

226. Liu, C., Y. Zhang, and J. Huang, "Well-Defined Star Polymers with Mixed-Arms by Sequential Polymerization of Atom Transfer Radical Polymerization and Reverse Addition - Fragmentation Chain Transfer on a Hyperbranched Polyglycerol Core", *Macromolecules*, Vol. 41, pp. 325–331, 2008.

227. Taton, D., M. Saule, J. Logan, R. Duran, S. Hou, E. L. Chaikof, and Y. Gnanou, "Polymerization of ethylene oxide with a calixarene-based precursor: Synthesis of eight-arm poly(ethylene oxide) stars by the core-first methodology", *Journal of Polymer Science: Part A: Polymer Chemistry*, Vol. 41, No. 11, pp. 1669–1676, 2003.

228. Stenzel, M. H., and T. P. Davis, "Star polymer synthesis using trithiocarbonate functional-cyclodextrin cores (reversible addition-fragmentation chain-transfer polymerization)", *Journal of Polymer Science: Part A: Polymer Chemistry*, Vol. 40, No. 24, pp. 4498–4512, 2002.

229. Schramm, O. G., G. M. Pavlov, H. P. van Erp, M. a. R. Meier, R. Hoogenboom, and U. S. Schubert, "A Versatile Approach to Unimolecular Water-Soluble Carriers: ATRP of PEGMA with Hydrophobic Star-Shaped Polymeric Core Molecules as an Alternative for PEGylation", *Macromolecules*, Vol. 42, No. 6, pp. 1808–1816, 2009.

230. Puts, R. D., and D. Y. Sogah, "Universal Multifunctional Initiator Containing Orthogonal Reactive Sites: Synthesis of Macromonomers and Comb Polymers Using Consecutive Controlled Free Radical and Cationic Ring-Opening Polymerizations", Macromolecules, Vol. 9297, No. 97, pp. 7050–7055, 1997.

231. Simanek, E. E., and J. Lim, "Toward the next generation drug delivery vehicle: Synthesis of a dendrimer with four orthogonally reactive groups", *Molecular Pharmaceutics*, Vol. 2, No. 4, pp. 273–277, 2005.

232. Matyjaszewski, K., "Atom Transfer Radical Polymerization (ATRP): Current status and future perspectives", *Macromolecules*, Vol. 45, pp. 4015–4039, 2012.

233. Siegwart, D. J., J. K. Oh, and K. Matyjaszewski, "ATRP in the design of functional materials for biomedical applications", *Progress in Polymer Science*, Vol. 37, pp. 18–37, 2012.

234. Theato, P., "Synthesis of Well-Defined Polymeric Activated Esters", *Journal of Polymer Science: Part A: Polymer Chemistry*, Vol. 46, pp. 6677–6687, 2008.

235. Heredia, K. L., Z. P. Tolstyka, H. D. Maynard, R. V February, V. Re, M. Recei, and V. April, "Aminooxy End-Functionalized Polymers Synthesized by ATRP for Chemoselective Conjugation to Proteins", Macromolecules, pp. 4772–4779, 2007.

236. Plunkett, W., P. Huang, and V. Gandhi, "Preclinical characteristics of gemcitabine", *Anticancer Drugs*, Vol. 6, pp. 7–13, 1995.

237. Xu, B., Z. Jiang, S. B. Kim, S. Yu, J. Feng, A. Malzyner, A. Del Giglio, H. C. Chung, L. J. Shen, and D. L. K. Pen, "Biweekly gemcitabine-paclitaxel, gemcitabine-carboplatin, or gemcitabine-cisplatin as first-line treatment in metastatic breast cancer after anthracycline failure: A phase II randomized selection trial", *Breast Cancer*, Vol. 18, pp. 203–212, 2011.

238. Pfisterer, J., M. Plante, I. Vergote, A. du Bois, H. Hirte, A. J. Lacave, U. Wagner, A. Stähle, G. Stuart, R. Kimmig, S. Olbricht, T. Le, J. Emerich, W. Kuhn, J. Bentley, C. Jackisch, H.-J. Lück, J. Rochon, A. H. Zimmermann, and E. Eisenhauer, "Gemcitabine plus carboplatin compared with carboplatin in patients with platinum-sensitive recurrent ovarian cancer: an intergroup trial of the AGO-OVAR, the NCIC CTG, and the EORTC GCG", *Journal of Clinical Oncology*, Vol. 24, pp. 4699–4707, 2006.

239. Edeiman, M. J., H. Quam, and B. Mullins, "Interactions of gemcitabine, carboplatin and paclitaxel in molecularly defined non-small-cell lung cancer cell lines", *Cancer Chemotherapy Pharmacology*, Vol. 48, pp. 141–144, 2001.

240. Pfisterer, J., I. Vergote, A. Du Bois, and E. Eisenhauer, "Combination therapy with gemcitabine and carboplatin in recurrent ovarian cancer", *International Journal of Gynecological Cancer*, Vol. 15, pp. 36–41, 2005.

241. Wong, A., R. A. Soo, W.-P. Yong, and F. Innocenti, "Clinical pharmacology and pharmacogenetics of gemcitabine", *Drug Metabolism Reviews*, Vol. 41, pp. 77–88, 2009.

242. Pasut, G., F. Canal, L. Dalla, S. Arpicco, F. M. Veronese, and O. Schiavon, "Antitumoral activity of PEG – gemcitabine prodrugs targeted by folic acid", *Journal of Controlled Release*, Vol. 127, pp. 239–248, 2008.

243. Khare, V., S. Kour, N. Alam, R. D. Dubey, A. Saneja, M. Koul, A. P. Gupta, D. Singh, S. K. Singh, A. K. Saxena, and P. N. Gupta, "Synthesis, characterization and mechanistic-insight into the anti-proliferative potential of PLGA-gemcitabine conjugate", *International Journal of Pharmaceutics*, Vol. 470, No. 1–2, pp. 51–62, 2014.

244. Vandana, M., and S. K. Sahoo, "Long circulation and cytotoxicity of PEGylated gemcitabine and its potential for the treatment of pancreatic cancer", *Biomaterials*, Vol. 31, No. 35, pp. 9340–56, 2010.

245. Monge, S., and D. M. Haddleton, "Synthesis of precursors of poly(acryl amides) by copper mediated living radical polymerization in DMSO", *European Polymer Journal*, Vol. 40, pp. 37–45, 2004.

246. Liu, Z., C. Dong, X. Wang, H. Wang, W. Li, J. Tan, and J. Chang, "Self-assembled biodegradable protein-polymer vesicle as a tumor-targeted nanocarrier", *ACS Applied Materials and Interfaces*, Vol. 6, No. 4, pp. 2393–400, 2014.

247. Zhang, J., Y. Lei, A. Dhaliwal, Q. K. Ng, J. Du, M. Yan, Y. Lu, and T. Segura, "Protein-polymer nanoparticles for nonviral gene delivery", *Biomacromolecules*, Vol. 12, No. 4, pp. 1006–14, 2011.

248. Qi, Y., and A. Chilkoti, "Growing polymers from peptides and proteins: a biomedical perspective", *Polymer Chemistry*, Vol. 5, p. 266, 2014.

249. Kulhari, H., D. Pooja, S. Shrivastava, N. V G M, and R. Sistla, "Peptide conjugated polymeric nanoparticles as a carrier for targeted delivery of docetaxel", *Colloids and Surfaces B: Biointerfaces*, Vol. 117, pp. 166–73, 2014.

250. He, C., X. Zhuang, Z. Tang, H. Tian, and X. Chen, "Stimuli-sensitive synthetic polypeptide-based materials for drug and gene delivery", *Advanced Healthcare Materials*, Vol. 1, No. 1, pp. 48–78, 2012.

251. Grover, G. N., and H. D. Maynard, "Protein-polymer conjugates: Synthetic approaches by controlled radical polymerizations and interesting applications", *Current Opinion in Chemical Biology*, Vol. 14. pp. 818–827, 2010.

252. Sharma, K. P., A. M. Collins, A. W. Perriman, and S. Mann, "Enzymatically active self-standing protein-polymer surfactant films prepared by hierarchical self-assembly", *Advanced Materials*, Vol. 25, pp. 2005–2010, 2013.

253. Biedermann, F., U. Rauwald, J. M. Zayed, and O. A. Scherman, "A supramolecular route for reversible protein-polymer conjugation", *Chemical Science*, Vol. 2. p. 279, 2011.

254. Shakya, A. K., H. Sami, A. Srivastava, and A. Kumar, "Stability of responsive polymer-protein bioconjugates", *Progress in Polymer Science (Oxford)*, Vol. 35. pp. 459–486, 2010.

255. Tao, L., G. Mantovani, F. Lecolley, and D. M. Haddleton, "Alpha-aldehyde terminally functional methacrylic polymers from living radical polymerization: application in protein conjugation “pegylation”", *Journal of American Chemistry Society*, Vol. 126, No. 41, pp. 13220–1, 2004.

256. Bontempo, D., K. L. Heredia, B. a Fish, and H. D. Maynard, "Cysteine-reactive polymers synthesized by atom transfer radical polymerization for conjugation to

proteins", *Journal of American Chemistry Society*, Vol. 126, No. 47, pp. 15372–3, 2004.

257. Kerr, J., J. L. Schlosser, D. R. Gri, D. Y. Wong, and A. M. Kasko, "Steric Eff ects in Peptide and Protein Exchange with Activated Disulfides", *Biomacromolecules*, Vol. 14, No. 8, pp. 10–17, 2013.

258. Wang, Y., Y. Sun, H. Wang, P. Liu, W. Peng, and Y. Duan, "Synthesis of low-molecular weight protein (LMWP) lysozyme-curcumin conjugates for kidney drug targeting", *Journal of Biomaterials Science: Polymer Edition*, Vol. 24, No. 11, pp. 1360–1367, 2013.

259. Tao, L., J. Xu, D. Gell, and T. P. Davis, "Synthesis, Characterization, and Bioactivity of Mid-Functional PolyHPMA−Lysozyme Bioconjugates", *Macromolecules*, Vol. 43, No. 8, pp. 3721–3727, 2010.

260. Saito, G., J. a Swanson, and K.-D. Lee, "Drug delivery strategy utilizing conjugation via reversible disulfide linkages: role and site of cellular reducing activities", *Advanced Drug Delivery Reviews*, Vol. 55, No. 2, pp. 199–215, 2003.

261. Mcrae, S., X. Chen, K. Kratz, D. Samanta, E. Henchey, S. Schneider, and T. Emrick, "Penta fluorophenyl Ester-Functionalized Phosphorylcholine Polymers: Preparation of Linear, Two-Arm, and Grafted Polymer − Protein Conjugates", Biomacromolecules, Vol. 13, No. 7, pp. 2099-2109, 2012.

262. McDowall, L., G. Chen, and M. H. Stenzel, "Synthesis of Seven-Arm Poly(vinyl pyrrolidone) Star Polymers with Lysozyme Core Prepared by MADIX/RAFT Polymerization", *Macromolacular Rapid Communications*, Vol. 29, No. 20, pp. 1666–1671, 2008.